Perception of Objective Parameter Variations in Virtual Acoustic Spaces

Aglaia Foteinou

Doctor of Philosophy

University of York

Department of Electronics

October 2013

Abstract

This thesis investigates if reliability in objective acoustic metrics obtained for an auralized space implies accuracy and reliability in terms of the subjective listening experience. Auralizations can be created based either on impulse response measurements of an existing space, or simulations using computer-based acoustic models. Validations of these methods usually focus on the observation of standard objective acoustic measures and how these vary under certain conditions. However, for accurate and believable auralization, the subjective quality of the resulting virtual auditory environment should be considered as being at least as important, if not more so.

This study is focused in the most part on St. Margaret's Church, York, UK. Impulse responses have been acquired in the actual space and virtual acoustic models created using CATT-Acoustic and ODEON-Auditorium auralization software, both based on geometric acoustic algorithms. Variations in objective acoustic parameters are examined by changing the physical characteristics of the space, the receiver position and the sound source orientation. It is hypothesised that the perceptual accuracy of the auralizations depends on optimising the model to minimise observed changes in objective acoustic parameters. This objective evaluation is used to ascertain the behaviour of certain standard acoustic parameters. From these results, impulse responses with suitable acoustic values are selected for subjective evaluation via listening tests.

These acoustic parameters, in combination with the physical factors that influence them, are examined, and the importance of variation in these values in relation to our perception of the result is investigated. Conclusions are drawn for both measurement and modelling approaches, demonstrating that model optimisation based on key acoustic parameters is not sufficient to guarantee perceptual accuracy as perceptual differences are still evident when only a simple acoustic parameter demonstrates a difference of greater than 1 JND. It is also essential to add that the overall perception of the changes in the acoustic parameters is independent of the auralization technique used. These results aim to give some confidence to acoustic designers working in architectural and archeoacoustic design in terms of how their models might be best created for optimal perceptual presentation.

Contents

Contents

Contents

Contents

Contents

List of Tables

List of Figures

Acknowledgements

It has been a great privilege to have Dr Damian Murphy as my supervisor for this journey, to whom I would like to express my gratitude for his support, constant guidance and major inspiration during my studies.

I would like to thank all my colleagues and friends, past and present, of the Audio Lab, one by one and all of them, particularly Andrew, Simon, Matt, Anocha and Christine, for their assistance, support, and encouragement. I would also like to thank Angelo Farina of the University of Parma; Jens Holger Rindel from ODEON; and Bengt-Inge Dalenbäck from CATT-Acoustic for their advices and guidance regarding their software which have been extensively used throughout this work. A huge thanks to those friends, students and staff from Electronics, Music and Theatre, Film and Television Departments who volunteered to participate in several "difficult" listening tests; their contribution to my research is sincerely appreciated. I would like also to thank Chris Mellor of the Maths Skills Centre of the University of York, for his help about statistics.

I am grateful to my great friends who despite the geographic distances, have always been very supportive and encouraged me throughout my experience as PhD student; especially Marina, Niki and Sarah, who agreed to performed in "cold" anechoic chambers or being covered in dust to measure the dimensions of acoustic panels. My gratitude goes also to Daniel for helping me with the final editing of this thesis and to my piano pupils who, maybe being unaware, had made me smile, feel confident and positive.

I would like to say a huge thanks to Pier Paolo, for the love and support he has given me throughout this work. Finally, I would like to thank my parents who have always been there for me. Their contribution to this work is greater than words can possibly express.

The opportunity to study this PhD course has been awarded by the Empirikion Foundation, Athens, Greece, in 2009, committing financial support for the full course, which is still expected.

Declaration

I declare that the contents of this thesis are entirely my own work and that all contributions from external sources, such as publications, websites or personal contact, have been explicitly stated and referenced appropriately.

In addition, I declare that some parts of this research has been previously presented at conferences. These publications are listed below:

- Foteinou, A., and Murphy, D.T., "The Control of Early Decay Time on Auralization Results based on Geometric Acoustic Modelling", Proc. of BNAM 2012, Odense, Denmark, June 2012

- Foteinou, A., and Murphy, D.T., "Perceptual validation in the acoustic modelling and auralization of heritage sites: The Acoustics Measurement and Modelling of St. Margaret's Church, York, UK", Proc. of Conference of Ancient Theatres, Greece, September 2011

- Foteinou, A., and Murphy, D.T., "Evaluation of the Psychoacoustic Perception of Geometric Acoustic Modelling Based Auralization", Proc. of the 130th AES Convention, London, UK, May, 2011

- Shelley, S., Foteinou, A., and Murphy, D.T., "OpenAir: An Online Auralization Web Resource with Applications for Game Audio Development", Proc. of the 41st International Conference of AES, Audio for Games, London, UK, February, 2011

- Foteinou, A., Murphy, D.T., and Masinton, A., "Investigation of Factors Influencing Acoustic Characteristics in Geometric Acoustics Based Auralization", Proc. of 13th International Conference on Digital Audio Effects (DAFx-10), p.171-181, Graz, Austria, September , 2010

- Foteinou, A., Murphy, D.T., and Masinton, A., "Verification of Geometric Acoustics-Based Auralization Using Room Acoustics Measurement Techniques", Proc. of the 128th AES Convention, London, UK, May 22-25, 2010, Convention paper 7968

Chapter 1.
Thesis Introduction

1.1 *Interest*

Over the last few decades, the creation of virtual acoustic spaces has aroused considerable interest and had an impact on several areas of modern life. The introduction of such spaces gives users the opportunity to listen to sounds placed within a virtual environment as if they, the listeners, were also present. This process is known as "Auralization" and there are several ways to create an auralized space. However, not all of these methods are reliable or convincing enough to create the impression amongst listeners of being present in a "real" space. Auralization methods can be categorised into: those which attempt to "capture" the acoustics of existing spaces and reproduce them in any auditory reproduction system; and those involving mathematical and computer models in place of an existing space, in a similar way to how architects use such models to create the visual representation of a space. An additional method combines elements of both these approaches through the use of a physical scale architectural model of the space to be auralized. This approach is not commonly used any more since the introduction of computer models, and so will not be considered further as part of this thesis.

To create an accurate auralized space, it is essential to have in-depth knowledge of the science of room acoustics and the principles of sound propagation. The sound energy in an enclosed space depends on the shape and volume of the space, the acoustic characteristics of the surfaces and the location of both sound source and sound receiver. In addition, it is important to take into consideration the field of psychoacoustics when seeking to understand and evaluate the perceived results and correlate them with the acoustic characteristics of the space.

This listening experience can be used in architectural and acoustic design, where the results of an acoustic treatment can be presented to the client before final decisions and construction have been finished [1-6]. In the music production industry, sound engineers or composers aim to create the impression that the recordings were made in an acoustic space different to the one that was actually used. In the entertainment industry, virtual spaces have become significant as part of film production and digital cinema, and especially the game audio industry where 3D is now considered essential. An application of such a virtual acoustic experience was demonstrated by the author in [7]. A walkthrough animation has been created based on a virtual acoustic model of St. Margaret's Church, York, where the viewer-listener moves through the virtual space, listening to the sound produced from a musical source placed within it.

1.2 *Acoustic Revival of Heritage Sites*

There is an abiding interest in the acoustic properties of archaeological or heritage sites and researchers have sought to revive and reproduce the sound of these places in order to better understand how they sounded in the past and to clarify their acoustic evolution over time.

Pre-historic sites such as Stonehenge in England, or Maes Howe in Orkney have often, until more recently, been overlooked by archaeological and archaeoacoustic studies [8, 9]. The acoustics of Greek and Roman Theatres has been the focus of research in several projects, with the aim to understand their cultural impact for historical, educational and even entertainment purposes [10-12]. The ERATO Project (identification Evaluation and Revival of the Acoustical heritage of ancient Theatres and Odea) [13-17] and the ATLAS project (Ancient Theatres Lighting and Acoustics Support) [18] attempted the virtual restitution of their past use based on historical descriptions of the theatres' history, clothing, hairstyles as well as acoustics, audience behaviour, sound and early music. As part of these projects, virtual acoustic spaces, as well as musical instruments, were constructed as reported in the primary literary sources. Additionally, the CAHRISMA project (Conservation of the Acoustical Heritage by the Revival and Identification of the Sinan's Mosques Acoustics) [19] considered acoustics as well as visual features for conservation and restoration projects.

As part of the CAMERA project (Centre for Acoustic and Musical Experiments in Renaissance Architecture), the acoustics of churches were studied in order to investigate what the audience's acoustic perception of such spaces would have been during the Renaissance period [20]. Several other projects which considered reviving the acoustics of potential historical spaces have been carried out, such as St. Patrick's Church near Hull (by the author [21, 22] and others [23]) the virtual reconstruction of the cathedrals of the region of Andalusia [24] and the reconstruction of the acoustics of the Temple of Decision (by the author), as part of the Re-sounding Falkland project [25].

Additionally, there is great interest in capturing the sound of existing spaces considered as being acoustically important, for posterity as in [9, 26, 27] and impulse responses libraries have been created recently for these purposes such as the Open AIR Library [28].

1.3 *Primary Aims and Thesis Hypothesis*

It is essential to create objectively accurate and perceptually believable auralizations for any space, in order to give the listener an experience that be considered authentic and as 'correct' as the designer is able to achieve. In recent works [29-34], the evaluation of an auralization is based on the observation of objective metrics, often comparing the results from a virtual space with those observed in an actual space. However, when reconstructing the sound of heritage sites that no longer exist or are partly ruined, where acoustic information about the real space is not available, these evaluation of the virtual acoustic environments becomes more problematic.

Hence, the subjective evaluation of an auralized space, together with the study of more readily available and standardised objective acoustic characteristics, is an essential step in its overall design. The primary aims of this thesis are to:

- address how changes made to the acoustic characteristics of a simulated space might affect the acoustic perceptions of a listener and,
- if so, what the physical factors are which influence these perceptual results.

It is hoped that the conclusions of this study will help acousticians working in architectural and archaeoacoustic design, in terms of how their auralizations might be best created for optimal perceptual presentation.

The main hypothesis of this research is as follows:

In virtual acoustic reconstructions, perceptual accuracy is dependent on minimising the changes in objective acoustic metrics through optimisation of physical parameters in the auralized space.

1.4 *Structure of Thesis*

The chapters that follow describe the process of the research as well as the results obtained, in order to support and assess the validity of the hypothesis of this thesis.

To begin with, in Chapter 2 there is an explanation of sound propagation as a physical phenomenon and the key properties of room acoustics are also considered. The main objective acoustic metrics are defined according to existing international standards and the theory about measuring their related subjective effects based on previous work is presented here as well.

In Chapter 3 the concept of auralization is considered along with the well-known auralization techniques that have been developed over the years. Auralization results can be produced from real measurements or synthesised impulse responses. The advantages and limitations of each of these methods, with respect to the excitation signal used as well as the sound source and microphone properties, are considered and the chapter concludes with an evaluation of which techniques are most suitable for the purposes of this study.

Chapter 4 describes the pilot experiments that were carried out in order to explore how, by controlling the physical factors and acoustic properties of an acoustic model, the user can influence the objective and subjective results obtained from the space. Important information has been extracted from these experiments and used for the investigation of the case study that focuses the main part of this thesis.

Chapter 5 presents the space chosen as the case study, used to test the studied hypothesis. The process followed for capturing and producing the impulse responses with three different auralization techniques is described in detail. The in-situ impulse response measurements and the modelling technique followed for the acoustic models based on two commercial geometric acoustic software packages, CATT-Acoustic and ODEON, are also detailed here.

Chapter 6 reviews the objective results observed from the impulse responses generated by these three auralization techniques. The chapter begins by explaining the reasons for focusing only on specific acoustic parameters in the current work and continues with a description of the calculation process for the acoustic parameters. The results are analysed and discussed based on the changes in the acoustic parameters obtained due to variations in the acoustic characteristics of the auralized spaces.

Chapter 7 outlines the strategy followed for the subjective evaluation of the results and the procedure of the listening tests is also described in detail. The results are analysed based on the changes obtained in the acoustic parameters compared with the perceptual results of the listening tests and conclusions are drawn relevant to the stated hypothesis.

A summary of the results and the main conclusions that can be drawn from the research are presented in Chapter 8. The novel contributions of the study are identified and in the final sections of the thesis, suggestions are made regarding future research in the area.

1.5 *Contributions to the Field*

The following contributions to the field are presented throughout the course of this work:

- An acoustic study of a space based on a wide data set obtained from varying the acoustic characteristics of the space, receiver position and sound source orientation.
- An investigation of the objective acoustic metrics observed from three different auralization techniques applied to a single space.
- The introduction of a novel way to represent data for multiple positions in the same space and with respect to their acoustic behaviour across frequency bands, by using the “acoustic floor maps”.
- An investigation based on both objective and subjective terms for the evaluation of the auralization results.

Chapter 2.
Room Acoustics

2.1 *Introduction*

Room acoustics is the study of how sound propagates within an enclosed space and how it is then perceived by a listener. The evaluation of the space can therefore be determined using both objective and subjective measures.

In order to understand the resulting sound and its propagation, it is necessary to approach it as a physical phenomenon while at the same time it has to be examined in terms of psychoacoustic perception. For this reason, in this chapter the following are discussed:

1) The characteristics of sound in a free field;
2) How sound behaves in an enclosed space;
3) How to measure the acoustic characteristics of a space;
4) How to measure their impact on the human perception of sound.

2.2 *Sound in a Free Field*

In a free field it is assumed that sound propagates freely from, ideally, a point source in all directions with no return and with no influence due to interactions from surrounding objects. The intensity of the sound therefore follows the **inverse square law** according to which the intensity of the sound is inversely proportional to the square of the distance from the source, as described by,

$$I = \frac{P}{4\pi r^2} \qquad (2.1)$$

where I is the intensity of the sound at any point (in watts/square metres), P is the power of the source (in watts) and r is the distance from the source to the receiver's point (in metres).

As the sound moves away from the source, S, in three dimensions (Figure 2.1), its energy will cover a wider area. When the distance from the source is doubled, $2r$, the intensity is reduced to one quarter of the initial value [35]. When the distance is tripled, $3r$, the intensity is reduced to one ninth of the initial value, and so on.

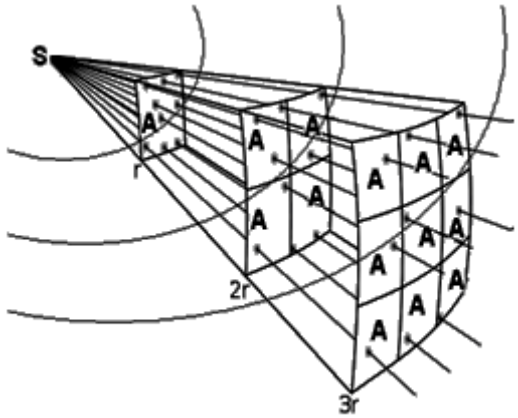

Figure 2.1 The measured sound intensity is inversely proportional to the square of the distance *r* from the source S (describing the phenomenon by 2D waves), after [36].

In practice, various factors such as air absorption will affect the intensity of the sound, especially at 1000Hz and above [35, 37-39]. Air absorption is dependent on air temperature and humidity, and more specifically it is directly proportional to temperature and frequency while it is inversely proportional to humidity.

Natural free fields are rarely found and heard in the real world, as there is always a surface which can act to reflect or absorb sound, such as the ground below the source location. For the purpose of acoustic research and measurement, **anechoic chambers** are built. These are rooms designed to have no reflections coming from the boundary surfaces as large wedges of absorbent material are used. These spaces behave as a "free field" and there is usually, in addition, a very low noise floor. This gives the listener the opportunity to hear only the direct sound from a given source [40].

2.3 *Sound in an Enclosed Space*

In an enclosed space, sound waves interact with the surrounding boundaries, as well as the air filling the space and any physical objects placed within these boundaries, influencing propagation through the space and contributing to the final audible result. The contributions of such acoustic interactions are described in the following section.

2.3.1 **Growth and Decay of Sound in a Room**

Consider a closed space, as shown in Figure 2.2, where a point-like sound source, *S*, emits a continuous sound in all directions, starting at time t_0. At the receiver position, *R*, the sound arrives through an infinite number of paths. The first sound is perceived by the receiver at t_1, such that $t_1 > t_0$, which is defined as the time needed for the sound to travel the shortest path from the source to the receiver. This is called the **direct sound** and behaves similarly to a sound source propagating in free space. The direct sound arrives at the receiver point with less sound energy than that emitted from the source, according to the inverse square law and due to air absorption losses. The level of the direct sound affects the perception of any sound heard within a given space, influencing the overall clarity and in particular the intelligibility of speech [41].

After a short time, t_2, the reflection $refl_1$ arrives at the receiver and adds its sound power to that of the direct sound, resulting in the energy $D + refl_1$. Thereafter, at t_3, the reflection $refl_2$ arrives and the sound energy at the receiver's position is increased to $D + refl_1 + refl_2$.

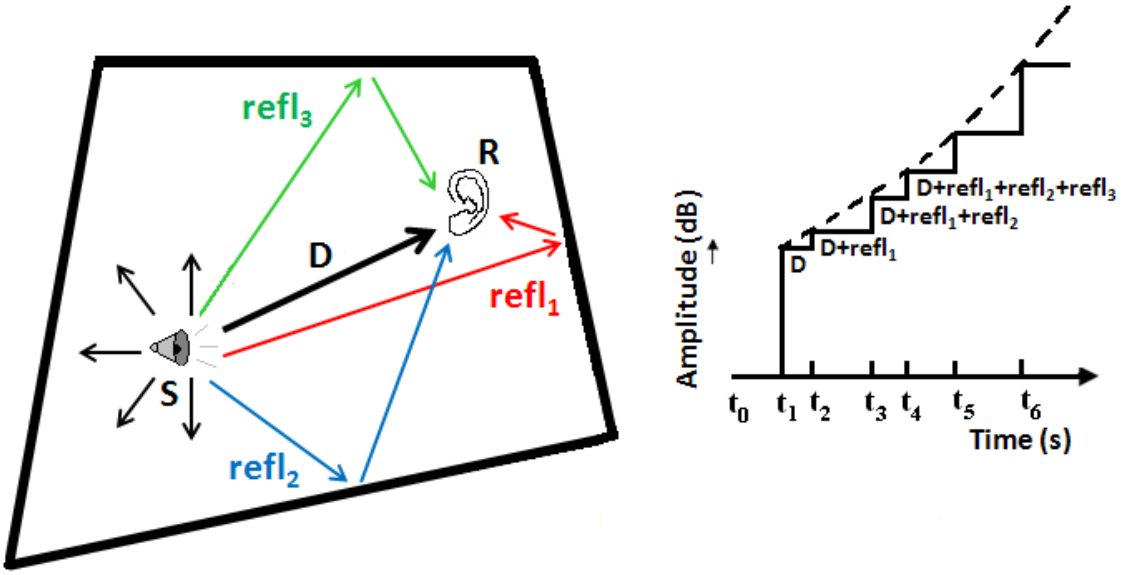

Figure 2.2 The growth of a sound at receiver R for a continuous sound source S based on the build-up of impulse arrivals. The direct sound D arrives at the receiver at time t_1 after a continuous sound source starts at time t_0 (left). The sound energy at the receiver point builds up from the added sound energy of the reflections $refl_1$, $refl_2$, $refl_3$ arrive at the receiver at times t_2, t_3, t_4 (right) (describing the phenomenon by 2D particles).

These sounds, produced by one or more reflections from surfaces in the space, are called **early reflections** and arrive at the receiver position at different times and from different directions. The energy of early reflections is reduced due to the distance travelled, air absorption, and also the absorption effect of the surface from which they are reflected. As with the direct sound, early reflections also contribute to the overall clarity of sound together with the perceived intelligibility of speech. Additionally, early reflections are responsible for the phenomenon of **echo**. This happens when a reflection arrives at the receiver position with a sufficient delay (typically greater than 50ms to 80ms [35]) after the previous sound such that the ear perceives it as a separate sound event.

After these early reflections, many more reflections arrive at the listener from all directions and as a result the sound loses its sense of perceived direction. This part of the sound is called the **reverberant sound**.

The above process continues until the source, *S,* stops producing sound. At this point the sound energy starts to decay as the energy in the space is absorbed by the surfaces, illustrated in Figure 2.3. At t_x, the sound source has stopped and the

direct sound produced as a consequence of this terminating sound event arrives at the receiver position at t_a, such that $t_a > t_x$. At t_b, the first reflection $refl_1$ arrives at the receiver position and so on.

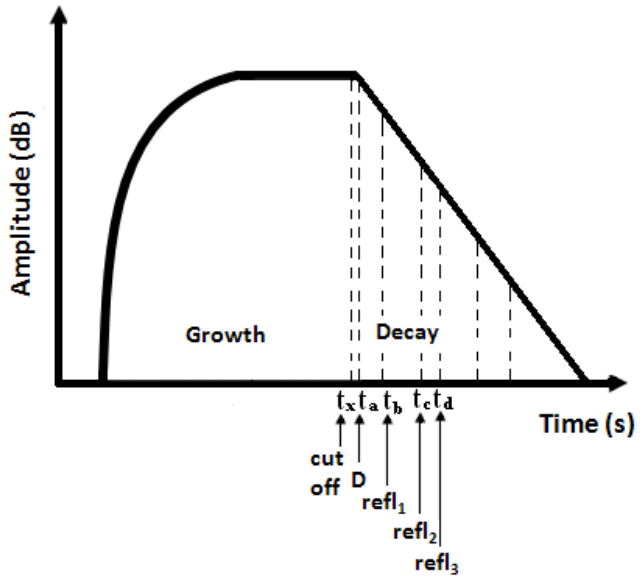

Figure 2.3 The sound energy related to the growth and the decay of sound for a continuous source *S* that is turned off at time $t = t_x$.

It takes some time for the sound to die away after the sound source is stopped. In Figure 2.3, the decay is a straight line, which is the ideal case, although, in reality, the energy of sequential reflections does not necessarily decay in such a linear manner.

By measuring this reverberant sound, important information can be obtained about how the sound is perceived in the space. This decay is dependent on the absorptive capacity of the surfaces in the space, the shape, the volume of the room and also the air conditions, such as humidity and temperature.

In an enclosed space, there are three distinct regions where sound can be characterised differently. These are 1) the near field, 2) the far field and 3) the reverberant field. The region which is very close to the sound source is known as the **near field**. In this area, the receiver perceives only the direct sound from the sound source and as a result, any acoustic measurements in this area cannot acquire the acoustic behaviour of the space.

Beyond the near field, in the **far field** the sound energy can be related to the inverse square law and the receiver perceives the direct sound as well as any early reflections that are strong enough to give information about the acoustic characteristics of the space.

An important term that needs to be defined at this point is the **critical distance**. In theory, this is the distance at which the sound energy of the direct and the reflected sound (or reverberation) are equal [35, 42]. In practice, it is determined by the room constant and the directivity of the sound source using the following equation [41]:

$$r = 0.141\sqrt{R_{room}\,Q} \qquad (2.2)$$

where r is the distance (in metres) and Q defines the source directivity and is equal to 1 for an omnidirectional source and equal to 2 for a semi-directional one. R_{room} is the room constant (in square metres), defined by the following equation:

$$R_{room} = \frac{S\alpha}{(1-\alpha)} \qquad (2.3)$$

where S is the total surface area (in square metres) and α is the average absorption coefficient associated with this total surface area, as will be explained in section 2.3.4.

Alternatively, if this information is not available, Sabine's approximation as a function of volume and reverberation time can be used:

$$r = 0.057\sqrt{\frac{V}{RT_{60}}} \qquad (2.4)$$

where r is the distance (in metres), V is the volume (in cubic metres) and RT_{60} is the reverberation time (in seconds). Reverberation time will be discussed in more detail in section 2.5.1.

It is clear that the critical distance is dependent on the complexity, the size, the absorptive materials of the space and the source directivity. For example, in large and complicated rooms, and where the sound source and receiver point are not

affected by surrounding objects, the critical distance is longer than in the case of a smaller room where the reflections from the boundaries arrive at the receiver point earlier. Following the same logic, the critical distance is shorter when an obstacle with a reflective surface is very close to the receiver point.

In the **reverberant field**, the perceived sound is a combination of direct sound from the source and reflected sound from the boundaries and any surrounding objects. These reflections arrive from all directions, thus due to their diffuse nature the sound energy remains approximately constant in this region.

2.3.2 **Sound Reflection**

When a sound meets a planar boundary, a specular reflection is the result, based on the **Law of Reflection**, where the angle of incidence ϑ_i is equal to the angle of reflection ϑ_r. It is assumed that the dimensions of the obstacle are sufficiently large in comparison to the wavelength of the incident sound.

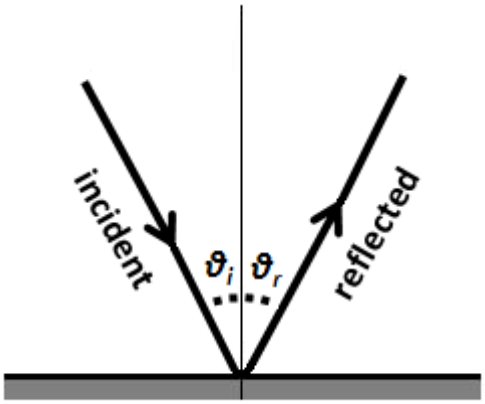

Figure 2.4 Sound Reflection, demonstrating specular reflection when the angle of incidence ϑ_i is equal to the angle of reflection ϑ_r according to Law of Reflection - (describing the phenomenon by 2D particles).

2.3.3 **Sound Diffusion/Scattering**

The Law of Reflection does not apply if the boundary under consideration is not flat and smooth. If the dimensions of the surface are smaller than the half the wavelength λ of the incident sound wave, it can be assumed smooth at low frequencies [43]. At high frequencies, however, the sound is reflected in different directions and the phenomenon is called **diffusion** or **scattering**. The ideal case of

calculating the direction of this reflected sound is based on **Lambert's cosine law** [44]. This law says that the intensity of the diffused sound is proportional to the cosine of the angle ϑ_i between the observer's line of sight and the projection of the surface (Figure 2.5), defined by the following equation:

$$I = I_0 \, dS \, \frac{\cos \vartheta_i \, \cos \vartheta_0}{\pi \, r^2} \qquad (2.5)$$

where I is the intensity of the sound (in watts/square metres) which is scattered in a direction characterised by an angle ϑ_0, I_0 is the intensity of the incident sound (in watts/square metres) which hits an area element dS under an angle ϑ_i, measured at distance r from dS and r is the distance from the source to the measured point (in metres).

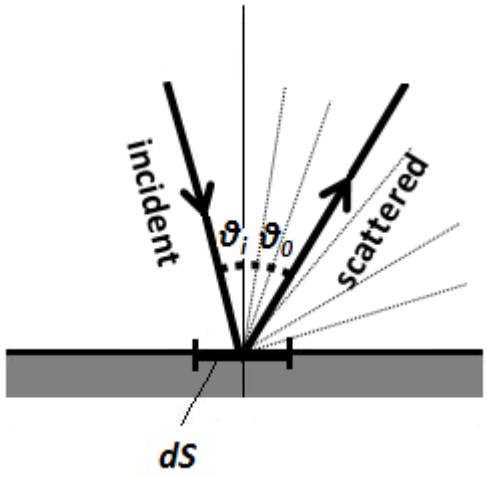

Figure 2.5 Sound Scattering according to Lambert's cosine law, demonstrating scattered reflection in angle ϑ_o when ϑ_i is the angle of incidence (describing the phenomenon by 2D particles)

2.3.4 **Sound Absorption**

In reality, the energy which is transmitted from the sound source and incident to a boundary is not equal to the energy of the reflected wave. This is because when the sound interacts with a surface it causes vibrations in the surface and energy is transferred. The amount of absorbed energy is dependent on the material that makes up the surface and this is defined by the absorption coefficient, α, of the material. This coefficient, according to Sabine, expresses the ratio between the

absorbed and the incident energy of the sound at the surface. It is defined with values from 0, for zero absorption, to 1 being a completely absorbing surface. In practice the values of 0 and 1 only occur in theoretically ideal conditions.

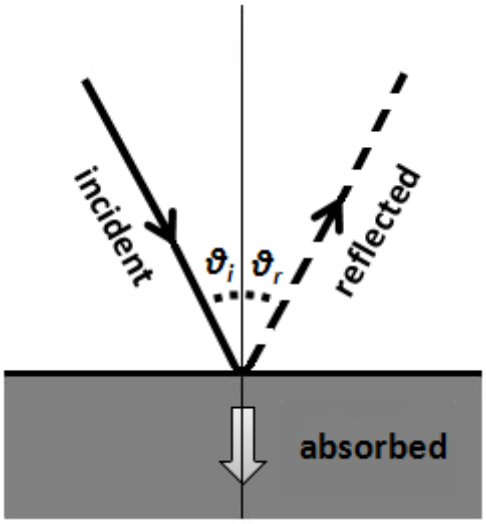

Figure 2.6 Sound Absorption, demonstrating the energy absorbed by the surface while the remaining energy is reflected according to the Law of Reflection (describing the phenomenon by 2D particles).

Sound is not only absorbed by the surfaces in the room but also from the air through which it travels. In the case of small rooms, the boundaries are sufficiently close to each other such that the sound spends a relatively small amount of time in the air between reflections. Thus, air absorption is not a major factor in the resulting sound at the receiver. However, in large rooms (greater than about 500m^3) [45] such as concert halls or churches, air absorption has a much more noticeable effect. In particular, reverberation sound falls off at higher frequencies (above 1000Hz) [46].

2.3.5 **Sound Diffraction**

Diffraction is the acoustic phenomenon where the propagated sound changes its direction due to obstructions in the space and as a result it apparently bends, spreads out and travels around such objects. The degree of diffraction depends on the wavelength of the sound. Thus, the effect is greater at low frequencies than high frequencies where the obstacle is large enough to become a reflecting surface. This also happens when sound passes through an opening in a surface, such as a

doorway. If the wavelength is large relative to the width of the opening, the sound is diffracted strongly.

2.3.6 Standing Waves

If a sound source is positioned between two reflective parallel surfaces, standing waves occur. Reflected sound interferes with the incident sound, which will have the same amplitude, speed and frequency, but be moving in the opposite direction. The effect of this interaction is a number of **nodes** and **anti-nodes**, as shown in Figure 2.7.

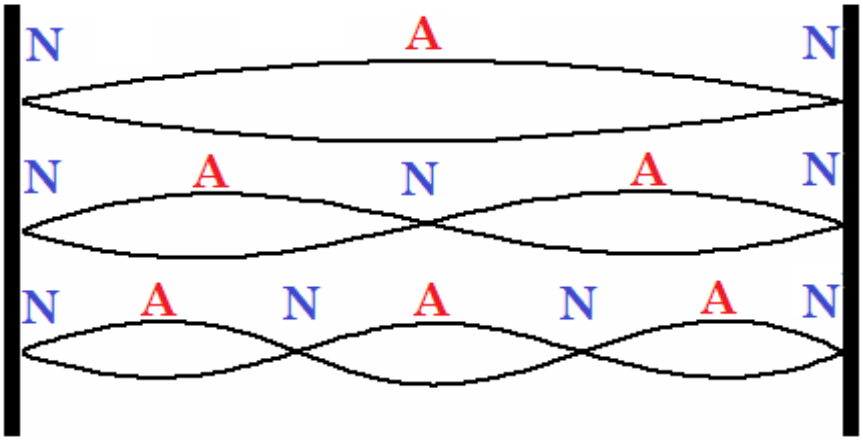

Figure 2.7 Nodes (*N*) and Anti-nodes (*A*) of three standing waves occurring between two fixed reflective barriers

At the nodes and at the boundary edges, the amplitude of the oscillation of the wave is zero, while the opposite phenomenon occurs at the antinodes, where the amplitude of the wave is at its maximum. The sound energy peaks in correspondence of the antinodes [41, 47-49].

2.3.7 Schroeder Frequency

The phenomenon of standing waves in an enclosed space has a significant impact on its acoustic characteristics, especially at low frequencies. In this region, the individual standing waves are sparsely distributed and highly position dependent, and the distribution of nodes and anti-nodes can, in some cases, be audible. In the high frequency region, standing waves are much more densely distributed and it is not possible to perceive specific resonant frequencies. The **critical frequency**, also

known as the **Schroeder frequency** [50, 51], between these two frequency regions is given by:

$$f_S = 2000\sqrt{\frac{RT_{60}}{V}} \qquad (2.6)$$

where RT_{60} is the reverberation time in seconds (defined in section 2.5.1) and V is the volume of the space in cubic metres.

2.4 *Room Impulse Response*

The perception of the acoustic characteristics of a room depends first of all on both the source and listener's position. These physical positions have an impact on the resulting effect of the direct sound and reflections from other surfaces within the room. Considering the room as a system into which a very brief sound is introduced as the input signal, the output signal is then determined by the interaction of the input signal with the room over time.

The **room impulse response** (RIR) is a time domain function that represents the response of the room measured at the receiver position to an ideal impulse-like sound at the source location. This ideal input signal includes all audible frequencies, has a flat frequency response, and is mathematically represented by the **Dirac Delta function**, which for a signal applied at $t=t_1$ is defined as

$$\delta(t) = \begin{cases} +\infty, & t = 0 \\ 0, & t \neq 0 \end{cases} \qquad (2.7)$$

with the condition

$$\int_{-\infty}^{\infty} \delta(t)\,dt = 1 \qquad (2.8).$$

Because of (2.8), this input is often referred to as unit impulse function. In this context, the value $t=0$ is chosen to be the time at which the excitation signal is applied to the system. The acoustic response of the system is therefore given by any output detected after the application of the initial impulse, as shown in Figure 2.8. The common assumption is that the system is **linear time invariant (LTI)**. This means that:

- as a linear system, the relationship between the input and the output of the system is a linear map
- and as a time-invariant system, the output does not depend on when the input is applied to the system.

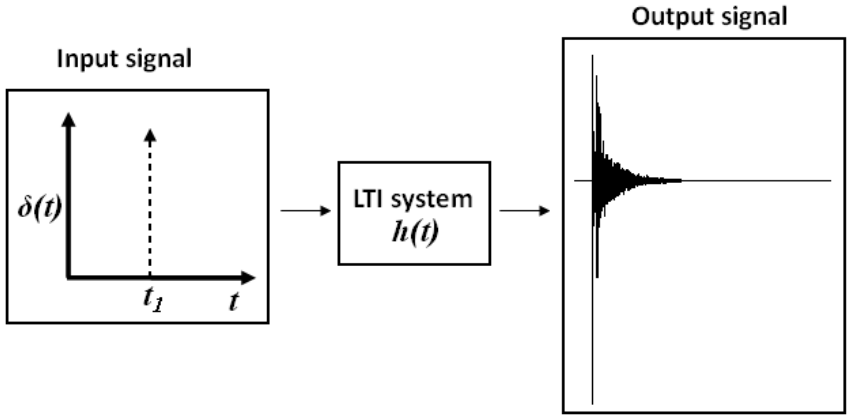

Figure 2.8 The input signal as the Dirac Delta Function interacts with the acoustic characteristics of a linear time invariant (LTI) system to give the output signal, the room impulse response (RIR) as a function of time.

The output signal *y(t)* in term of the input *x(t)* can be formally written as:

$$y(t) = F[x(t)], \tag{2.9}$$

where the function *F*, for an LTI system, assumes the form of the **convolution** between the input signal *x(t)* and the system impulse response *h(t)* [52]:

$$y(t) = x(t) \otimes h(t) \tag{2.10}$$

Convolution is the mathematical operation for determining the output signal of a LTI system resulting from the interaction of the input signal with the impulse response of the system [53]. In simple words, convolution can be considered as a form of superposition between the two signals [54].

In reality, LTI systems only exist in ideal circumstances. For example, non-linear distortions can occur due to the loudspeaker used to apply the input signal. Another case is non-time-invariance, where the impulse response changes in time perhaps due to air movement or an increase in air temperature. As long as this

variation is slow enough as is usually the case, there are no significant differences in the results obtained [52].

In order to appropriately describe the impulse response of a real space, it is necessary to take into consideration the noise, generated inside the system, which is the "added" to the ideal output signal, as shown in Figure 2.9.

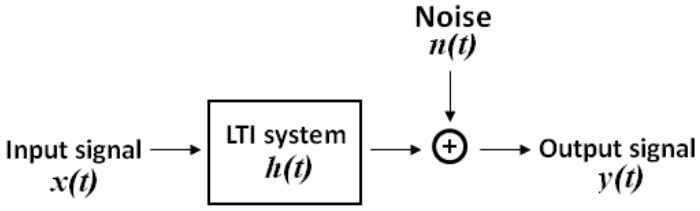

Figure 2.9 Input and Output Signal of a Linear Time Invariant (LTI) system with added noise at the output.

2.5 *Acoustic Parameters*

In order to measure the impact of acoustic space on the human perception of sound, subjective terms such as "reverberant", "dry" or "clear" in isolation cannot give reliable and useful information for further analysis. Therefore, some of the most important objective parameters commonly used for acoustic analysis are defined below, according to ISO3382 [55]. For the calculation of these parameters the room impulse response (RIR) of a space, for a given source and receiver position, plays a central role.

For this purpose, a graphical representation of the decay of the acoustic energy of the impulse response as a function of time is used, based on the **Schroeder Decay** method, or **Energy Decay Curve** (EDC), as introduced in [56]. This makes use of the backwards integrated squared impulse response for each frequency band, using the following equation, according to [55]:

$$E(t) = \int_t^{\infty} p^2(\tau) d\tau \qquad (2.11)$$

where *E(t)* is the energy of the decay curve (in decibels) as a function of time, *p* is the sound pressure of the impulse response (in Pascal) as a function of time and *t* is time (in seconds).

Thus, the EDC is the total amount of energy remaining in the RIR at time *t*. It gives a much smoother decay than the RIR itself and is much more suitable for acoustic calculations. Figure 2.10 shows such an EDC as obtained using this process, for the room impulse response shown in Figure 2.8.

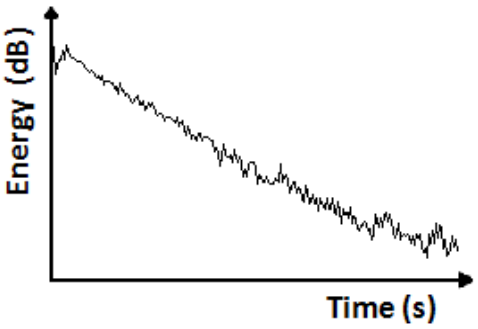

Figure 2.10 The backwards integrated decay curve obtained from the squared impulse response presented in Figure 2.8, as a function of time.

2.5.1 **Reverberation Time**

In theory, reverberation refers to the time that it takes for sound to die away in a room after the source has stopped. This is dependent on the time required for the sound to reach the receiver point after interacting with the surfaces within the space.

There are many ways to calculate this time value. The most commonly used definition is the well-known Reverberation Time RT_{60} [41]. This is the time expressed in seconds that a sound takes to decrease by 60dB from its original sound pressure level at the receiver. In order to measure this reverberation time, the energy decay curve (EDC) as defined in section 2.5, is used, an example of which is shown in Figure 2.11.

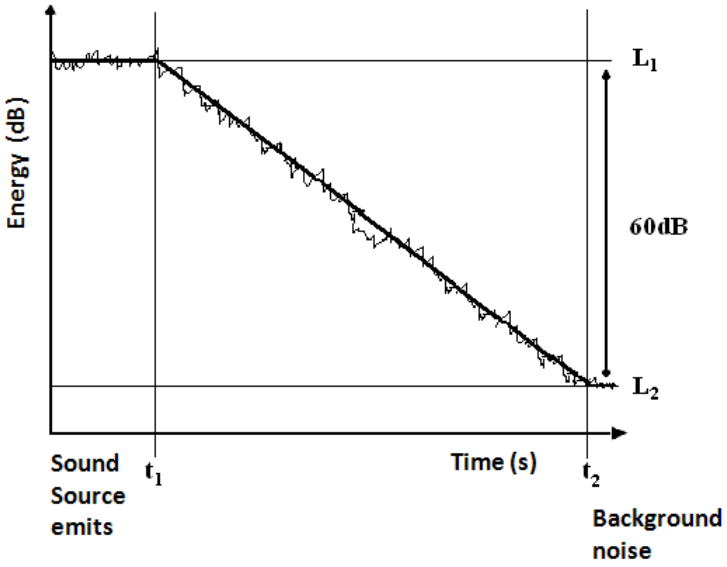

Figure 2.11 Reverberation Time, RT_{60}, measured by the time difference $t_2 - t_1$, from the initial slope of the obtained energy decay curve, determined when the sound energy level has decreased by 30dB.

At t_1 the sound source is switched off and the level L_1 from the source starts to decrease until the time t_2 when it can no longer be distinguished from the level of ambient noise. The reverberation time is the time equal to $t_2 - t_1$ when the difference between the L_1 and L_2 is 60dB. In reality, this time is not so simple to be measured because a) any noise floor in the system or room, being constant (not sufficiently low), may prevent an acoustic measure of decay from being taken and b). the decay is not linear (the relationship between the sound energy level and time is not linear).For example, double-slope decay occurs when the sound absorption is not evenly distributed across the surface materials of the space, there is poor diffusion of the sound or the space includes coupled volumes [57]. Thus, according to ISO3382 [55] the reverberation time is measured as the rate of decay given by linear least squares regression of the measured decay curve from a level 5dB below the initial level to 35dB below. When the decay rate used is measured between these levels, RT_{60} is referred to as T_{30}, as shown in Figure 2.12. When the decay rate used is measured from 5dB below the initial level to 25dB below, RT_{60} is referred as T_{20}.

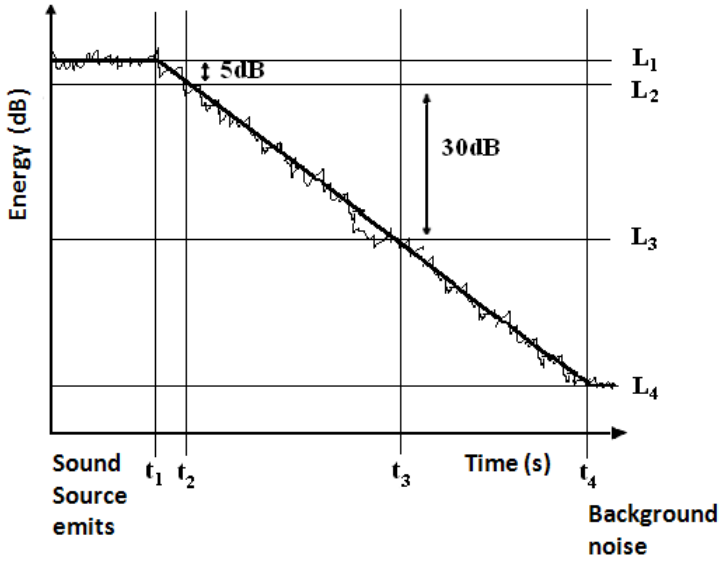

Figure 2.12 T_{30}, measured using the time difference $t_3 - t_2$, from the slope of the obtained energy decay curve determining when the sound level has decreased by 30dB.

2.5.2 Early Decay Time (EDT)

Early Decay Time (EDT) is the time, in seconds, needed for the reverberant sound to decay 10dB. This means that in comparison with RT_{60}, T_{30} or even T_{20}, EDT gives a more detailed indication of the behaviour of early reflections in the impulse response from the initial 10dB of the decay, and is considered to give a more detailed indication of the perception of the reverberation in a space [55]. The slope of the decay curve is determined from the slope of the best linear regression line. In the following diagram, EDT is the time between t_2 and t_1, in which the level has reduced $L_1 - L_2 = 10$dB.

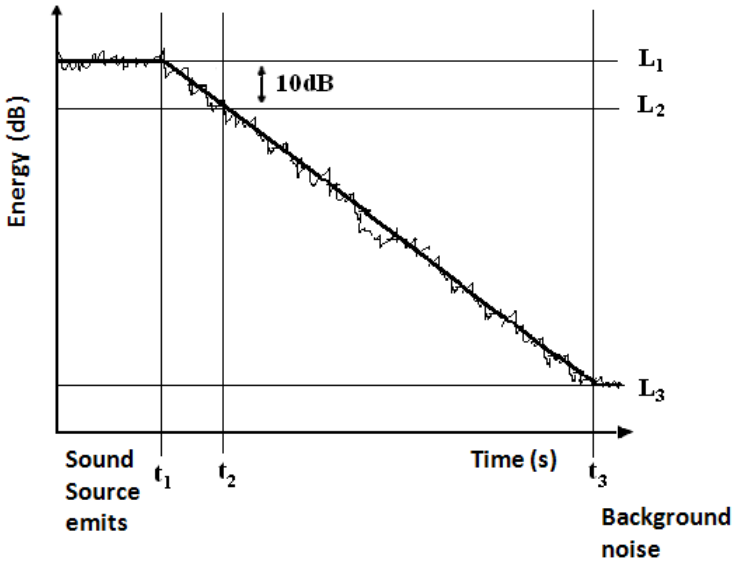

Figure 2.13 Early Decay Time, EDT, measured using the time differences $t_2 - t_1$, from the slope of the obtained energy decay curve determining when the sound level has decreased by 10dB.

2.5.3 Initial Time Delay Gap (ITDG)

Initial Time Delay Gap (ITDG) is defined as the time delay, in seconds, from the direct sound to the first reflection. In the case of small spaces or short distances between the sound source and the receiver points, the ITDG is shorter than when the sound source is far away. Thus, this parameter is normally used in order to determine the size of a space or the distance between the sound source and the receiver point. It corresponds with the subjective impression of "intimacy" [58, 59].

2.5.4 Centre Time (Ts)

The Centre Time (Ts) corresponds to the centre of the gravity of the squared impulse response [60] and determines the time (in seconds) where the energy of the early part is equal to the energy of the later part of the impulse response [61]. It is defined by:

$$T_S = \frac{\int_0^{\infty} t\, p^2(t)\, dt}{\int_0^{\infty} p^2(t)\, dt} \qquad (2.12)$$

A small value of Ts in comparison with the overall length of the impulse response means that the energy is concentrated in the early part.

2.5.5 **Clarity C_{50}/C_{80}**

Clarity is the early-to-late arriving sound energy ratio, expressed in decibels. More specifically, it describes the importance of the direct sound and early reflections (in the far field) in comparison with the late reflections that cause reverberation, as shown in Figure 2.14. With C_{50}, clarity is determined according to the first 50ms, which is more associated with the study of the perception of speech. C_{80} is clarity determined according to the first 80ms of the impulse response and is used in studies relating to the perception of music. Clarity is especially important for the study of speech, because it helps to describe the perceived intelligibility of words and is formally defined according to [60] by:

$$C_{t_e} = 10 \log \left(\frac{\int_0^{t_e} p^2(t)\, dt}{\int_{t_e}^{\infty} p^2(t)\, dt} \right) \qquad (2.13)$$

where C_{t_e} is termed the early-to-late sound index, t_e is the early time limit of either 50ms or 80ms and $p(t)$ is the pressure of the measured impulse response (in Pascal).

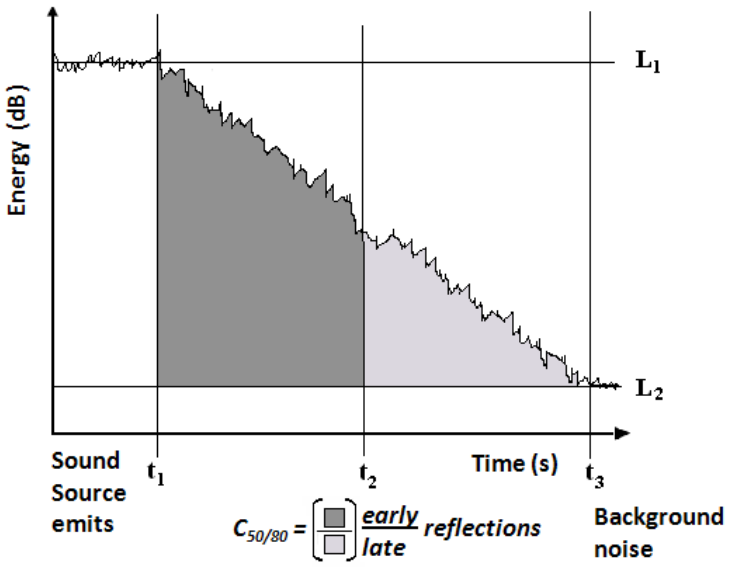

Figure 2.14 Clarity (C_{50}/C_{80}) defined as the early-to-late sound index, with the early sound threshold defined at t_2=50 ms or 80 ms according to application.

2.5.6 Definition (D_{50})

Definition (D_{50}) is related to C_{50}/C_{80} as it is the ratio of the early to total sound energy. This parameter is also often used in cases of speech intelligibility and is defined according to [60] by:

$$D_{50} = \frac{\int_0^{0.050} p^2(t)dt}{\int_0^{\infty} p^2(t)dt} \qquad (2.14)$$

in which *p(t)* is the pressure of the measured impulse response (in Pascal). This parameter is directly related to C_{50} as follows:

$$C_{50} = 10\log\left(\frac{D_{50}}{1-D_{50}}\right) \qquad (2.15).$$

2.5.7 Sound Strength (G)

Sound Strength (G) is the difference, expressed in decibels, between the pressure level of the measured sound and that produced by the same omnidirectional source in a free field, at 10m distance from its centre. It is defined as follows [60]:

$$G = 10 \log_{10} \frac{\int_0^\infty p^2(t)\,dt}{\int_0^\infty p_{10}^2(t)\,dt} \qquad (2.16)$$

in which $p(t)$ is the pressure of measured impulse response (in Pascal) and $p_{10}(t)$ is that measured at a distance of 10m from the source in a free field.

2.5.8 **Early Lateral Energy Fraction (LF)**

Early Lateral Energy Fraction (LF) is the fraction of energy arriving within the first 80ms from lateral directions and can be measured from impulse responses obtained from an omnidirectional and a figure-of-eight pattern microphone. It is defined by the following equation [60]:

$$LF = \frac{\int_{0.005}^{0.080} p_L^2(t)\,dt}{\int_0^{0.080} p^2(t)\,dt} \qquad (2.17)$$

where $p_L^2(t)$ is measured with a figure-of-eight pattern microphone and $p^2(t)$ is the response from the omnidirectional microphone (in Pascal).

2.5.9 **Inter-Aural Cross-Correlation (IACC)**

Inter-Aural Cross-Correlation (IACC) is a parameter associated with binaural measures and is obtained via a dummy head or with small microphones at the entrance of the ear canals of a real head. It measures the correlation of the pressure impulse responses received at the two ears in the first 50ms. The inter-aural cross-correlation coefficient, IACC, is given by [60]:

$$IACC_{t_1 t_2} = \max\left|IACF_{t_1 t_2}(\tau)\right|, \text{ for } -1\text{ms} < \tau < +1\text{ms} \qquad (2.18).$$

The normalised inter-aural cross correlation function, IACF is defined as:

$$IACF_{t_1 t_2}(\tau) = \frac{\left(\int_{t_1}^{t_2} p_L\, p_r(t+\tau)\, dt\right)}{\sqrt{\left(\int_{t_1}^{t_2} p_L^2(t)\, dt \int_{t_1}^{t_2} p_r^2(t)\, dt\right)}} \qquad (2.19)$$

where $p_L(t)$ is the impulse response at the entrance to the left ear canal, and $p_r(t)$ is that for the right ear canal.

2.6 *Just Noticeable Difference (JND)*

The measurable acoustic parameters described above do not provide, enough information about the subjective perception of these objective measures, as the human ear is always the final receiver of these sound events.

Just noticeable difference is defined as the smallest perceived/detectable difference between changes of the values in a given objective measured parameter.

As in any other area of psychoacoustics, the just noticeable difference (JND) or just audible difference, as described by Kuttruff [44], has aroused interest in several previous works in which the JND of various parameters have been determined through laboratory listening tests. An earlier approach to study the sensitivity of listeners to changes was made by Reichardt et al. [62]. In that study, the limens for the delay and the level of individual lateral and ceiling reflections in an impulse response were investigated. However, the samples were not based on properly simulated concert hall conditions and the results are not considered reliable. In Cremer et al.'s work [63], the JND for reverberation values is reported to be about 4% for RT_{60} value greater than 0.6s, while an absolute subjective limen equal to 0.024s is noticed for RT_{60} < 0.06s. Following study by Niaounakis et al. [64] has been shown that RT_{60} values below 0.6s, the same difference limen of RT_{60} is 0.042 ± 0.015s, based on realistic binaural reproduction of sound fields.

Cox et al. [65] used artificial simulated impulse responses, more similar to those typically observed in concert-halls, for reverberation time of 2.1s. Their study was focused on changes in the early sound field and measured the difference limens for early lateral energy fraction (LF), centre time (Ts), clarity (C_{80}) and initial time delay gap (ITDG). They found that the JND for centre time (Ts) was 8.6 ± 1.6ms for a reference value of 80ms and the JND values for clarity (C_{80}) to be 0.67 ± 0.13dB. These values, however, were the average values observed by investigating the

effect of two different musical motifs. Another interesting point of the study was that, for the simulation of the used impulse responses, information was derived from actual measurements in auditoria, as well as simulated impulse responses based on hybrid ray-tracing and Mirror Image-Source models of existing halls. Following this work, Bradley et al. [66], focused their study on clarity of speech and showed that the JND for C_{50} is independent of reverberation time and measured at 1.1dB, for conditions varying from 0.5s to 2.0s for RT. They used synthetic sound fields based on acoustic conditions typically found in concert halls or auditoria [67, 68]. In Ahearn et al. [69], by using synthetic sound fields, C_{80} gave an average JND of 1.6dB, with significant variations as a function of musical motifs and RT_{60} (1.6s and 2.1s). More recent surveys have determined this value to be around 2.5dB [R.Höhne, in German, cited in [70]],[71]. Martellota [72] focused on Ts and C_{80}, as a function of reverberation values from 2s to 6s, showing that the relationship between C_{80} and Ts changes when the reverberation time increases, even though the JND remains the same (1dB) for C_{80}. It was also shown that the JND of C_{80} and Ts were independent of musical motif.

From the results of these studies it can be determined that the JND values vary with the range of the reverberation times of the studied space, the acoustic conditions applied for each examination (real or artificial sound fields), as well as the sound motif used. ISO3382 Standard [55] (after Vorländer [73]) states an approximation of the JND for the acoustic parameters, as shown in Table 2.1;

Table 2.1 Just noticeable differences for the acoustic parameters, according to ISO3382.

Subjective listener aspect	**Acoustic quantity**	**Single number frequency averaging (Hz)**	**Just Noticeable Difference (JND)**
Subjective Level of sound	G (in decibels)	500 to 1000	1dB
Perceived Reverberance	EDT (in seconds)	500 to 1000	5%
Perceived clarity of sound	C_{80} (in decibels) D50 Ts (in millisecons)	500 to 1000 500 to 1000 500 to 1000	1dB 0.05 10ms
Apparent source width (ASW)	LF	125 to 1000	0.05

Although doubts about the "accuracy" of the JND have been expressed [29, 74], these values are commonly used as a guideline to evaluate the accuracy of measured acoustic parameters, the accuracy of computer models to predict acoustic parameters, as well as by acousticians for designing acoustic spaces based on listener's perception [29, 30, 33, 73].

2.7 *Summary*

In this chapter, sound is approached as a physical phenomenon and its behaviour is studied in a free field and in an enclosed space. The propagation of sound is explained along with the key properties of this phenomenon. The room impulse response is introduced as an output of a system excited by an input signal and ideally the room impulse response contains all the acoustic characteristics of the system. The main objective acoustic parameters used for measuring the impact of sound on human perception have also been define based on the ISO3382 standard [55].

The just noticeable difference (JND) is defined as the smallest perceived difference between changes in the acoustic parameters and is introduced as a guideline to evaluate the variations of the acoustic parameters values. The uncertainties of the recommended values by ISO3382 standard are also expressed, as the JND values vary with

- the range of the reverberation time
- different types of impulse responses (mesured or synthetic) and
- the sound motif used (different musical motifs, speech, noise).

The above points are carefully considered throughout this thesis.

Chapter 3.
Auralization

3.1 *Introduction*

"Auralization is the technique for creating audible sound files from numerical (simulated, measured, synthesized) data" [43].

Auralization can be considered as the audio equivalent to visualization and through its application we are able to synthesize the acoustics of either a complete virtual environment or a particular building, and listen to sounds placed within this virtual space as if we, the listener, were also present.

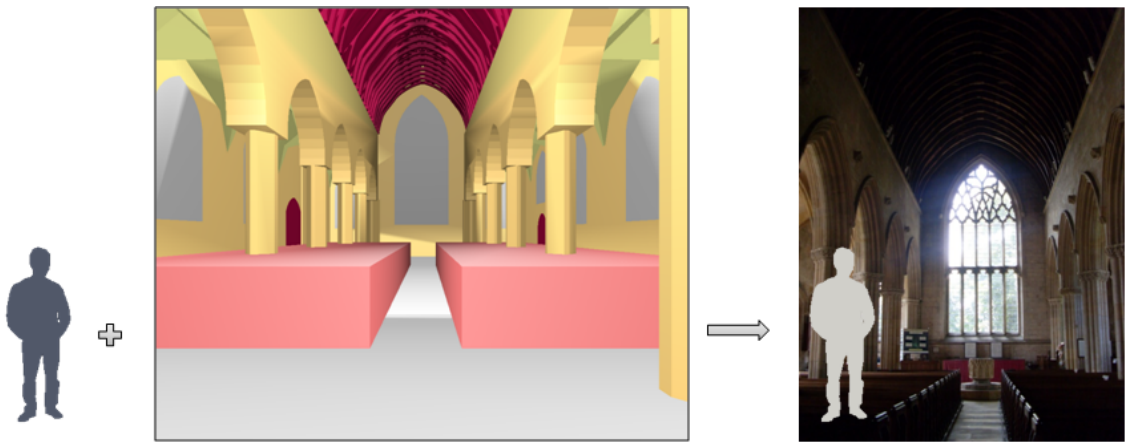

Figure 3.1 Visual demonstration of the auralization concept, where a listener is "placed" in a virtual acoustic realisation of St. Patrick's Church, Patrington, UK [21, 22].

Auralization techniques are commonly applied nowadays for presentation of building design proposals, for the revival of the acoustics of heritage sites, in the sound recording and music production industry, and for 3D acoustic reconstruction in the fields of animation, computer games and digital cinema.

Although the term auralization was introduced by Kleiner et al. [75] in 1993, the concept and methodology actually date back further to 1962, with the paper titled "Digital computers in room acoustics" by Schroeder et al. at the ICA in Copenhagen (cited in [76]). This was when the main steps necessary to be able to listen to a computerised simulation of the acoustics of a space were first defined:

- Convolution of impulse response with anechoic music,
- Cross-talk cancellation technique for reproduction of binaural signal over two sound sources (loudspeakers) in an anechoic room, and
- "the development of a natural sounding reverberation unit without needing to carry out a convolution with a huge number of discrete reflections" [76].

The technique of convolving the response of an artificial reverberator with a stimulus for the impression of a simulated space as carried out by a digital computer was already in use in 1970, by Allen and Berkley [42]. Nowadays, due to the development of computing power and recording techniques, auralization results can be produced from both real measurements, or synthesised, artificial impulse responses.

Due to the complexity of the nature of sound propagation within an enclosed space, the study of room acoustics is considered difficult. Accurate and practical measurement techniques were the goal of scientists from the beginning of the 20th century. Measurements of impulse responses have been used more recently, starting with very simple techniques (based on gunshots and balloons as the sound source) [77, 78] and developing into the very high quality, accurate and repeatable measurements used today. This data can also be used for auralization, where the impulse responses obtained are applied to anechoic recordings. The result being that these recordings are heard as if they had been produced within the space being studied.

Additionally, acoustic simulation software has improved in terms of the quality of the artificial impulse responses produced and the methods used to produce them. They are now commonly used for acoustic research and architectural acoustic design [77], as well as for auralization and perceptual studies.

In this chapter, the most well-known auralization techniques will be described together with their advantages and disadvantages, in order to establish the most suitable techniques for this research.

3.2 *Measurements of Impulse Responses*

Several techniques are documented for how impulse response measurements can be obtained, often based on the ISO3382 standard [55]. More recent approaches tend to differ from this recommended method however, as more accurate and reliable results can be obtained with alternative techniques based on parallel improvements in both computing power and recording methods during the last decades. Acoustic measurements have often been used in order to collect more information about the acoustic characteristics of the measured space but more and more, these impulse responses are used also for auralization purposes and related perceptual studies.

3.2.1 **Excitation signal**

The excitation signal used in the measurement process must have sufficient energy across the whole audible spectrum to decay properly without being covered by background noise from either the space itself or the equipment used in the measured position [35, 79]. Based on ISO standards [55], the pressure level of the impulse source should be sufficient to ensure a decay curve starting at least 35dB above the background noise and at least 45dB above if the quantity T_{30} is to be considered. As a measure to compare the level of the desired signal with the background noise, the **signal-to-noise ratio** is used, defined as the ratio of the peak value of the excitation signal to the background noise observed at the end of the signal.

Based on the definition of the room impulse response given, it is deduced that the excitation signal should include all audible frequencies, from 20Hz to 20,000Hz and the spectrum should be flat across this range of frequencies.

The duration of the excitation signal needs to be sufficient to let the sound field achieve a steady state before any decay. The minimum duration should be half of the estimated reverberation time and at least a few seconds for large volumes [55].

Below, different types of measurements with respect to the excitation signal are presented and grouped in two methods: a) interrupted noise method and b) integrated impulse response method, based on the ISO3382 standard [55].

Interrupted Noise Method

With this method, the excitation signal is a random or pseudo-random broadband noise, played from a loudspeaker. The advantage of this method is that the required instrumentation is simple. The decay curve is then obtained by measuring directly the decay of the excitation signal at the receiver point once the source has been turned off (as used for example for acoustic measurements at St. Paul's Cathedral, London, in 1951 (cited in [80]). However, the big disadvantage is that only reverberation time parameters can be calculated as other acoustic parameters are based on the obtained impulse response [60], which is not measured directly using this approach.

Integrated Impulse Response Method

Direct Method - Measurements using Impulsive Source

In this type of measurement developed by Schroeder [56], an impulse-like source such as a cannon, pistol, or powerful electrical spark discharge is used as the excitation signal [81, 82]. The measured response is then squared and integrated, such that greater accuracy for measuring reverberation time is obtained when compared with the Interrupted Noise Method, and early decay time is able to be measured as well [80].

This method does not need any post-processing for the recordings obtained, which is one of the reasons why it is still being used for acoustic measurements. Its main disadvantage, however, is that the excitation signal does not have a perfectly flat frequency response [77, 83, 84].

Additionally, it cannot always be guaranteed that the energy of the signal will be sufficient to ensure that the decay curve starts at least 45dB above the noise floor (as required by ISO3382 [55]). Another problem with this method is that the signal and any signal distortion cannot be separated from the impulse response as they occur simultaneously [26].

Indirect Method – Electro-acoustic Impulse Responses

Due to the developments of electro-acoustic techniques, the background noise of the space can be overcome and high signal-to-noise ratios achieved by determining the characteristics of a test signal reproduced via loudspeaker(s). The most commonly used signals are; a) MLS and b) sine sweep signals.

Maximum Length Sequence Signal Analysis (MLSSA) measurement method

MLS measurements use a binary sequence of pulses switched between two values (1 and 0) in a pseudo-random manner. For N defined as the group of the binary elements, the number of the possible values for a binary number with N digits is 2^N. Thus, the maximum length L of an MLS signal must be $L = 2^N-1$, from which the set of all zeros has been excluded as that only leads to another zero state, and this equation also defines the periodicity of the signal. The signal is reproduced by a loudspeaker and the subjective perception of the result is a system excited by noise. The cross-correlation of such a signal resembles the Dirac Delta function, with a flat spectrum as all frequency components have the same amplitude [26].

This method has been widely used for acoustic measurements [29, 43, 77], although there are several problems which need to be taken into account [27]. Firstly, the risk of this method is the time aliasing error which could happen if the MLS signal length is no longer or at least the same length as the impulse response of the system (its reverberation time). As a result, parts of the end of the impulse response overlap the beginning part. To avoid this aliasing problem the excitation signal used should be longer (higher order N) than the reverberation time of the system. One of the main problems is the requirement for an LTI system [52, 77], otherwise underestimations of calculated acoustic parameters can be caused by signal distortion which might affect the measurements. Another undesired property of the MLS method is the flat spectrum of the source signal [26]. Low frequencies do not have sufficient time to disperse especially for large spaces and high frequencies can be affected by ambient noise.

Sine Sweep Measurements Method

Time-Delay Spectrometry (TDS) Method

For this method, suggested by Heyser, the excitation signal for TDS is a linear sine sweep wave which means that the frequencies across the whole range of excitation increase equally per time unit. With this signal, it has been possible to avoid problems of time-variant systems [27]. However, due to the linearity of the signal, its spectrum is flat, as was the case with MLS method.

Both MLS and TDS are commonly used in measurement studies, as they generally provide better results in terms of the signal-to-noise ratio obtained, and the frequency response is wider and flatter than with previous methods based on an impulsive source. However, as has been mentioned, they are based on perfect linearity and time-invariance (LTI) of the system during the measurement process.

Another important disadvantage of these methods is that, in order to improve the signal-to-noise ratio, multiple repetitions of the input signal are required for post measurement averaging. Thus, these methods are considered time consuming and with the added risk of time-variant aspects of the system being introduced by using this technique [26].

Exponential-Swept Sine (ESS) Method

This method can be used with *non-linear* systems, as suggested by Farina [52]. Historically, this method is based on one of the oldest methods, where a logarithmic sweep was generated by an analogue generator and the resulting voltage was drawn by a writing pen on a sheet of paper [79]. The excitation signal used for this new method is a logarithmic sweep. A logarithmic sine sweep means that the frequency increases constantly per time unit. The sequence of low frequencies sweeps slowly and continues more quickly over an increasing bandwidth [52, 79, 85]. As the signal amplitude is constant (as shown in Figure 3.2), this results in a pink spectrum attenuated by 3dB/octave, with each octave having the same energy. This decay of the magnitude corresponds roughly to the magnitude spectra of the background of a typical measured room, which shows the need of more energy for low frequencies [86].

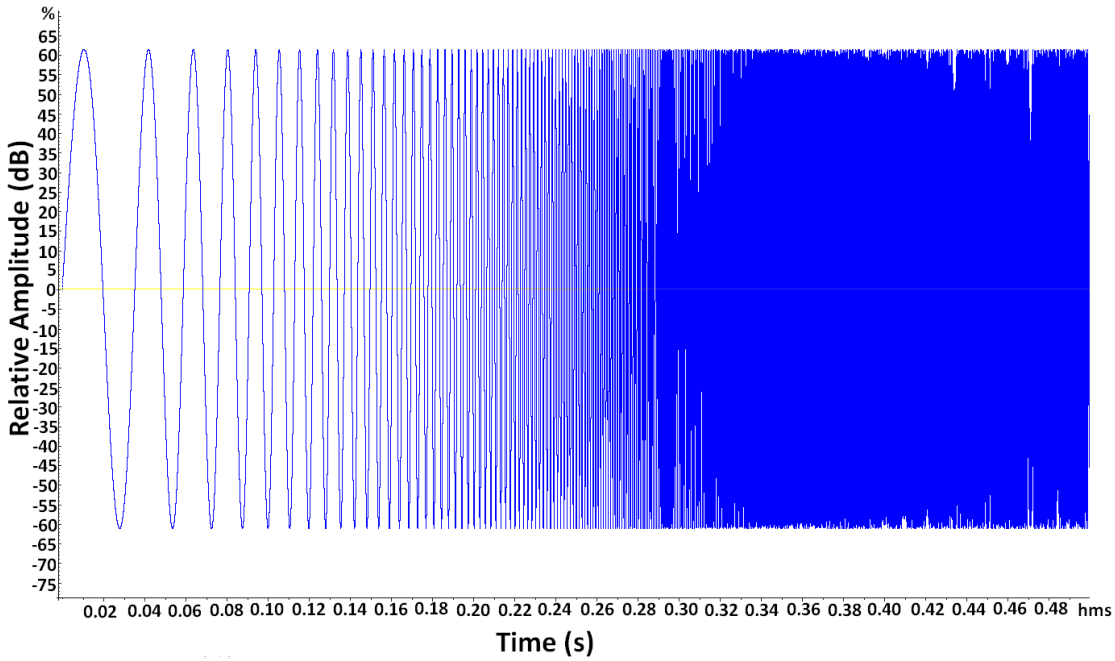

Figure 3.2 Time Domain representation of an input logarithmic sine sweep, from 22Hz to 22kHz and lasting 0.5s.

The linear impulse response of the system is deconvolved from the recorded output sine signal. This is done by convolving the output signal with an inverse filter of the input sine sweep. This results in the linear response of the system appearing as an almost perfect impulse response, with a delay equal to the length of the input signal [27].

The generation of the inverse filter is the reverse of the input signal along the time axis. Additionally, an amplitude modulation is necessary, in order to get a flat spectrum by applying to it an amplitude envelope to generate the different energy from low to high frequencies [87]. This is done by reducing the level by 3dB/octave [83], starting from 0dB and ending at $-6\log_2(\omega_2/\omega_1)$, in which ω_1 is the start frequency and ω_2 is the end frequency of the sine sweep [52].

Additionally, the harmonic distortion of the output signal produced by the loudspeaker can be observed now in the time domain, as a sequence of impulse responses clearly separate and before the impulse response of the system, as shown in Figure 3.3. For this example, the length of the input sine sweep for this example was 15s. The impulse response of the system can be observed exactly after that length of the input signal, while the harmonic distortions are now clearly noticeable before the impulse response.

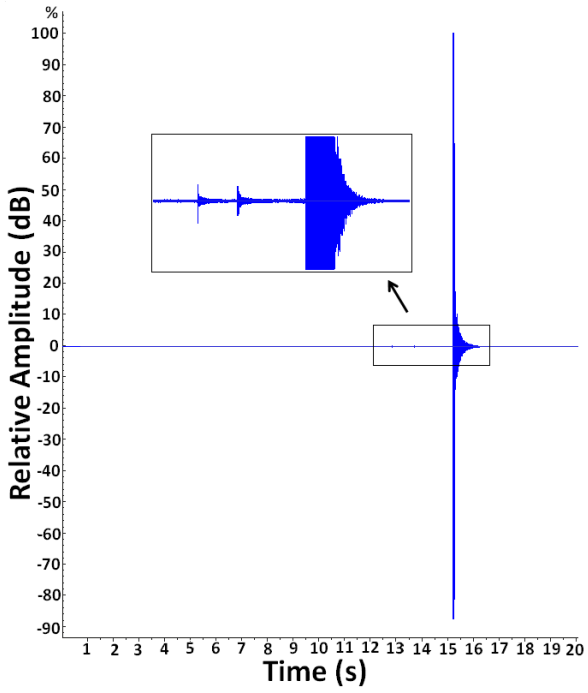

Figure 3.3 The resulting output signal after deconvolution with the inverse filter. The harmonic distortions are easily observed before the required system impulse response.

In addition, it is possible to use a suitable frequency range of the input signal based on each transducer requirements, avoiding speaker damage in out-of-range frequencies [77, 78].

This method has been commonly accepted during the last decade for in-situ acoustic measurements of buildings such as churches [20], auditoriums, concert halls [86, 88] or opera houses [77, 78, 89].

Despite the advantages of the ESS method there are still some problems. The deconvolved impulse response is not a perfect Dirac delta function, which the MLS method can provide, as some oscillations before and after the main pulse can be observed [83]. Proposed solutions using different filters have been suggested, although no one result has as yet been proposed as an optimal solution.

3.2.2 **Sound Source Directivity**

According to ISO3382 [55], the sound source and the microphone should be as close to omnidirectional as possible, even if in reality the source (such as human voice, musical instruments or loudspeakers) and the receivers (such as human ears) could

never be perfectly omnidirectional. This helps to avoid the potential for the source focusing unevenly on specific points of the tested space.

An omnidirectional source is usually based on using an electroacoustic system, as omnidirectivity is not always achievable with mechanical/physical sources such as balloons or pistols. A common method for this purpose is to use a dodecahedron speaker, with 12 full-range drivers [18, 20, 52].

However, these types of loudspeakers, designed typically for noise-based acoustic measurements, have three main problems [27, 85, 90]:

- non-flat frequency response across the frequency range,
- cannot radiate efficiently below 100Hz and above 5kHz,
- the homogeneity of the spherical directivity at higher frequencies cannot be guaranteed.

This means that there is a systematic error introduced into the measured parameters for specific frequencies [26, 91]. As a solution for the first problem, previous studies suggested equalisation to create a flat frequency response [26, 85, 88, 89]. However, the overall power of the loudspeaker is sacrificed as a result [27, 86]. In order to obtain a flat frequency response in the lowest frequency bands, a subwoofer is used, with a typical upper limit of 120Hz [5, 8, 20, 26, 86, 88, 89, 92]. However, due to its complexity, this could cause further difficulties at the measurement stage such as further equalisation between the two sound sources being required or spatial distribution of the two sources.

The non-uniform directivity of a dodecahedral loudspeaker at high frequencies is dependent on the size of the loudspeaker driver. A smaller driver could be used where the cut-off point of the response is at a higher frequency [27, 89, 90, 93].

An interesting experiment in [83] measures the polar patterns of three different dodecahedron systems and shows significant differences at medium and high frequencies, such that omnidirectional characteristics can no longer be assumed. Differences have been shown in similar studies at low frequencies as well [86, 90].

3.2.3 **Microphones**

The ISO3382 standard [55] for the purpose of calculating the acoustic parameters also requires an omnidirectional microphone to be used for obtaining monaural impulse responses. Additionally, ISO3382 requires binaural impulse responses for IACC calculation, as well as a figure-of-eight microphone for the calculation of lateral-energy parameters such as LE or LF [85].

Furthermore, recent studies focus on the performance of 3D auralization and relevant 3D acoustic parameters. By using omnidirectional equipment (either sound source or microphones) as recommended in ISO3382, any spatial information relating to the directivity of the source and the spatial perception of the receiver is lost. Depending on the measurement method, and more specifically on the microphones being used for each case, multichannel impulse responses and spatial information should be captured when possible [8, 84, 90, 94].

The collection of 3D impulse responses was first proposed by Gerzon [94]. Due to the improved performance of personal computers and the availability of sophisticated digital signal processing (DSP) techniques, that were not available at the time of this original proposal, this has only more recently started to become common practice [9, 21, 22, 26, 27, 85, 86, 88, 90, 92, 95-97]. Generalizing, for these studies, a binaural dummy head, a pair of cardioids in ORTF configuration, and a 4-channel Soundfield microphone are combined with a rotating turntable such that they are able to capture 8 impulse responses at 36 positions, measured every 10° around a circle, centred exactly to the axis of the turntable. With this set up, it is possible to reproduce stereo and ITU 5.1 surround-sound based on either the ORTF configuration of the cardioid pair, or from the appropriate azimuth at positions of the Soundfield microphone.

It is important to note that the polar patterns of existing microphones do not match the theoretical required ones. Measurements of the polar patterns of four Soundfield microphones are presented in [83] showing significant differences at medium and high frequencies, for both figure-of-eight and omnidirectional patterns. It is also observed that the gain of these patterns is not always properly matched across the frequency range.

3.2.4 **Measured Uncertainties**

This chapter so far demonstrates how methods for room acoustic measurements have been improved and standardised over recent years, offering significant improvement in both the quantity and quality of the data obtained. International Round Robin surveys [98] or relevant research workshops [84] have been carried out on various room acoustic measurement systems with the goal being to solve common problems and point out any variations in the analysis of the results that are greater than accepted just noticeable differences (JND). A common observation from these tests is that good measurements are often not observed across the whole frequency range. This could be due to background noise, or transducer limitations. The main uncertainties are caused by differences in the estimation of the initial response level, decay rate and noise floor level [99], as is explained below.

In the 2004 International Round Robin [98], the calculated results obtained from a given room impulse response were discussed. The task for the 37 participants was to filter the signal into various frequency bands, to identify the start of the impulse response and to detect the noise-floor level (the last used data point for the acoustic parameters calculation). Extremely wide deviations were observed for the calculations of reverberation time values, especially T_{30} for the low frequencies of 125 and 250Hz, as shown in Figure 3.4. This highlights the difficulty in detecting the noise-floor level in real measurements. Similar results were observed with C_{50}/C_{80} values with good agreement at high frequencies and less at low frequencies. These variations are due to difficulties in identifying the start of the impulse response. Also, it was shown that calculations based on human interactions had smaller standard deviation values than those produced via automatic or semiautomatic methods, which also clearly indicates the limitations of automatic software calculations.

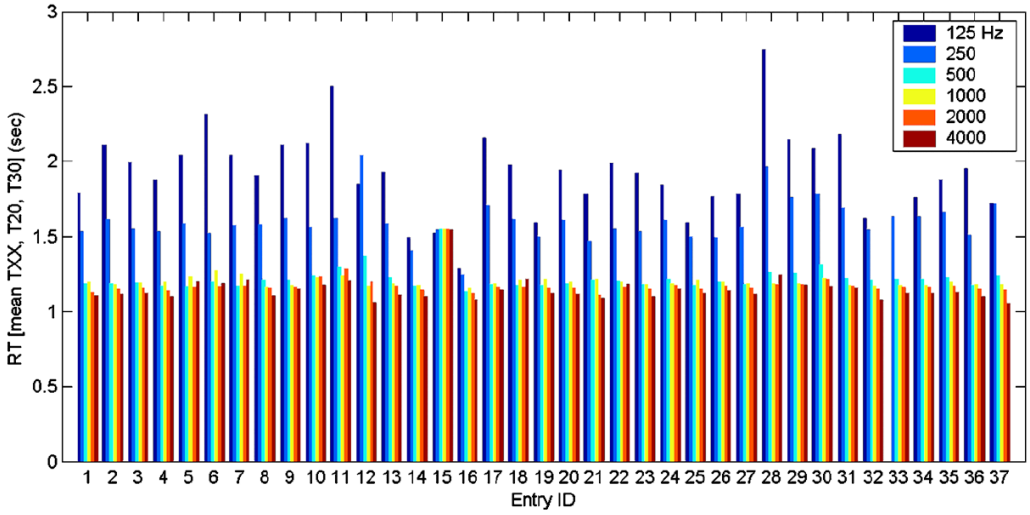

Figure 3.4 Differentiations observed at low frequencies for the calculation of RT from 37 different participants, from [98].

For a round robin comparison of room acoustics measurement methods based on artificial impulse responses [100], approximately one-third of the participants diverged significantly from the average calculated values for each of ISO parameter considered. The remaining measurements agreed very closely. Any deviations observed between these best-case results were caused for two reasons: 1) uncertainties in the determination of the best fit regression line to the decay curve for the calculation of EDT values [101], as defined in ISO3382 [55] and 2) small differences in the starting point of the impulse response giving variations in C_{50}/C_{80} values due to strong reflections close to the time boundary of 50/80ms.

For determining the reverberation time, the backwards integrated squared impulse response is calculated based on Schroeder's method. In reality though, a recorded impulse response could contain background noise and a systematic error could be introduced to the calculation methods of the acoustic parameters as a result. Thus, different noise-removal algorithms have been introduced in order to minimise such errors [27, 61, 93, 102, 103]. This adds additional uncertainties to the results obtained, depending on what algorithm has been applied.

Additionally, it has been mentioned in a few previous studies [21, 30, 70, 84, 104], that slight changes (of the order of 15cm) in the position of the source and receivers can cause significant differences in the measured results - with respect to the just noticeable difference (JND). These changes, as will explained in detail in Chapter 6, are specifically observed in parameters that are position dependent, such as EDT

and C_{50}/C_{80}. Finally, as already discussed in sections 3.2.2 and 3.2.3, the measurement equipment itself can cause inaccuracies in the measured impulse responses obtained.

3.3 *Computer Modelling - Introduction*

An alternative to the direct acoustic measurement of a given space is to use an appropriate computer modelling method to synthesise the impulse response for a given set of initial conditions and obtain the acoustic parameters indirectly. For the production of a synthesized room impulse response, the general requirements for accurate and convincing auralization results are available information about the architectural characteristics of the studied space, information about the nature and the characteristics of the source and receiver and the calculation algorithm used for sound propagation.

In recent decades, there has been huge progress in auralization and the prediction of room acoustics using computer modelling software, a development that has been made possible because of the improvements in the capability of personal computers. Following initial scale modelling experiments, where optical rays were used to measure the mean free path for the prediction of reverberation time, computers offered a solution to collect this data more quickly and with greater accuracy [76]. The first reference to the use of a ray-tracing computation system was made by Allred and Newhouse [105] in 1958, who used the system for prediction purposes and more specifically for determining the mean free path. That study was followed by Krokstad et al., in 1968 [106], who developed the first ray-tracing based room acoustic software for actually simulating of the impulse response in a 3D model.

More recent developments give the capability to calculate the acoustics of a space with more complex algorithms, based on fewer assumptions and incorporating more accurate modelling of sound propagation behaviour.

The basic question for computer modelling of room acoustics is whether the phenomenon of sound will be described by particles or by waves [107]. This section introduces commonly used modelling techniques and considers their accuracy in

simulating the behaviour of sound propagation in a given space together with the resulting acoustic parameters.

3.3.1 **Wave Models**

Algorithms representing sound as a wave are based on the wave equation; hence, wave phenomena such as interference and diffraction are included.

Element Methods, such as the Finite Element Method (FEM) and Boundary Element Method (BEM) approximate the computation of a complicated system by discretising the acoustic space in small, finite volumes whose boundary are defined by a mesh of nodes. The relevant physical parameters and equations are then defined for each nodes so that the total system will be represented by a system of equations (one for each node).

Finite Difference Time Domain (FDTD) schemes produce impulse responses by calculating the 2D or 3D equation for the wave propagation in time domain. The volume of geometric space is represented by a 2D or 3D grid of points or nodes, while the time is discretised as t_0, t_1, t_2, ..., t_n with t_0 and t_n initial and final time of the simulation. At each time t_m ($t_0<t_m<t_n$) the value of the quantity under study at each node is defined in terms of the values of this quantity at its neighbouring nodes (including the node itself) at the time t_{m-1} [108-111].

Digital waveguide mesh (DWM), as a variant of FDTD method, is based on the d'Alembert solution of the 1D wave equation which is the given by the sum of two waves propagating in opposite direction [53, 111]. This method is used for the simulation of wave propagation in strings and tubes with 1D meshes and is extended to membranes and plates simulations with 2D meshes and rooms and musical instruments simulations with 3D meshes [112, 113].

Although these models are very accurate for single frequencies, especially low frequencies and small rooms or two dimensional representation of rooms [107], the level of computation and their computation times are very high due to the large number of calculations. For example, FDTD method requires a large number of nodes in order to reliably approximate a real space. Due to these aforementioned limitations and the fact that this research focuses on large real-world spaces, the geometrical acoustic algorithms will be used instead of the wave-based methods.

Therefore, any detailed description of the wave-based methods is beyond the scope of this thesis. The interest is referred to the relevant literature for more detailed explanations of the wave-based methods.

3.3.2 **Acoustic Radiance Transfer/Radiosity Method**

The acoustic radiance transfer method is an element-based method, like the BEM method, but the modelled acoustic quantity is energy [114-116]. The acoustic radiance transfer method, or known also as radiosity method, is based on the room acoustics rendering equation in which each surface of the room model is subdivided into surface elements. Starting with the energy sent from the sound source to each element, the energy transferred between elements is calculated and stored. For the final calculations, the energy is collected from all the elements to the receiver point. The method cannot account for diffraction effects or specular reflections, which limits its current application for auralization purposes.

3.3.3 **Geometrical Acoustic Models**

Geometrical acoustic models describe sound propagation by calculating the path of particles moving along sound rays, following the ray-tracing technique used in optical model experiments, and based on the geometrical/physical characteristics of the space. A number of rays *N* are emitted from a source and each ray is repeatedly reflected until it is absorbed or it becomes longer than the defined computing time. It is assumed that the ray is totally absorbed if it strikes the defined receiver position [106]. By calculating the energy and the direction of each and every one of the rays received at a specific position in terms of time, an approximation to the impulse response is generated for each ray, which can be represented as an **Echogram, Echo Diagram**, **Reflectogram** or **Histogram** (Figure 3.5).

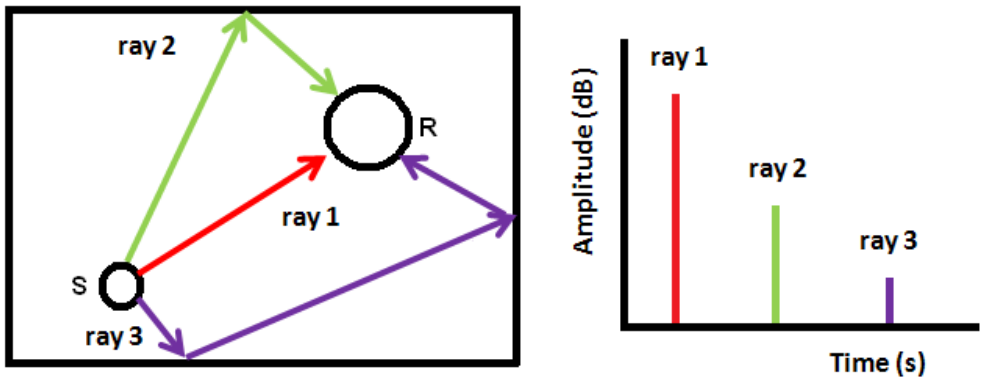

Figure 3.5 Ray tracing emitted from sound a source S in a 2D environment and the representation of the impulse responses from each of the example rays as registered at receiver R.

The energy of each ray is dependent on the atmospheric conditions defined in the computer model for air absorption (temperature and humidity) and the absorption coefficients which characterise the properties of the reflective boundaries.

There are two methods to calculate and simulate the propagation paths of the particles: 1) the Mirror Image-Source Method (MISM) and 2) the ray tracing Method.

Mirror Image-Source Method (MISM)

Image methods were commonly used in very early analyses of the acoustic properties of a space [106, 117, 118], the principle being that a mirror image of the original sound source is created in the plane represented by the reflecting surface. The distance between this image source and the receiver is equal to the reflection path from the original source to the receiver. The method was first used to predict the acoustic properties of small rectangular rooms using a digital computer [42]. In a rectangular box-shaped room, all image sources are easily constructed up to a certain order of reflection and the number of the image sources, N, can be calculated according to:

$$N = \frac{4\pi c^3}{3V} t^3 \qquad (3.1)$$

where V is the volume of the space, c is the speed of sound in the air and t is the time of the emission of the sound from the source to the receiver point, and statistically this can be applied to any geometry [119].

All image sources are visible from the receiver and the calculation of the arrival time of each one is efficient as it is determined only by the distance between these images and the receiver.

Figure 3.6 represents an example of the image source method in the simplest case of a two dimensional rectangular space. The source S emits rays which are reflected by a surface before they arrive to the receiver R. A first-order reflection i.e. meaning that the ray has been reflected only once before R at the point A, creates an image source S1 on the opposite side of that boundary. The path length that the ray has to travel from S to R, through this first-order reflection is equivalent to the distance between S1 and R. A second-order reflection, where the ray has been reflected twice before it arrives at the receiver, requires a new image source, added after the reflection at point C, on the opposite side of this second boundary. Here, the same effect happens: the path length of the ray travelling from S to R via C is equal to the distance between R and S2.

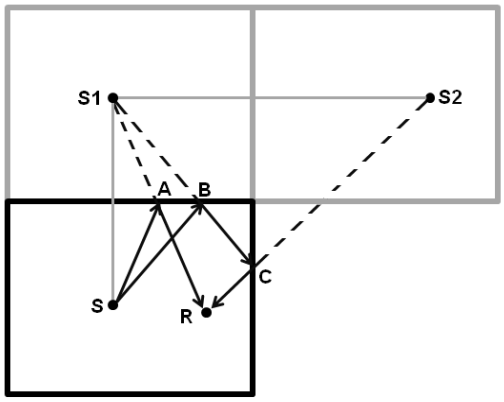

Figure 3.6 Demonstrating the Mirror Image-Source method. Reflections are calculated by building up the paths from the sources to the receiver point. An image source S1 is created on the opposite side of the boundary, after the first-order reflection at point A. After the second-order reflection at points B and C, a second image source S2 is created on the opposite side of the second boundary.

Computer modelling software based on this theory creates a mirror image source, every time a ray is reflected from a surface. If it is characterised as visible, then the corresponding reflection from it is added to the echogram. Every reflection is counted only once, even if it has been detected several times by different rays [120].

This algorithm is considered the fastest and simplest way for the prediction of simple rectangular acoustic models, however, calculations with this method become more complicated in the case of irregular spaces where image sources are not always visible from the receiver. Figure 3.7 shows an example of such an irregular room, with a source S and two receiver points, R1 and R2. The first-order reflection from the source S to the receiver R1 is calculated as the distance between the valid image source S1 and R1. The receiver R2 is not visible from the source S1, as the reflection path between S1 and R2 is intercepted by the boundary surfaces D, E and F. Thus, further reflection orders are needed for this source to be considered visible via reflections by this receiver point.

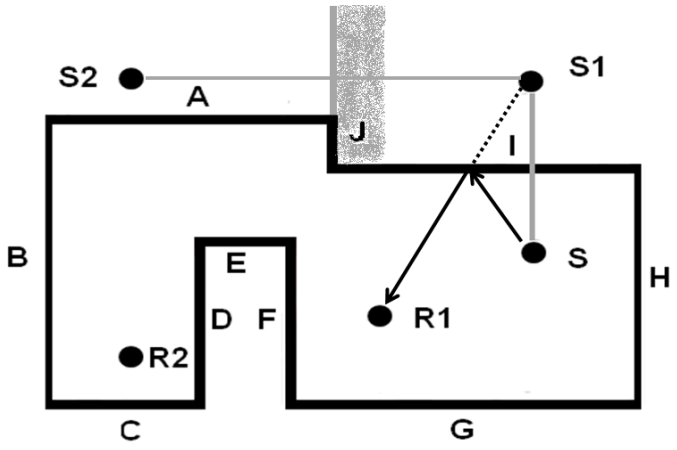

Figure 3.7 Demonstrating a likely case in the Mirror Image-Source method, where the created image source S1, while detected by R1, is not visible via reflections by R2.

Borish [117] extended the Mirror Image-Source method to include non-rectangular spaces by introducing three criteria in order to assure that the created image source is valid for the calculations of the reflection paths between source and receiver points. The first criterion is called "validity" and checks that the image sources are created by reflecting across the non-reflective side of the boundary, as the invalid S2 image source in Figure 3.7 created by the non-reflective side of the boundary surface J. The second criterion is "proximity" and discards image sources

which are further from the listener than a distance defined by the user. The third is "visibility" and tests if an extended line between the image source and the listener lies inside the boundary of the reflecting side. If all of these criteria are satisfied the examined image source contributes to the sound received by the listener. However, there are still limitations on the application of this method. As the order of the reflections increases, the number of the image sources increases exponentially and influences the initial calculation time.

Ray-Tracing Method

In ray-tracing, the sound source emits a large number of sound rays in all directions. Sound particles are traced along these rays and they are reflected from surfaces in the space according to the geometrical law of reflection and depending also on the geometrical data of the room. The results are plotted using an echogram or histogram based on the energy and arrival time of each ray/particle at a receiver position.

Detection of the receiver position

Due to the fact that a point-like receiver would require an infinite number of rays to be detected accurately, two calculation methods are used in order to detect the reflections passing by a specific receiver position.

The first is to define the receiver position not as a point, but as a region around the receiver, centred on its geometrical location [121]. When a ray arrives in this region, it is considered as having been detected and contributes to the output. Figure 3.8 represents such an example of ray-tracing. A point source S propagates rays across different directions. The rays are reflected from boundary surfaces with some reflections passing across the defined receiver area around the receiver R.

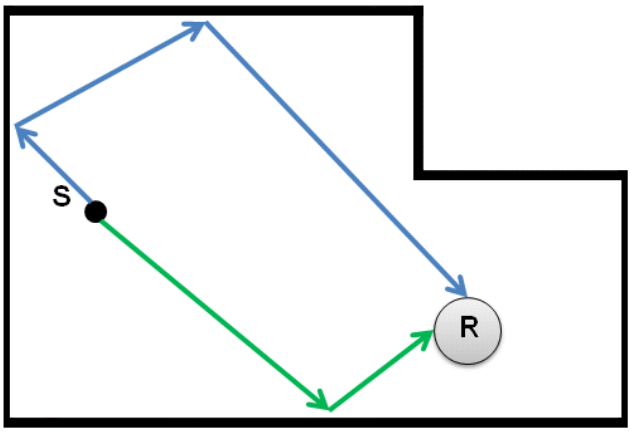

Figure 3.8 Ray Tracing method, where the source S emits sound rays in different directions and is detected by the receiver position R, defined as an area.

The second method, known generally as Beam Tracing, replaces rays with "thick" rays, or volumetric beams, in order to detect the receiver position with more accuracy and greater computational efficiency. The beam of rays is uniformly propagated from the centre of the defined spherical source, and the rays propagate with the same angle between them [106].

In cone-tracing, circular cones are propagated from the source. As a spherical/omnidirectional source is required, due to the shape of the cones, there are overlapping areas between the adjacent cones, as shown in Figure 3.9 (left image) which cause multiple detections of the same paths [122, 123].

In triangular/pyramidal tracing, a pyramidal beam is used to represent a group of rays, and is emitted from the source avoiding the overlapping areas possible in cone-tracing leading to the same path being detected more than once [107, 124, 125]. The pyramids perfectly cover the surface of the spherical source and there is no overlap as shown in Figure 3.9 (right image).

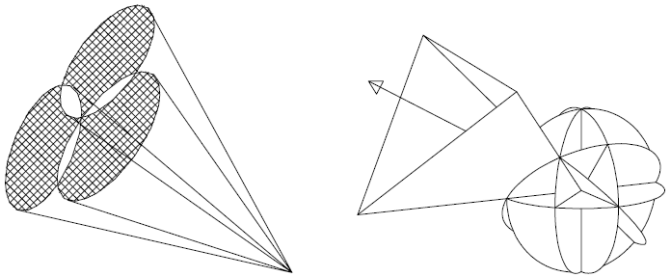

Figure 3.9 Cone and Pyramidal tracing as emitted from a spherical source, from [124].

When the beams hit a wall, new beams are reflected based on a newly created image source S, as shown in the Figure 3.10. These sequences of beam structures are called a **beam tree**, with the sound source to be the root of the tree and the first level beams to be the branches. The next level of beams is reflected from the boundary surface A, then from the boundary surface B and C, and so on [126].

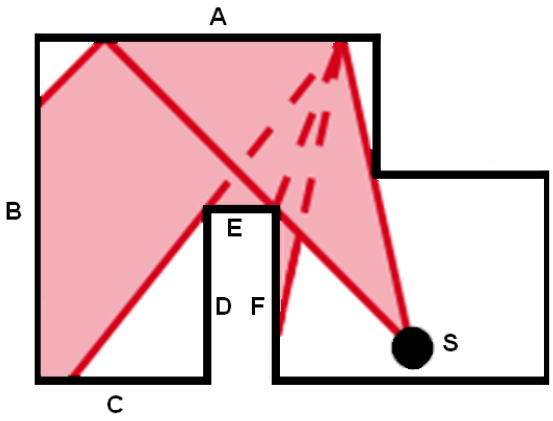

Figure 3.10 Representation of the beam tree. The beam is emitted from the source S to the surface area A where the beam is flipped to the surface areas B, E and F, after [126].

When a cone or beam passes by the receiver position, an individual hitting ray, from the central path (the axis of each beam) between source and receiver, is determined and calculated [125]. This fact introduces a risk, however, that a number of image sources will not be detected, or false impressions are created in the case where the beam does not pass exactly through the receiver position.

Beam tracing methods, as an improvement of the basic ray-tracing method, have provided a noticeable reduction in computation time compared with normal ray-tracing methods [125, 127]. However, corrections are required for the underestimated reverberation tail, due to the increase of the base of the beam that becomes larger than the room [128, 129]. A typical way to deal with this problem is to add a statistically generated reverberant tail at the late part of the impulse response resulting in a "hybrid" model [130]. Various studies are working to correct these problems and different implementations have been used in the field going back to the Godot system, in 1982 [131], till more recent software such as Ramsete [124, 128] and EVERTims based on [132].

Avoiding false reflections in the Ray-Tracing method

Another problem with ray-tracing methods is the generation of false reflections or the non-calculation of true reflections. Based on the probability that a ray is incident upon a surface, the minimum number of used rays N can be calculated from the following equation,

$$N \geq \frac{8\pi c^2}{A} t^2 \qquad (3.2)$$

where A is the area of the surface, c is the speed of sound in air and t is the travelling time needed from the source to the receiver area [107]. Although a smaller number of rays can underestimate acoustic behaviour within the space, no major changes have been observed by increasing the number of rays above the recommended number [16, 133].

Ray-Tracing is applicable to more irregularly shaped rooms, in contrast with the Mirror Image-Source method. However, the Mirror Image-Source method is considered more accurate as it is unlikely to miss important early reflections.

The limitations of geometric algorithms

Geometric acoustic algorithms generally assume that boundary surfaces are flat and reflect specularly, and so diffusion effects cannot be described. Recently solutions have been introduced [29, 119] by suggesting the use of diffusion/scattering for each surface, which has improved reliability of the results. Thus, in addition to air absorption and the absorption characteristics of the surfaces, scattering has an important impact in the calculation of the reflection energy. Depending on the defined scattering coefficient for each surface, the reflections can be modified to have perfectly specular direction, based on the Law of Reflection, or scattered more or less at random [107] with directions determined according to Lambert's Law [134]. However, after this treatment, the differences between a real impulse response and a ray-based one are still obvious in the time domain, as shown in Figure 3.11. In the simulated response (Figure 3.11, top), there is still no comparable diffuse sound energy between the early reflections as evidenced in the real response (Figure 3.11, bottom) [135].

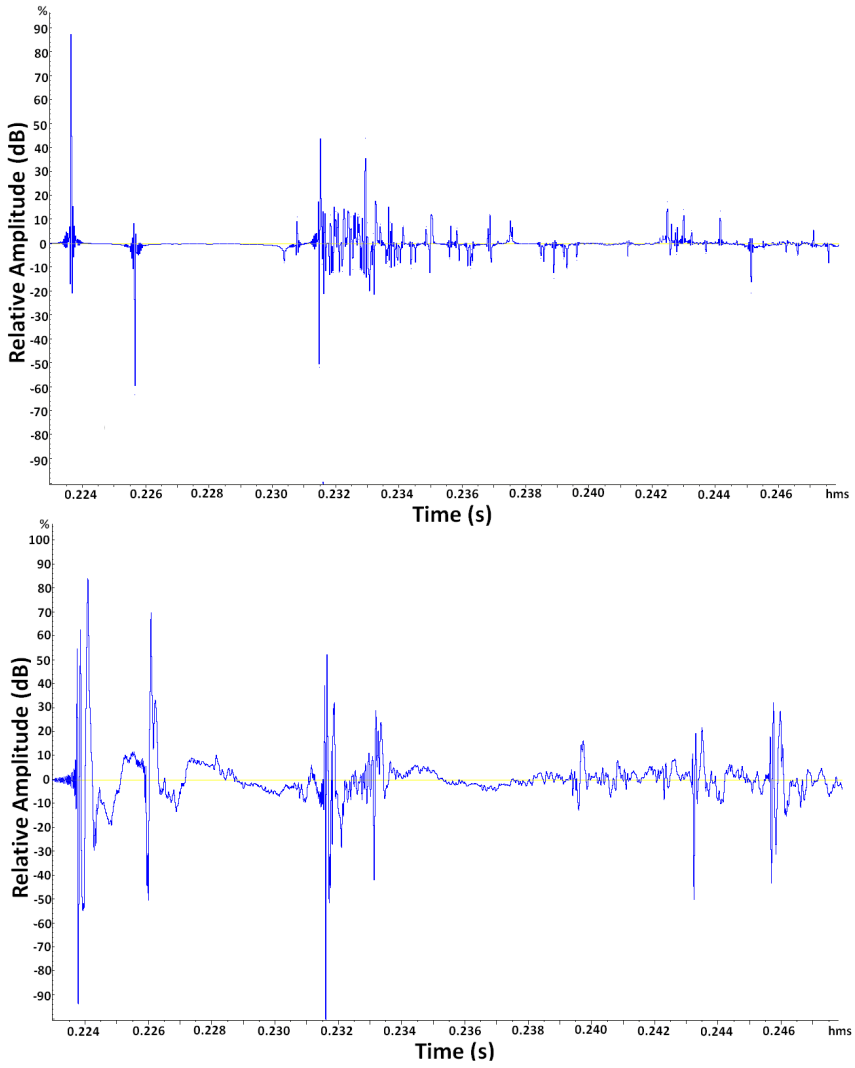

Figure 3.11 Comparing early reflection for the first 0.025s of a ray-based impulse response (top) and a real impulse response (bottom). The lack of diffuse sound is clear for the first case due to the limitation of geometric acoustic algorithms to describe accurately diffusion effects.

Additionally due to the consideration of sound as particles, and not as waves, wave based phenomena are disregarded by these algorithms. For example, the phenomenon of interference cannot be taken into account with the calculations, as these algorithms do not consider and calculate the phase components of a "ray" and their changes after a reflection occurs [136]. According to [137] this is a problem especially for absorptive surfaces, where the phase change effect is more critical. Harder and more reflective surfaces will provide more accurate results in these cases. Additionally lack of phase information means that the effects of standing waves cannot be simulated.

Diffraction effects cannot be described by considering the straight line propagation of sound rays. Thus, the method tends to create high-order reflections which do not occur in the real world. This leads to poor accuracy, especially for low frequencies where diffraction can have a significant effect.

Additionally, assuming that the full audio spectrum ranges from 22Hz to 22kHz, geometric acoustic methods are only really valid for spaces and surfaces with dimensions in the range of 15.5m to 1.55cm. If the dimensions of an object are smaller than this range, the rays instead of propagating through and around it are assumed to be reflected by the object. Thus, as a modelling technique it is recommended to avoid surfaces that are very small and to simplify the architectural representation of the room in order to obtain a reasonable degree of precision, compatible with this modelling technique [106].

Hybrid Method

Similar to the example of a "hybrid" algorithm discussed above adding statistically generated reverberant tail at beam tracing method in order to improve the method (p.49), several acoustic simulation methods have used hybrid approaches by combining the best features of individual modelling types. Vorländer in [138] introduced a hybrid method where Mirror Image-Source and ray-tracing methods are combined for improved accuracy of the early reflection paths of an impulse response. An algorithm introduced by Lewers combines beam tracing and radiance transfer method, which replaces surfaces with nodes and south paths with lines, in order to correct the diffuse reverberant tail of an impulse response [125]. Since then, several other approaches have been introduced based on different hybrid

algorithms, combining geometric models with wave based algorithms, acoustic radiance transfer methods, or even scale model measurements such as in the DIVA software [135], HAM [139], Epidaure software [140], RAIOS software [141, 142], EASE-AURA [5] and other research focused algorithms [110, 143-147].

In summary, algorithms based on geometric acoustic methods are considered accurate at high frequencies, within certain limitations (as they neglect wave effects), and can deal very well with large and complicated spaces [107] in a time efficient manner. Hence, these methods have been identified as suitable for use in this study. Two leading commercial acoustic simulation software packages, both based on hybrid calculation methods, have been used and their main properties are described below.

CATT Acoustic

CATT Acoustic is a hybrid simulation software, combining Mirror Image-Source, ray-tracing and cone-tracing methods [148-150]. The software provides three independent prediction methods options to the user. The "Early part detailed Mirror Image-Source Model (ISM)" calculates all the image sources on the boundary surfaces, up to a requested maximum order of reflection or defined length of time. From each detected image source, rays are reflected in both specular and diffuse ways, avoiding an exponential growth of the reflected sound. To calculate the diffuse reflection, each diffusing surface is subdivided into square patches which act as secondary sources, radiating according to Lambert's Law (see section 2.3.3) in a frequency dependent manner [148].

The "Audience area mapping" is based on the classical method of ray-tracing with a receiver point defined as a spherical region. The rays, after hitting a boundary surface, are reflected based on Lambert's Law, in a frequency-dependent manner. Due to the nature of this method, the echograms of the ray-tracing method are basically used for predictions and mapping of energy parameters (such as Clarity C_{80}) in a regular grid across the audience area. Hence, this method is not suitable for auralization purposes.

The "Full detailed calculation" is based on a randomised tail-corrected cone-tracing (RTC) algorithm which combines features of specular cone-tracing, classic ray-tracing and image-source algorithms. The first- and second-order specular

reflections are calculated based on the Mirror Image-Source method. The first-order diffuse reflection is calculated based on the secondary patch sources, as described above in the ISM method [150]. For higher-order reflections, randomised cone-tracing method, or "approximate" cone-tracing, as was first introduced by Dalenbäck [148], is used, where the calculated ray directions are randomised, unlike with the specular cone-tracing method where only the centre ray is traced.

CATT-Acoustic has been used for research purposes, in objective and subjective studies of room acoustics, as well as by acoustic consultants for providing predictions during the acoustic design process, some of which are reported in the following [5, 24, 73, 126, 143, 151-157].

ODEON

The ODEON room acoustic software is a hybrid model that contains elements of both the Mirror Image-Source and ray-tracing methods [158, 159]. As the early part of the reflections in an impulse response requires accuracy for efficient results, for this part of the echogram, a combination method between ray-tracing and Mirror Image-Source methods is used in order to calculate the early reflections. Rays are emitted to all directions from the source, creating image sources behind the surfaces from which they have been reflected. The data relating to the reflection paths is stored and these image sources are evaluated for their contribution at the receiver point, with visibility checks [134, 160]. It is also checked that each reflection is not duplicated. Once the reflection paths have been stored, the same ones can be used for any different receiver points. The transition from early-to-late reflections is abrupt, defined by the "Transition Order" (T.O.), a term introduced by ODEON. This defines the reflection order of the early reflections below when the hybrid method of combining ray-tracing and Mirror Image-Source methods, as described above is used.

For the later part of the reflections, the "secondary source" method is used. Above the reflection order defined by the Transition Order, secondary sources are created on the reflecting surfaces and emit rays into a hemisphere, carrying energy following Lambert's Law. With this method for the late reflection, a sufficient mixing of the specular and diffused reflections is obtained [107, 119, 160].

The two calculation methods for early and late reflection parts are overlapped for a time interval. A transition order of 0 means that the calculation method is based

only on the "secondary source" method, which does not guarantee, however, that all early reflections will be captured. It is recommended by the developers of ODEON that the Transition Order be estimated according to the complexity and the shape of the room [16, 158].

ODEON has been used in studies for research purposes, in the objective and subjective study of room acoustics as a reference tool for new experimental approaches in room acoustic modelling, and as a tool for acoustic consultants providing predictions during the acoustic design process, some of which are reported in the following [6, 10, 12, 13, 16-18, 20, 39, 73, 161-176].

3.3.4 **Round Robin for Acoustic Computer Simulations**

Just as Round Robin surveys have been carried out in order to identify variations in the various acoustic impulse response measurement systems, International Round Robin surveys have been carried out on room acoustic computer simulation systems, mainly based on Mirror Image-Source, ray-tracing or hybrid geometric algorithms. The goal of these surveys is to perform validity checks on their algorithms, with respect to the JND of the acoustic parameters.

Individual participants using different simulation software have been given the task of comparing their results for a specific space, based on the calculation of acoustic parameters according to ISO3382. The followed process for these surveys comprises two phases. Firstly, the room geometry and material data are provided with basic architectural plans, photos or drawings and material descriptions in words. Additionally, the location of the sources and the receivers is given and in some cases the climatic conditions are also described [29]. Thus, the results are based on the "guesses" and experience of each participant. In the second phase, common absorption coefficients (and diffusion data wherever is applicable) for the materials are given to the participants, thus the examination is focused on the algorithms rather than the users' estimations. The results are compared with the results observed from impulse response measurements performed in the actual space.

In 1994, the 1st International Round Robin was organised by Physikalisch – Technische Bundesanstalt, in German, for a speech auditorium, the PTB Audirorium [73]. Fourteen software packages were compared based on the simulations by sixteen participants, most of them developers of the software. The

results were observed for eight acoustic parameters (T, EDT, D, C, Ts, G, LF and LFC) as an average of the measured positions (two source and five receiver positions) for the 1kHz octave band. Significant differences were reported between the results of the simulations and those observed from the measurements, with respect to the JND values, even for the second phase (by applying general absorption data).

In 1997-8, for the 2nd International Round Robin, the ELMIA concert hall in Sweden was selected as the test space and it was modelled by sixteen participants (the developers themselves and also software users)[29]. The results for nine acoustic parameters (T_{30}, EDT, D_{50}, C_{80}, G, Ts, LF, LFC and IACC) within six octave bands (from 125Hz to 4kHz) were observed as well an average of the measured positions (two source and six receiver positions).

For the 3rd International Round Robin in 2002, the music recording studio of the Physikalisch-Technische Bundesanstalt Braunschweig was the test space [31-34]. It was modelled by twenty-one participants using nine software packages and the results were observed in six octave bands for the same nine acoustic parameters as in the 2nd Round Robin. In order to minimise any bias due to users' experience and guesses, this Round Robin was performed in three phases, providing more information to the users each time. For the first phase, a simple model was employed, giving the dimensions of the space and applying the same frequency-independent absorption and scattering coefficients. For the second phase, a more detailed model was used, with frequency-dependent coefficients applied to the diffusing walls. For the third phase, geometrical details were given for the diffusing elements of these walls. In addition, variations of the room acoustic properties were examined by varying the use of the curtains which covered the two boundary walls. Important deviations in the results were observed in terms of JND values, that also showed the importance of applying frequency-dependent absorption and scattering coefficients, as well that using very detailed geometrical models does not necessarily guarantee accuracy at the results stage.

In 2008, the Danish Acoustical Society [30], organised a Round Robin where all eight participants used them the same software, ODEON. Significant differences were observed even in this case, proving that the skills and the experience of the users are very important factors for the accuracy of the results.

The conclusions of the Round Robin tests provide a "rough" overview of the accuracy of different algorithms and highlight the important issues that need to be resolved or clarified for accurate predictions and auralization results [177-180]. The main issues are:

- the required level of detail in a geometrical models and their geometrical accuracy,
- the uncertainties of the impulse response measurement techniques, as already discussed in 3.2.4, which do not provide reliable results for using them as reference for the evaluation of the modelled results,
- the accuracy of the absorption and scattering coefficients, estimated by the users, as in-situ measurement techniques for these data are still not readily available,
- the neglect of wave-phenomena in ray-based techniques, pointing out once more the importance of including diffuse reflections in the algorithms,
- the vast number of settings and parameters available to the users for each software,
- the fact that the results are mainly observed by averaging the results of various measured positions and frequency bands, rather than studying the acoustic behaviour of the simulations for individual positions within the space.

The most interesting observation though from the results of the Round Robins is that a single mean value across all the measured positions does not provide sufficient information about the acoustic behaviour of the space and further more about the accuracy of the different algorithms, as a lot of individual information is lost. Additionally, after the 2nd and 3rd Round Robin conclusions the need for listening tests of the analysis of the auralization results has been even more emphasised [29, 34, 178], as optimisation of the results based on the just noticeable difference (JND) between the variations of the results for each calculated acoustic parameter does not necessarily guarantee optimisation at their auralization results.

3.4 *Summary*

In this chapter, the concept of Auralization, and the most well-known auralization techniques have been described based on real and synthesised impulse responses. For the capture of the impulse responses in an actual space, a number of different techniques have been applied. Their advantages and their limitations have been explained, dependent on the excitation signal used, the sound source and microphone properties, as well as the calculation process used for the analysis of the impulse responses.

Synthesised impulse responses are generated through computer-based models, where different algorithms simulate the physical and acoustic characteristics of the studied space. The main different between these algorithms is the consideration of the phenomenon of sound as particles or as waves. Geometric acoustic algorithms were examined in detail and the state-of-the-art described, in order to identify the most suitable technique for the purposes of this study. It is also clarified that, even if geometric acoustic algorithms are considered accurate at high frequencies, they have a limitation to low frequencies calculation. This is because these methods neglect wave effects, such as diffraction effects. Thus, the methods tend to create high-order reflections, leading to poor accuracy for low frequencies, where diffraction can occur.

Chapter 4.
The Perception of Changes in Objective Acoustic Parameters – A Pilot Study

4.1 *Introduction*

It is common in acoustic design to use 3D computer models and simulation methods to investigate how changes in the physical characteristics of the space relate to changes in the resulting acoustic experience [77]. However, the exact relationship between design parameters, objective acoustic metrics and the perception of the sound heard within the designed space are not well understood. Several studies have aimed to explain these correlations in more detail, often based on simulations in which the acoustic properties of the space could be easily controlled and changed by the researcher [42].

Tsingos et al. [181] motivated by the experimental use of the "Cornell Box", a simply constructed real-world space for the simulation of light in computer graphics, built their own simple test space for investigating sound propagation algorithms. Due to the simplicity of this space, the researchers were able to carefully control a variety of geometric configurations and check how accurately these phenomena can be acoustically simulated, based on the beam tracing method (as explained in section 3.3.3).

Klosak et al. [170] examined the influence of room shape and room volume using a virtual rectangular “shoebox” type concert hall using ODEON. In 24 models with a variety of room dimensions and three different room volumes, results were

averaged over 300-850 receiver points, spread over the audience area based on a 1x1 metre grid. It was concluded that there was a linear relationship between variations in Clarity (C_{80}) and Strength (G) and the changes in the geometric characteristics of the models. Changes in the values of these two parameters became wider as the volume and the dimensions of the models were increased. However, conclusions could not be drawn with confidence about the effect of the variations of room dimensions on Early Lateral Energy Fraction (LF_{80}) values.

Similarly, in Berardi's work [157], 25 box-shaped church models were used to study the influence of geometrical dimensions, volume and source position on acoustic parameters, derived from simulations based on CATT-Acoustic. As with the work conducted by Klosak et al. [170], it was shown that C_{80} and Ts values increase in direct proportion to an increase in the length-to-width ratios of the space.

Motivated by these previous works, a preliminary study was carried out for this thesis using a 3D shoebox-shaped room in ODEON, which allows the user to control a range of physical acoustic properties relating to the simulation. The aim was to better understand how physical factors relate to variations in derived acoustic parameters that might influence the perception of resulting auralizations. This chapter describes the pilot study and presents the results, which will be then used to influence the direction of the main modelling and measurement work that follows (Chapter 5).

4.2 *Methodology*

For this pilot study, the dimensions of the modelled room were 10m x 8m x 5m, based approximately on the dimensions of existing large reverberation chambers. The reason for this was to have the opportunity to investigate different source/receiver positions in a large space and observe the results in both objective and subjective terms. As a geometric based algorithm is used for this model and standing waves cannot generally be taken into account using this method, it was therefore not necessary to select room dimensions without common factors, to avoid this sound effect.

For each case study, different versions of the model were created wherein different variables such as variations in source directivity, source orientation, absorption

and scattering coefficients, calculation settings, and source/receiver positions were examined in turn. The results of these variations were verified through objective comparisons of the most relevant acoustic parameters and a series of listening tests, considering the critical distance for each case and the JND values for each acoustic parameter (results which have partly been published in [74, 182]).

For the listening tests, six experienced subjects (all of whom musicians, acousticians or musicologists) listened to pairs of samples, each of them based on different versions of the model, and were asked to express the degree of similarity between the paired sounds by choosing a number on a scale of values from 1, very similar to 10, very different.

4.2.1 **Case Study A**

The aim of this case study [74] was to investigate the influence of source directivity, source position, absorption and scattering coefficients, as well as the ODEON specific parameter, Transition Order (T.O.), on the three main acoustic parameters, T_{30}, EDT and C_{50}. The perceptual effects of these changes observed in these acoustic parameters were then investigated through a series of listening tests. For an appropriate coverage of the space, a grid of 12 equidistant receiver points (as shown in blue and identified with the numbers 1-12 in Figure 4.1) and five different positions of a single sound source (as shown in red and identified with the letters A-E in Figure 4.1) were used. The distance of the source and receiver positions was no closer than 1m away from the boundaries, as recommended in ISO3382-2 [183] in order to avoid strong reflections in the results.

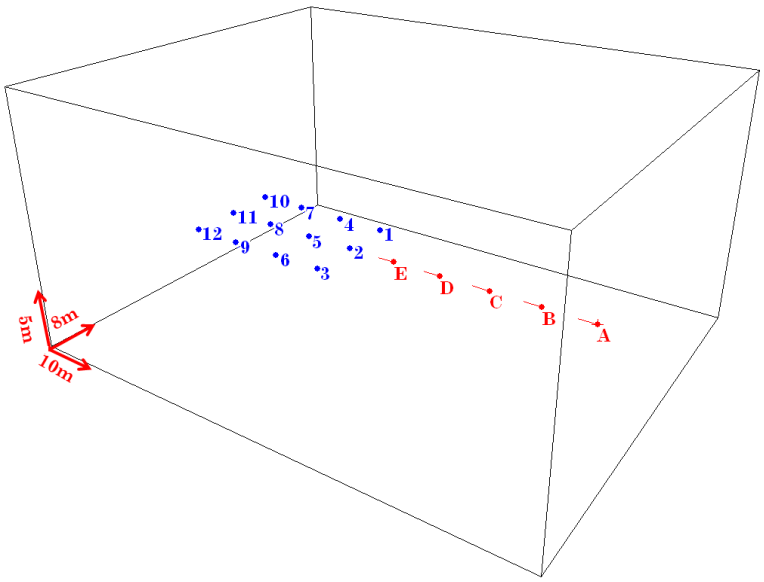

Figure 4.1 Demonstrating the virtual shoebox model, where the grid of 12 receiver points is represented in blue and the variation in source position (A-E) are represented in red.

Different versions of the model were studied, in which a different factor was changed and examined by observing T_{30}, EDT and C_{50} averaged across all receiver positions. For the subjective evaluations, the impulse response for the middle receiver point (R8) of the grid was used and convolved with an anechoic male speech.

The versions of the model used for this experiment were based on changes in the following factors:

Source Directivity and Position

The influence of the source directivity was examined by changing the directivity from an omnidirectional to a semidirectional source, as shown in Figure 4.2.

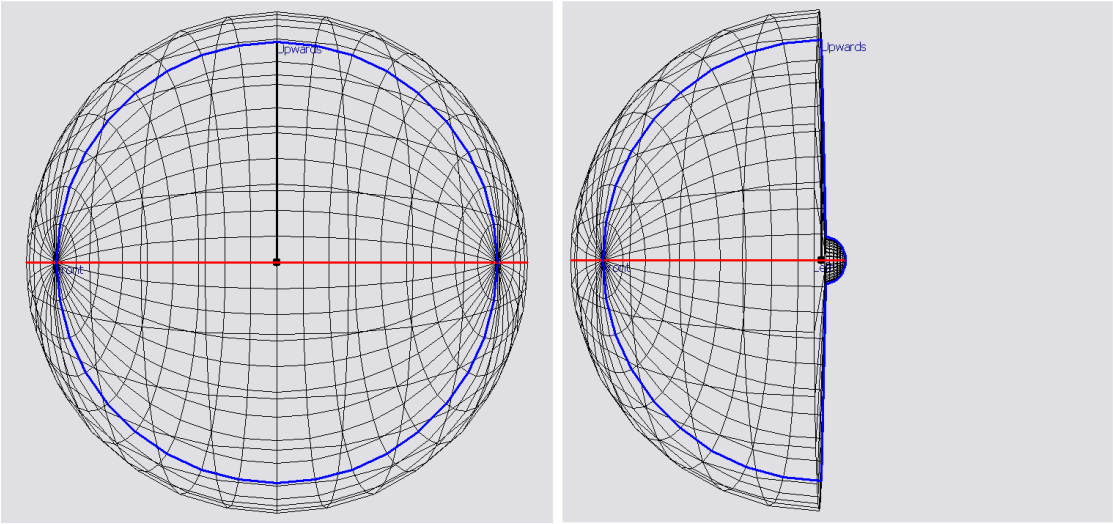

Figure 4.2 3D Directivity plots of the virtual source in ODEON: the left plot demonstrates an omnidirectional source and the right plot a semidirectional source (both in elevation view). Both sources have the same directivity characteristics across all octave bands.

In addition, the source position was moved across the equidistantly spaced positions A to E as shown in Figure 4.1. From the objective results, it was observed that the effect of source directivity was correlated to the distance between source and receiver positions. For instance, as shown in Figure 4.3, C_{50} increases as the source is moved progressively closer to the grid of receivers. However, this was not confirmed, in the subjective tests, where subjects could only detect minimal changes.

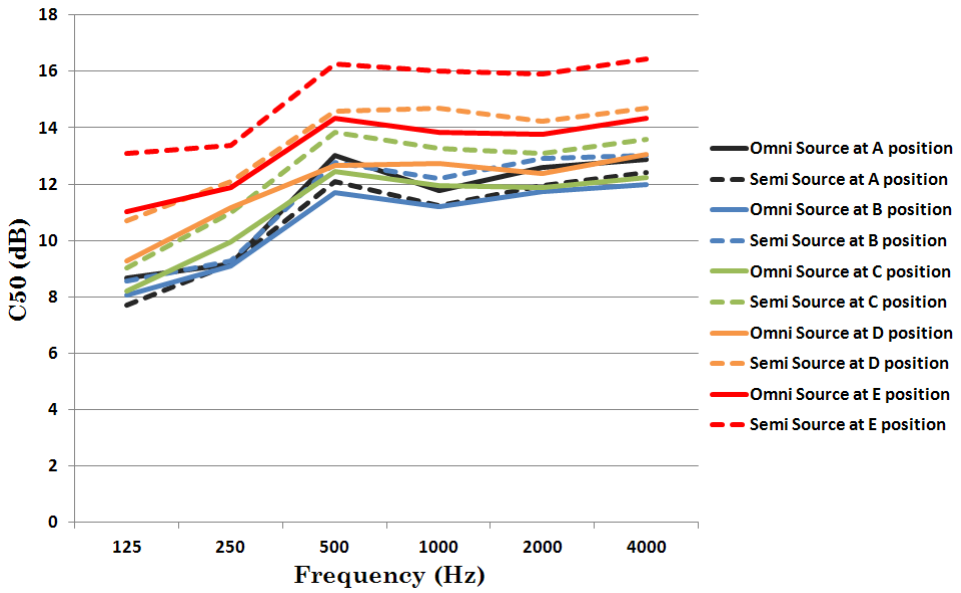

Figure 4.3 Mean values of C_{50} observed across the 12 receiver points by varying the source positions and directivity. The colours indicate the same source position (from position A to E respectively), while solid lines represent an omnidirectional source and dashed lines a semidirectional source.

Absorption Coefficients

To study the effect of varying absorption coefficients, the same value was applied to all boundaries in the shoebox model. These values were chosen to be 0.4, 0.45, 0.49 to 0.5. Using the model with absorption coefficient of 0.5 as a reference, it is noted that T_{30} changed noticeably, with even the smallest changes in absorption coefficient (compare the cases with absorption coefficient values of 0.49 and 0.5), as shown in Figure 4.4. In the listening tests the subjects clearly perceived absorption coefficient differences between values of 0.5 and 0.4, scoring the perceived difference at points 6 and 7 of the scale being used. For absorption coefficient values of 0.45 and 0.49 with 0.5 as the reference model, the subjects marked the perceived difference at points 1 and 2 on the scale.

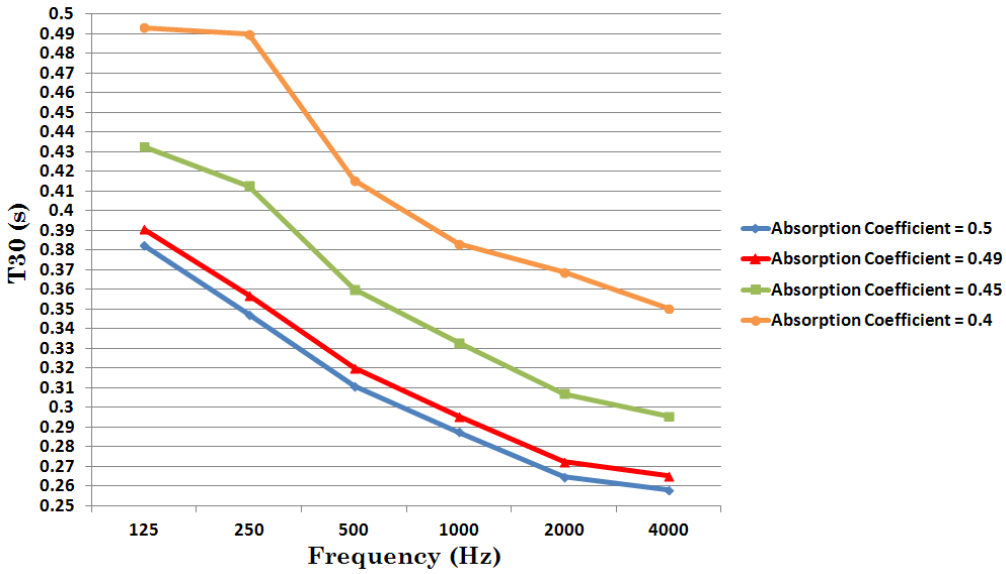

Figure 4.4 Mean values of T_{30} observed across the 12 receiver points by varying the absorption coefficient values at the boundaries (0.4, 0.45, 0.49, 0.5).

Scattering Coefficients

Significant differences in the objective results are observed when the scattering coefficient at the boundaries was varied between the values of 0.05, 0.1, 0.6 and 0.9 used. The absorption coefficient was set at 0.5 in all surfaces. Note here that the acoustic parameters responded differently across octave bands, as shown in Figure 4.5 and Figure 4.6 for T_{30} and C_{50} respectively. However, from the subjective evaluations it was observed that the listeners were not able to discern these changes.

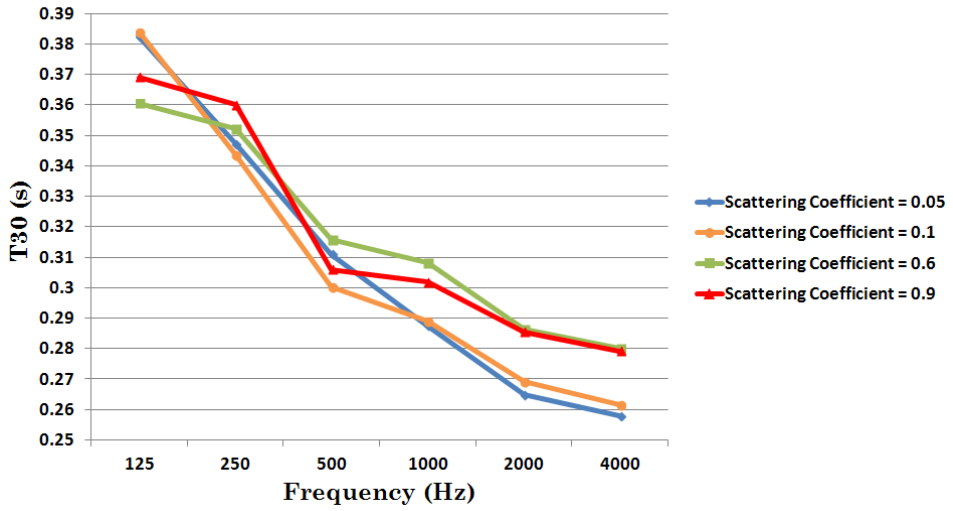

Figure 4.5 Mean values of T_{30} observed across the 12 receiver points by varying scattering coefficient values (0.05, 0.1, 0.6, 0.9).

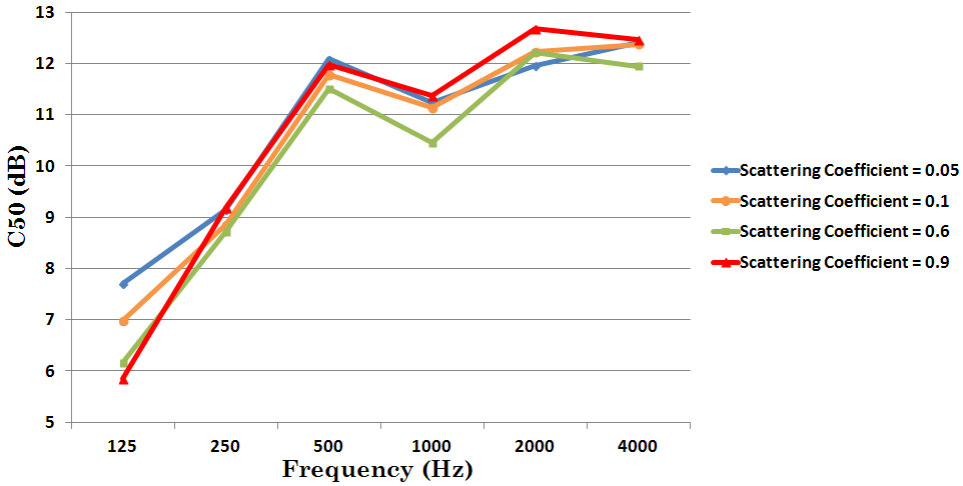

Figure 4.6 Mean values of C_{50} observed across the 12 receiver points by varying scattering coefficient values (0.05, 0.1, 0.6, 0.9).

Transition Order (T.O.)

Additionally, the effect of T.O. was investigated, using three different values of 0, 1 and 5. From the objective results, changes slightly greater than the JND for T_{30} and C_{50} were observed, as shown in Figure 4.7 and Figure 4.8 respectively. A more significant change in EDT was noted, as shown in Figure 4.9. Despite these variations in T.O. directly affecting the presence of early reflections (as discussed

in section 3.3.3), leading to them being absent with a T.O. = 0, there was no consensus between the listeners about this obvious change at the early reflections.

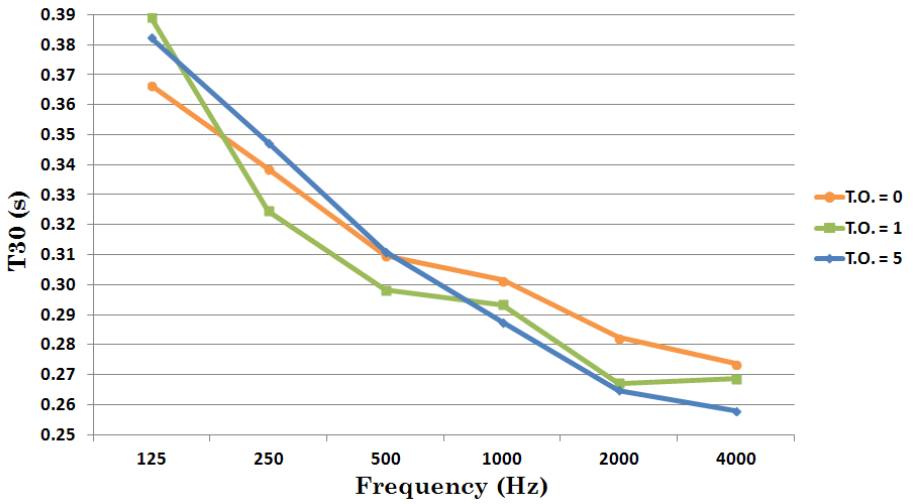

Figure 4.7 Mean values of T_{30} observed across the 12 receiver points by varying Transition Order (T.O.) (0, 1, 5).

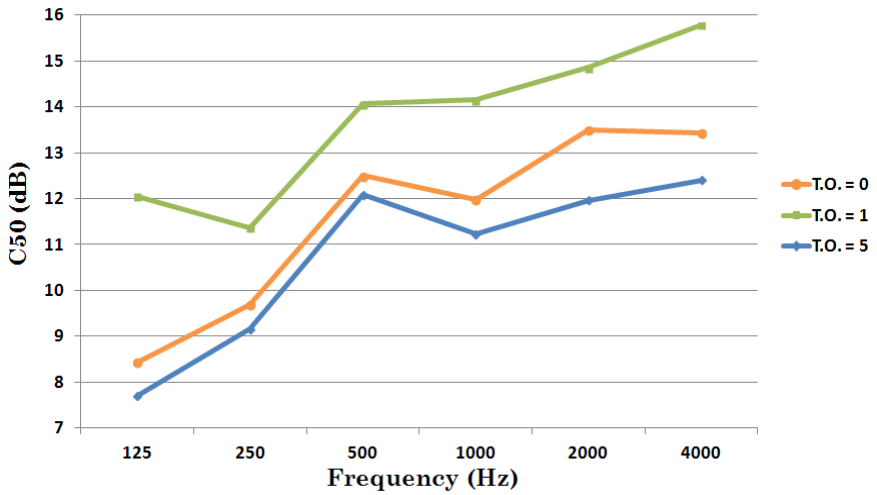

Figure 4.8 Mean values of C_{50} observed across the 12 receiver points by varying Transition Order (T.O.) (0, 1, 5).

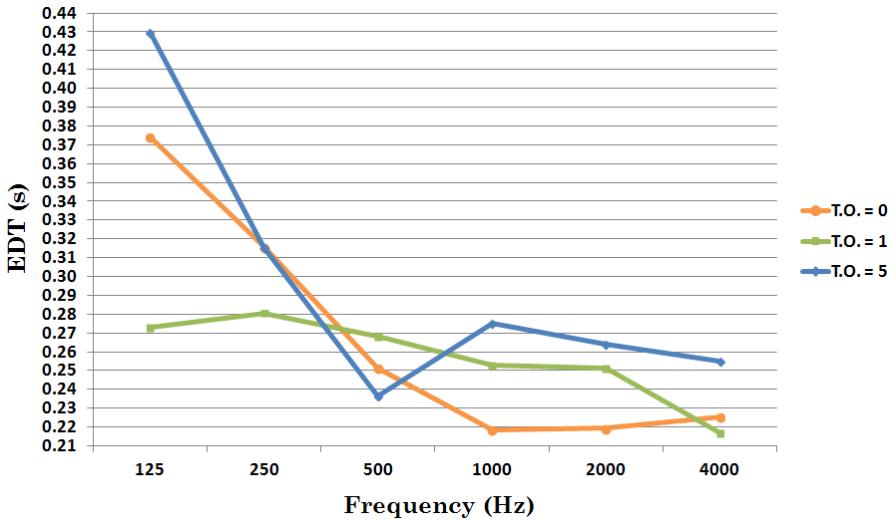

Figure 4.9 Mean values of EDT observed across the 12 receiver points by varying Transition Order (T.O.) (0, 1, 5).

4.2.2 Case Study B

EDT is considered an important acoustic parameter for evaluation of auralization, as it is related to the perception of reverberance, as referred to in ISO3382. Hence, the interest for Case Study B [182] focused on investigating how physical changes in source-boundary and source-receiver distances, together with source directivity, influence EDT. The results were based on the mean values observed from a grid of 80 equally spaced receiver points (shown in Figure 4.10).

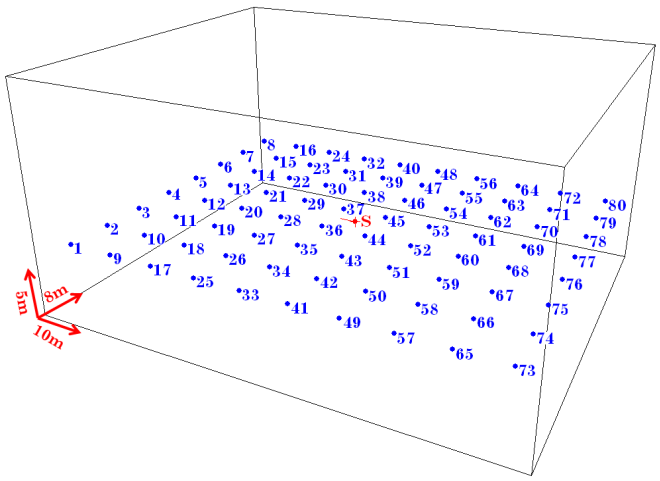

Figure 4.10 The virtual shoebox model used in Case Study B, where a grid of 80 receiver points is represented in blue and the source position is represented in red, at the centre of the space.

In order to control the energy of the early reflections, only specular reflections were used for the calculations, as scattering coefficient value greater than 0 results in random changes to the energy of early reflection. Variations in EDT values for an omnidirectional source, placed at the centre of the space, were obtained directly from ODEON and examined using colour-mapping across the grid of receiver positions. This is shown in Figure 4.11 below.

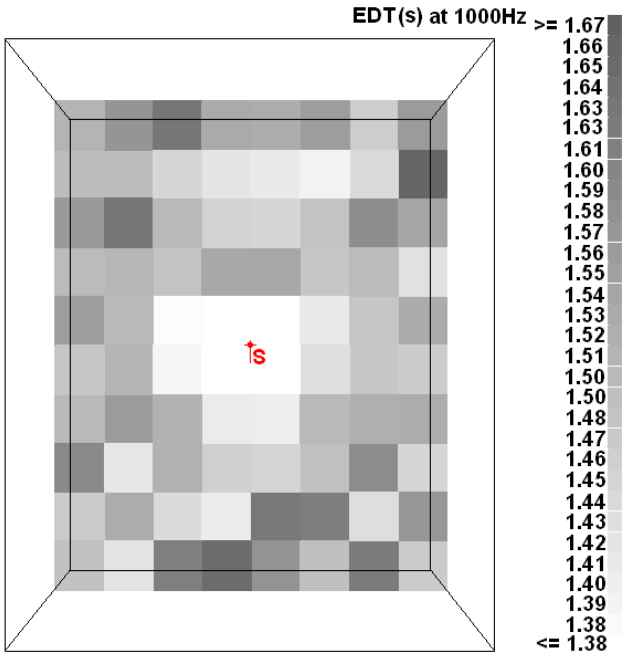

Figure 4.11 Colour-map showing EDT (s) at 1000Hz across the grid of 80 receiver points based on an omnidirectional source, placed at the centre of the space.

The scale on the right side of the colour-map shows the range of the EDT values in seconds for 1000Hz. Results were also obtained with the same methodology for a semidirectional source placed at the centre and oriented to 30°, 60° and 90° (Figure 4.12) and an omnidirectional source, placed 2m away from the upper boundary, shown in Figure 4.13.

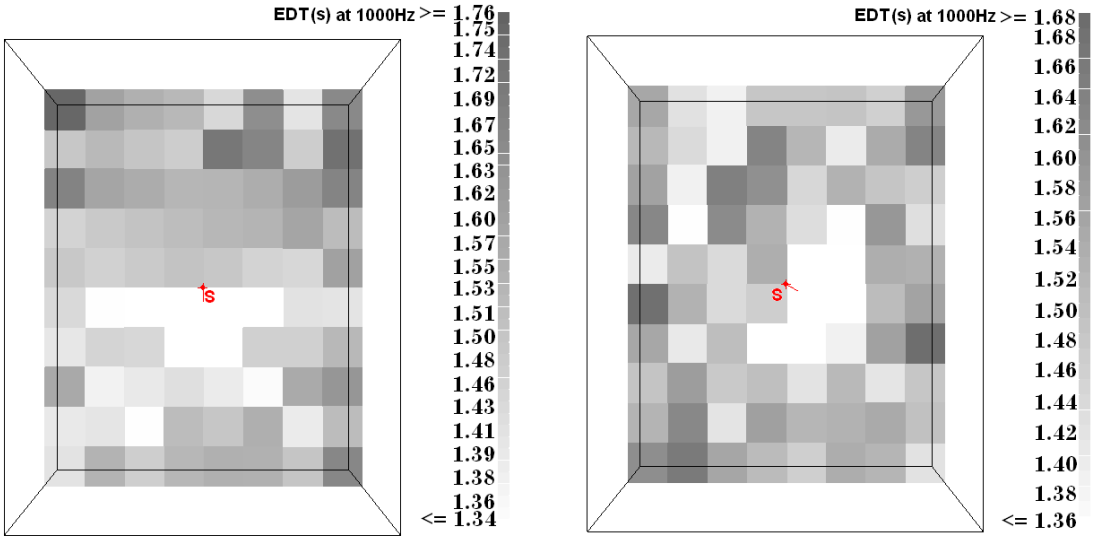

Figure 4.12 Colour-map showing EDT (s) at 1000Hz across the grid of 80 receiver points with a semidirectional source, placed at the centre of the space (left), and with the semidirectional source oriented 60° (anti-clockwise rotation) (right).

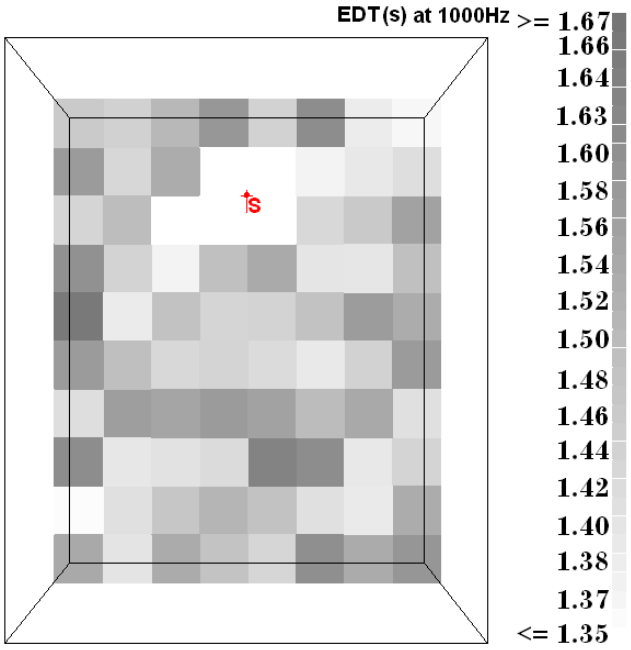

Figure 4.13 Colour-map showing EDT (s) at 1000Hz across the grid of 80 receiver points with an omnidirectional source, placed 2m away from the upper boundary.

Non-symmetric behaviour of EDT values were observed across the space, especially at low and middle frequencies, which means we cannot be confident about the conclusions reached regarding the behaviour of EDT for these physical variations in the space. Nevertheless, although this experiment did not offer additional

information about the behaviour of EDT values, it did show from this non-symmetric behaviour of EDT that specular reflections are not sufficient for an accurate simulation of the acoustic characteristics of a space, even with a very simplified model like this. The experiment thus confirmed the importance of using appropriate scattering coefficient value in geometrical acoustic algorithms.

4.2.3 **Case Study C**

A directional sound source, a Genelec S30D, was used for the investigation that forms the main part of this thesis (Chapter 5). In order to consider the influence of speaker directionality, a 3D version of this source was created (the modelling technique of which will be explained further in section 5.5.3) and tested in the shoebox shaped acoustic model. The source was rotated anti-clockwise from 0° to 10°, 40° and 70°, and changes in T_{30} and C_{80} were measured and noted, as shown in Figure 4.14 and Figure 4.15. A more detailed inspection reveals that T_{30} values have changed slightly across the octave bands, but more significant changes were observed in C_{80} parameters in the middle and high octave bands (above 500Hz).

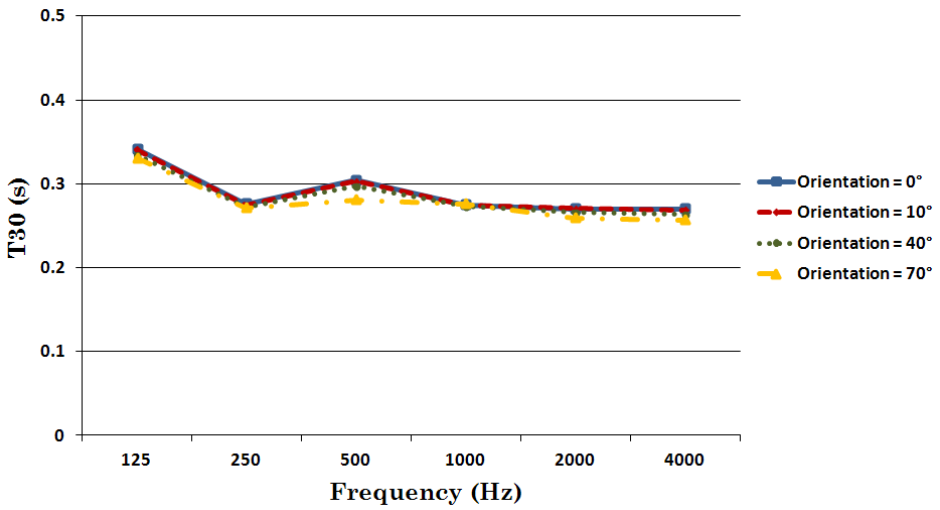

Figure 4.14 Comparing T_{30} values observed from a single receiver point (R8 as shown in Figure 4.1) from the ODEON shoebox model by varying the orientation of the virtual Genelec S30D sound source (0°, 10°, 40°, 70°).

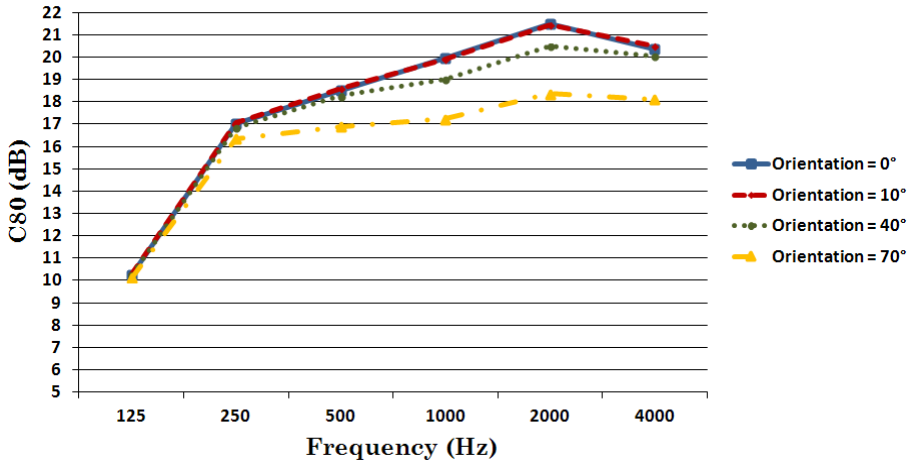

Figure 4.15 Comparing C_{80} values observed from a single receiver point (R8 as shown in Figure 4.1) from the ODEON shoebox model by varying the orientation of the virtual Genelec S30D sound source (0°, 10°, 40°, 70°).

4.3 *Summary*

An experimental shoebox shaped acoustic model was created using ODEON in order to study and control different physical factors and acoustic properties, and to investigate their influence on both objective and subjective results. Source directivity, source orientation, absorption and scattering coefficients, together with Transition Order (T.O.) calculation settings and source/receiver positions, were examined, based on T_{30}, EDT and C_{50}/C_{80} objective metrics. For the subjective evaluations, listening tests were carried out for the first two case studies.

From Case Study A, it was observed that C_{50} values are directly affected by source directivity and thus this relationship was also influenced by source-receiver distance. It was further observed that variations in absorption coefficient values resulted in similar variations in the objective results, as expected. The acoustic parameters studied did not respond evenly across octave bands when the application of variations in the scattering coefficients and Transition Order values. In most cases, subjects were not able to confirm these objective changes in a series of listening tests.

From Case Study B, conclusions could not be drawn with confidence about the influence of source/receiver positions and source orientation and directivity. The main reason being that the results of such acoustic simulations are realistic only

when they reflect the geometry, absorption, diffusion and so forth of real spaces. Thus, setting scattering coefficient to zero, an unnatural acoustic space was created, as the non-symmetric behaviour of EDT evidenced.

From Case Study C, useful information were extracted about the influence of the Genelec S30D sound source in the acoustic parameters studied, which will be used in the main part of this thesis, detailed in the following chapter.

Chapter 5.
Capturing the Acoustic Impulse Responses in St. Margaret's Church

5.1 *Introduction*

In order to validate and generalise how changes in objective acoustic metrics, caused by variations of the physical parameters of an auralization space, influence the resulting subjective experience, a huge number of spaces would need to be tested. However, this would be impractical, very time consuming and beyond the scope of this research. This study therefore focuses mainly on the results of one specific space, in which measurements of impulse responses in-situ can be applied and used for auralization purposes. The main requirement, being that the physical acoustic characteristics of the space could be easily changed in order to achieve variations in the values of the derived acoustic parameters, controlled as much possible by the researcher. Additionally, the space should have a sufficiently long reverberation time and relatively simple architectural characteristics.

The chosen space, St. Margaret's Church located in York, UK, was considered suitable as it has been redeveloped and acoustically treated in 1998 for concerts and conference use. The church's physical acoustic characteristics can be easily changed through variable reversible wall acoustic panels with a reflective and an absorptive side, and drapes arranged throughout the space, depending on the acoustic requirements of the activity within the venue [184].

5.2 *History of St. Margaret's Church*

St. Margaret's Church was founded in the 12th century and rebuilt a number of times before falling into disuse in 1974. The building was held in trust by the York Civic Trust until 1997, when the York Early Music Foundation secured a grant from the Arts Council Lottery Fund, in order to create the National Centre for Early Music, as it is currently known.

Only one feature remains from the original 12th century building, the section between the west wall and the first pillar of the arcade, which formed the north-west corner of the original rectangular church (the shape and size of the current nave). When the church was first built, the sanctuary was on the eastern side and the congregation sat on in the western side. In 1308, the church was rebuilt and enlarged by adding a tower to the north-west side. The English Reformation in the 16th century also affected the internal structure of the church, removing the altar and the sanctuary screen. In the 19th century more changes were made, with features such as pews, a new pulpit, choir stalls and an organ installed. The church continued to be used until 1974, when it was declared pleonastic and therefore became a store for the Theatre Royal of York [185].

Figure 5.1 The outside view of St. Margaret's Church, in York, UK, looking at the west side of the church and its tower.

The main feature of this work, of considerable architectural significance, is an ornate Romanesque doorway from the 12th century, with carvings of mythological

beasts, such as signs of the Zodiac and the Labours of the Month or illustrations from bestiaries and Aesop's Fables on the outer side. Another notable characteristic of the architecture is the unusual brick bell tower, which was rebuilt in the 17th century after the steeple collapsed on the nave.

The east and west windows are lancet type, while the windows on the north and south walls are rectangular, most of them decorated with stained glass. There are still several memorial tablets "which witness the gentle way of life at the beginning of 18th century" [186].

5.3 *Renovation of St. Margaret's Church*

As part of the York Civic Trust's plans to redevelop abandoned churches into places for activities and public events, St. Margaret's Church, which is located on Walmgate, was handed over to the York Early Music Foundation Trustees, thereby creating the National Centre for Early Music. The refurbishment included spaces for offices, rehearsals, recordings and conferences and the work involved professionals in architecture, interior design and acoustics.

Figure 5.2 St. Margaret's Church before the refurbishment, towards the east-south (left) and the east (right) side of the church [184, 185].

Figure 5.3 St. Margaret's Church after the refurbishment, towards the east-south (left) and the west-north (right) side of the church.

The maximum dimensions of the space are approximately 24.3m in width, 12.5m in length and 11.2m in height and the volume is approximately calculated to be 2,700m^3.

The floor has been reconstructed with huge, smooth flagstone plates. Due to many decades of rain entry, a further coat of lime-wash to the stonework had to be added and it was also necessary to install underfloor heating. Most of the stonework of the walls has been repaired and covered with lime and paint, except for the memorial tables which have remained untouched. The five columns and their arches that divide the north aisle from the main nave have kept their original stonework and no changes have been made to the wooden beam ceiling. A wooden frame, 0.955m high, was repaired and extended across the length of the bottom of the walls, while some storage cupboards, 2.00m in height, covered half of the west side wall. Extra doors have been built for the needs of the current use of the space and the windows have been covered internally with double glazing, keeping the view of the old stained glass. The ground floor of the tower has been opened and is now directly connected with the nave, being used mainly for storage.

The architectural plans for the refurbishment (1999) were received for this research from the archive of the National Centre for Early Music, and are presented in the following figures.

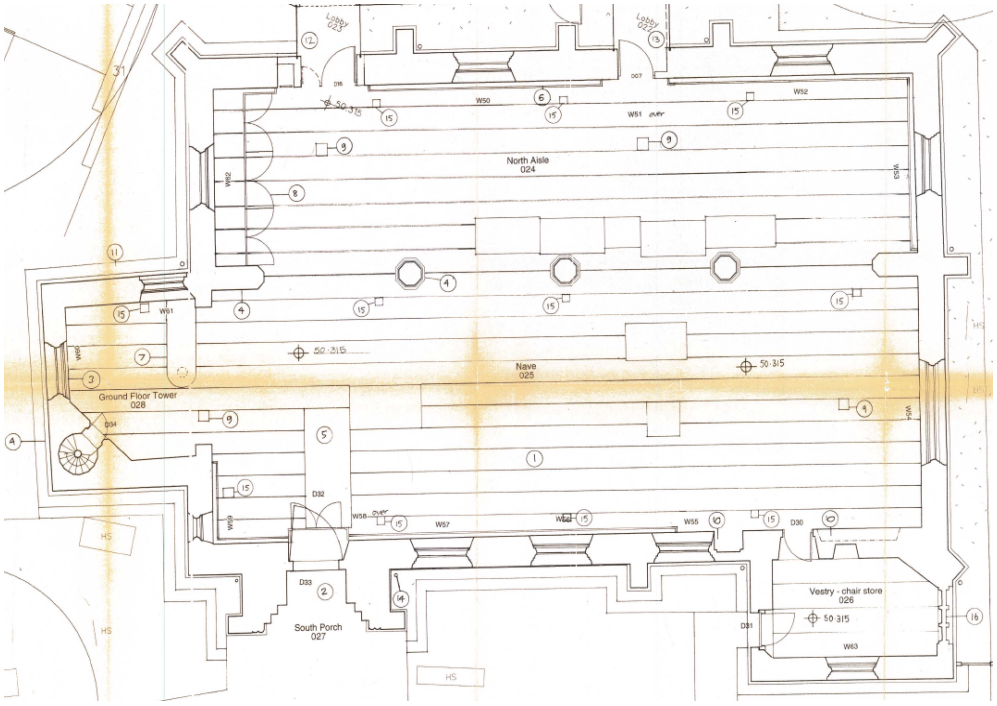

Figure 5.4 Ground Floor Plan of St. Margaret's Church as proposed [187].

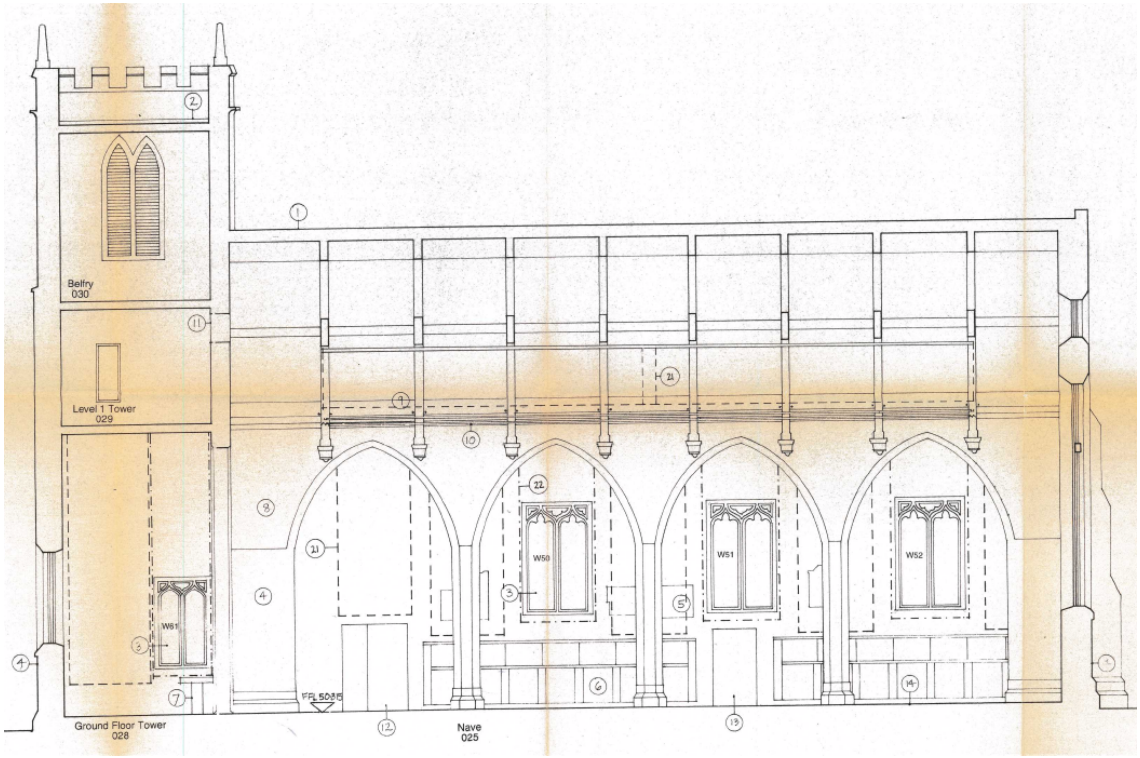

Figure 5.5 Long Section North of St. Margaret's Church as proposed [187].

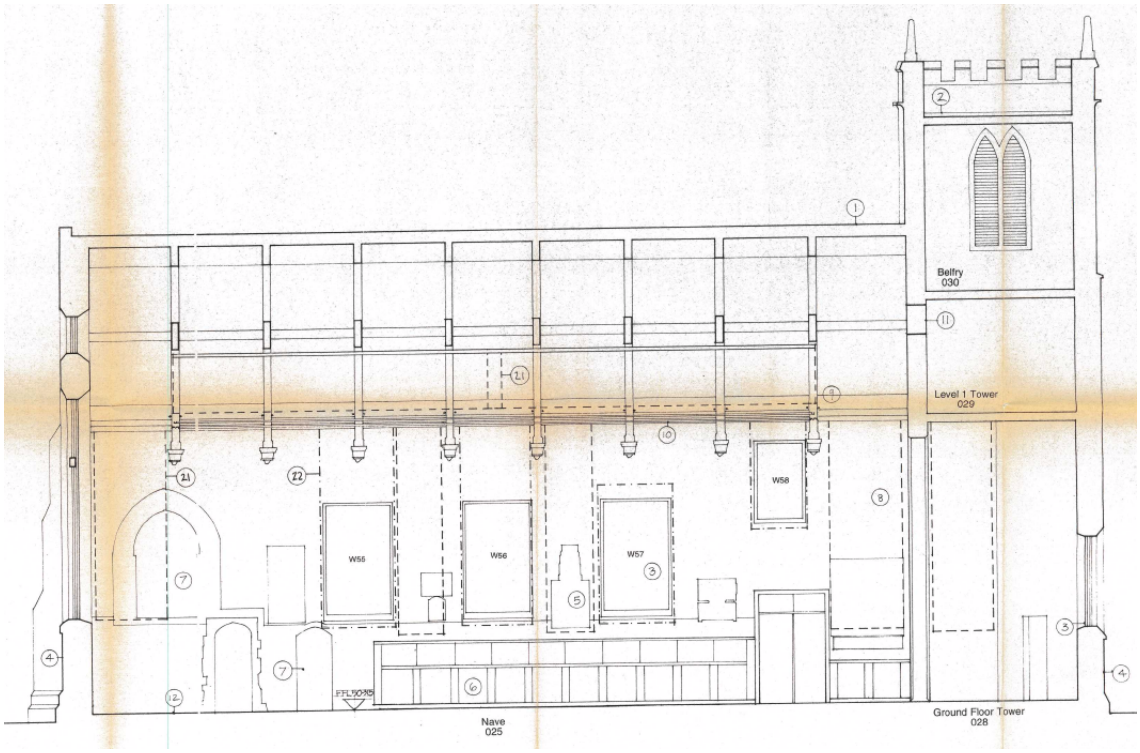

Figure 5.6 Long Section South of St. Margaret's Church as proposed [187].

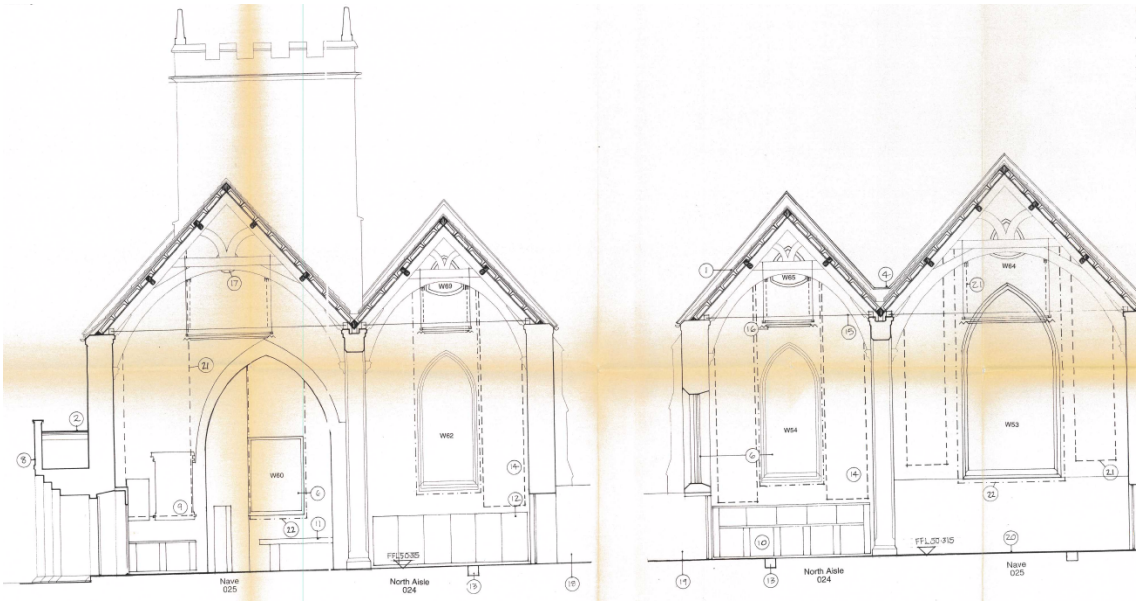

Figure 5.7 West and East Cross Sections of St. Margaret's Church as proposed [187].

Chapter 5. Capturing the Acoustic Impulse Responses in St. Margaret's Church

Arup Acoustics were consulted during the acoustic design of St. Margaret's Church. The aim was to create a space acoustically suitable for the variety of events that were planned to be held in the venue, from conferences (implying a short reverberation time) to classical and early music recitals (requiring longer reverberation time). Absorbing acoustic panels and drapes were also considered in the architectural redevelopment, as the quote below illustrates;

> "*Variable Acoustic Absorption. In ceiling – Acoustic drapes on Unistrut, stored bunched up at end archbrace truss positions, total surface area of fabric = 100sqm (comprising 4 no. drapes of 15sqm in nave and 4 no. drapes of 10sqm in north aisle). On walls – Acoustic banners, stored rolled up at internal eaves level, total surface area of fabric = 270sqm (the individual dimensions vary to suit internal elevations, each wall banner comprises double thickness of fabric, a constant gap between the two layers is maintained by aluminium framing, banner is handle operated*" [187].

It is worth noting that just as the quote above indicates, the dimensions and the exact position of the acoustic panels as well as the dimensions of the space were approximated to the states specified in the architectural plans. The original plans recommended: "*All dimensions to be checked on site*" (see Appendix A for the original architectural plans [187]).

The total number of acoustic panels is 58, spread in groups of two to ten across the north and south walls as well as the ground floor tower area and corners of the space. Each group of panels can be folded in half, so that the absorbing front faces are covered, revealing only a hard reflecting rear panel, as shown in Figure 5.8 and Figure 5.9.

Figure 5.8 Acoustic panels set at the south wall. The 4 square absorbing panels (on the left) are folded in half, replaced by 2 reflecting panels (on the right).

Figure 5.9 Acoustic panels set at the south-east walls. The 26 square absorbing panels (on the left) are folded in half, replaced by 13 reflecting panels (on the right).

Acoustic drapes were also mounted on two rails in the nave and north aisle ceilings, thus enabling them to be opened or closed as needed, as shown in Figure 5.10.

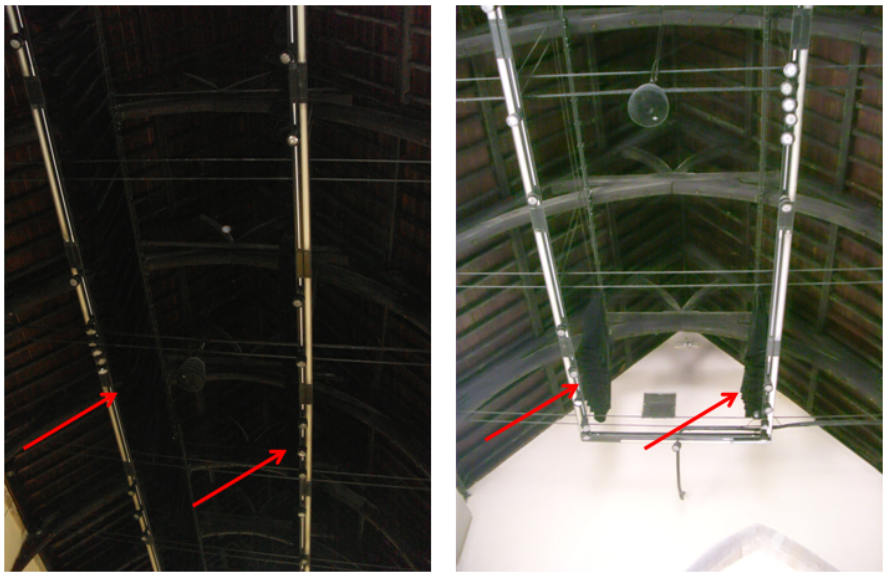

Figure 5.10 Acoustic drapes set on the ceiling; drapes out (on the left) and drapes back (on the right).

By changing the configurations of panels and drapes arranged throughout the space, it is possible to vary the acoustic qualities to cater for a range of different activities. The acoustic characteristics of the space for each recommended configuration are given in Table 5.1. Note that the panels are referred as 'boxes'.

Table 5.1 Guidance notes for the various acoustic qualities, provided by Arup Acoustics [185].

Activity	**Acoustic boxes: absorption exposure**	**Drapes: absorption exposure**	**Acoustic qualities of space**	**RT (s) (Based on Arup measurements)**
Large choral	All boxes closed	All drawn back	Highest reverberation, warmth, spaciousness	2-2.6
Music recitals	All boxes closed	All drawn out	Even balance between clarity and reverberation; discrete sounds stand apart clearly, but ample reverberation	1.5–1.8
Small ensembles	25% of boxes open	All drawn out	Balance towards clarity (assume 100+ padded seats)	1.4
Opera/ musicals	75% of boxes open	All drawn out	High degree of clarity, modest reverberation	1.2
Lectures/ speech	All fully open	All drawn out	Sound absorbent space, giving maximum clarity for speech	1.0

5.4 *Impulse Response Measurements*

To fully exploit the opportunity to acoustically survey and measure impulse responses in St. Margaret's Church, different physical factors were changed and their acoustic effects recorded for further study. First, changes in the acoustic characteristics of the space were applied by considering the configurations of panels and drapes. Additionally, changes in the orientation of the sound source were applied to test for the effects of source directionality.

Measurement technique and Excitation Signal

The Exponential-Swept Sine (ESS) Method was used as it is considered the best solution for auralization purposes [79], as explained in section 3.2.1. It gives a flat frequency response and a strong input signal compared with the ambient noise (high signal-to-noise ratio) but, more importantly, separates the nonlinear harmonic distortion of the speaker from the linear response. The logarithmic sine-sweep excitation signal was generated using the Aurora Plug-in [188]. The frequency range of the sweep is from 22Hz to 22kHz, approximately the audible range of

frequencies, and it lasts 15 seconds. In ISO3382 [55] it is strongly recommended to use sweeps with a length of two to four times the longest reverberation time, in order to increase the total radiated energy and reduce the influence of external noise. The length of the silence after the sweep depends on the reverberation of the room where the sine sweep is recorded. In order to minimise onset/offset effects, a fade-in and fade-out has been applied at the beginning and end of the test signal [61].

Table 5.2 Settings for the generation of the logarithmic sine sweep in Aurora plug-in.

Log Sweep	
Start Frequency (Hz)	22
End Frequency (Hz)	22000
Duration (s)	15
Fade-in and Fade-out duration	
Fade-in (s)	0.1
Fade-out (s)	0.1
Silence	
Duration (s)	10

Sound Source

For this study, a Genelec S30D was used as the source transducer. This is a directional three-way active tri-amplified system with 96kHz/24-bit AES/EBU digital input. Its directivity tends to be omnidirectional at low frequencies, while at mid-range and high frequencies it tends to a more consistent cardioid characteristic, as shown in Figure 5.11.

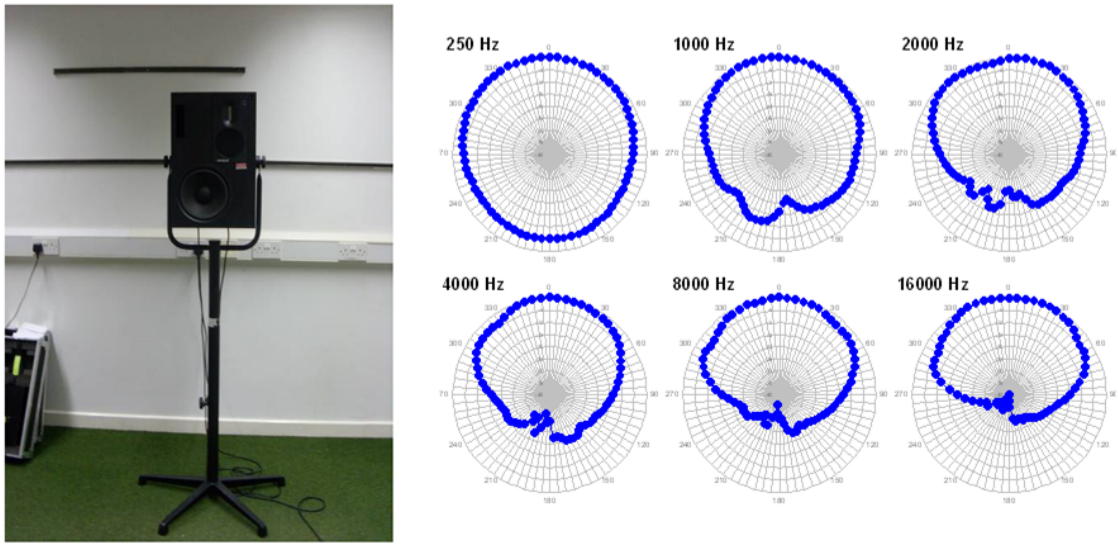

Figure 5.11 Genelec S30D (left) and its horizontal polar plots with 0° facing up for the octave bands of 250Hz, 1kHz, 2kHz, 4kHz, 8kHz and 16kHz, from [189] (right).

The main reason for using this directional source, instead of the omnidirectional source recommended in ISO3382 [55], is that the acoustic measurements for this study have been performed for auralization purposes, rather than for directly analysing the acoustic characteristics of the space. The measured impulse responses will be convolved with directional anechoic sources, such as voice or music [176, 190, 191]. Thus, any bias from effects caused by omnidirectional excitation should be avoided.

Secondly, the frequency response of the speaker, rated from 36Hz to 48kHz, has small variations in SPL (dB) values, as shown in Figure 5.12, and it is considered almost flat for the audible spectrum and so does not require any additional equalization [27] for the purposes of this study.

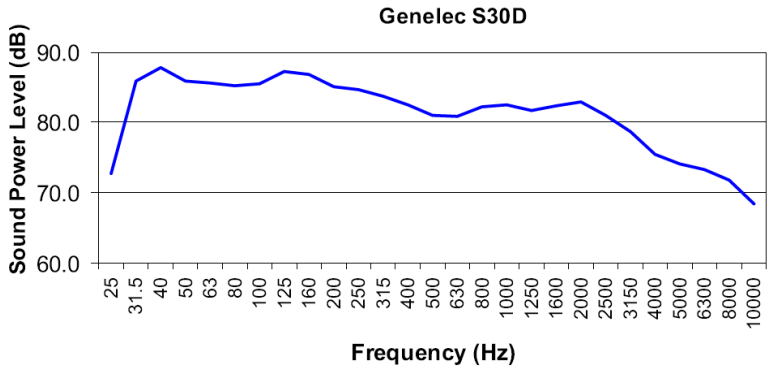

Figure 5.12 Frequency response of Genelec S30D cited in [27].

In addition, this loudspeaker is very convenient for in-situ measurements as it is both active, and can supplied with a digital input.

Microphone

For this study, a Soundfield SPS422B was used as the main receiver microphone. The Soundfield microphone captures B-format signals and consists of 4 channels: W, the omnidirectional component, and three figure-of-eight signals on the Cartesian axes, X for the horizontal axis, with position orientation pointing towards the front, Y for the horizontal axis pointing to the left, and Z for the vertical axis. The quoted frequency range of the Soundfield SPS422B is from 20Hz to 20kHz [192].

Playback system, hardware and software

For playback and recording, Steinberg Nuendo 2 was used. The chosen soundcard for this project was the RME Fireface 800, providing balanced mic/line inputs to record the microphone signals and a digital output to feed the Genelec. The signals were stored directly on the laptop during the recording process as 32 bit floating point files at 96kHz. This same equipment and measuring technique has been used for measurements in previous studies [9, 26].

Measurement Conditions

The atmospheric conditions are relatively stable in the studied space, as the leaded windows are internally supported with double glazing and the temperature and humidity are permanently controlled by the underfloor heating system. Thus,

during the measurement process the temperature was measured at a constant 21.5°C and the relative humidity at 44.5-45%, even though the measurements were taken over two complete days. The space was empty when the measurements were performed, without any audience or seating. A piano and harpsichord were the only additional features in the main space, with any other smaller items stored in the ground floor tower space.

Measured Positions of Sound Source and Microphone

The sound source was placed at a position within the space typical in terms of performer location, approximately at the middle of the length of the south wall and 1.66m distant from it, facing towards the north wall. Its height was set at 1.5 m. The SPL level during the measurements was calibrated at 94-95dBA at 1m distance from the source in order for the signal-to-noise ratio to be sufficient to limit background noise and avoid too much distortion at the speaker due to peak levels. For the microphone measurement positions, 26 receiver positions were used, for an appropriate acoustic coverage of the space, as shown in the following floor plan (Figure 5.13).

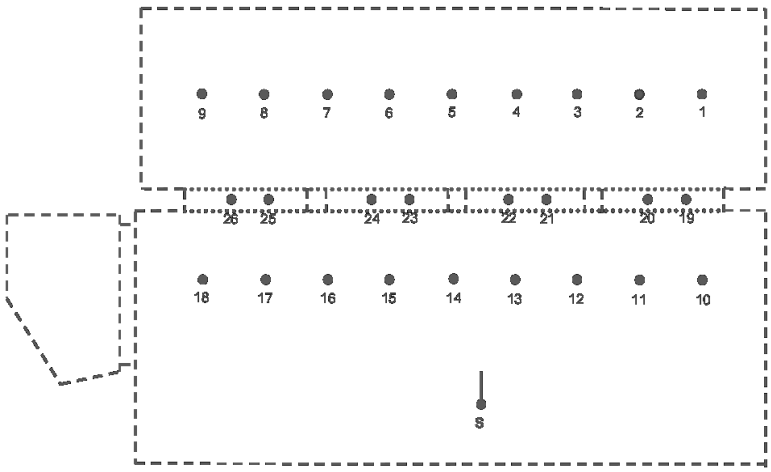

Figure 5.13 Floor plan of the church. The position of the sound source (S) and the 26 measurement positions are represented.

The receivers were placed in a marked grid (shown in Figure 5.14) consisting of three rows across the length; a first row of 9 receivers at the middle of the north

aisle, a second row of 9 receivers in the nave, symmetrical with the first one and a third row of 8 receivers between the columns.

Figure 5.14 Marked Grid on the floor for the positions.

According to the recommendations in ISO3382-2 [183] the distance of the source and receivers from the walls should be at least ¼ of a wavelength, which is approximately 1m for 125Hz. The distances between each measurement position and from the walls and columns are represented in Figure 5.15. The microphone was set at a height of 1.5m, in order to be at the same height as the source.

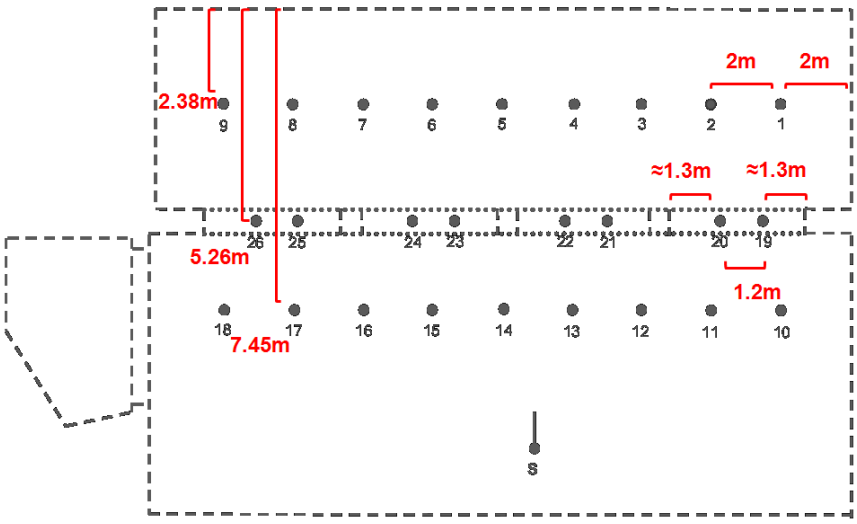

Figure 5.15 Floor plan of the church. Distances between the measurement positions and the boundary surfaces.

Each receiver was orientated towards the south wall of the church. As was explained in section 2.3.1, the critical distance is defined, based on Sabine's

approximation (equation 2.4), as a function of volume and reverberation time. Thus, as for these measurements the same positions were required for each of the acoustic configurations studied, the distances of each measurement position from the sound source were based on the maximum critical distance calculated from the three studied configurations of the panels and drapes, depending on the acoustic characteristics of the space. The longest critical distance calculated was 2.88m (observed from the less reverberant configuration, being Congifuration B), while the closest receiver, (R14), was placed at a distance of 3.6m from the sound source.

The final distance between sound source and each receiver position is listed in Table 5.3. It is worth mentioning, however, that receivers R2 and R5 have no direct line-of sight with the source.

Table 5.3 Distance between sound source and each of the 26 receiver positions. Left (L) is defined as the left side of the sound source.

Row 1		**Row 2**		**Row 3**	
Receiver Position	Distance from the source (m)	Receiver Position	Distance from the source (m)	Receiver Position	Distance from the source (m)
R1	11L	R10	7.8L	R19	8.6L
R2	9.9L	R11	6.1L	R20	7.7L
R3	9L	R12	4.6L	R21	6L
R4	8.5L	R13	3.6L	R22	5.7L
R5	8.5R	R14	3.5R	R23	6R
R6	9R	R15	4.5R	R24	6.6R
R7	9.8R	R16	6R	R25	8.8R
R8	11R	R17	7.7R	R26	9.8R
R9	12.3R	R18	9.6R		

Acoustic Characteristics and Configurations

Three configurations of panels and drapes were used during the impulse response measurements of this study based on the recommendations in Table 5.1:

- Configuration A, for "Opera/Musical" events, with RT values of 1.2s,
- Configuration B, for "Lectures/speech" events, with RT values of 1s, and

- Configuration C, for "Music recitals" events, with RT values of 1.5-1.8s.

For the measurements in configuration A, the acoustic panels of the north wall were folded in half as shown in Figure 5.16.

Figure 5.16 Acoustic panels set at the north wall. The 28 square absorbing panels (on the left) are folded in half, replaced by 14 reflecting panels (on the left).

During the measurements, the loudspeaker remained in the same position while the acoustic panels and drapes were set respectively for configurations A, B and C. The Soundfield microphone then captured the usual responses for each configuration, for each receiver position and source orientation.

Sound Directivity

The influence of the directionality of the source was also examined in this study and hence, during the acoustic measurement, impulse responses were captured with the Genelec rotated on its axis for the same receiver positions for configuration A. As shown in section 4.2.3, through the shoebox experimental model, the effects of Genelec orientation was studied by observing the variations in T30 and C80 values. Based on these results, the loudspeaker was rotated 40° and 70° right respective to its original orientation.

5.5 *Computer Modelling*

The acoustic model of St. Margaret's Church was designed by using two commercial software packages, CATT-Acoustic v8.0j and ODEON 10.1 Auditorium,

both based on hybrid geometrical algorithms, as described in detail in section 3.3.3. The acoustic modelling of a space depends on many factors and not all of which can be controlled by the user. However, depending on the software, some of these parameters can be manipulated by a user with the necessary skills and experience. In the Round Robin tests [29, 73] of room acoustic computer modelling, variations in modelling methods were observed regarding:

- the level of geometric details (number of surfaces),
- the number of rays used for the calculations,
- reflection order,
- inclusion of diffuse reflections and edge diffraction,
- length of impulse response.

For the modelling process in this current study, for both of the simulation software packages used, previous acoustic modelling projects as well as personal communications between the author and the software developers have been used as guidelines. The aim was to examine the perceptual effect of variations in obtained acoustic parameters, and different versions of the space were designed based on the actual acoustic configurations used during the acoustic measurements process. The models were created in such a way that existing acoustic panels and drapes will be easily altered by any other user from opened to closed. The modelling procedure followed with both software packages was the same;

1) import the geometrical data of the space (after considering which surfaces and how detailed a model was necessary),

2) determine the absorption and scattering coefficients for the materials included,

3) define the source and receiver positions,

4) choose appropriate settings for the calculation process,

the steps of which are explained in more detail below.

5.5.1 **Designing the model**

Architectural characteristics

The first draft of the model was developed based on the architectural plans created during the refurbishment of the space [187]. However, as the space was not symmetric and the outer walls were not exactly parallel to each other in the supplied plans, it was considered best to have an accurate model in terms of the main dimensions. Hence, these dimensions were later altered based on physical measurements of St. Margaret's Church in its current state. This also incorporated the physical measurements of additional objects and furniture which had not been included in the original architectural plans.

Modelling process

It is possible to convert the geometry data for the space from other CAD-platforms in both CATT-Acoustic and ODEON. However, for the current study the geometries were imported manually for each included surface based on a coordinate system. This method was a much more time consuming process, but the user has total control of surface corner locations and their identifications. The data for surfaces and corners is listed and numbered based on the modelling order, which has the advantage of making changes very easy if necessary for future studies.

There are no standards providing recommendations about the level of the geometric details which should be modelled - this depends mainly on the skills and the experience of the user. Previous studies have shown that the final results can be modified either by the user, or depend on the algorithm that has been used [73]. In the 2nd Round Robin [29], the number of surfaces in the participating models varied from 94 to 3530 surfaces. There were also participants that had used the same .DXF files as the basis for their models, although significant differences were observed between results. However, there is an important rule that should be followed for acoustic modelling. Apart from being impossible to simulate every detailed object and structure within a space, an extremely detailed model would cause an increase in the number of the reflection order, leading to a loss of accuracy in the results, especially for low frequencies (as discussed in section

3.3.3). Some exceptions have been reported, such as in open air ancient theatres, where due to the lack of strong reflections for the ceiling, geometrically detailed surfaces are necessary for the accurate prediction of early reflections [16].

Following recommendations in previous works about the steps to be taken in the modelling procedure [16], the construction of the model geometry started with the basic boundary elements of the space.

The floor and the ceiling were modelled as flat large planes. As the vaults in the ceiling (shown in Figure 5.10) were not modelled in detail, the sloping flat surfaces of the ceiling were defined with higher values of scattering, as will be explained below.

For modelling the boundary walls, in order to include the surfaces of the windows and doors, a different process was followed due to differences in the modelling requirements of CATT-Acoustic and ODEON [193, 194]. In CATT-Acoustic, the walls were subdivided in smaller surfaces, as shown in the example in Figure 5.17, modelling the north wall. In ODEON, the walls are modelled as single surfaces around the window areas, as shown in Figure 5.18.

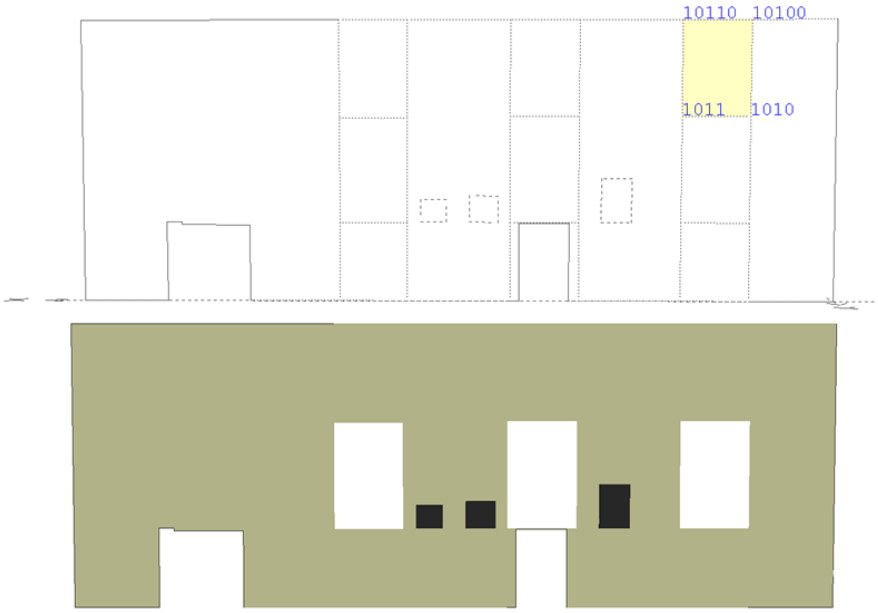

Figure 5.17 Modelling walls using subdivision of surfaces in CATT-Acoustic. This represents an example of the north wall. In the top image, the wall subdivisions can be observed, while in the bottom image, the wall is represented as a single surface using the 3D viewer tool. The stone memorials were also included as subdivisions in the wall surfaces.

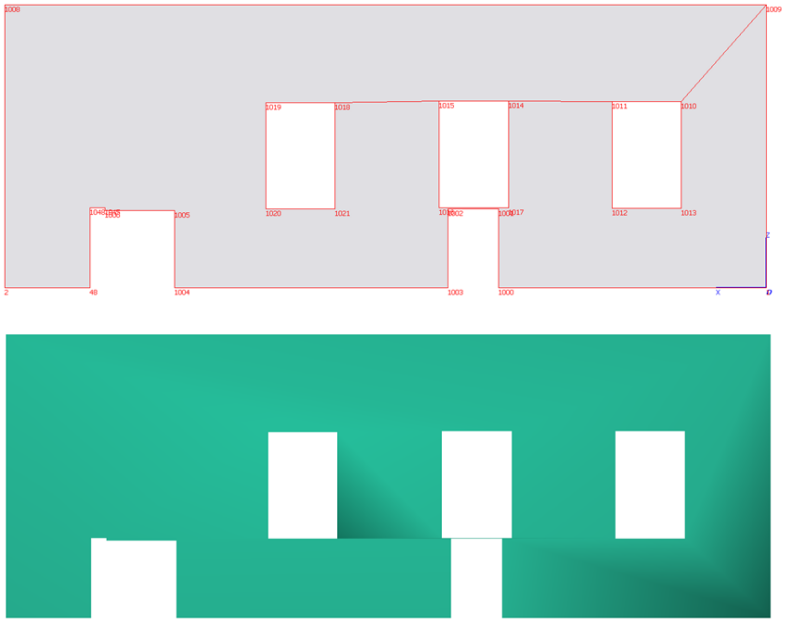

Figure 5.18 Modelling walls as a single surface in ODEON. This represents an example of the north wall. In the top image, the wall has been modelled as a single surface, while in the bottom image, the wall is represented using the 3D OpenGL tool.

The door and window surfaces were then mounted on the appropriately defined areas of the walls, and thus, overlapping surfaces were avoided for these main parts of the structure.

The simulation of curved surfaces is a general problem in such acoustic models, as only straight lines can be defined. As a result, curved surfaces can only be designed as a summary of subdivided plane surfaces. This does mean that scattering and absorption effects can be calculated differently than what might occur in reality. This was a problem for the current model, when it came to defining the arches on the top of the columns and some of the windows. These surfaces had to be modelled in a more detailed fashion, including small subdivision of surfaces, as shown in Figure 5.19.

Figure 5.19 Modelling arches between the columns and at the top of the windows using subdivision of surfaces. On the top left, the CATT-Acoustic model is represented, on the top right, the ODEON model, and at the bottom, the actual space is pictured.

In previous work [30], tables were modelled either as 2D plates, 3D planes or boxes. In this model, large interior objects such as tables, pianos, cupboards or the wooden frame across the length of the bottom of the walls were simulated as simple

boxes, excluding those surfaces of these objects which were abutting on other main structure surfaces.

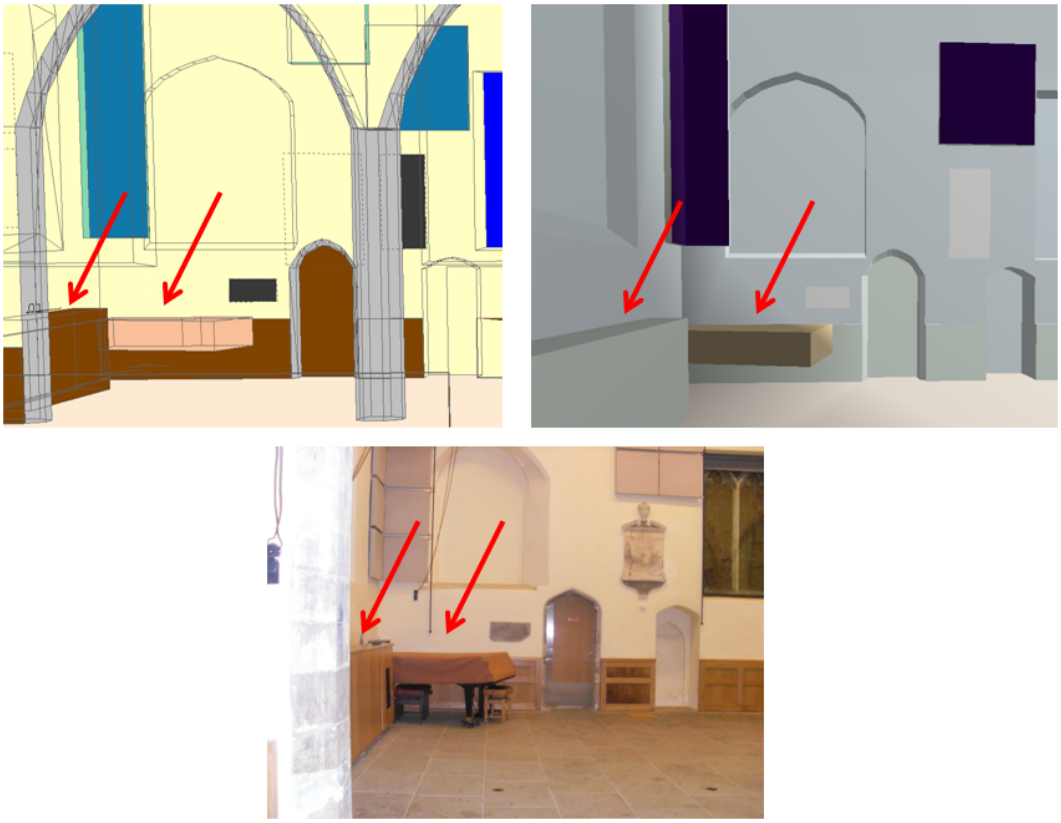

Figure 5.20 Modelling interior objects; a piano and a wooden cupboard, in CATT-Acoustic (top left) and in ODEON (top right) based on their dimensions and locations in the actual space (picture at the bottom).

The stone memorials on the walls were simulated as 2D plates. In CATT-Acoustic, they were included as subdivided surfaces in the main wall surfaces, as shown in Figure 5.17. In ODEON, the stone memorials were modelled at a distance of 5mm from the walls, in order to avoid overlapping surfaces. This was because in some cases of overlapping surfaces, it might not be clear which absorption characteristics should be used by ODEON between two overlapping surfaces with different absorption [30].

Both sides of the reversible absorbing panels were simulated, giving the user the ability to exert a great deal of control over which ones should be activated; the opened or closed one, depending on the requirements of the configuration in each case. An example of these settings is presented in Appendix B, for both CATT-

Acoustic and ODEON. However, the groups of two to ten panels were modelled as single surfaces, as shown in Figure 5.21, demonstrating the north wall (as pictured in Figure 5.16).

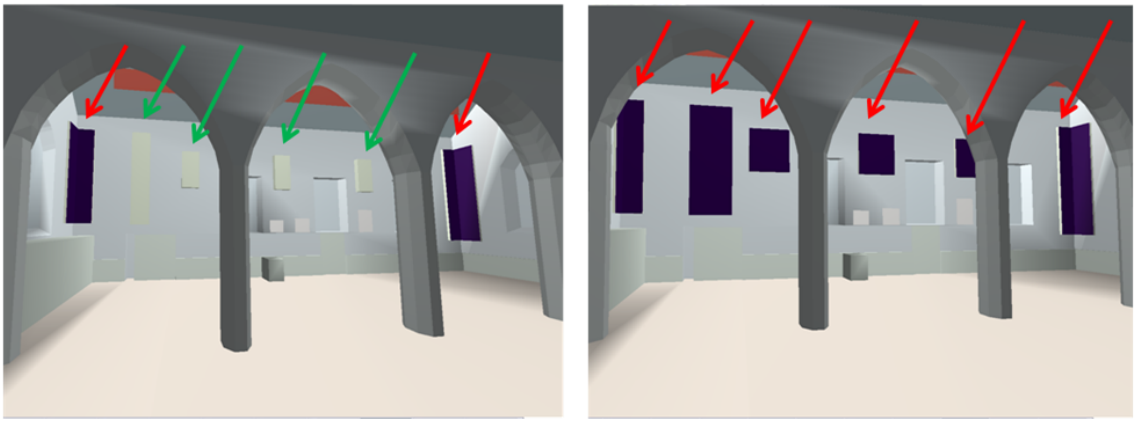

Figure 5.21 Modelling groups of acoustic panels, as demonstrated with ODEON. The red arrows are pointing at the opened panels, the green arrows at those closed. The left model is based on configuration A and the right model on configuration B.

As it was considered better to model the drapes on the ceiling as single 2D plates, it was necessary in CATT-Acoustic, to duplicate and flip one of them, as the software takes into account the acoustic properties of a surface from only one side.

Finally, the models were checked for overlapping or wrapped surfaces, which can lead to incorrect calculation of the related absorption characteristics. The 3D tools (such as the 3D viewer, 3D OpenGL, and 3D Investigate rays) provided in both software were used to detect these kind of error during the modelling process. In addition, the models were checked for loss of rays.

5.5.2 Calibrating the Model

The defined acoustic characteristics of the surfaces in the model plays a crucial role in the accuracy of the acoustic results of the simulated space. Defining these characteristics is quite a challenge for acousticians [6, 30, 173] and users of such computer modelling software, and depends on their skills and experience [29, 34]. The main limitation is that the user has to rely on the materials provided in the existing libraries for absorption and scattering coefficients. It is not likely that an exact material will be found for the specific materials of a given project and it must

also be remembered that these characteristics will be both frequency and angle dependent, and the current state-of-the-art does not provide acousticians with sufficient data for these requirements. Round Robin tests (as discussed in section 3.3.4) have shown that such data is of the underestimated when based on the users' judgement [29, 30, 73].

The scarce availability of absorption coefficient data in the literature can be circumvented by taking in-situ absorption coefficient measurements of the boundaries. A considerable number of relevant previous studies have been performed to describe absorption coefficient measurements for surfaces used in computer modelling [5, 33, 34, 195]. There are also interesting measurements of absorption coefficients performed in-situ, mainly based on the method proposed by Garai [196]. However, the methods are still at a preliminary stage and cannot be used for reliability acoustic modelling purposes with the required accuracy. The main problem that still needs solving is how to factor into the geometric algorithms the angle dependent absorption coefficients, as previous experiments have shown that the values can vary significantly depending on the incident angle of the reflection [197].

For the acoustic characterisation of the surfaces included in the St. Margaret's Church model, existing libraries have been searched, as well as absorption and scattering coefficient data used in previous work, modelling similar spaces [16, 20, 24, 29, 30, 155, 157, 168, 170, 198]. This also includes ODEON software default models based on the ERATO projects, for the Hagia Irene church and Jerash theatre.

As well as gathering information about absorption coefficients from the literature, it is commonplace to use acoustic measurements of the actual space, when these are available, as a reference for the model calibration [16, 153, 155].

For the current study, it was considered that optimisation based on matching the average values of reverberation parameters, as often applied in prior work, does not guarantee the accuracy of the results, as explained in the following chapter. Thus, the absorption coefficients of the walls were adjusted after a more detailed examination of early reflection energy observed in W-channel B-format waveforms obtained from modelled and measured impulse responses for each measurement

position. It was observed that by varying the wall absorption coefficients provided by CATT-Acoustic and ODEON material libraries between several "wall materials" with plaster or without, painted or not, significant changes in the results were obtained. This optimisation was based on the measured impulse responses for configuration A, with the assumption that these measurement results are sufficiently accurate. Thus, the model calibration was based on the results of configuration A, with the same coefficients then copied for configurations B and C. As an example, Figure 5.22 and Figure 5.23 present the values of T30 obtained for R17, for configurations A, B, C for both models and measurements.

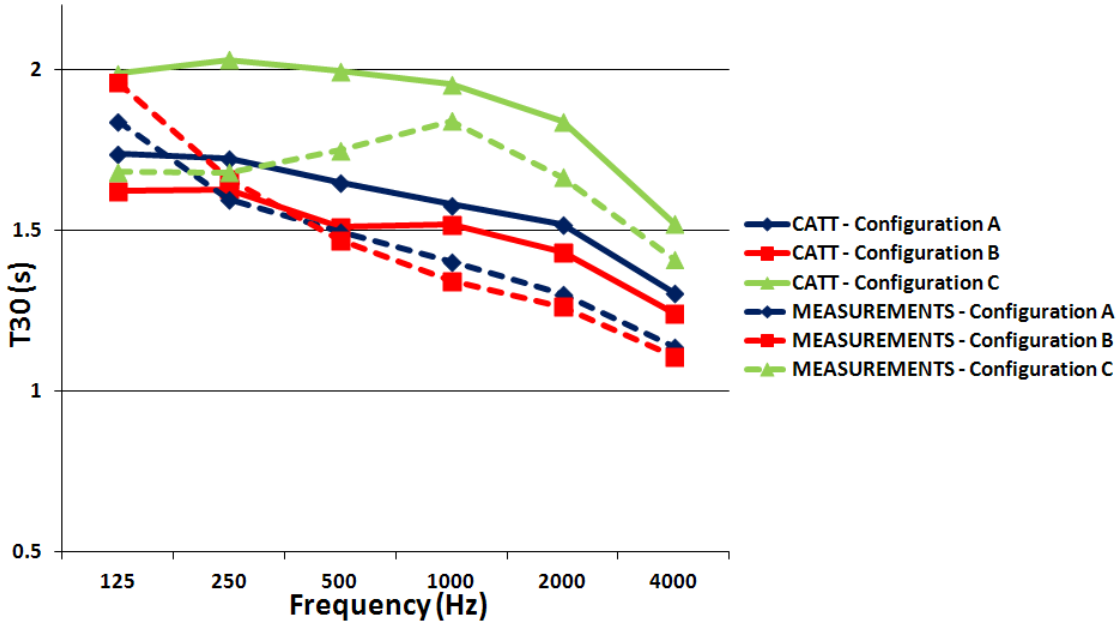

Figure 5.22 Comparing T_{30} values observed from R17 in CATT-Acoustic models and impulse response measurements for the three configurations.

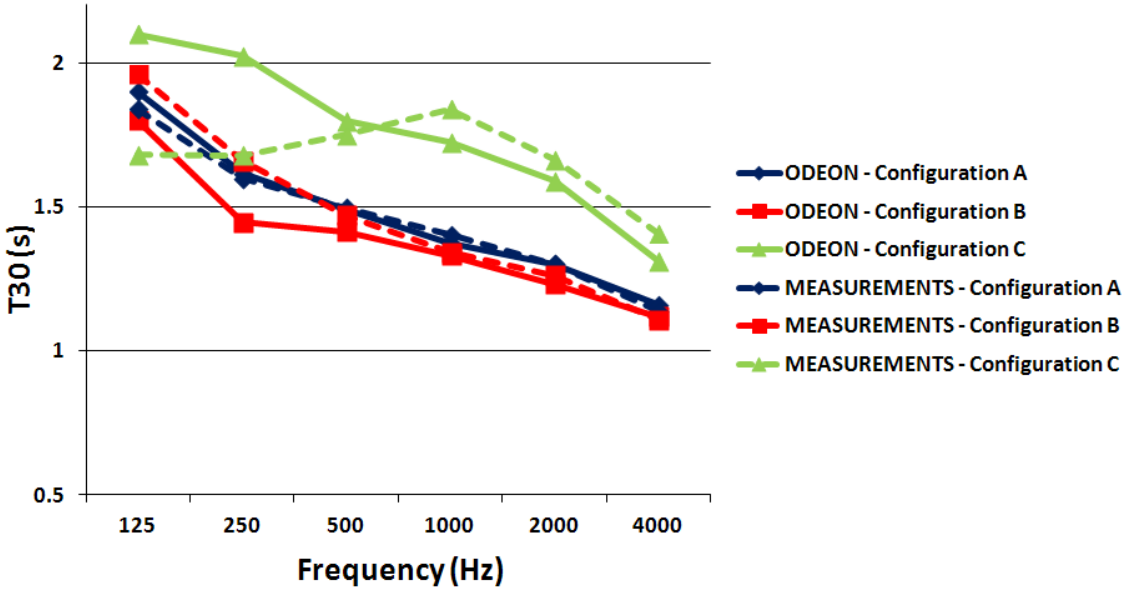

Figure 5.23 Comparing T_{30} values observed from R17 in ODEON models and impulse response measurements for the three configurations.

It can be observed from these results that even if the values of the T30 parameter for configuration A are in agreement, clear differences can be observed for the same values across configurations and modelling software.

Additional experimentation could be undertaken at this stage to optimise the results further. However, the aim of this study is not to create accurate acoustic models and compare the results, in either objective or subjective terms, with those obtained from the acoustic measurements. Rather the aim is to investigate the perception of variations in objective acoustic parameters via auralization; hence the conditions studied are based on the experience of the author and the acoustic information available about the surface materials used. Thus, further optimisation of the models against the measurement data is not desirable for this work.

Note also, that the results do not agree with the acoustic characteristics provided by the designers in Table 5.1. This could be due to differences in the measurement methods used as the approach taken here has been developed after the original design and construction work took place, as evidenced in Figure 5.24.

Figure 5.24 Evidence for the gunshot method used by Arup Acoustics for the acoustic measurements carried out in St. Margaret's Church during the development of the space in 1998 [185].

Summarising, for the calibration of the model the following steps were followed:

- gathering information about absorption coefficients from the existing libraries and literature of previous modelling work,
- using the W-channel B-format waveforms of the measured impulse responses of the actual space as a reference for the model calibration, and comparing their early reflection energy with those observed from the corresponding modelled positions, the absorption coefficients of the walls were re-adjusted,
- this detailed examination was carried out for each measurement position from configuration A, instead of optimising the average values of reverberation parameters, as often applied in previous work,
- scattering coefficients were based on user's estimation of the roughness and dimensions of the surfaces, compared and confirmed for their validity with previous modelling works, and finally,
- the same absorption and scattering coefficients were then copied for configurations B and C.

Hence, the final absorption coefficients used to define the acoustic properties of the surfaces in CATT-Acoustic and ODEON are listed in able 5.4 and Table 5.5, respectively [199].

Table 5.4 Absorption coefficients of the materials used for modelling St. Margaret's church in CATT-Acoustic, values presented in %.

Materials	125Hz	250Hz	500Hz	1000Hz	2000Hz	4000Hz
Main Floor	1	2	3	7	9	10
Main Wall	11	8	7	6	5	5
Windows	1	7	5	3	2	2
Wood	10	7	5	4	4	10
Stone	8	06	6	4.5	4.5	6.5
Ceiling	10	15	13	7	10	8
Black Hole (open gate for the tower) *	80	80	80	80	80	80
Plastic	10	25	45	58	65	70
Fabric	3	4	11	17	24	35
Marble	1	1	1	1	2	2
Dark Wood	10	7	5	4	4	10
Reflector	15	3	3	4	5	14
Absorption	90	92	100	98	83	6
Drapes	14	35	55	72	7	65

*The surfaces marked in grey were less important as they cover small areas.

Table 5.5 Absorption coefficients of the materials used for modelling St. Margaret's church in ODEON on a scale from 0 to 1.

Materials	63Hz	125Hz	250Hz	500Hz	1000Hz	2000Hz	4000Hz	8000Hz
Main Floor	0.01	0.01	0.02	0.03	0.07	0.09	0.1	0.1
Main	0.11	0.11	0.08	0.07	0.06	0.05	0.05	0.05
Windows	0.1	0.1	0.07	0.05	0.03	0.02	0.02	0.02
Wood	0.1	0.1	0.07	0.05	0.04	0.04	0.1	0.1
Stone	0.1	0.08	0.06	0.06	0.045	0.045	0.065	0.055
Ceiling	0.3	0.1	0.15	0.13	0.07	0.1	0.08	0.08
Black Hole (open gate for the tower) *	0.8	0.8	0.8	0.8	0.8	0.8	0.8	0.8
Plastic	0.1	0.1	0.25	0.45	0.58	0.65	0.7	0.7
Fabric	0.03	0.03	0.04	0.11	0.17	0.24	0.35	0.35
Marble	0.01	0.01	0.01	0.01	0.01	0.02	0.02	0.02
Dark Wood	0.1	0.1	0.07	0.05	0.04	0.04	0.1	0.1
Reflector	0.03	0.15	0.03	0.03	0.04	0.05	0.14	0.14
Absorption	0.66	0.9	0.92	1.00	0.98	0.83	0.6	0.69
Drapes	0.14	0.14	0.35	0.55	0.72	0.7	0.65	0.65

*The surfaces marked in grey were less important as they cover small areas.

In reality, scattering effects depend on the wavelength of the sound (as a wave) being compared with the dimensions of the reflecting surfaces. In practice, this means that the scattering coefficients increase at high frequencies, as explained in the previous chapter (section 3.3.2). Geometric acoustic software designers have found different ways to include this wave-based effect in ray-tracing calculations, but require that the users define the scattering coefficients of the surfaces modelled. The available data, relating to the scattering characteristics of materials is, however, very limited and at a relatively early stage of research [195, 200-203].

Empirical information is provided for only a limited number of octave bands, even though the importance of frequency dependence in relation to scattering has been repeatedly discussed in the literature [20-22, 74, 127, 147, 182]. Hence, an accepted solution for this problem is to estimate the coefficients, mainly by the size of the geometrical irregularities [153]. The guidelines provided by the acoustic simulation software developers suggest using high scattering coefficients for large surfaces that have not been modelled with significant detail [34, 193, 194]. This is a way to simplify complicated geometries and to achieve sufficiently accurate results, a method that has been used in the current study for modelling the ceiling as flat single surfaces and to define high scattering coefficients for the materials, in order to take into account the non-modelled vaults of the ceiling. Additionally, it is suggested not to use the extreme values of 0 and 1, while it is recommended for highly irregular surfaces to use a maximum value of 0.7, and for smooth, large surfaces, values between 0.05-0.1 [107, 166].

The scattering coefficients for the St. Margaret's model are defined and implemented differently for CATT-Acoustic and ODEON simulation software. With ODEON, the user specifies the scattering coefficient for the middle frequency of 707Hz, and then ODEON expands these coefficients into values for each octave band based on the curves provided in Figure 5.25 [166, 194, 204].

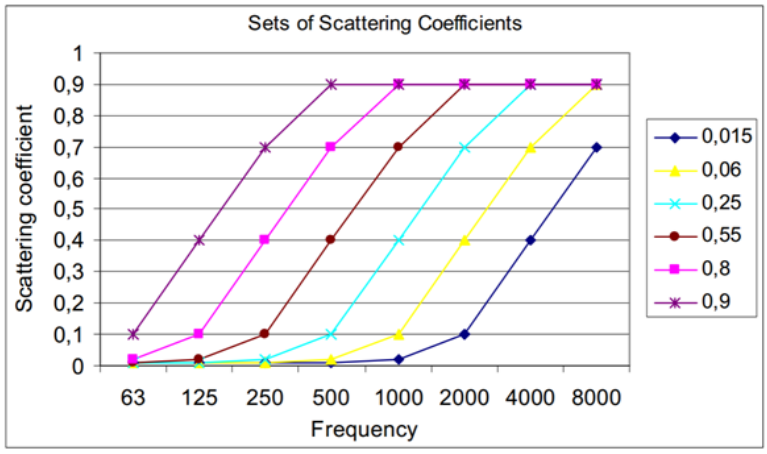

Figure 5.25 Frequency dependent scattering coefficients for materials with different surface roughness as used in ODEON [204].

The scattering coefficients used for the ODEON model were defined separately for each surface, based on their irregularities. This means that different surfaces with

the same material do not necessarily have the same scattering coefficients. Generally, scattering coefficients values were defined as 0.1 for large planar surfaces, wooden doors, smooth wooden furniture, absorbing panels; 0.05 for smaller wall surfaces (such as walls around windows) as well as glazed window surfaces; 0.15 for wooden carved surfaces (such as cupboards and frames across the walls); 0.2 for stone surfaces; 0.5 for the wooden beamed ceiling which was modelled without considering the details of the structure. The stone memorial scattering coefficients varied between 0.1 and 0.2 depending on the amount of carving they featured. There are all listed in Table 5.6.

Table 5.6 Scattering coefficients of the materials used in the ODEON model, on a scale from 0 to 1.

Materials	**707Hz (default value)**
Main Floor	0.1
Main Wall	0.1
Windows	0.05
Wood	0.1 – 0.15
Stone	0.2
Ceiling	0.5
Black Hole (open gate for the tower)	0.05
Plastic	0.1
Fabric	0.1
Marble	0.1 – 0.2
Dark Wood	0.1
Reflector	0.1
Absorption	0.1
Drapes	0.1

In CATT-Acoustic, scattering coefficients are defined for each of the materials used (not for individual surfaces, as occurs with ODEON) and the user is required to specify the scattering coefficients for each of the octave bands. To simplify the estimation, the function "*estimate (x.xx m)*" was used for some of the materials. With this function, the scattering coefficients across the octave bands are estimated based on the roughness of the surfaces, calculated in metres. For instance, if the vaults of a corrugated ceiling are 0.4m in depth, the user should use the function as follows: "*estimate (0.40 m)*" [193]. Thus, for the current study the roughness of the wooden surfaces, the vaults of the ceiling and the featured marbles of the stone memorials were estimated by the author for this model. For the rest of the materials, as the definition of scattering coefficients in a frequency dependent manner is a challenge, it was considered better to estimate these values based on

the curves provided by ODEON (Figure 5.25). Additionally, the values were compared and confirmed for their validity with previous modelling works in CATT-Acoustic, where scattering coefficients were reported [24, 157]. The final scattering coefficients used for CATT-Acoustic model are listed in Table 5.7.

Table 5.7 Scattering coefficients of the materials used with the CATT-Acoustic model, values presented in %.

Materials	125Hz	250Hz	500Hz	1000Hz	2000Hz	4000Hz
Main Floor	12	14	14	15	16	17
Main Wall	12	14	14	15	16	17
Windows	12	14	14	15	16	17
Wood	(estimate (0.02)					
Stone	12	14	14	15	16	17
Ceiling	(estimate (0.4)					
Black Hole (open gate for the tower)	12	14	14	15	16	17
Plastic	12	14	14	15	16	17
Fabric	12	14	14	15	16	17
Marble	(estimate (0.05)					
Dark Wood	12	14	14	15	16	17
Reflector	12	14	14	15	16	17
Absorption	12	14	14	15	16	17
Drapes	12	14	14	15	16	17

However, it is very important to note that there is a strong inter-dependent relationship between the defined absorption and scattering coefficients. It has been reported in several works that by changing one of these parameters, a re-adjustment of the other will be necessary for matching real world sound propagation behaviour [16, 22, 34].

5.5.3 **Virtual sound source and receivers**

The source and receiver points in the acoustic models were located at exactly the same positions as they were for the measurement process (section 1.1). The data was imported with the use of the model coordinate system. Both CATT-Acoustic and ODEON software consider receivers and sound sources as points with no physical size. However, the directivity of the source is taken into account and the user can select the appropriate one from the libraries provided in both packages, or create a directivity pattern in plot editors in a frequency dependent manner, as shown in Figure 5.26.

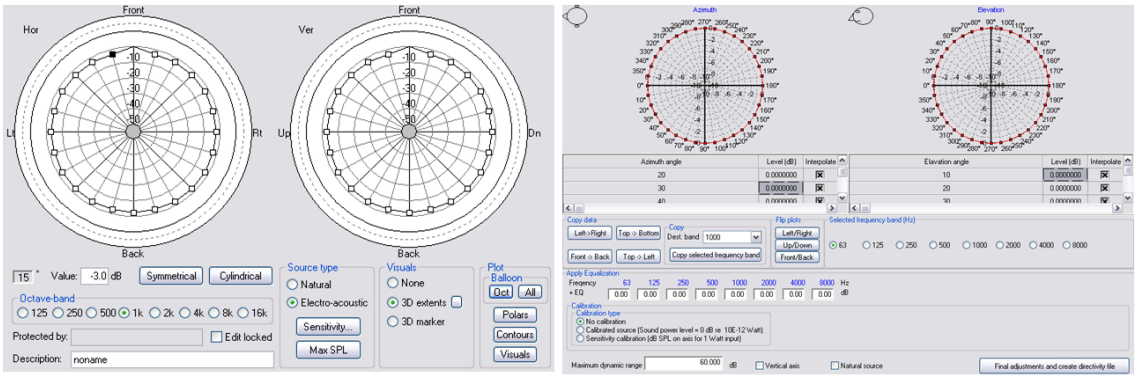

Figure 5.26 Editor tools for creating source directivity patterns in CATT-Acoustic (left) and ODEON (right).

For the current study, the user designed the characteristics of the sound source, based on the 2D source directivity data for the Genelec S30D, available from [189] and shown in Figure 5.11. Thus, an approximate 3D plot for the virtual source in the simulated model was created, as shown in Figure 5.27.

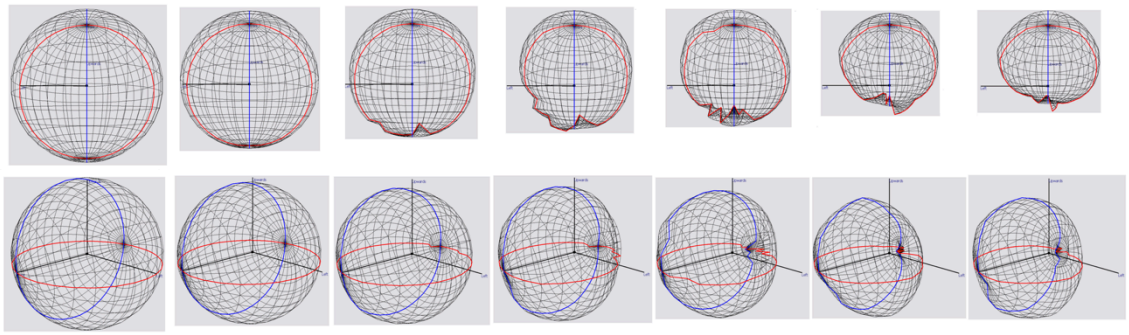

Figure 5.27 3D Directivity plots of the virtual Genelec S30D as used in the simulation source (azimuth top, and elevation bottom), across the octave bands 125Hz, 250Hz, 500Hz, 1000Hz, 2000Hz, 4000Hz and 8000Hz.

In addition, the receiver's head direction was defined, as the microphone was aligned towards the south wall for each location during the acoustic measurements in the actual space.

With CATT-Acoustic, the head direction of each receiver is defined by adding optional coordinates to the receiver data, such as;

```
r id        r x , r v , r z          h x , h v , h z
Receiver    Receiver  location       Optional individual head direction
```

With ODEON, the option for the receiver's head direction is limited to the option of pointing the receiver towards a source. For this reason, as the Genelec location was not ideal for this scenario, additional virtual non-active sources were created as mirror "receiver" points toward the south wall. Hence, each receiver position was matched with the corresponding mirror source, while the sound was produced only from the main Genelec location, as shown in Figure 5.28.

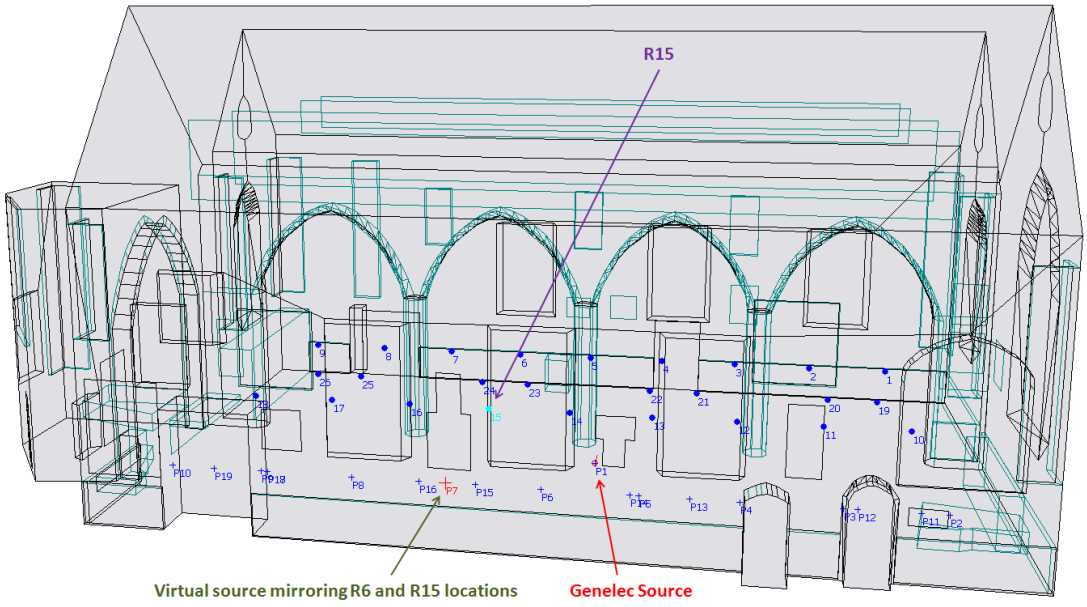

Figure 5.28 Demonstration of the virtual non-active sources at the south wall, represented with a cross symbol. The active source is indicated as P1 at the middle of the length of the south wall. In this example, the R15 is pointing towards the non-active P7 source, while the sound is produced by the virtual Genelec source.

5.5.4 General Settings in Geometric Software

The total number of surfaces used for the St. Margaret's model, as well as the total surface area calculated varied, depending on the software and the different versions of the model, according to the acoustic configurations A, B and C. The average number of surfaces across all three configurations in both simulation software CATT-Acoustic and ODEON was 980, while the approximate average surface area was estimated to be 1900 m^2.

The number of rays used for the calculations was defined at 50,000 and this was considered sufficient for all the model versions, as results did not show significant changes in the calculated acoustic parameters as this number was increased [133,

159]. The impulse response length was defined at 2000ms and atmospheric conditions were set to those noted during the actual measurement process i.e. 45% humidity and 21.5 °C.

Additional settings in CATT–Acoustic fixed the ray truncation time at 2500ms. This is the time needed for rays to be traced and it is recommended that it is set to be greater than the estimation of the reverberation time [193].

For ODEON, the settings included a Transition Order (T.O.) of 2, as the "safe" recommendation by the developers [194]. As explained in p.54, the developers of ODEON originally recommended the adjustment of T.O. values according to the complexity and shape of the space [30, 198]. However, from version ODEON 8 onwards, results are no longer significantly affected by the value of T.O..

As has been mentioned already, good results can be obtained regardless of how detailed the model is providing the appropriate settings in the software are applied, based on the skills and experience of the user [12, 16, 34, 155, 168]. Hence, the settings for the software reported in this section are considered appropriate for the current models but re-adjustments will be necessary when other parameters in the models change. For example, if the number of surfaces changes the number of rays used will also need to change.

5.6 *Summary*

In this chapter, St. Margaret's church has been introduced and its architectural and physical characteristics have been described. With respect to the hypothesis of this thesis, the space was chosen to apply the three different auralization techniques being considered. The advantage of this specific space, St. Margaret's Church, in York, is that after the renovation and the acoustic treatment, its physical acoustic characteristics can be easily changed through sets of acoustic panels and drapes. Hence, variations in the obtained acoustic parameters can be easily changed and controlled by the researcher. For the purpose, of this study, three configurations of panels and drapes have been used.

The basis of these three auralization techniques have been described in detail. First, impulse response measurements were carried out in the actual space, by using the currently most reliable measurement technique, which is based on the

exponential sine sweep signal. The equipment, the sound source and the microphone used for the measurements have been introduced. The space was tested in different acoustic conditions, across a grid of 26 receiver points covering the audience area and with variations in the orientation of the loudspeaker.

Additionally, two commercial acoustic simulation software packages, CATT-Acoustic and ODEON, were used for modelling the same space based on geometric algorithms. The modelling technique has been described in detail, with respect to the requirements of each package. The models were firstly developed based on the architectural plans and physical measurements of St. Margaret's Church in its state. The level of geometric details was discussed based on recommendations in previous works. The models have been calibrated by using suitable absorption and scattering. Different versions of the model have been used in order to simulate the different acoustic configurations, while a virtual grid of 26 receiver points was used for generating impulse responses, corresponding to those captured during the in-situ impulse response measurements.

The next chapter will consider the objective data derived from the obtained impulse responses, by observing the relevant acoustic parameters for each of the three auralization methods, for each configuration and source/receiver combination.

Chapter 6.
Analysis of Objective Acoustic Parameters of St. Margaret's Church

6.1 *Introduction*

So far, the methodology that was followed in order to capture/produce the impulse responses required for the auralizations proposed in this study, have been explained. The three auralization techniques have been introduced in detail and the studied space, wherein these techniques were applied, described based on the space's physical acoustic characteristics and their exploitation for the investigation of the hypothesis of this thesis.

It was considered necessary to determine a common method for the calculation of the objective acoustic parameters derived from these impulse responses. These have been obtained from both acoustic measurements and acoustic simulation models, using CATT-Acoustic and ODEON. The calculation method is described in detail in the current chapter, followed by the analysis of the results obtained from the acoustic parameters. For the representation of this data, "acoustic floor maps" are introduced, combining position and frequency dependent characteristics.

6.2 *Acoustic Parameters as Design Variables*

Room acoustic parameters are the traditional way to represent and understand the acoustic characteristics of a space in objective terms. However, the observed parameters are often not strongly related to the perception of the acoustics of a given space [205]. The goal of this study is to establish an interpretation of the observed objective results in relation to the perceptual results also obtained. The

key parameters are clearly listed in ISO3382 [55], and most commonly presented and interpreted in related literature.

The acoustic parameters can be categorised into time relative parameters (RT_{60}, T_{30}, T_{20}, EDT) and energetic parameters (C_{50}/C_{80}, Ts, D_{50}, LF, IACC). Another important categorisation of these parameters is based on the spatial information that they might provide. Thus, RT_{60}, T_{30}, T_{20}, EDT, Clarity, Ts, D_{50} are defined as *monoaural* ISO parameters, while LF and IACC are *3D spatial parameters*.

With respect to the most important subjective aspects of the acoustic perception of a space, Jordan [206] suggested a group of parameters where each of them express a) the reverberance of the space, b) location variations or c) the sense of involvement, considering the influence of the frequency dependence of the parameters as well.

Reverberance impression

Of the time relative parameters, reverberation time (RT_{60}) is the oldest and most commonly used parameter for the description of room acoustics. It describes the time it takes for a sound to decay 60dB in the space after the source has been turned off. However, as stated in recent approaches [16, 18], optimisation of reverberation time in an acoustic simulation model does not imply optimisation of the remaining parameters. This is because the reverberation time is a global parameter for the space and it is not expected to change significantly with spatial variation.

A more detailed view of the first 10dB of decay of sound is provided by the early decay time (EDT). However, in practice reverberation time (RT_{60}) and EDT differ as the latter depends more on the energy of early reflections and hence on the geometry of the space and the source/receiver positions within it [34]. Based on Jordan [206], EDT is assigned "the role of leading criterion" and as referred into ISO3382 [55] is strongly related with perceived reverberance.

Sense of source directivity

In addition to EDT, acoustic position dependent variation and the sense of source directivity can be very well expressed with the Clarity (C_{80}/C_{50}) parameter. As defined, C_{80}/C_{50} expresses the ratio of early-to-late energy and is dependent on the

geometry of the space [170] and the distance from the source. C_{80}/C_{50} is inversely correlated with the reverberation parameters, and directly with sound pressure level (SPL) [30, 206]. However, positions with the same observed reverberation time could have significant differentiation in EDT and Clarity values as an effect of the changes in early reflections.

Sense of spatial impression

Spatial impression is correlated with a sense of involvement, of being "immersed" in the sound [206], and depends on the ratio of lateral and total energy arriving at the receiver. Hence, it is also related to LF which is also dependent on these quantities [55].

For this study, as measured high definition impulse responses from the actual space using the Soundfield microphone, spatial parameters can also be studied based on the W and Y channels, and as used in [26, 85, 88]. However, factors that cannot be completely controlled should be taken into account when considering 3D parameters. As the aim of this thesis is to investigate the influence of the variations of acoustic parameters on our perception, we were trying to avoid any bias irrelevant to the hypothesis factor, caused for example from the reproduction system used, or the physical aspects of the listening room. Thus, it was decided that the current study be limited to monoaural parameters only.

It is reasonable to consider that the same principles that determine the use of the objective parameters presented above for the acoustic perception of the space, should be considered similarly for auralization. Previous studies have been based on the study of T_{30}, EDT, Clarity (C_{50}/C_{80}), and in some cases Centre Time and Definition [5, 18, 73, 81, 89]. It is worth mentioning in Round Robins surveys, computer simulation programs had shown a relatively higher error, in respect to the JND values, for the calculations of T_{30} and EDT [34] and EDT and Clarity (C_{50}/C_{80}) [73], while parameters such as Ts, G, LF and LFC can be calculated more easily with values close or below the JND values.

Therefore, for the investigation of how variations of the acoustic characteristics of a simulated space might affect the perceptual results, the current work will focus on those parameters which are commonly used in room acoustics and auralization studies, namely T_{30}, EDT, C_{80} and C_{50}. In addition, as described above, the values of these acoustic parameters have shown higher level of variations, in respect to the

JND values, than Ts, G, LF and LFC. Once these first parameters be studied, further work of this research could focus on to the less common parameters, as well as to the study of the spatial parameters.

A common approach for studying the acoustics of spaces, such as concert halls and churches, based on either actual impulse response measurements or simulated ones, is to measure across different positions and use average values of the acoustic parameters obtained in order to describe the acoustics of the space [5, 18, 20, 33, 73, 86, 89, 168, 170, 207-209]. For example, in the Round Robin surveys, conclusions were mainly drawn based on the average values observed across a few measurement positions. However, some results were reported by comparing the results of individual combinations of source and receiver positions, which showed a significant difference between the computer-based impulse responses and the measured impulse responses in the actual space across measured positions [73], or across octave bands [29]. This observation highlights the importance of studying the acoustic behaviour of the simulations for individual positions, rather than using spatial averaging.

For the current study, the average measures of T_{30}, EDT and C_{80} across the 26 measured positions (as discussed in Chapter 5) are presented in order to study the overall acoustic behaviour of the space, as shown in Figure 6.1, Figure 6.2 and Figure 6.3 for acoustic configurations A, B and C. Across these configurations, the acoustic treatment of the space can be easily noticed. The values of T_{30} from configuration C, in which the acoustic panels are all closed and only the drapes are out (in use), establish that this configuration is the one with the least acoustic modifications. Generally, in large halls and churches, there is a drop in the reverberation time values at high frequencies due to the effect of air absorption, as described in 2.3.4. Acoustic designers aim to create a smooth reduction in the reverberation curve as frequency increases and at the same time to increase clarity (C_{50}/C_{80}), as these two parameters are inversely related. Acoustic changes due to the 'designed in' acoustic treatment can be observed in the results of configurations A and B, in which 75% of the panels are open or all the panels are open, respectively.

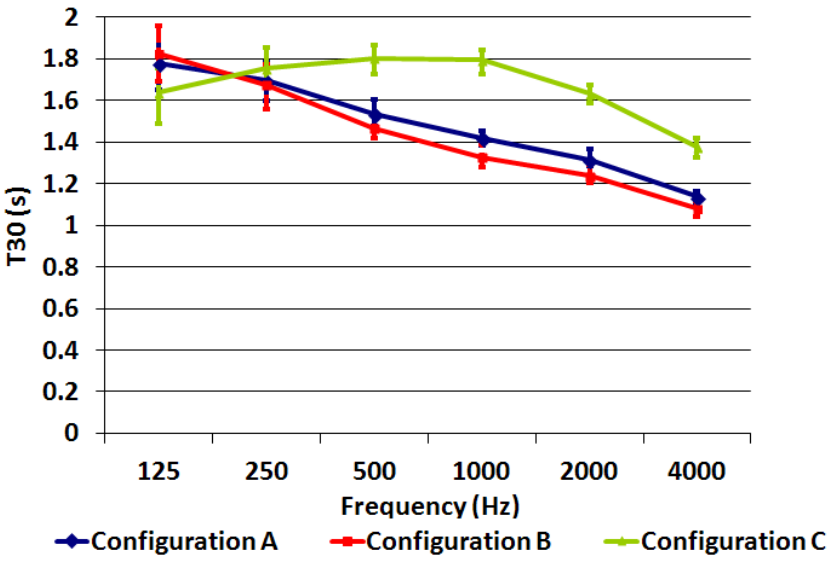

Figure 6.1 Mean values and standard deviation of T_{30} observed across the 26 receiver points for configurations A, B and C.

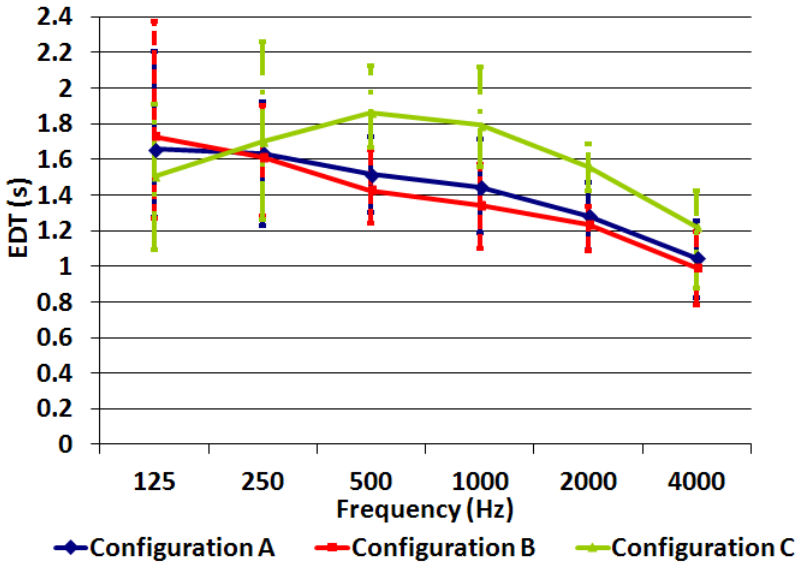

Figure 6.2 Mean values and standard deviation of EDT observed across the 26 receiver points for configurations A, B and C.

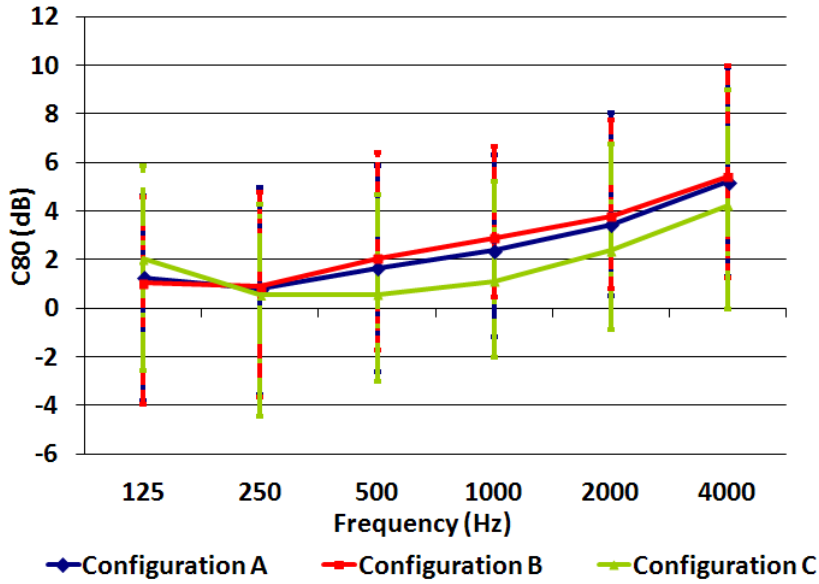

Figure 6.3 Mean values and standard deviation of C_{80} observed across the 26 receiver points for configurations A, B and C.

However, the results obtained from averaging the values of the acoustic parameters are not very useful in terms of determining the quantity of the resulting subjective experience, an issue which several other studies have also raised [70, 82, 91, 170, 205, 210]. The values averaged across different measurement positions cannot represent the acoustic characteristics at a given point and consequently the acoustic result perceived by a listener at this specific position. In addition, the acoustic parameters can vary significantly from one position to another across the same space, as described in section 3.2.4, especially for position dependent parameters such as EDT, Strength (G) and Clarity (C_{80}/C_{50}), as observed from the wide standard deviation values across octave bands in Figure 6.2 and Figure 6.3.

Thus, the analysis of this study will based on position dependent results, instead of the mean values for each parameter, in order to investigate which changes in acoustic parameters, significant or not, could change the perceptual accuracy of these auralizations for a specific point within the space.

6.3 *Calculation Process*

For the study of the main monoaural acoustic parameters, the results are based on impulse responses captured from the W (omnidirectional pressure) channel of the Soundfield microphone as used in the actual measurements, and the corresponding

W-channel of the B-format impulse responses generated from the acoustic simulation software.

As discussed previously (section 3.2.4), the acoustic parameter derivations can differ significantly, especially at low frequencies, depending on the analysis and calculation algorithms applied to the impulse responses. This was confirmed by using the same impulse response for acoustic parameter calculations in Aurora, CATT-Acoustic and ODEON, where important variations were observed. In order to avoid any bias caused by this fact, only Aurora will be used for all calculations. Thus, the W-channel of the B-format impulse responses from both computer simulations were imported into Adobe Audition, and the same acoustic parameter calculation method, as used for the measured impulse responses, was followed[1].

Deconvolution for the recorded sine sweeps

The logarithmic sine sweep, recorded in the actual space, had to be deconvolved with the inverse sine sweep of the system in order to obtain the impulse response. Before this step, however, the recorded files were edited in order to remove the silence at the end of each measurement. The duration of the silent part was estimated to be at least as long as the reverberation time, based on the values provided by Arup measurements.

Deconvolution was performed in Matlab, where normalization was applied for each set of measurements with respect to the level of the individual position, so that the difference between levels across measurement positions can be maintained.

Editing the impulse response

The first 15s were removed from each impulse response in order to remove the harmonic distortion that appears in the first 15s (as described in section 3.2.1).

A common problem which can cause variations in obtained acoustic parameters ,is the definition of the beginning and end points of the impulse response file, especially for Clarity (C_{80}/C_{50}) and Ts. Ripples observed due to onset effects from

[1] It should be mentioned here that the necessity of using of the same calculation method has been already recognized by ODEON, where in the latest update, measured impulse responses can be imported and calculated by the software itself.

the speaker before the direct sound arrives should not be included in the calculations as part of the impulse response data. By setting a threshold in Aurora, the acoustic parameter calculation only starts at a point in time where the signal amplitude is greater than 5% of full scale. For these results, the threshold point was not defined higher, as it is sometimes applied, as it was observed in few measurements that the early reflections were stronger than the direct sound, due to the nature of the source directivity, as shown in Figure 6.4 and Figure 6.5.

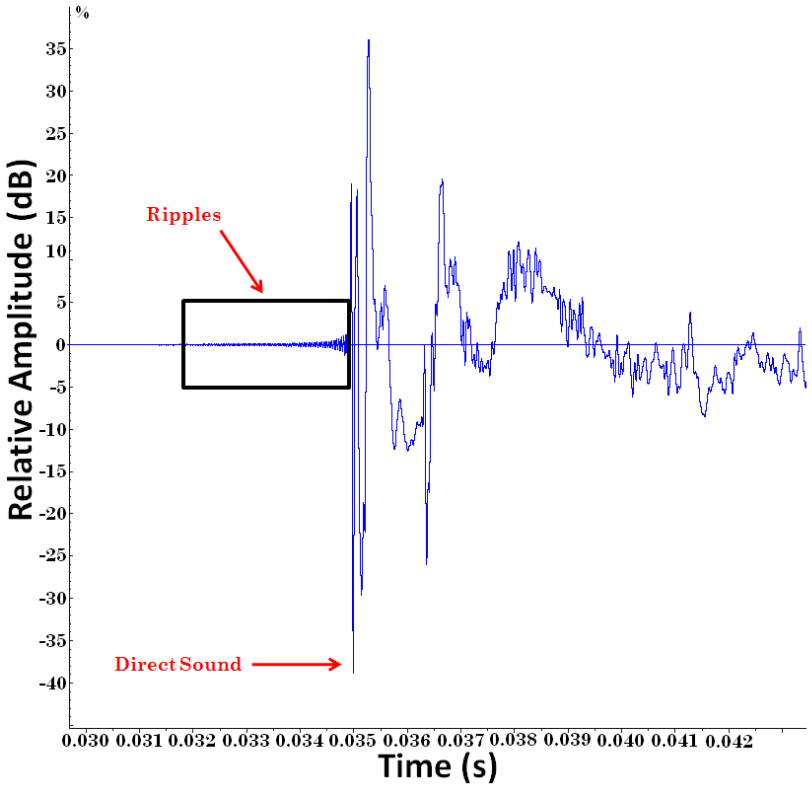

Figure 6.4 A closer observation of R2, configuration A, 0° sound source orientation at the beginning of the measured impulse response, where ripples can be observed just before the direct sound (as the arrow shows).

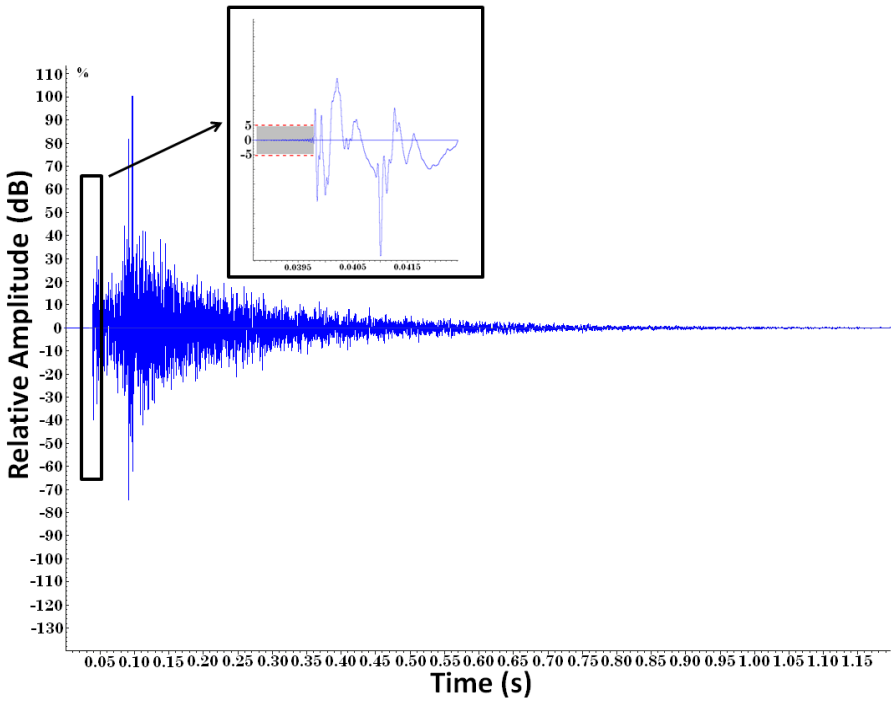

Figure 6.5 A closer observation of R9, configuration A, 70° source orientation. In this example the early reflections are stronger than the direct sound. The defined threshold from where the acoustic parameter calculation starts, is after the grey area where the signal amplitude is less than 5% of full scale level.

It is important to mention that the two receiver positions (R2 and R5) are not visible from the source, which implies that there was no direct sound reaching these positions.

In addition, a section had to be removed from the beginning of each impulse response, due to the recording system latency calculated approximately at 200ms. This correction was not essential for the calculations of the acoustic parameters, as the threshold for the starting point of the calculations had been already defined. However, this helps to ensure the correct time of the direct sound for each receiver position.

Also, the determination of the end of the room impulse response is significant for the calculations of energy parameters [211]. According to ISO3382 [55], Ts, Clarity (C_{80}/C_{50}), Definition and Strength parameters are calculated based on equations (2.7), (2.8), (2.9), (2.11), where the end of room impulse response is defined with infinite measurement times, which obviously is not realistic. Furthermore, additional "silence" after the end of the impulse response could include background noise in the calculations and give error values. Thus, the files were trimmed to 3 seconds in total, as after detailed examination, it was observed that the

reverberation tail of all the measured impulse responses was never greater than 2.5 seconds.

Acoustic parameter calculation

Aurora makes its calculations according to the ISO3382 standard; first the impulse response is octave-band filtered by means of IIR IEC-compliant filters. The impulse response is then squared in order to obtain the energy for the estimation of the energy parameters. The squared impulse response is then backwards-integrated to obtain the Schroeder delay curve and a noise-removal algorithm is also applied. A linear regression is performed over the required dB range, for the reverberation parameters and EDT.

It should also be noted that, before the calculation process, the impulse responses were all normalised for the purposes of the listening tests, which will be explained in Chapter 7. It was checked that the acoustic information was not affected by this modification, as no changes at the values of the acoustic parameters were observed by comparing the results before and after the normalisation.

Moreover, it is important to note here how EDT is calculated in Aurora. Based on ISO3382 [55], EDT is estimated from the best-fit regression line of the first 10dB. It was observed, however, that Aurora calculates EDT for a different portion of the decay curve, starting at 0.1dB and dropping down to the first 10.1dB. The reason for this is to avoid the ripples caused by the onset effects of the speaker when recording in-situ impulse responses[2]. As this phenomenon does not occur with the computer based impulse responses for this modelled data, the T-user parameter value was used for calculating EDT between the values of 0dB-10dB.

The frequency range of interest is limited to 125Hz to 4000Hz in one-octave bands, as the absorption and scattering coefficient values based on existing libraries, used for the calibration of the simulated models, are available for these octave bands. Additionally, these octave bands are considered sufficient for the frequency range of the stimuli used for auralization examples, for the purposes of this current study, as will be described in section 7.4. It should be mentioned here that the Schroeder frequency for this space varies, based on the equation (2.6)

[2] After personal communication with the developer of Aurora, Prof. Angelo Farina.

(explained in section 2.3.7), from 39Hz to 44Hz, depending on the chosen configuration of the acoustic panels. Thus, the acoustic parameters at the examined frequencies can be assumed to give accurate results, based on the assumption of a diffuse field.

For handling the huge amount of data and avoiding typing errors, all the data calculated by Aurora was copied with the "copy to clipboard" feature to Excel files, where they were categorised according to the auralization method, acoustic configurations, and receiver positions.

6.4 *"Acoustic Floor Maps"*

In the analysis that follows, the results from the three auralization techniques studied (acoustic measurements, acoustic simulations in CATT-Acoustic and ODEON software), which were collected at exactly the same positions and using the same process to calculate the acoustic parameters described above, are considered in more detail.

As discussed above, it was considered necessary to observe the overall acoustic behaviour for each individual measurement position and variations according to configuration A, B, C, and source orientation. One method of presenting data across spatially distant measurement positions is the use of colour-maps, as used in section 4.2.2. This function is a feature of both CATT-Acoustic and ODEON.

Stenner [212] had introduced a different way to represent multivariate data across many measured positions in a space, as shown at Figure 6.6. By using 3D images with shape and colour variations dependent on the measured values, Stenner achieved a visualisation of the acoustic parameter information for individual measured positions in the simulations.

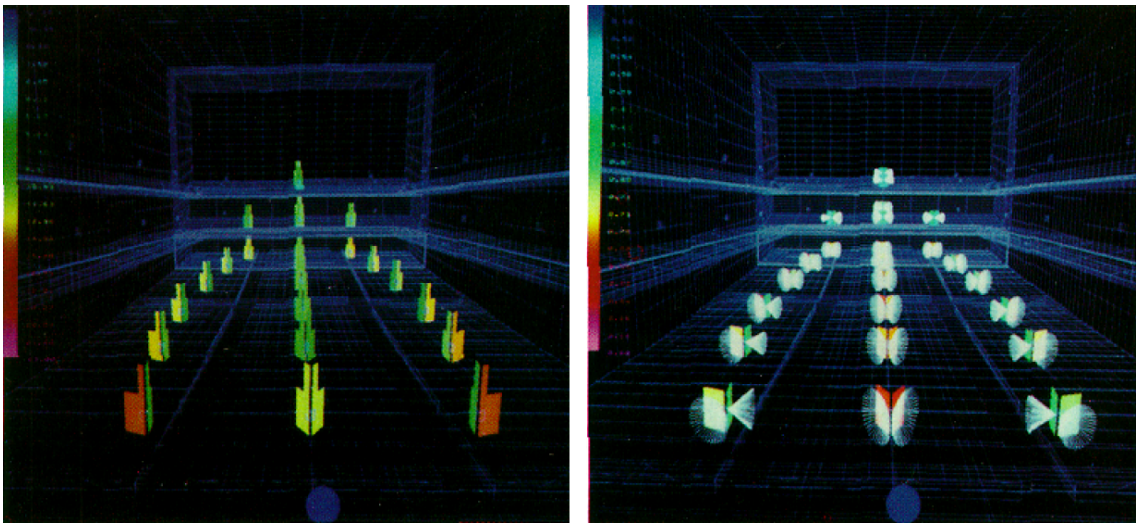

Figure 6.6 Visualisation of Clarity (C_{80}) and Spatial Impression parameters across different measurement positions in a space. The differences of early-to-late energy (left) and left-to-right energy (right) for the corresponding parameters are presented with further details, from [212].

For the current study, "acoustic floor maps" have been used, combining the position dependent characteristics of the space and frequency dependence of each acoustic parameter. Thus, the grid of measurement positions has been replaced with a grid of radar charts, as shown in Figure 6.7. These radar charts are centred at the numbered measurement positions, across the three rows of receiver positions and the values of the acoustic parameters studied are presented clockwise across the six octave bands, 125Hz, 250Hz, 500Hz, 1000Hz, 2000Hz and 4000Hz. Position of the source S is represented at the corresponding position and an arrow points out the orientation of the source. The bottom right floor plan within the main figure is a guide of the source/receiver positions being used.

It is important also to mention that the axes for each radar chart are set depending on the overall maximum and minimum values for each parameter. In this way, the differences of the values between positions are much easier to observe, although careful attention is necessary to avoid underestimating JND values.

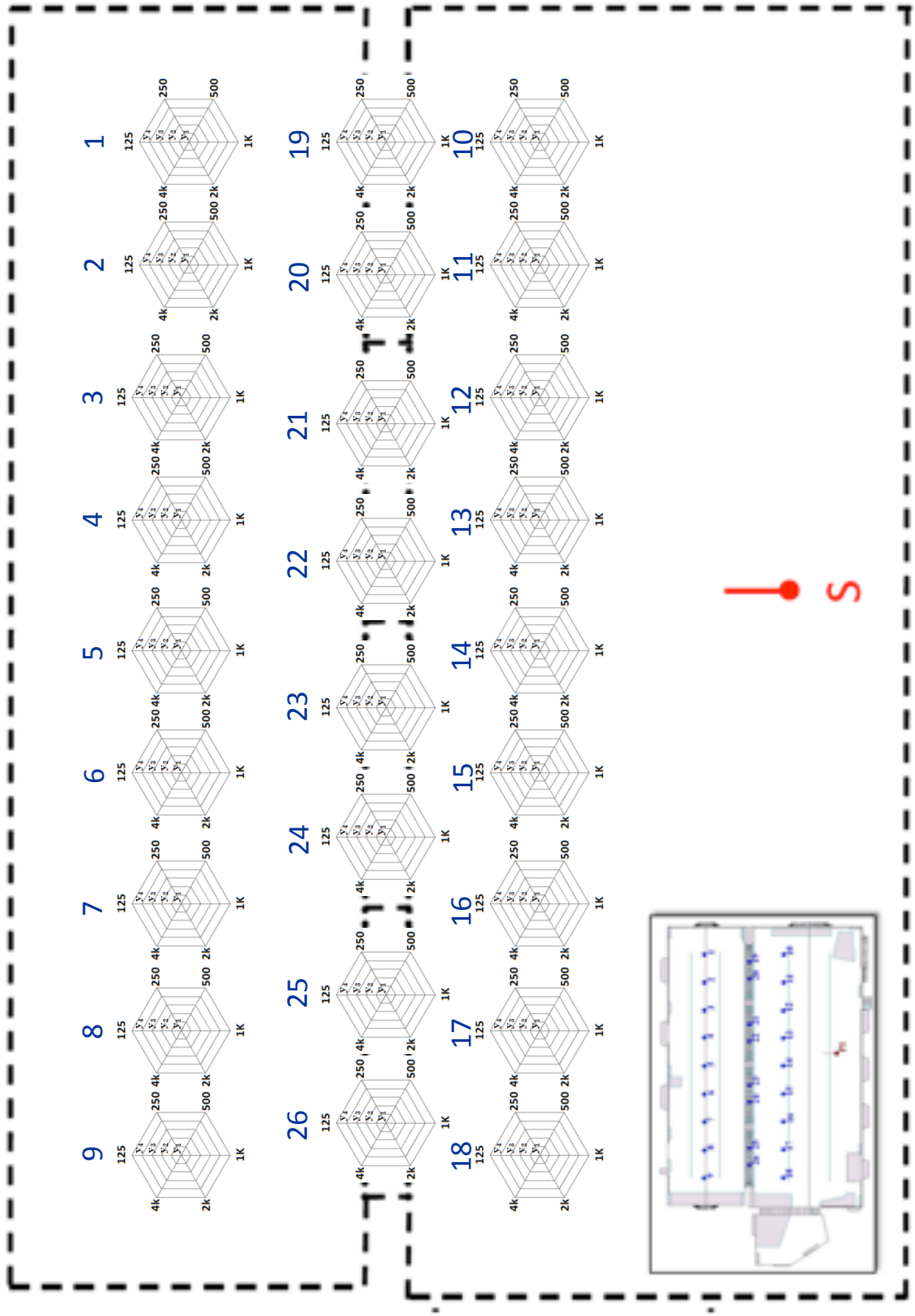

Figure 6.7 Acoustic floor map with radar charts centred at each receiver position across the grid, representing values across the six octave bands.

6.5 *Acoustic Impulse Response Measurements*

6.5.1 Results obtained from changes in acoustic configuration

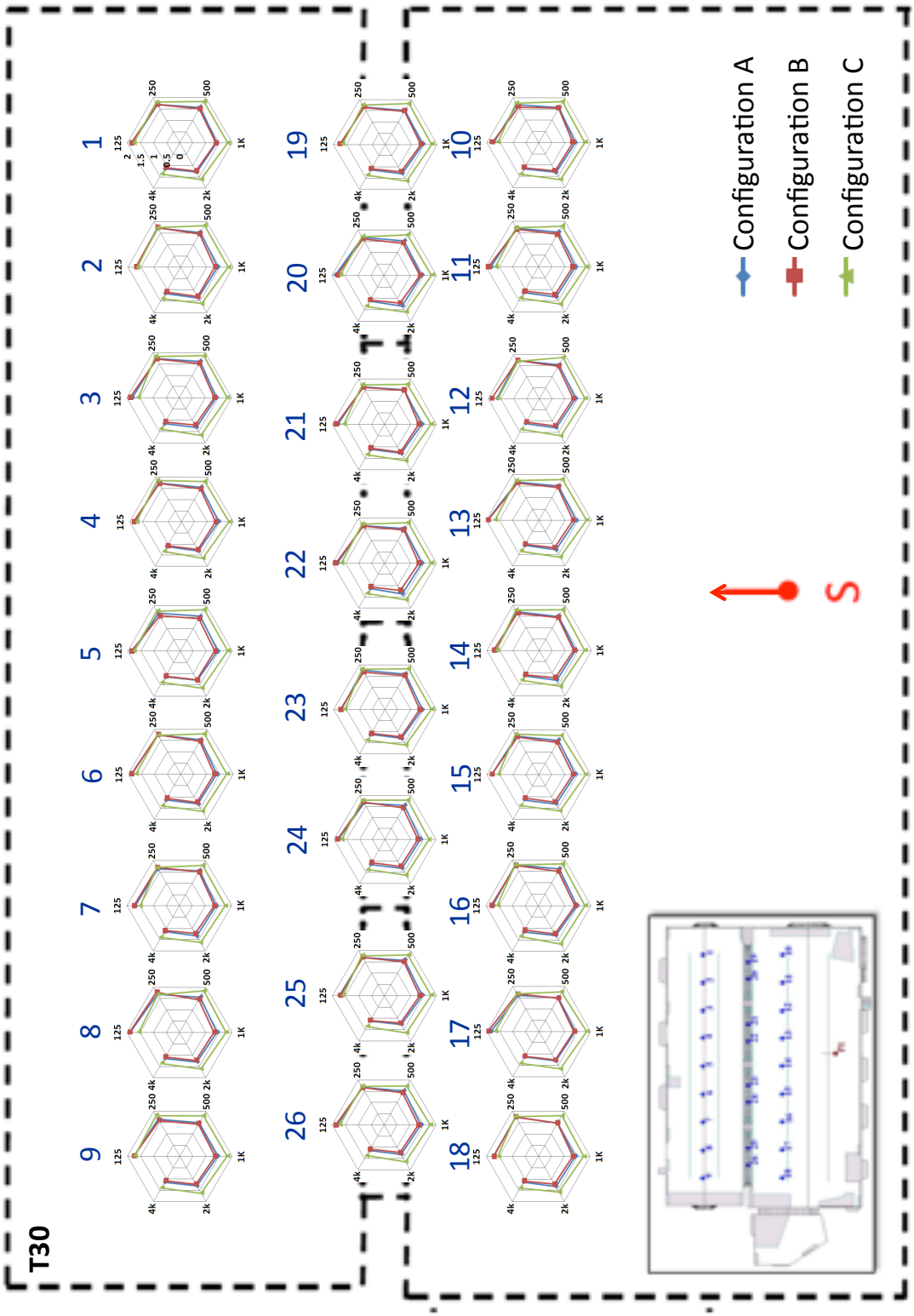

Figure 6.8 Acoustic floor map of T_{30} values obtained from the measurements varying with configurations A, B and C across the grid of 26 receiver positions.

Figure 6.8 shows the changes in T30 values by varying with configuration, across the six octave bands, from 125Hz to 4000Hz, and across the 26 measurement positions.

Analysing the results across all the measurement positions, the values of T_{30} have similar behaviour, showing once more that T_{30} is a global parameter. There are minimal differences observed, mainly in the 125Hz and 250Hz bands. In Figure 6.9, the relative variation for T_{30}, based on the JND values is represented for each configuration and across the six octave bands. Note that the reference value of 1 indicates the order of magnitude of the JND value for each configuration, while the grey area marks variations with less than 1 JND value. For the calculations of these variations, the JND for the average of the 26 measurement positions has been calculated for each configuration. The variations were calculated from the maximum (V_{max}) and minimum values (V_{min}) observed from each octave band across the 26 results, with respect to the average values ($JND_{average}$), in a similar way to [16], according to:

$$Variation = \frac{|V_{\max} - V_{\min}|}{JND_{average}} \qquad (6.1)$$

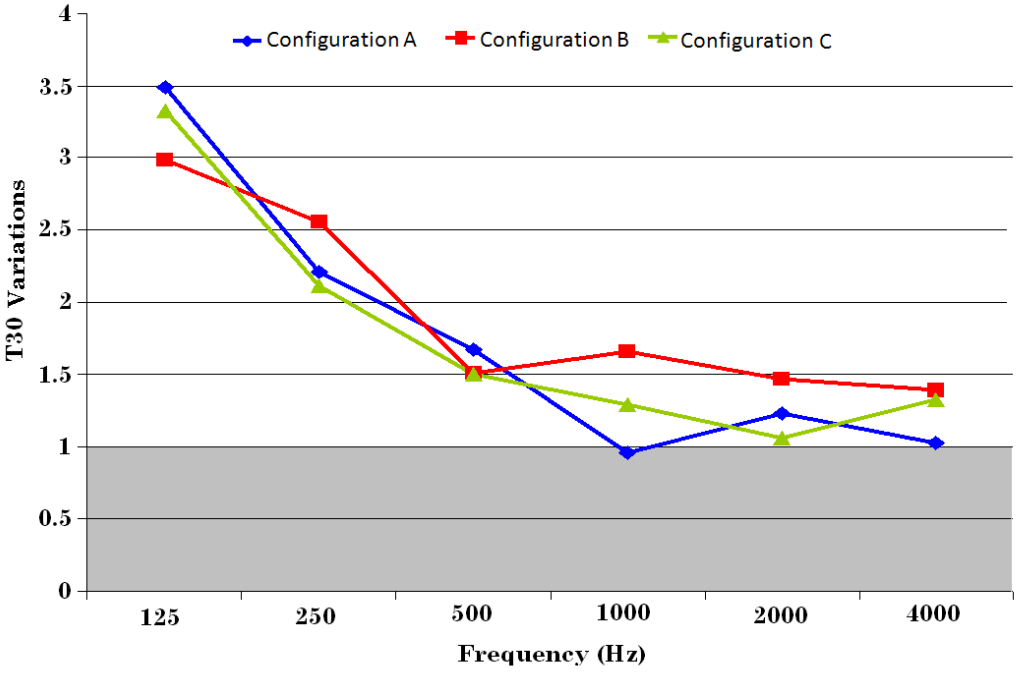

Figure 6.9 Degree of variation in average values of T_{30} based on ISO3382 JND, observed for each acoustic configuration, A, B and C.

Analysing each individual position, there is an obvious difference in the T_{30} values for configuration C (all the acoustic panels closed), compared to those observed with configurations A and B. However, the differences between configuration A (75% of the acoustic panels open) and configuration B (all the acoustic panels open) are minimal, with the maximum value of 2.38 JND (as will be explained further in 7.2 and represented in Appendix D).

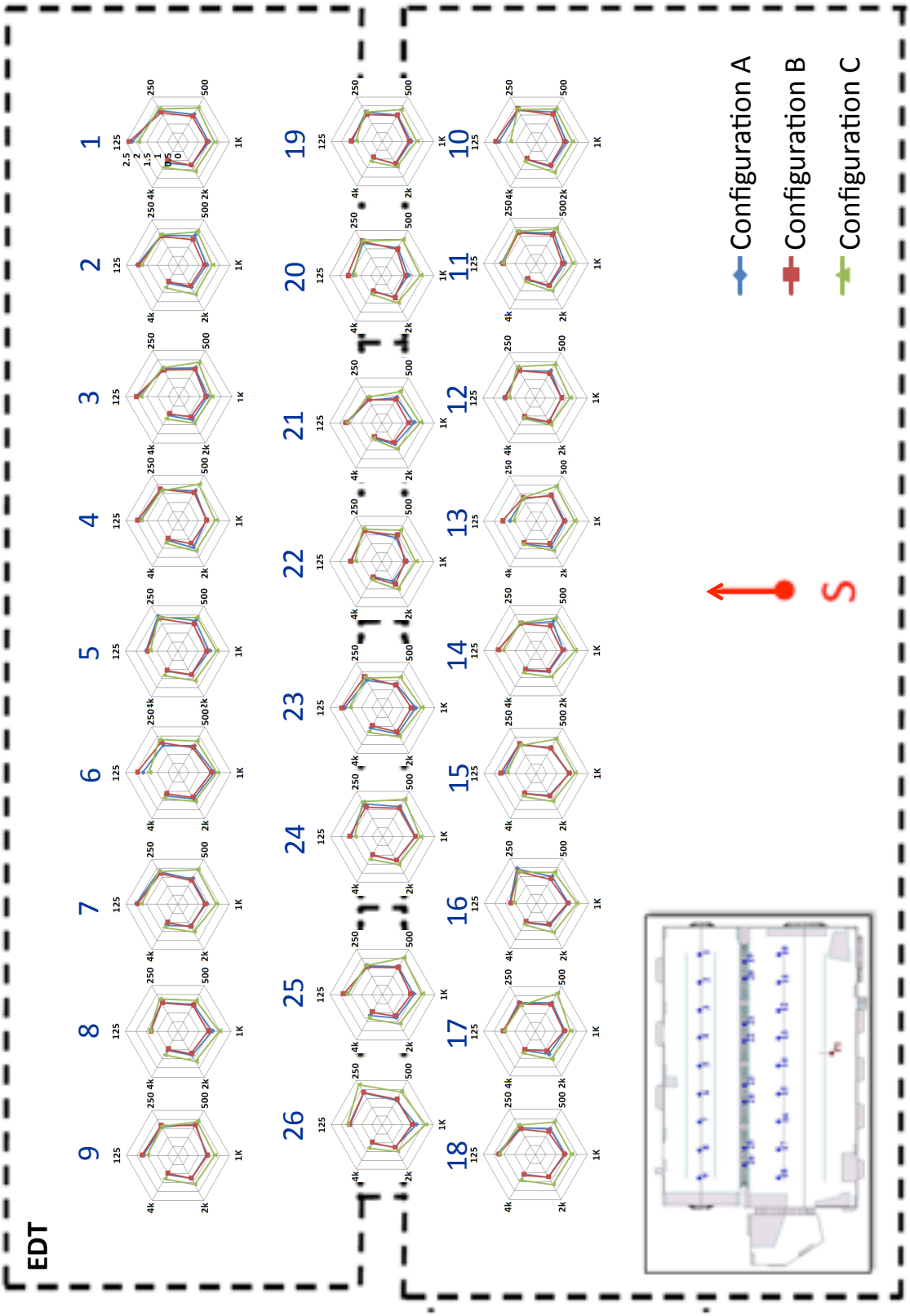

Figure 6.10 Acoustic floor map of EDT values obtained from the measurements varying with configurations A, B and C across the grid of 26 receiver positions.

Figure 6.10 shows the changes in EDT values across all measurement positions, for configurations A, B and C. It is observed that firstly, the behaviour of EDT follows that observed for T30 values (Figure 6.8), although differences in the results across positions are more noticeable. As Behler [91] notes, EDT seems to be more sensitive to position than T30, as it considers the effect of early reflections. However, from these results the effects of walls, corners, or columns on EDT values are not obvious at adjacent measurement positions. It is interesting to note that, for the north wall, changes had been made by closing and opening panels according to configurations A and B. However this change does not have significant effects on the observed EDT values.

The differences across the positions are calculated to be more than the quoted JND for this parameter, according to ISO3382 [55]. At shorter distances between source and receiver positions, where the direct sound level is higher, lower EDT values are expected to be observed, as explained in [34]. However, this phenomenon is only more obvious for the low frequencies of 125Hz and 250Hz, as due to air absorption (as described in section 2.3.4) the phenomenon is masked for the high frequencies, especially above 1000Hz. For example in the results observed at R4, R22 and R13 where values increase with an increase in distance for 125Hz an 250 Hz, while values are approximately the same for higher frequencies. The acoustic floor maps for each configuration are presented in Appendix C, Measurements, for a more detailed observation.

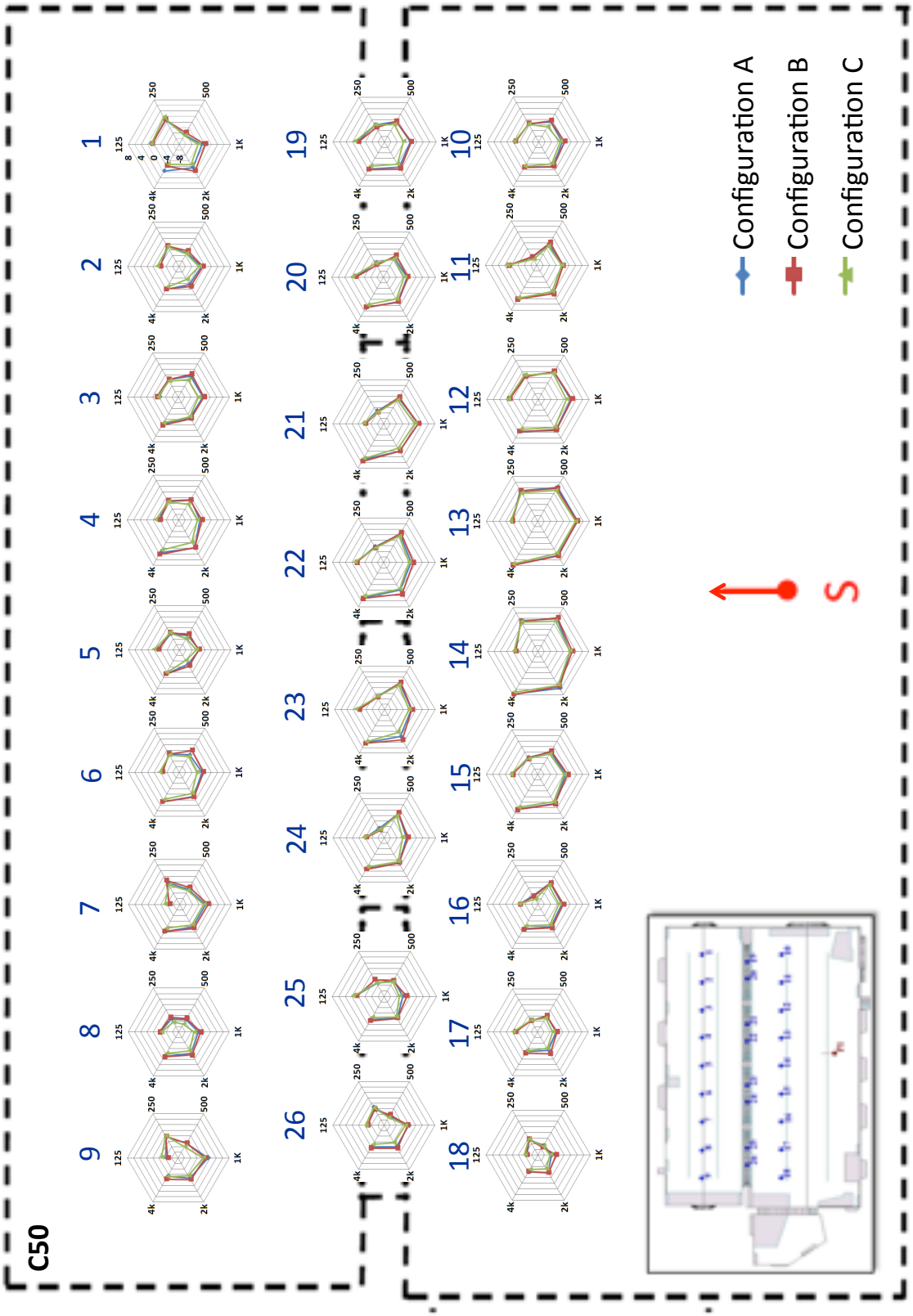

Figure 6.11 Acoustic floor map of C_{50} values obtained from the measurements varying with configuration A, B and C across the grid of 26 receiver positions.

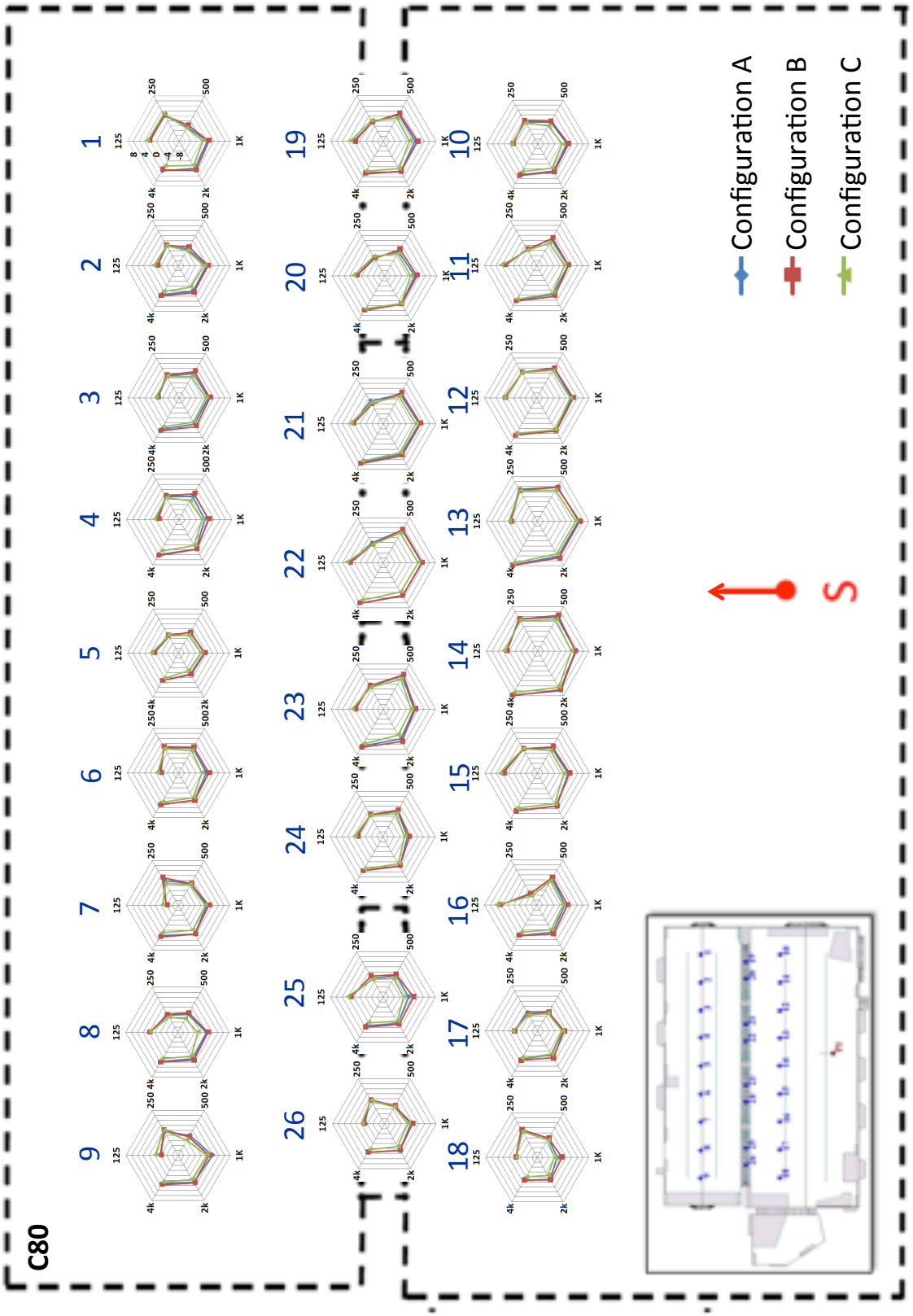

Figure 6.12 Acoustic floor map of C_{80} values obtained from the measurements varying with configuration A, B and C across the grid of 26 receiver positions.

It has been discussed in previous works [70, 74, 182], how C_{80} and C_{50} change over a space, depending on the shape of the room and the distance from the source. The results presented in Figure 6.11 and Figure 6.12 confirm that both parameters, C_{50} and C_{80} are position dependent parameters.

It is also observed that for each individual measurement position, C_{50}/C_{80} values are very similar for each of the configurations, A, B and C. This does not necessarily mean, however, that the same early and late energy is arriving at the receiver positions for all acoustic configurations, as clarity (C_{50}/C_{80}), from definition, describes the ratio of energy. This implies that if a physical change in the space influences both early and late reflections in the same way, the values of Clarity (C_{50}/C_{80}) and LF will remain similar but the audible results and reverberation times (T_{30} and EDT) will significantly change. This could also explain the "unexpected" results of Clarity and LF when seats have been present in a concert hall project [88], where the resulting longer reverberation and increased values for strength (G) did not influence the energetic parameters.

Comparing the results of the measurement positions row by row, one would expect that positions closer to the source to have better (higher) values for C_{50}/C_{80}. Going further away from the source, one would expect to observe more energy in the later part of the impulse response, due to the greater diffusion of sound, and as a result of that, lower values for C_{50}/C_{80}, as shown in [104]. However, in this study case, these expected results are not observed across all the measured positions in a similar way. Dividing the space into region (a), region (b), and region (c), as shown in Figure 6.13, it is noticeable that the expected results can be observed in region (a) and to an even greater extent in region (b). In particular, the receivers R13, R14, R15, which are closest to the source, have higher values for C_{50}/C_{80}. However, in region (c), C_{50}/C_{80} has smaller values for all 3 rows. This could be the result of later reflections coming from the floor tower section, at the south west side of the church.

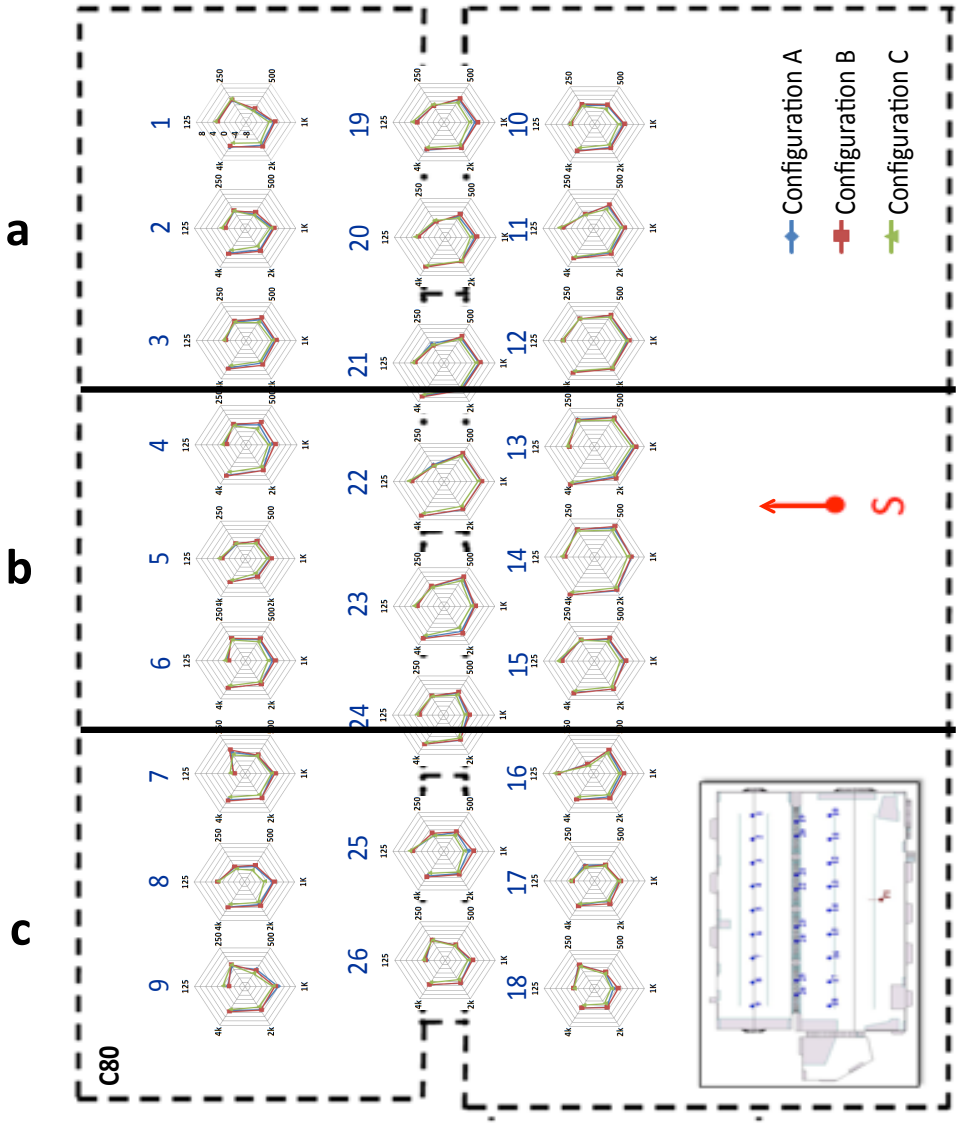

Figure 6.13 Observing C_{80} values across measurement positions in divided into three regions, (a), (b) and (c).

For 125Hz and 250Hz especially, at a few measurement positions there is a steep incline in C_{50}/C_{80} values compared with the rest of the charts. For example, at R18 there is a sharp increase of C_{50}/C_{80} values at 250Hz, while at R16, the opposite behaviour is observed for 125Hz and 250Hz. A further investigation was carried out for these measured positions by comparing the frequency domain analysis obtained from these two impulse responses, at positions R18 and R16 and comparing them with R10, which has more regular curve at these frequencies (Figure 6.14). The observed differences at the frequency range between 150Hz and 400Hz could be explained due to nodes/anti-nodes of standing waves, which as discussed in section 2.3.6 influence the sound energy.

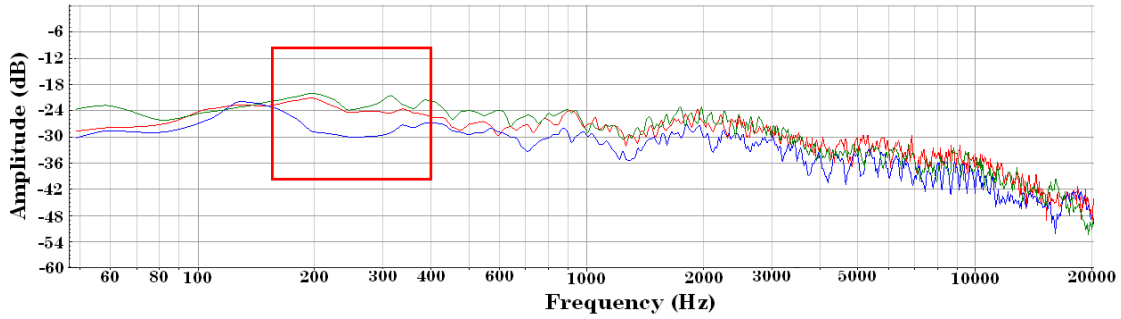

Figure 6.14 Frequency domain analysis of R10 (red line), R16 (blue line) and R18 (green line) for configuration A (using Hamming window and with FFT size at 4096).

As with the EDT values, the effects of specific walls, corners, or columns on adjacent measurement positions cannot be observed with C_{50}/C_{80} parameters.

Even though the critical distance had been considered for the measurement positions, from the results observed in Figure 6.11 and Figure 6.12, much higher C_{50}/C_{80} values R13 and R14 have been noted compared with the rest. Hence, it is assumed that their distance is not sufficiently far away from the source and these measurement positions should not be used for the purposes of the current study.

6.5.2 Results obtained from changes in source orientations

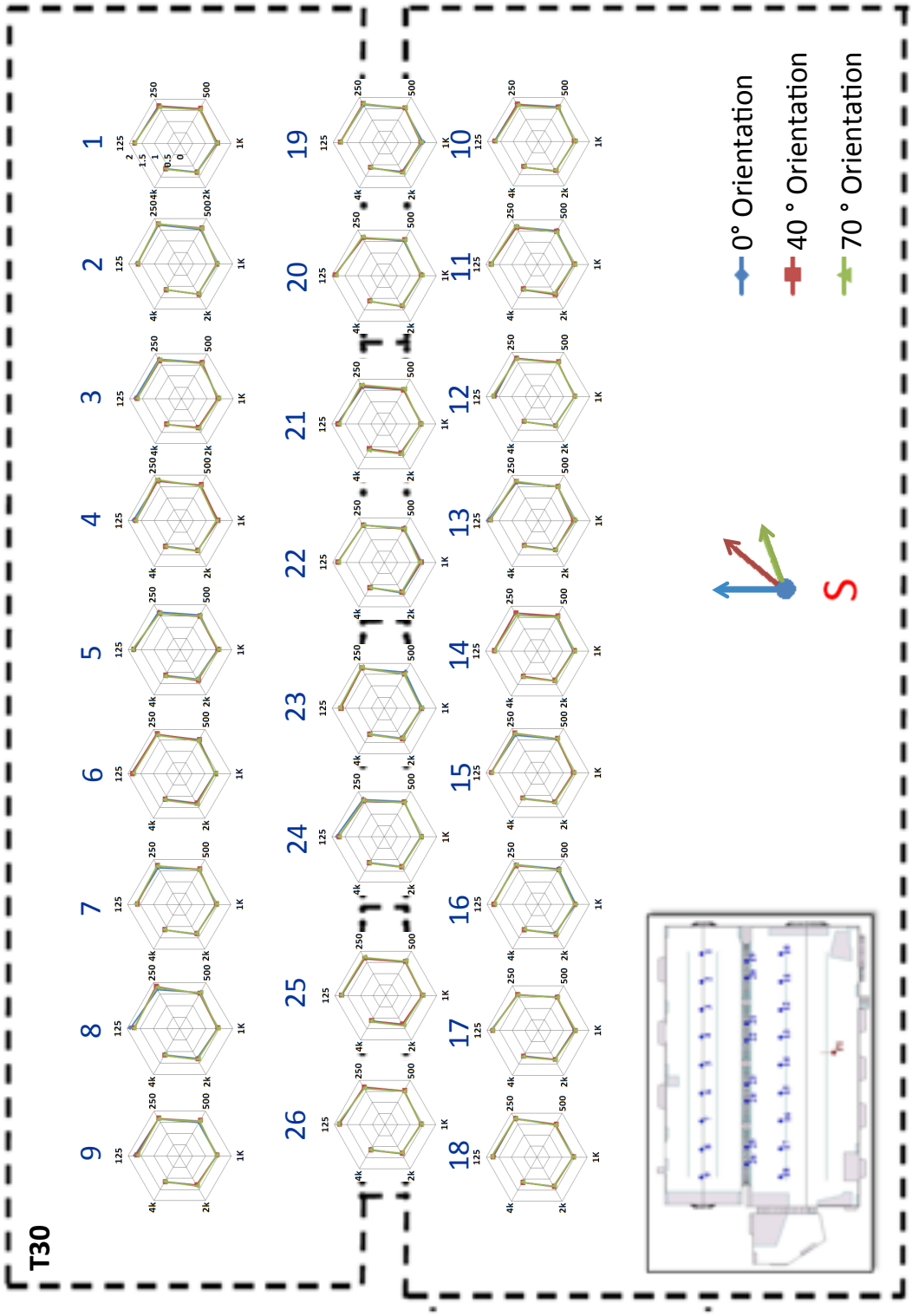

Figure 6.15 Acoustic floor map of T_{30} values obtained from the measurements varying with source orientation 0°, 40° and 70°, across the grid of 26 receiver positions.

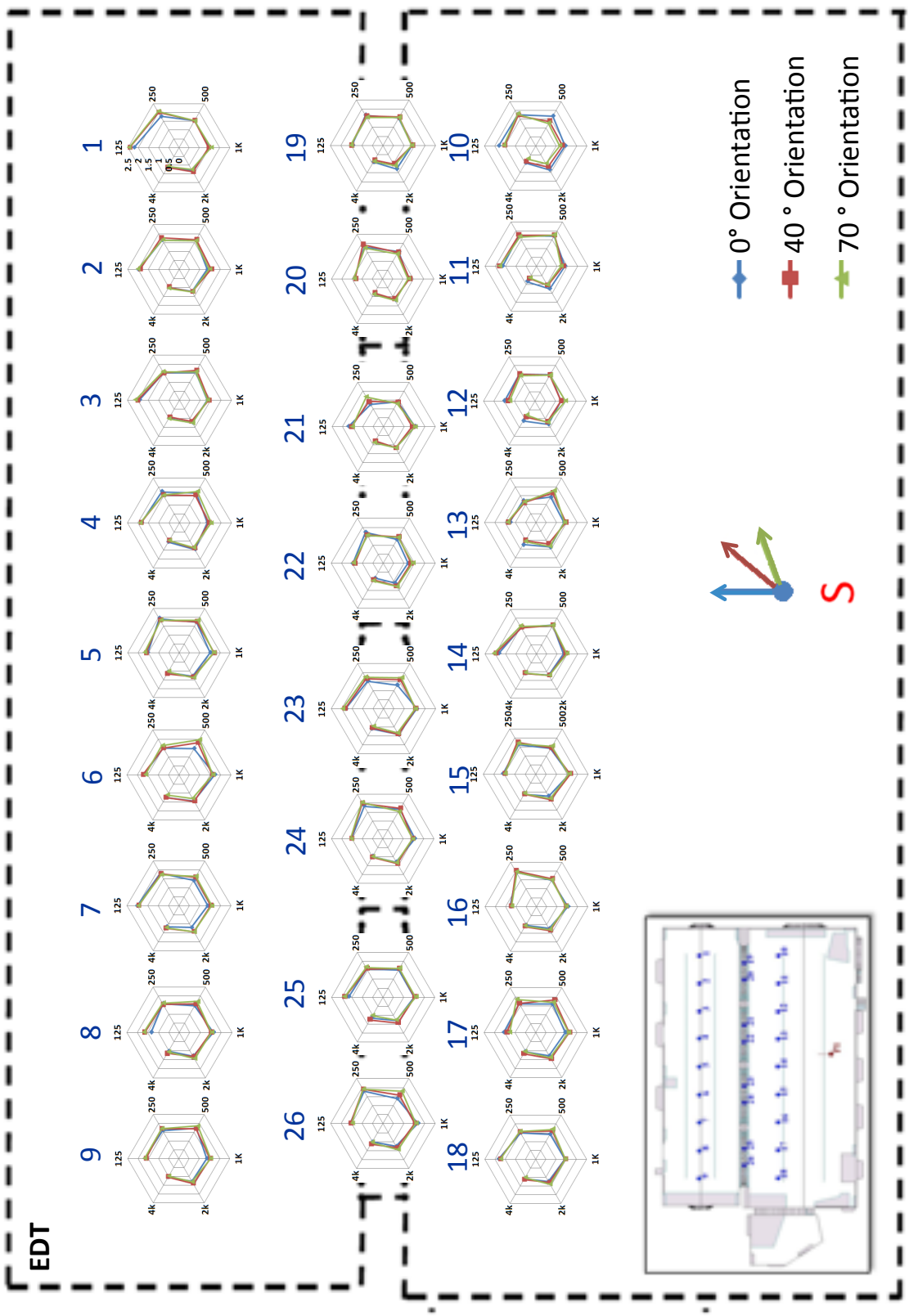

Figure 6.16 Acoustic floor map of EDT values obtained from the measurements varying with source orientation 0°, 40° and 70°, across the grid of 26 receiver positions.

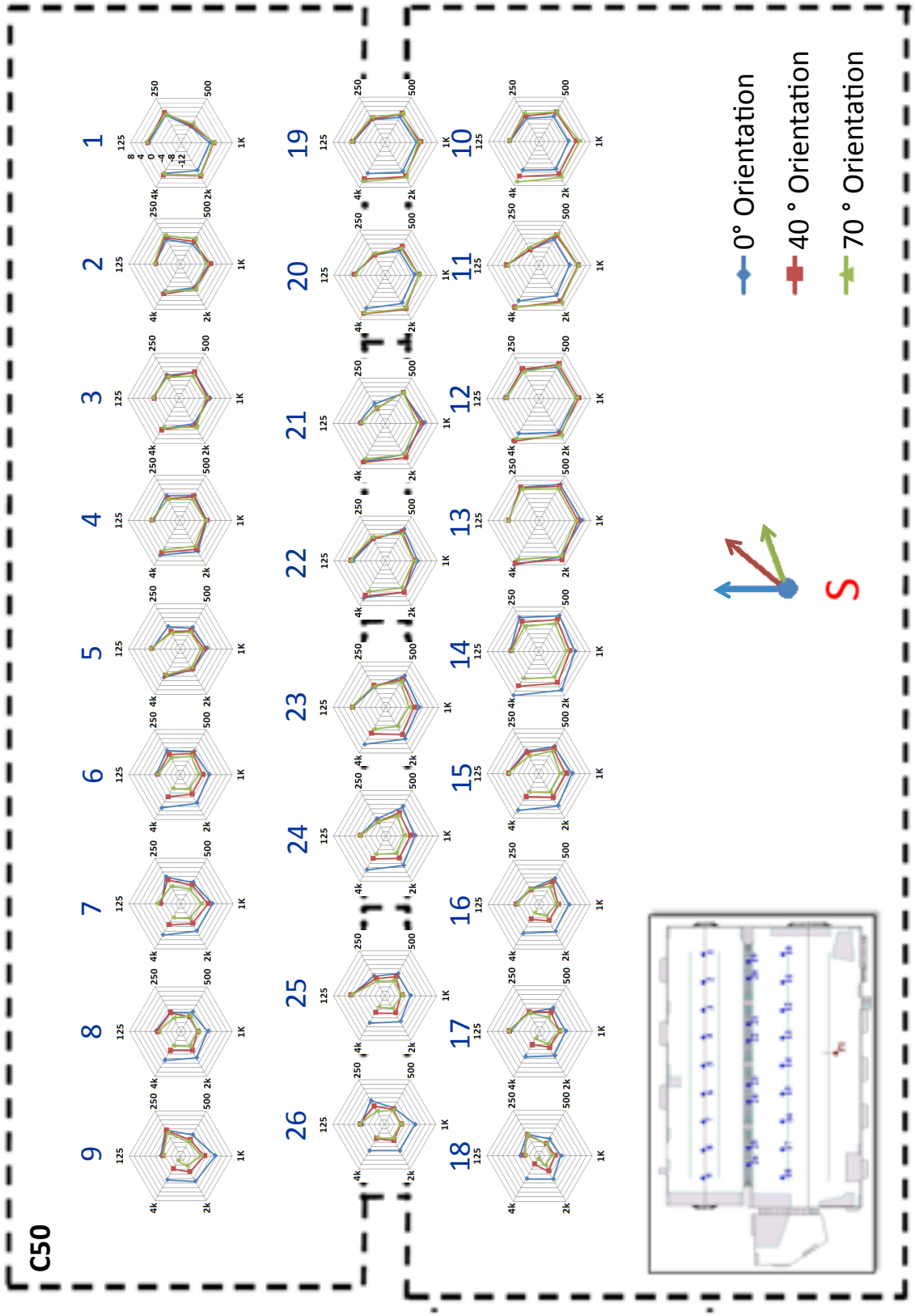

Figure 6.17 Acoustic floor map of C_{50} values obtained from the measurements varying with source orientation, 0°, 40° and 70°, across the grid of 26 receiver positions.

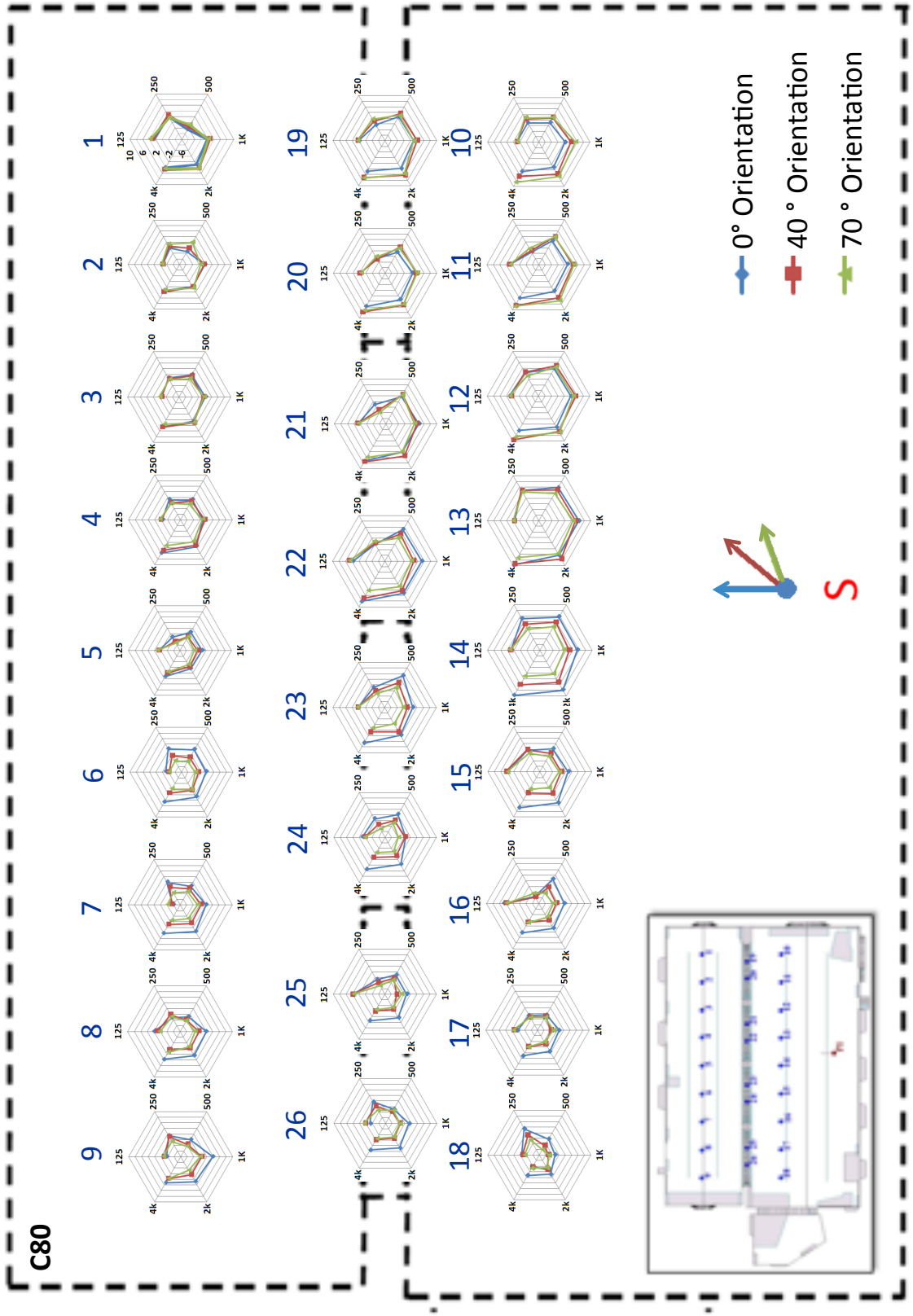

Figure 6.18 Acoustic floor map of C_{80} values obtained from the measurements varying with source orientation, 0°, 40° and 70°, across the grid of 26 receiver positions.

As described in section 5.4, the orientation of the Genelec loudspeaker used for the impulse response measurements was changed from 0°, facing the "audience", to 40° and 70° respectively on its axis. The set up of the acoustic panels was the same as that of configuration A. From Figure 6.15 and Figure 6.16, it can be observed that the effects on the reverberation parameters range from no change (in T_{30} values) to minimal changes only (in EDT values), if the changes in each measurement position are considered individually. It is interesting to note that most of the changes in EDT values are obtained at positions where the physical characteristics of the space (such as nearly walls or columns), combined with the effects of source directivity influence the energy of the early reflections. This is because by rotating the on axis position of the loudspeaker, stronger reflections arrive at the measurement positions, after their interaction with the boundaries of the space.

In the waveforms of the impulse responses, as discussed at Figure 6.5 above, the first reflections appear much stronger than the direct sound, as a result of the non-omnidirectivity of the sound source. These strong early reflections influence the related EDT values (even if the changes are minimal) and even more obviously the C_{50}/C_{80} parameters.

By comparing the behaviour of C_{50} and C_{80} across measurement positions and source orientation, there was a greater variation in C_{80} across individual positions than for corresponding C_{50} results, as shown in Figure 6.17and Figure 6.18. The acoustic floor maps for each configuration are presented in Appendix C, Measurements, for a more detailed observation.

6.6 *CATT-Acoustic IRs*

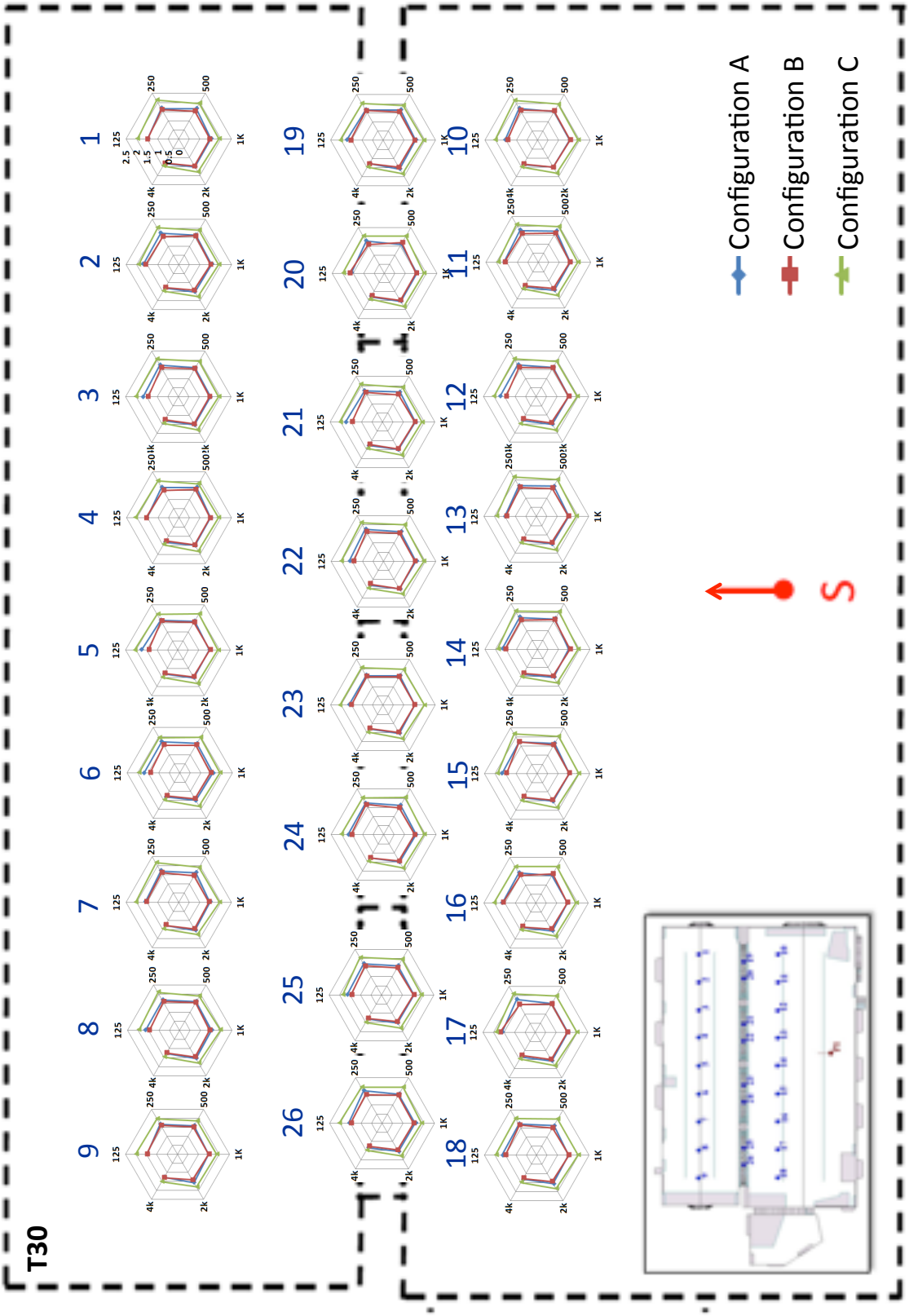

Figure 6.19 Acoustic floor map of T_{30} values obtained from the CATT-Acoustic model varying with configuration A, B and C across the grid of 26 receiver positions.

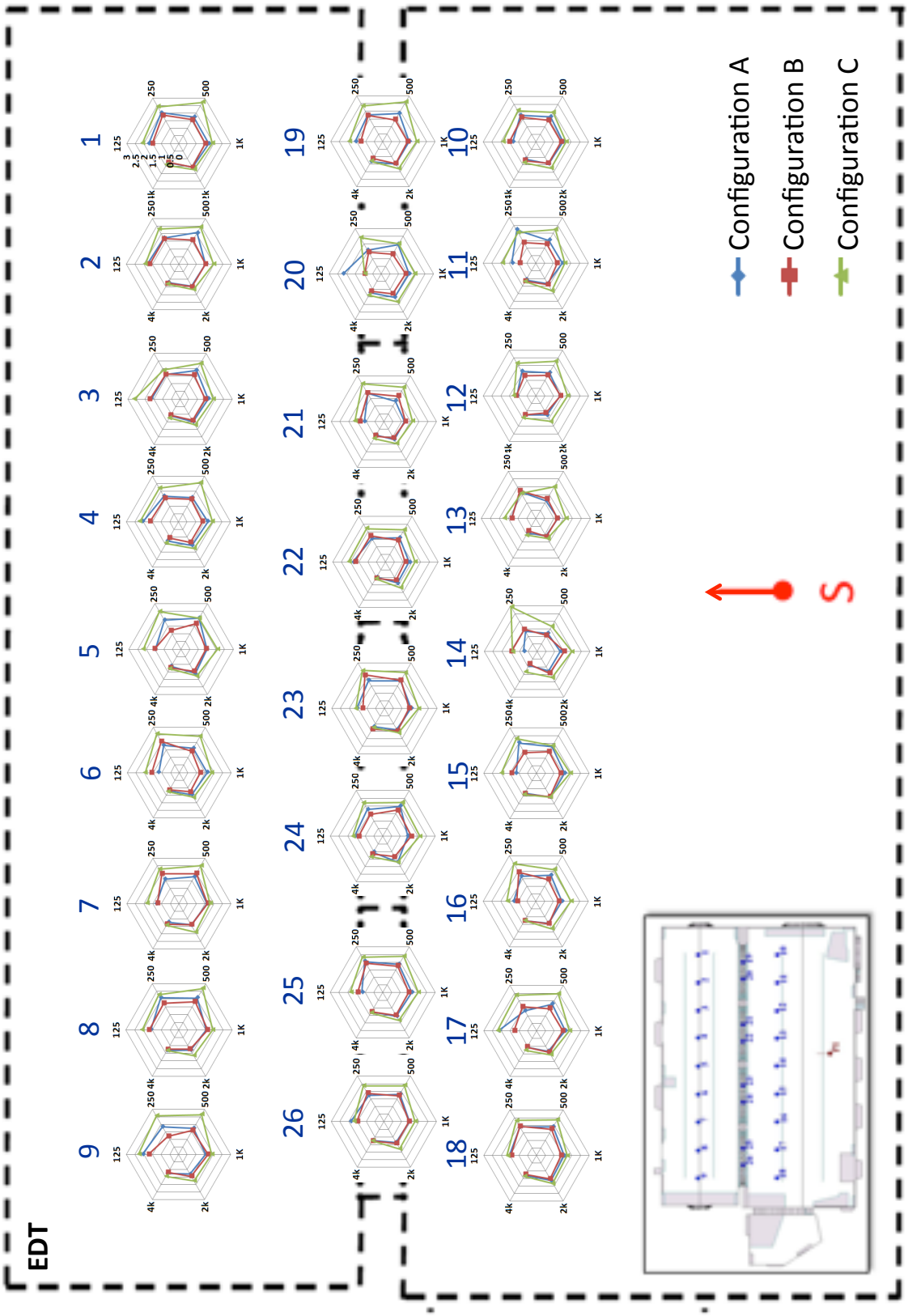

Figure 6.20 Acoustic floor map of EDT values obtained from the CATT-Acoustic model varying with configuration A, B and C across the grid of 26 receiver positions.

In Figure 6.19, T_{30} values are represented across the 26 measurement positions for configurations A, B and C across the six octave bands studied, from 125Hz to 4000Hz. It is important to note that the values of T_{30} vary with acoustic configuration, as the curves of the three configurations change respectively from the less (configuration B) to the most reverberant (configuration C). T_{30} values have small variations across all receiver positions. The largest differences were observed mainly at 125Hz and 250Hz for configuration A. By observing individual positions and the T_{30} values, between the configuration A and configuration B there are only minimal differences, while T_{30} values for configuration C have increased up to 0.5s more than those observed for the other two configurations across all the octave bands.

Figure 6.20 shows the changes in EDT values across all measurement positions, for each of the three configurations. It can be observed that EDT has similar behaviour with T_{30} values, across the three configurations studied, as the curves change respectively from the less to the most reverberant. However, the curves have some steep changes across octave bands, which are not comparable with the corresponding T_{30} values. This could indicate the direct influence of specific surfaces, such as walls or columns, on early reflections. It is difficult to draw more definite conclusions as these effects do not seem to demonstrate any repeated and/or symmetric behaviour across the measurement positions.

Appendix C, CATT-Acoustic, contain corresponding figures, showing in more detail the behaviour of EDT across the space for each configuration.

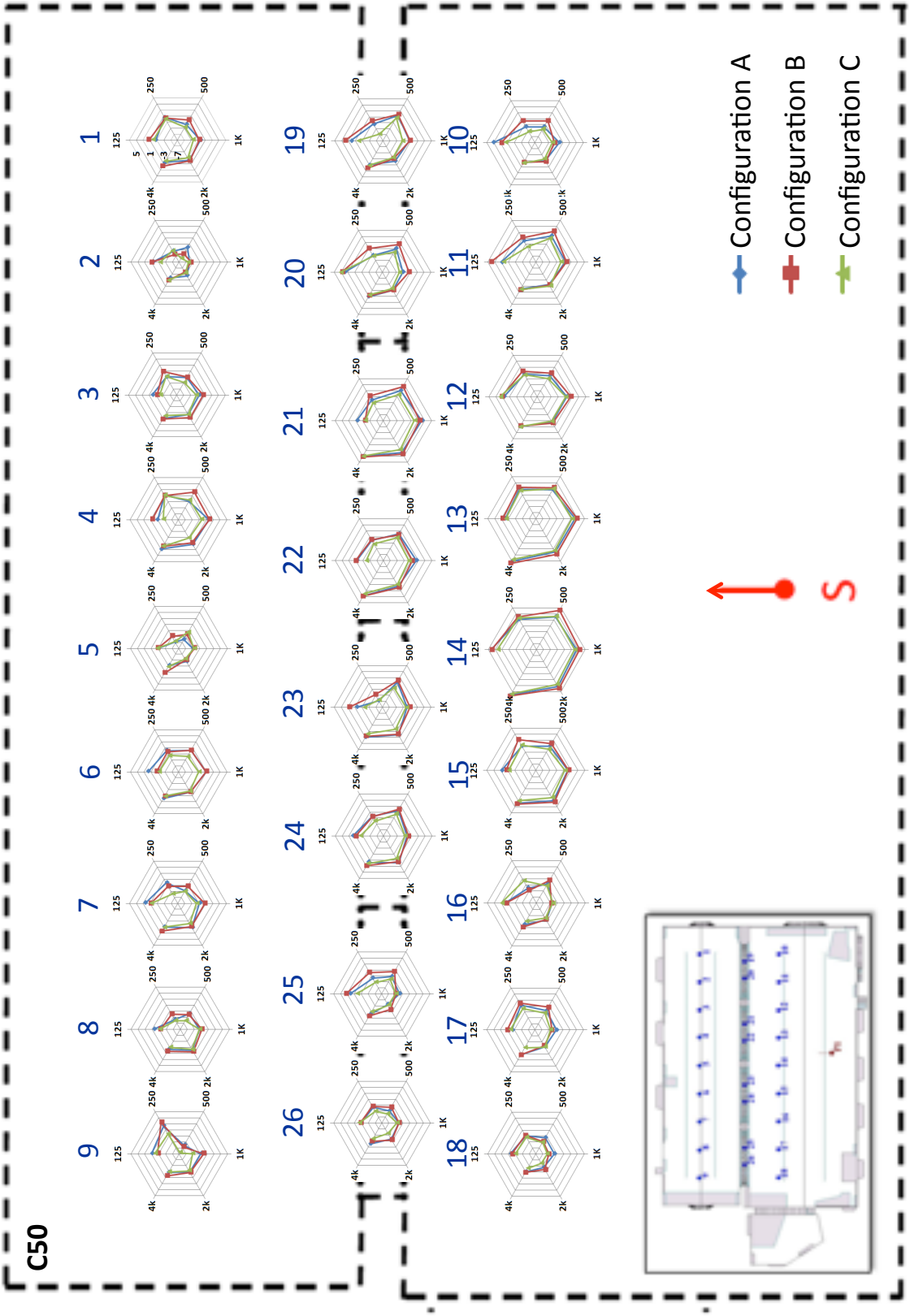

Figure 6.21 Acoustic floor map of C_{50} values obtained from the CATT-Acoustic model varying with configurations A, B and C across the grid of 26 receiver positions.

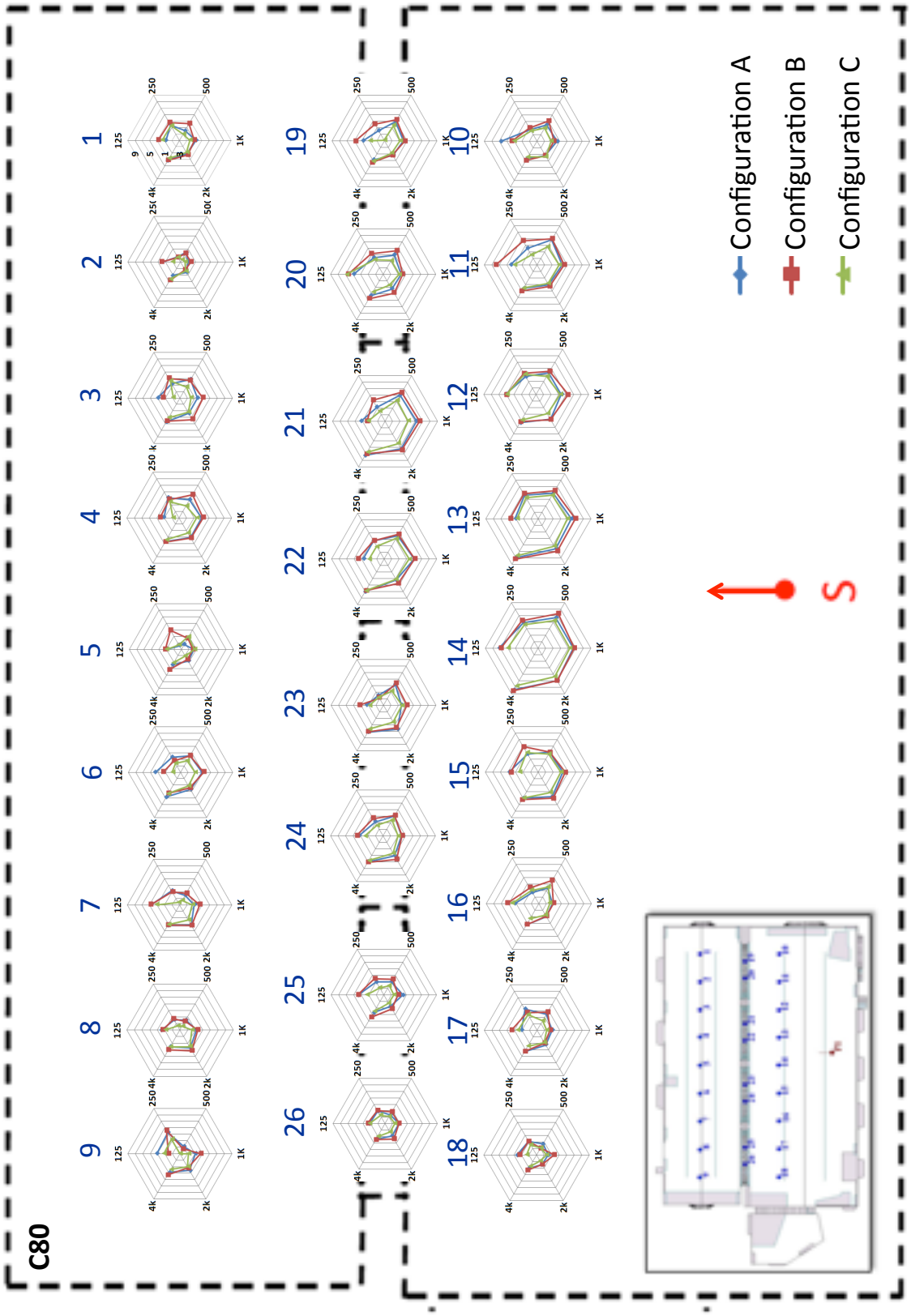

Figure 6.22 Acoustic floor map of C_{80} values obtained from CATT-Acoustic model varying with configurations A, B and C across the grid of 26 receiver positions.

C_{50} (Figure 6.21) and C_{80} (Figure 6.22) change over the space, confirming that both parameters are position dependent, as C_{50} and C_{80} vary across the receiver positions. It is also observed that for each individual measurement position, C_{50}/C_{80} curves have quite similar behaviour across the three configurations.

Dividing the space into three regions as before, shown in Figure 6.13, it is noticeable that in the regions (a) and (b) (with the exception of R10) the further away from the source the receiver positions are, the lower the values for C_{50}/C_{80}, while C_{50}/C_{80} increases for positions closer to the source. This cannot be noticed however, in region (c), where low values for C_{50}/C_{80} are observed for all 3 rows.

Finally, as was the case with the measurement results, higher values of C_{50}/C_{80} are observed for R13 and R14 here as well, which confirms that these impulse responses are unsuitable for the purposes of this study.

Appendix C, CATT-Acoustic contains corresponding figures, showing in more detail the behaviour of C_{80} across the space, separately for each configuration.

6.7 *ODEON IRs*

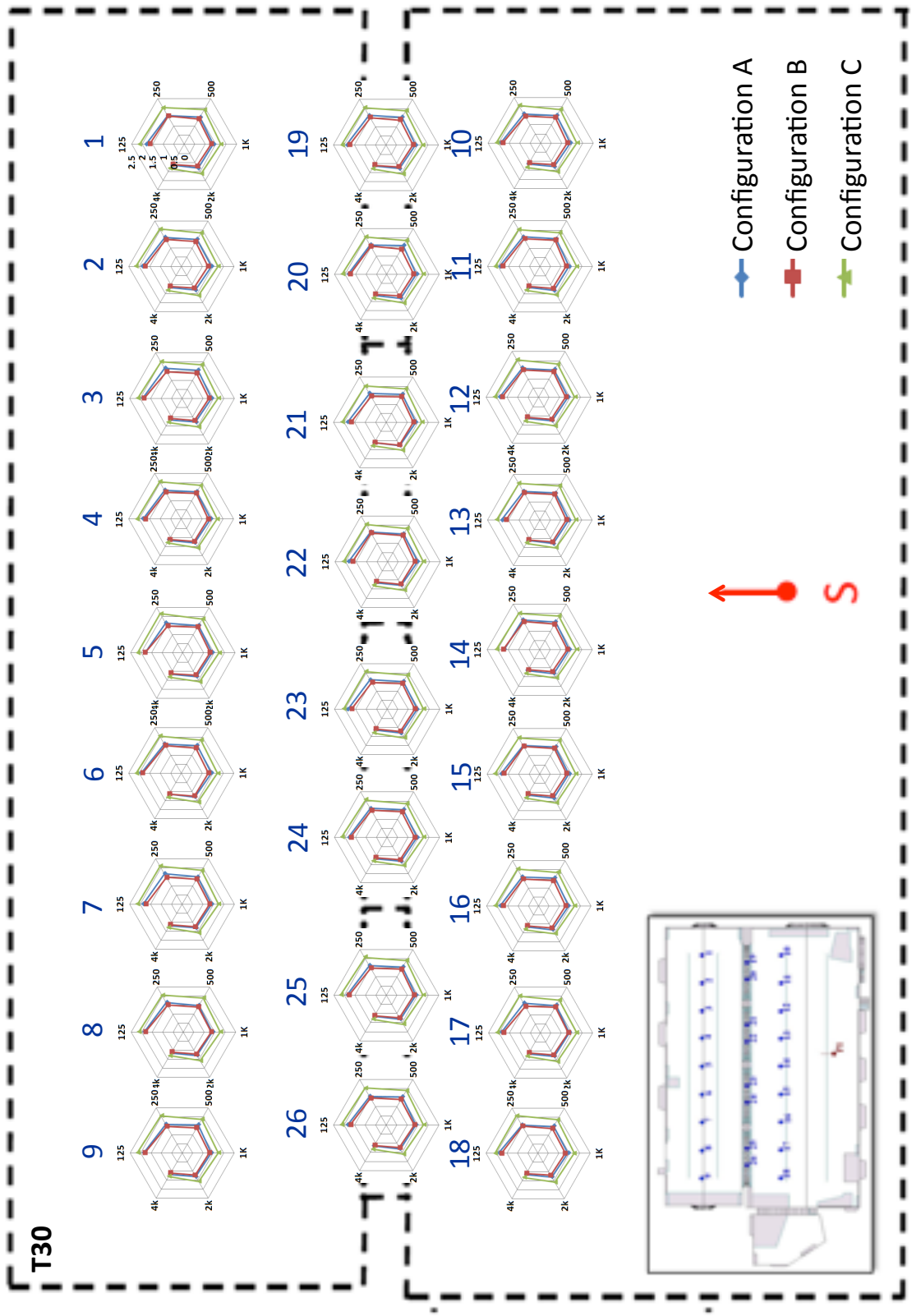

Figure 6.23 Acoustic floor map of T_{30} values obtained from the ODEON model varying with configurations A, B and C across the grid of 26 receiver positions.

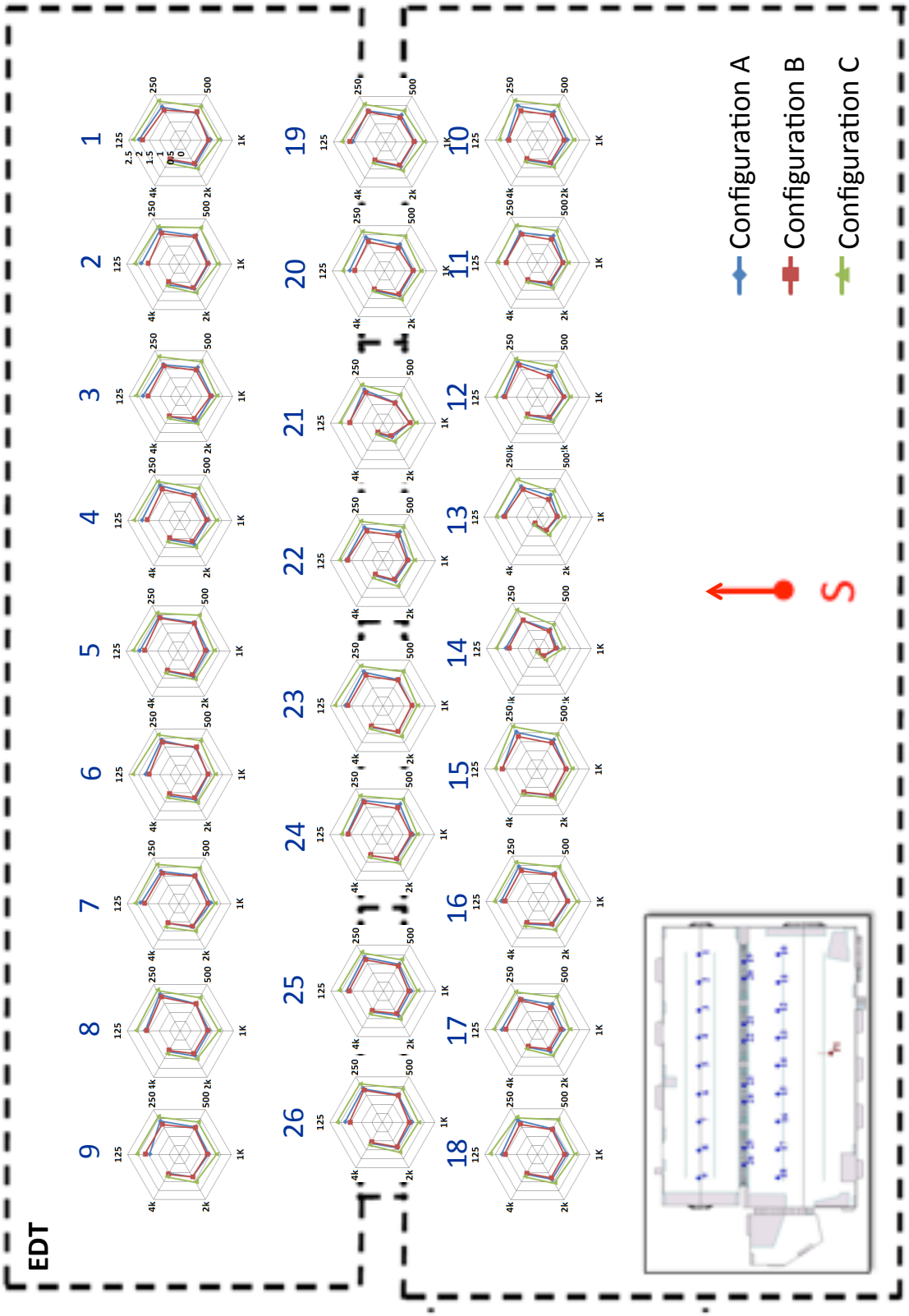

Figure 6.24 Acoustic floor map of EDT values obtained from the ODEON model varying with configurations A, B and C across the grid of 26 receiver positions.

The T_{30} values are increased respectively across the three configurations, from the less (configuration B) to the most reverberant configuration (configuration C), as shown in Figure 6.23.

Across all receiver positions, there are minimal variations in T_{30}. For the individual positions, small differences are noted, especially between configurations A and B, with configuration A slightly more reverberant, as would be expected. T_{30} values for configuration C have increased up to 0.5s more than those observed for the other two configurations across all the octave bands.

Figure 6.24 shows that changes in EDT across all measured positions are minimal for the three configurations. It is also observed that EDT has behaviour corresponding to that of T_{30}, across each of the three configurations studied.

Additionally, it can be noticed once more that higher values of C_{50}/C_{80} are observed for R13 and R14, as observed in measurements and CATT-Acoustic results as well.

Appendix C, ODEON, contains corresponging figures, showing in more detail the behaviour of EDT across the space, separately for each configuration.

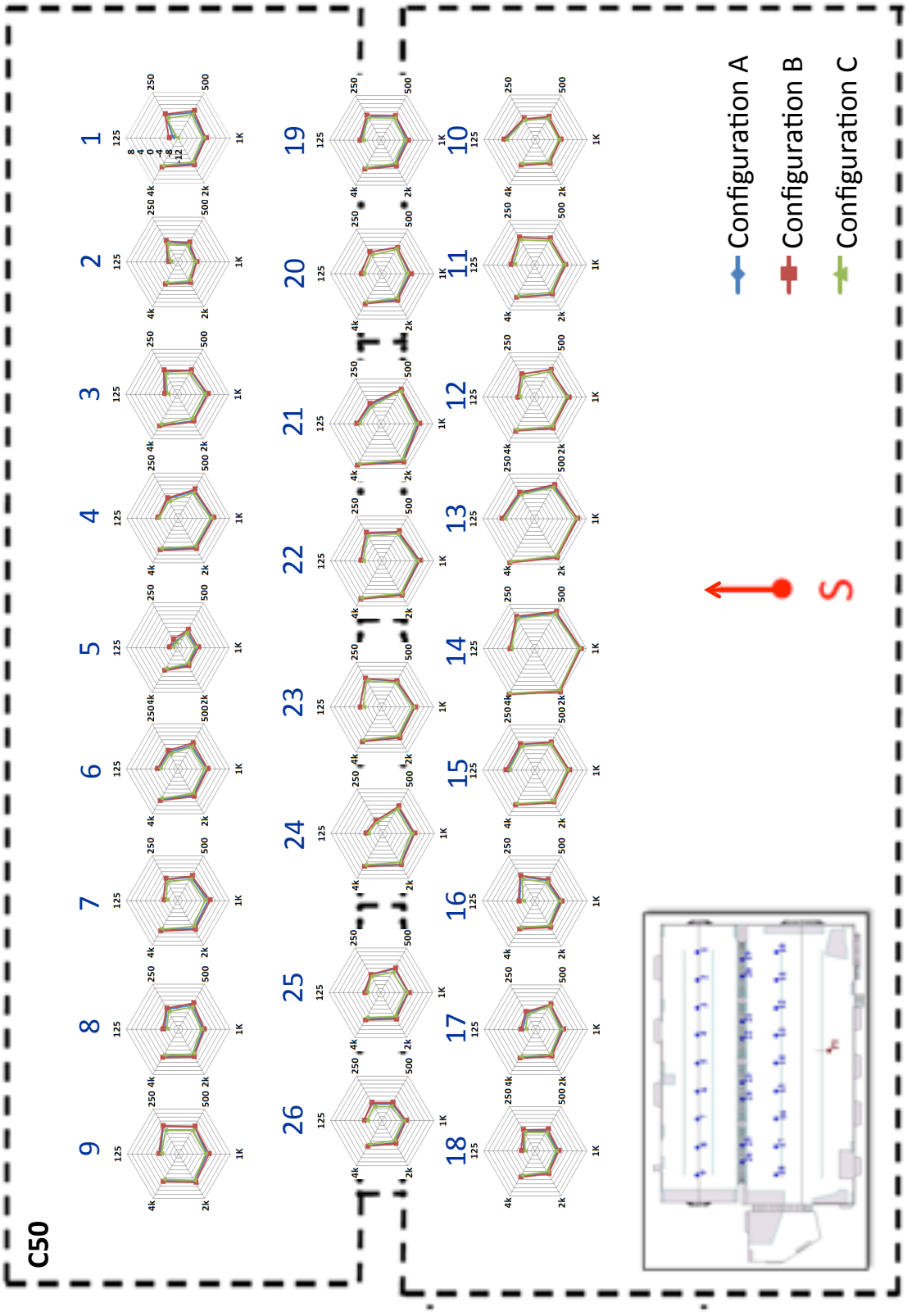

Figure 6.25 Acoustic floor map of C_{50} values obtained from the ODEON model varying with configurations A, B and C across the grid of 26 receiver positions.

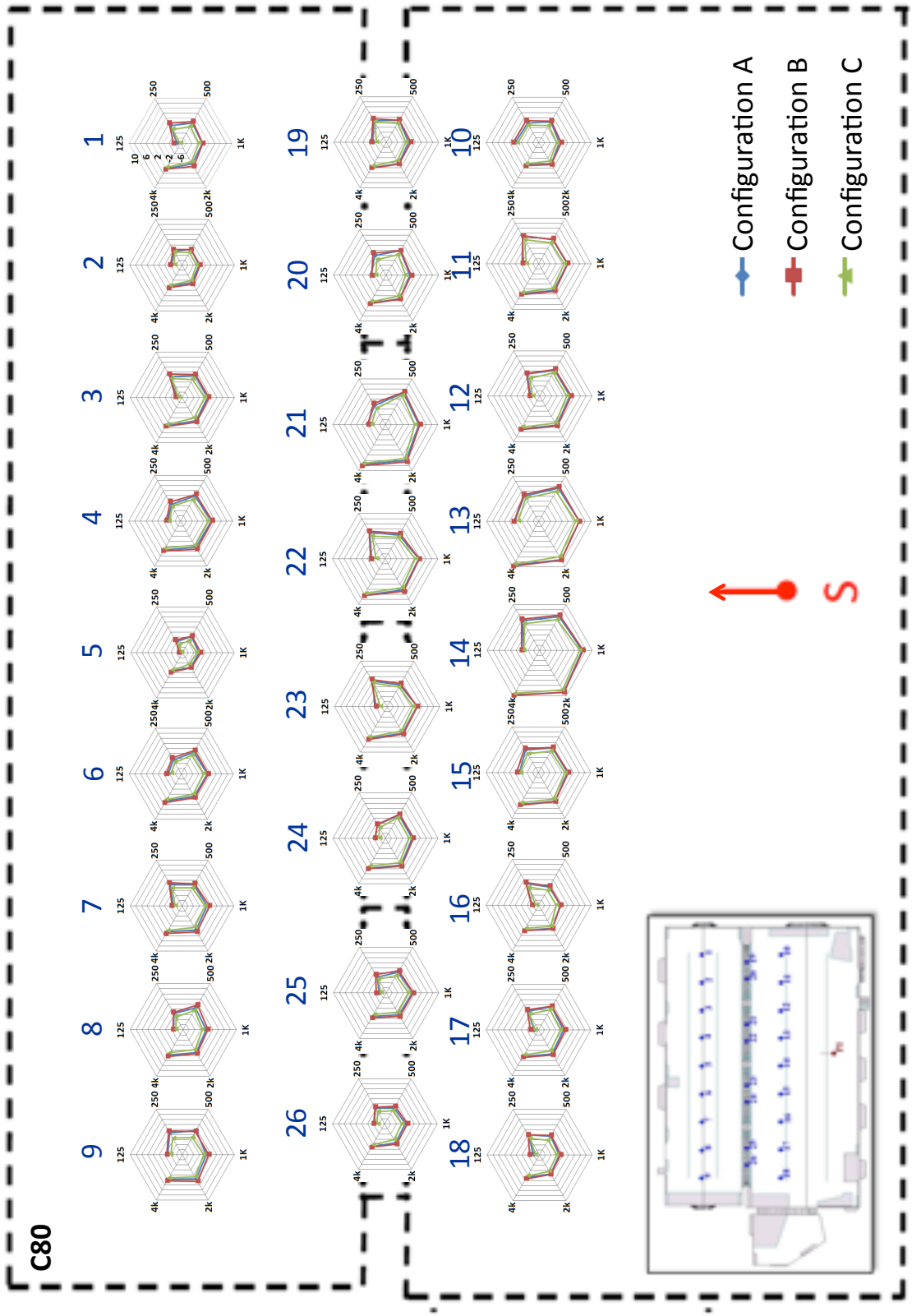

Figure 6.26 Acoustic floor map of C_{80} values obtained from the ODEON model varying with configurations A, B and C across the grid of 26 receiver positions.

As expected C_{50}, (Figure 6.25) and C_{80} (Figure 6.26) vary across the space, as these are highly position dependent parameters. It is also observed that for each individual measurement position, C_{50}/C_{80} values are similar for each of the three configurations. It is important to note here once more though that this does not necessarily mean the same early and late energy is arriving at the receiver positions for all acoustic configurations, as C_{50}/C_{80}, from definition, describes the ratio of early to late energy.

Dividing the space into three regions, as previously shown in Figure 6.13, it is noticeable that in the regions (a) and (b), the receiver positions further away from the source have lower C_{50}/C_{80} values, while C_{50}/C_{80} increases for positions closer to the source. This cannot be noticed however, in region (c), where low values for C_{50}/C_{80} are observed for all 3 rows, and as explained before this could be the influence of the late reflections arriving from the ground tower area, in region (c) of the space. Higher values of C_{50}/C_{80} for R13 and R14 are observed as well. Appendix C, ODEON, contains corresponding figures, showing in more detail the behaviour of C_{80} across the space, separately for each configuration.

6.8 *Summary*

In this chapter, the process used to calculate the acoustic parameters is explained in more detail, followed by a description of the methodology, which involved deconvolution of the recorded sine sweeps obtained from the actual space, as well as a discussion of the reasons for choosing the parameters considered for this current study. A novel to analyse and represent the data collected - "acoustic floor maps" – is also described, along with the data for the multiple positions studied, based on their behaviour across octave bands.

The analysis includes data obtained from the measured impulse responses, and the impulses responses produced by CATT-Acoustic and ODEON models. The results of these three different auralization techniques were presented separately, as there was not any intention in this study to make comparisons between them. The simulated models, as described in the previous chapter, were created quite independently from the measurement results, as the optimisation of the models was not necessary for the purposes of this study.

The next step, explained in the following chapter, is to select the appropriate impulse responses from this wide data set, based on observed acoustic parameters values for the purposed listening tests leading to confirmation of the hypothesis under investigation.

Chapter 7.
Subjective evaluations of Auralized St. Margaret's Church

7.1 *Introduction*

A considerable amount of literature exists regarding various procedures for evaluating the acoustic quality of spaces, both real and virtual. Over the years researchers have sought to build a framework capable of explaining the subjective sense of these acoustic effects and to correlate them with the objective parameters values [43, 80, 82, 101, 163, 207, 213-219].

The common approach to studying the psychoacoustic impression of a space is to analyse the perceptual results obtained from asking listeners who have visited the space, either in the audience or as music performers. Surveys of such cases are based on questionnaires administered to the listeners during or after their presence in the space [82, 219, 220].

Auralization applications have introduced an additional approach for the study of these psychoacoustic effects. Anechoic recording samples are convolved with impulse responses, either obtained from measurements in-situ or from computer models. Convolution can be applied in real-time in laboratories, in conditions where researchers can control the reproduction and rendering process [26, 42, 65, 72, 161, 221], as shown in Figure 7.1.

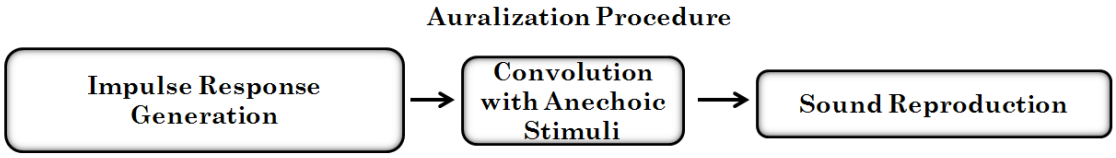

Figure 7.1 For auralization, impulse responses are convolved with anechoic stimuli and the output is reproduced in laboratories applying multi-channel reproduction, under the control of the researchers.

However, acoustic perception has a variety of aspects and is influenced by factors such as the loudness of the sound, its intelligibility, the reverberation and the spatial information [209, 222]. Hence, even "after a hundred years of reverberation time" [205], we still cannot describe with accuracy what we listen to nor the correlation of subjective and objective measures.

As stated in this thesis, the subjective quality of the auralization results of a virtual acoustic environment is at least as important as the objective evaluation of the relevant acoustic parameters. In order to investigate the sensitivity of listeners to auralization changes occurring in a particular space, changes have been made to the physical acoustic characteristics of St. Margaret's Church. In the previous chapters, the methodology followed for the purpose of this work was described in detail. It has been explained how the required impulse responses of real spaces were measured in situ or produced by acoustic simulation, using CATT-Acoustic and ODEON software (Chapter 5). The four main objective measures of these impulse responses were then analysed and presented in Chapter 6.

For the subjective evaluation of these changes, listening tests were performed for each of the three different auralization techniques. In this chapter, the procedure followed for the selection of the auralization examples as well as the procedure for carrying out the listening tests conducted, are described in detail and the results are analysed in-depth.

7.2 *Pilot Experiment from Auralized St. Margaret's Church*

Before introducing the listening tests conducted for the purposes of this research, the results of a preliminary listening test are worth mentioning [133]. The experiment was also based on impulse responses obtained from in-situ

measurements of St. Margaret's Church and the two simulation models in CATT-Acoustic and ODEON. These tests were based on preliminary versions of the models, with less appropriately defined material for the walls. The results ultimately showed longer reverberation time for the models than those observed with the final versions, were used in the main test (Figure 5.22 and Figure 5.23).

The goal of the initial listening tests was to validate the objective results observed using the three different auralization techniques in each of the three acoustic configurations. Six subjects were asked to listen to 16 pairs of samples, which were created by convolving impulse responses of the three acoustic configurations and the three auralization techniques with female singing and male speech. The subjects' first task was to identify the most reverberant sound of each pair and then to express the degree of similarity in terms of the perceived reverberation by marking a point on a scale with values from 1 (very similar) to 10 (very different).

The results shown a clear perceptual difference between the real and virtual cases. However, a very interesting point was that all participants indicated that the measurement results were more reverberant than either the ODEON or CATT models when comparison between them was taking place, even though both models had significantly longer reverberation times than the actual measurements. This confirmed the importance of looking at parameters other than reverberation time when optimising such models even if the study is focused on the perception of reverberance.

7.3 *Selection of the Impulse Responses for Auralization*

Three different auralization methods are examined for the current hypothesis; based on impulse responses: 1) measured in the actual space and generated in virtual acoustic models by using 2) CATT-Acoustic and 3) ODEON software. Thus, for the evaluation of the results, it was necessary to conduct listening tests separately for each case, but following exactly the same procedure.

It was crucial to find a suitable method to compare the values of the parameters studied across configurations A, B and C, and over the different receiver positions. Following the precedent set by previous studies [29], the corresponding JND values for each parameter, averaged over 500Hz and 1000Hz octave bands were used as a

reference value for these comparisons. According to ISO3382 [55] (section 2.6), the JND for parameters such as T_{30} and EDT, are defined to be within 5% of the measured values, assuming a typical range of 1.0s to 3.0s. For clarity (C_{50}/C_{80}) JND is defined to be 1dB, for a typical range of values from -5dB to +5dB.

Thus, in order to include all the results obtained from the study, from all the 26 receiver positions for each of the three acoustic configurations, A, B, and C, the values of the four acoustic parameters were sorted in increasing order. The JND of the minimum observed value was calculated and used as a reference value for the comparison of the changes for each of the parameters. For the calculation of the JND, the average values of T30, EDT, C50 and C80 over 500 and 1000Hz octave bands were used, based on the recommendations of ISO3382 [55]. The lists are represented in Appendix D.

From these lists, the R13 and R14 positions were excluded as their distance from the source was not considered large enough for reliable results, even if they were placed further away from the corresponding critical distance in each measurement configuration (theoretically calculated). The direct sound was too strong and there was not as good a balance between early and late reflections.

Note that the goal of this study is not to compare the different auralization methods. As explained previously in the thesis, such a comparison is not accurate and will not give scientific results about the perceptual differences that occur due to observed changes in the related acoustic parameters. Their comparison is used in other work as a guide for acoustic designers and developers of acoustic simulation software, as discussed in previous chapters. In this study, it is necessary to focus on the results of each auralization method individually in order to examine the perceptual differences of different acoustic metrics and parameters.

The method for the evaluation of these changes was to ask the subjects if they could perceive differences by comparing pairs using the A/B comparison method as in [72, 190, 213, 222]. The pairs were categorised in different groups according to the parameter(s) studied. For each pair in the group, the samples differed from each other in terms of the JND variations, which were increased for each pair, while keeping the rest of the acoustic parameters studied within 1 JND variation.

Due to this methodology, the selected samples differed in terms of physical acoustic changes as well. Hence, pairs would compare samples from different acoustic configurations, different orientation of the source (for the samples obtained from the actual measurements), or from different measurement positions within the space. As mentioned earlier (in section 6.3), the impulse responses were all normalised so that the level of the direct sound was equal in each of them, as in [190].

The same methodology was followed for all the impulse responses observed from each of the three different auralization techniques, the characteristics of which are presented in detail in the following section. Hence, the first step of the auralization procedure was completed with the selection of suitable impulse responses from all three auralization techniques, as represented in Figure 7.2.

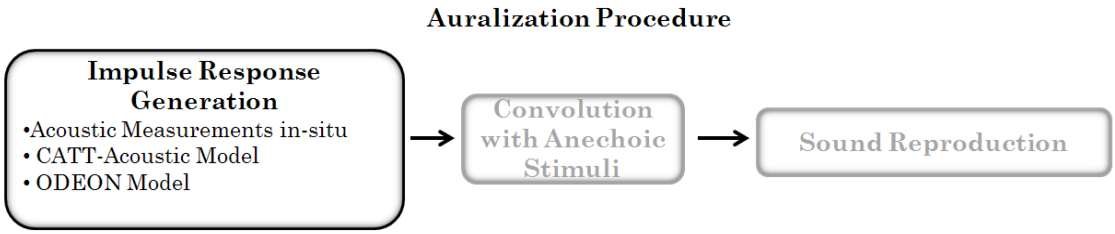

Figure 7.2 The impulse responses required for the first step of the auralization procedure are selected from the impulse responses obtained from the acoustic measurements in-situ, and from the impulse responses generated by both acoustic models, in CATT-Acoustic and ODEON software.

7.3.1 Impulse responses from measurements

For the perceptual evaluation of the variations of the four acoustic parameters observed from the acoustic measurements in-situ, data from all three acoustic configurations and from the three source orientation configurations were included. The selected examples were based on different groups based on the values of the acoustic parameters and the relative JND values, as shown in Table 7.1 and Table 7.2 based on the measurements of the three acoustic configurations and the three source orientations respectively.

Table 7.1 Calculating the JNDs obtained from the single number averaged across 500Hz and 1000Hz octave bands, for each parameter based on the minimum observed values (Appendix D, Measurements, Configurations A, B and C) from the measured impulse responses of the three acoustic configurations.

	T30		EDT		C50		C80	
Minimum Values	R24	1.358	R22	1.2535	R18	-4.6015	R8	-1.787
JND		0.0679		0.062675		1		1

Table 7.2 Calculating the JNDs obtained from the single number averaged across 500Hz and 1000Hz octave bands, for each parameter based on the minimum observed values (Appendix D, Measurements, Source Orientations 0°, 40°, 70°) from the measured impulse responses of the three source orientations.

	T30		EDT		C50		C80	
Minimum Values	R18	1.4305	R10	1.2115	R18	-7.0295	R18	-3.547
JND		0.071525		0.060575		1		1

As shown in Table 7.3 and Table 7.4, the pairs of examples for the A/B comparison differed in each group, based on a defined characteristic. The colours indicate the acoustic configuration from which each impulse response was captured, while the examples defined with (*) include the impulse responses captured from the different source orientation configurations. Out of the 130 possible total recordings from the actual space, 33 were used for the listening tests and 20 pairs of impulse responses were selected as appropriate for the purpose of this study.

Table 7.3 The groups of pairs from the in-situ measured impulse responses. 20 pairs of A/B impulse responses were selected based on the calculated acoustic parameter values. The colours indicate the acoustic configurations for each impulse response (Blue for Configuration A, Red for configuration B and Green for configuration C). The pairs defined with (*) are impulse responses from the source orientation configurations (Blue for the 0° orientation of the source, Red for the 40° and Green for the 70°).

Selected Pairs for Measurements										
Pair	A	B	T30		EDT		C50		C80	
1	R26	R5	1.378	1.3825	1.4425	1.4395	-2.357	-2.1815	0.472	0.7875
2*	R1	R15	1.475	1.4625	1.5505	1.546	-1.471	-1.1735	0.6465	0.601
3	R8	R18	1.795	1.7755	1.8045	1.7555	-4.195	-4.6015	-1.787	-1.5025
4	R23	R12	1.8165	1.8165[3]	1.767	1.761	0.3285	1.175	2.785	3.1355
5	R6	R6	1.454	1.373	1.5875	1.468	-1.3155	-0.3575	1.788	2.4065
6	R6	R6	1.454	1.78	1.5875	1.7865	-1.3155	-2.437	1.788	0.4985
7	R6	R6	1.373	1.78	1.468	1.7865	-0.3575	-2.437	2.4065	0.4985
8	R23	R24	1.4385	1.358	1.3145	1.5555	1.36	0.133	4.3455	1.8025
9	R17	R17	1.4495	1.794	1.5065	1.9075	-2.1595	-3.0455	0.085	-0.3015
10	R9	R8	1.3855	1.4905	1.5325	1.533	-1.078	-2.6455	0.9905	0.5185
11	R22	R21	1.476	1.41	1.2535	1.275	1.292	2.2455	5.101	4.5365
12	R24	R11	1.358	1.366	1.5555	1.416	0.133	0.09	1.8025	2.8795
13	R3	R20	1.8495	1.7935	1.705	1.9165	-1.7435	-1.564	0.886	0.84
14	R5	R2	1.3825	1.3785	1.4395	1.314	-2.1815	-1.555	0.7875	0.7575
15	R20	R21	1.387	1.41	1.2775	1.275	-0.426	2.2455	2.7935	4.5365
16*	R20	R20	1.468	1.476	1.394	1.3995	-1.01	0.7755	2.01	3.444
17	R11	R17	1.4465	1.4495	1.5105	1.5065	2.235	-2.1595	4.1775	0.085
18	R18	R15	1.7755	1.7765	1.7555	1.873	-4.6015	-0.2605	-1.5025	1.1455
19	R3	R1	1.514	1.4935	1.4555	1.517	-0.4155	-2.796	1.963	-0.38
20*	R18	R18	1.4505	1.4305	1.4275	1.5695	-4.2625	-7.0295	-0.745	-3.547

[3] These two positions had exactly the same calculated T30 values, as an average of 500Hz and 1000Hz octave bands.

Table 7.4 The groups of pairs from the in-situ measured impulse responses. 20 pairs of A/B impulse responses were selected based on their difference in absolute JND values (approximated at the second decimal) obtained from the single number averaged across 500Hz and 1000Hz octave bands. The colours indicate the acoustic configurations for each impulse response (Blue for Configuration A, Red for configuration B and Green for configuration C), while the differences with more than 1 JND value are highlighted in grey. The pairs defined with (*) are impulse responses from the source orientation configurations (Blue for the 0° orientation of the source, Red for the 40° and Green for the 70°).

Differences in JND values							
Pair	A	B	T30	EDT	C50	C80	
1	R26	R5	0.0662739	0.047866	0.1755	0.3155	T30/EDT/C50/C80 < JND
2*	R1	R15	0.1747641	0.0742881	0.2975	0.0455	T30/EDT/C50/C80 < JND
3	R8	R18	0.287187	0.7818109	0.4065	0.2845	T30/EDT/C50/C80 < JND
4	R23	R12	0	0.095732	0.8465	0.3505	T30/EDT/C50/C80 < JND
5	R6	R6	1.1929308	1.9066613	0.958	0.6185	C50/C80 < JND, **T30/EDT ≥ JND**
6	R6	R6	4.8011782	3.1751097	1.1215	1.2895	**T30/EDT/C50/C80 ≥ JND**
7	R6	R6	5.994109	5.081771	2.0795	1.908	**T30/EDT/C50/C80 ≥ JND**
8	R23	R24	1.185567	3.8452333	1.227	2.543	**T30/EDT/C50/C80 ≥ JND**
9	R17	R17	5.0736377	6.3980854	0.886	0.3865	C50/C80 < JND, **T30/EDT ≥ JND**
10	R9	R8	1.5463918	0.0079777	1.5675	0.472	EDT/C80 < JND, **T30/C50 ≥ JND**
11	R22	R21	0.9720177	0.3430395	0.9535	0.5645	EDT/C80 < JND, **T30/C50 ≥ JND**
12	R24	R11	0.1178203	2.2257679	0.043	1.077	T30/C50 < JND, **EDT/C80 ≥JND**
13	R3	R20	0.8247423	3.3745513	0.1795	0.046	T30/C50/C80 < JND, **EDT >JND**
14	R5	R2	0.0589102	2.0023933	0.6265	0.03	T30/C50/C80 < JND, **EDT >JND**
15	R20	R21	0.3387334	0.0398883	2.6715	1.743	T30/EDT < JND, **C50/C80 > JND**
16*	R20	R20	0.111849	0.0907965	1.7855	1.434	T30/EDT < JND, **C50/C80 > JND**
17*	R11	R17	0.0419434	0.0660338	4.3945	4.0925	T30/EDT < JND, **C50/C80 > JND**
18	R18	R15	0.0147275	1.8747507	4.341	2.648	T30 < JND, **C50/C80/EDT ≥ JND**
19	R3	R1	0.3019146	0.9812525	2.3805	2.343	T30 < JND, **C50/C80/EDT ≥ JND**
20*	R18	R18	0.2796225	2.3442014	2.767	2.802	T30 < JND, **C50/C80/EDT ≥ JND**

Note from Table 7.3 that R17 (blue) (as A in the 9th pair and as B at the 17th pair) is the same measured impulse response. However, for the comparison of the pairs, variations between acoustic configurations and variations in source orientations, different JND values were used in each case as reference, which resulted in different JND values in Table 7.4.

7.3.2 Impulse responses from the CATT-Acoustic model

For the perceptual evaluation of the variations in the four acoustic parameters observed from the CATT-Acoustic model, data from all three acoustic configurations (but not the source orientation) were included. The selected examples were based on the same groups as those presented for the in-situ measurement impulse responses (Table 7.3 and Table 7.4) according to the values of the acoustic parameters and the relative JND values, as shown in Table 7.5.

Table 7.5 Calculating the JNDs obtained from the single number averaged across 500Hz and 1000Hz octave bands, for each parameter based on the minimum observed values (Appendix D, CATT-Acoustic, Configurations A, B and C) from the measured impulse responses of the three acoustic configurations in CATT-Acoustic.

	T30	EDT	C50	C80
Minimum Values	R26 1.4685	R21 1.08	R2 -3.882	R18 -1.428
JND	0.073425	0.054	1	1

As shown in Table 7.6 and Table 7.7, the pairs of examples for the A/B comparison differed in each group based on a defined characteristic. The colours indicate the acoustic configuration from which each impulse response was captured. Out of the 78 possible total recordings from the actual space, 29 of them were used for the listening tests and 18 pairs of impulse responses were selected as appropriate for the purpose of this study.

Table 7.6 The groups of pairs from the impulse responses of the CATT-Acoustic model. 18 pairs of A/B impulse responses were selected based on the calculated acoustic parameter values. The colours indicate the acoustic configurations for each impulse response (Blue for Configuration A, Red for configuration B and Green for configuration C).

Selected Pairs for CATT-Acoustic										
Pair	A	B	T30		EDT		C50		C80	
1	R26	R9	1.4685	1.4985	1.579	1.599	-2.343	-1.432	0.6285	1.5685
2	R1	R10	1.5515	1.577	1.8635	1.845	-0.1635	-0.219	1.3875	1.761
3	R19	R24	1.9235	1.9475	2.174	2.1375	-0.8005	-0.6235	0.828	1.195
4	R7	R20	1.947	1.9605	2.3165	2.334	-0.8165	-0.9315	1.083	1.3335
5	R6	R6	1.4845	1.599	1.545	1.64	0.791	0.6185	2.341	2.844
6	R6	R6	1.4845	1.9375	1.545	2.1005	0.791	-0.776	2.341	0.606
7	R6	R6	1.599	1.9375	1.64	2.1005	0.6185	-0.776	2.844	0.606
8	R12	R12	1.6405	1.5035	1.6745	1.7115	1.548	2.3345	4.1215	4.6885
9	R9	R25	1.4985	1.59	1.599	1.628	-1.432	-1.2105	1.5685	1.2595
10	R22	R21	1.5225	1.5385	1.1455	1.08	2.0935	2.6825	4.9475	4.81
11	R8	R1	1.8845	1.918	2.403	2.252	-3.209	-2.7805	-0.923	0.2705
12	R22	R11	1.6285	1.633	1.476	1.212	1.9635	1.968	4.042	4.6395
13	R25	R6	1.59	1.599	1.628	1.64	-1.2105	0.6185	1.2595	2.844
14	R8	R4	1.5845	1.6235	1.6635	1.6435	-2.3475	1.165	0.768	2.751
15	R21	R17	1.9205	1.975	1.9515	2.0025	2.1135	-3.0545	3.2915	-1.103
16	R20	R26	1.565	1.566	1.3175	1.7655	0.3715	-2.74	3.5865	0.8205
17	R2	R17	1.5195	1.5135	1.6195	1.4685	-2.734	-0.965	0.137	1.799
18	R21	R10	1.9205	1.9075	1.9515	2.1365	2.1135	-1.3665	3.2915	1.0025

Table 7.7 The groups of the pairs from the impulse responses of the CATT-Acoustic model. 18 pairs of A/B impulse responses were selected based on their difference in absolute JND values (approximated at the second decimal) obtained from the single number averaged over 500Hz and 1000Hz octave bands. The colours indicate the acoustic configurations for each impulse response (Blue for Configuration A, Red for configuration B and Green for configuration C), while the differences with more than 1 JND value are highlighted in grey.

Differences in JND values							
Pair	A	B	T30	EDT	C50	C80	
1	R26	R9	0.41	0.37	0.91	0.94	T30/EDT/C50/C80 <JND
2	R1	R10	0.35	0.34	0.06	0.37	T30/EDT/C50/C80 <JND
3	R19	R24	0.33	0.68	0.18	0.37	T30/EDT/C50/C80 <JND
4	R7	R20	0.18	0.32	0.12	0.25	T30/EDT/C50/C80 <JND
5	R6	R6	1.56	1.76	0.17	0.50	C50/C80 < JND, **T30/EDT > JND**
6	R6	R6	6.17	10.29	1.57	1.74	**T30/EDT/C50/C80 ≥ JND**
7	R6	R6	4.61	8.53	1.39	2.24	**T30/EDT/C50/C80 ≥ JND**
8	R12	R12	1.87	0.69	0.79	0.57	EDT/C50/C80 < JND, **T30 > JND**
9	R9	R25	1.25	0.54	0.22	0.31	EDT/C50/C80 < JND, **T30 > JND**
10	R22	R21	0.22	1.21	0.59	0.14	T30/C50/C80 < JND, **EDT >JND**
11	R8	R1	0.46	2.80	0.43	1.19	T30/C50/C80 < JND, **EDT >JND**
12	R22	R11	0.06	4.89	0.00	0.60	T30/C50/C80 < JND, **EDT >JND**
13	R25	R6	0.12	0.22	1.83	1.58	T30/EDT < JND, **C50/C80 > JND**
14	R8	R4	0.53	0.37	3.51	1.98	T30/EDT < JND, **C50/C80 > JND**
15	R21	R17	0.74	0.94	5.17	4.39	T30/EDT < JND, **C50/C80 > JND**
16	R20	R26	0.014	8.30	3.11	2.77	T30 < JND, **C50/C80/EDT > JND**
17	R2	R17	0.082	2.80	1.77	1.66	T30 < JND, **C50/C80/EDT > JND**
18	R21	R10	0.18	3.43	3.48	2.29	T30 < JND, **C50/C80/EDT > JND**

7.3.3 Impulse responses from the ODEON model

For the perceptual evaluation of the variations in the four acoustic parameters observed from the ODEON model, data from all three acoustic configurations were included (but not the source orientation). The selected examples were based on the same groups, as those presented for the in-situ measurement impulse responses (Table 7.3 and Table 7.4) according to the values of the acoustic parameters and the relative JND values, as shown in Table 7.8.

Table 7.8 Calculating the JNDs obtained from the single number averaged across 500Hz and 1000Hz octave bands, for each parameter based on the minimum observed values (Appendix D, ODEON, Configurations A, B and C) from the impulse responses of the three acoustic configurations in ODEON.

	T30	EDT	C50	C80
Minimum Values	R2 1.307	R17 1.147	R5 -4.8025	R5 -1.237
JND	0.06535	0.05735	1	1

As shown in Table 7.9 and Table 7.10, the pairs of examples for the A/B comparison differed in each group based on a defined characteristic. The colours indicate the acoustic configuration from which each impulse response was captured. Out of the 78 possible total recordings in the actual space, 29 of them were used for the listening tests and 18 pairs of impulse responses were selected as appropriate for the purpose of this study.

Table 7.9 The groups of pairs from the impulse responses of the ODEON model. 18 pairs of A/B impulse responses were selected based on the calculated acoustic parameter values. The colours indicate the acoustic configurations for each impulse response (Blue for Configuration A, Red for configuration B and Green for configuration C).

Selected Pairs for ODEON										
Pair	A	B	T30		EDT		C50		C80	
1	R19	R25	1.3305	1.3645	1.3325	1.29	-0.173	-0.0465	2.5975	2.998
2	R19	R25	1.4635	1.473	1.4205	1.386	-0.6435	-0.4635	2.168	2.5515
3	R20	R9	1.792	1.7935	1.8155	1.779	-0.746	-0.6865	1.379	1.1065
4	R24	R23	1.352	1.3525	1.4	1.377	1.4695	1.49	3.527	3.69
5	R6	R6	1.3435	1.4725	1.3955	1.3805	0.5625	-0.1775	3.255	2.729
6	R6	R6	1.3435	1.7795	1.3955	1.75	0.5625	-1.1095	3.255	1.4455
7	R6	R6	1.4725	1.7795	1.3805	1.75	-0.1775	-1.1095	2.729	1.4455
8	R7	R23	1.335	1.475	1.4185	1.3975	0.812	1.3165	3.057	3.4385
9	R16	R8	1.341	1.431	1.4135	1.3935	-1.1985	-1.017	1.4925	2.0515
10	R1	R20	1.3265	1.318	1.425	1.29	0.375	0.59	2.2795	3.2375
11	R10	R25	1.4575	1.473	1.4755	1.386	-1.255	-0.4635	1.65	2.5515
12	R24	R11	1.789	1.805	1.8005	1.6035	0.02	0.0405	2.103	2.498
13	R19	R26	1.4635	1.47	1.4205	1.4475	-0.6435	-2.978	2.168	0.6435
14	R2	R3	1.307	1.335	1.415	1.4275	-3.29	0.3035	0.184	3.0655
15	R26	R24	1.8235	1.789	1.7965	1.8005	-4.112	0.02	-0.461	2.103
16	R25	R26	1.3645	1.361	1.29	1.3695	-0.0465	-2.511	2.998	1.35
17	R16	R17	1.7785	1.7615	1.8635	1.6675	-2.406	-1.0455	-0.016	1.7405
18	R10	R21	1.3315	1.351	1.313	1.176	-1.0195	4.4765	2.1015	6.397

Table 7.10 The groups of the pairs from the impulse responses of the ODEON model. 18 pairs of A/B impulse responses were selected based on their difference in absolute JND values (approximated at the second decimal) obtained from the single number averaged over 500Hz and 1000Hz octave bands. The colours indicate the acoustic configurations for each impulse response (Blue for Configuration A, Red for configuration B and Green for configuration C), while the differences with more than 1 JND value are highlighted in grey.

Differences in JND values							
Pair	A	B	T30	EDT	C50	C80	
1	R19	R25	0.52	0.74	0.13	0.40	T30/EDT/C50/C80 <JND
2	R19	R25	0.15	0.60	0.18	0.38	T30/EDT/C50/C80 <JND
3	R20	R9	0.02	0.64	0.06	0.27	T30/EDT/C50/C80 <JND
4	R24	R23	0.01	0.40	0.02	0.16	T30/EDT/C50/C80 <JND
5	R6	R6	1.97	0.26	0.74	0.53	C50/C80/EDT < JND, **T30 > JND**
6	R6	R6	6.67	6.18	1.67	1.81	**T30/EDT/C50/C80 > JND**
7	R6	R6	4.70	6.44	0.93	1.28	**T30/EDT/C50/C80 ≥ JND**
8	R7	R23	2.14	0.37	0.50	0.38	EDT/C50/C80 < JND, **T30 > JND**
9	R16	R8	1.38	0.35	0.18	0.56	EDT/C50/C80 < JND, **T30 > JND**
10	R1	R20	0.13	2.35	0.22	0.96	T30/C50/C80 < JND, **EDT >JND**
11	R10	R25	0.24	1.56	0.79	0.90	T30/C50/C80 < JND, **EDT >JND**
12	R24	R11	0.24	3.44	0.02	0.40	T30/C50/C80 < JND, **EDT >JND**
13	R19	R26	0.10	0.47	2.33	1.52	T30/EDT < JND, **C50/C80 > JND**
14	R2	R3	0.43	0.22	3.59	2.88	T30/EDT < JND, **C50/C80 > JND**
15	R26	R24	0.53	0.07	4.13	2.56	T30/EDT < JND, **C50/C80 > JND**
16	R25	R26	0.054	1.39	2.46	1.65	T30 < JND, **C50/C80/EDT > JND**
17	R16	R17	0.26	3.42	1.36	1.76	T30 < JND, **C50/C80/EDT > JND**
18	R10	R21	0.33	2.39	5.50	4.30	T30 < JND, **C50/C80/EDT > JND**

7.4 *Convolution with Anechoic Stimuli*

For auralization it is necessary to convolve a dry signal (anechoic recording) with the selected impulse responses (measured or artificial ones). In previous studies such as [65, 66, 72, 190, 206, 222, 223], it has been shown that perceived differences in the acoustic parameters, and more specifically the JND values, depend on the characteristics of the motif being tested.

There are three main types of signal that can be used for auralization proposes, after Bech et al.[224];

- Music (anechoic recordings),
- Speech (anechoic recordings),
- Noise (artificial signals by random noise generators).

Variations between these types of signal can significantly affect the perceived result. For instance, Cox et al. in [65] show that a slow excerpt from Mendelssohn's *Symphony No. 3 in A minor* and a fast moving piece from Handel's *Water Music Suite* have a significant effect on the JND values for Centre Time (Ts) and C_{80}, but not for Early Lateral Energy Fraction (LF).

Listening tests are assumed more robust when different types of stimuli are able to be tested for the same hypothesis, with respect to the main aims of the test. For the current study due to the large number of tested pairs and the time consuming process of the listening tests involved, two different source signals have been used, one for each anechoic recording type described above. Hence, an excerpt of speech and instrumental music were used, considering the recommended activities within the space by Arup (Table 5.1) for the corresponding configurations of this study. In addition, this choice of samples was suitable for studying in detail the changes in both at C_{50} and C_{80} values, as according to ISO 3382, C_{50} is more associated with the study of the perception of speech and C_{80} for music.

The first was an excerpt of the initial 9s of an anechoic recording from a theme for solo cello by Weber, and the second was a 7s excerpt of male speech (between 30s and 37s from the original recording), both from the "Archimedes" project [225]. The passages of the cello are shorter than the human voice [72] and were considered a

suitable example for listening to the attacks and the effect of early reflections. Additionally, these stimuli were characterised by different spectra, as observed in Figure 7.3. The spectrum of the male speech can be characterised as flatter than the spectrum of the cello which demonstrates a wider variation across the frequency range.

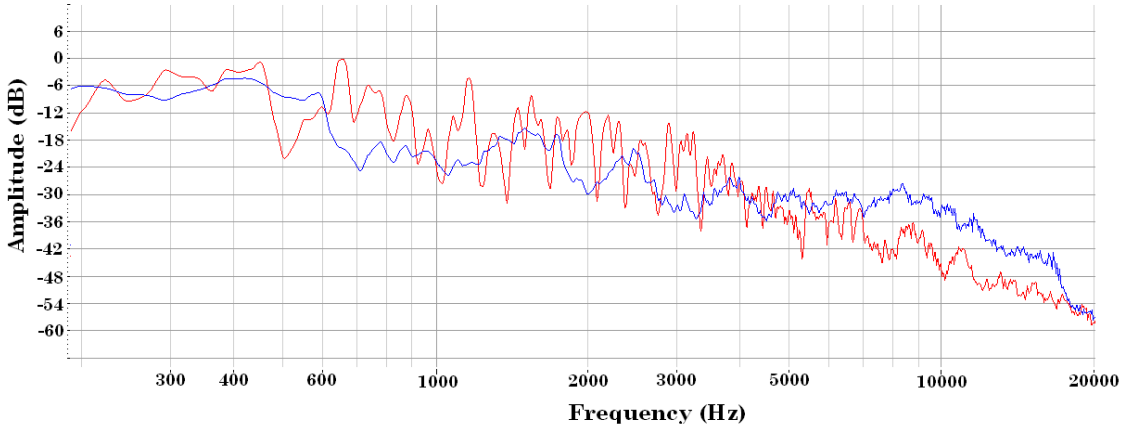

Figure 7.3 Frequency domain analysis (using Hamming window and with FFT size at 4096) of the two anechoic examples selected for the listening tests. The excerpt of male speech is represented in blue and the excerpt of cello in red.

Once the anechoic stimuli had been chosen they were convolved with the selected impulse responses (as described in the previous section) using Aurora [226].

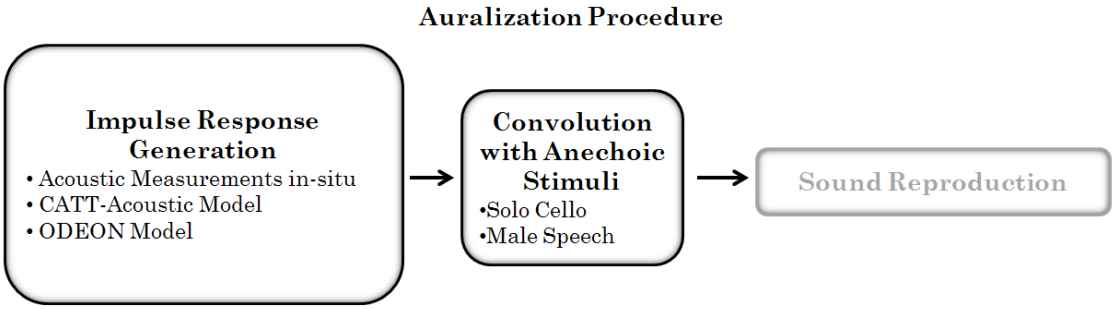

Figure 7.4 For the auralization procedure the impulse responses are convolved with anechoic stimuli (a) an excerpt of solo cello by Weber and (b) an excerpt of male speech.

7.5 *Sound Reproduction*

The development of both auralization and sound reproduction techniques in recent years means that it is now possible to reproduce 3D spatial audio environments with a high degree of accuracy and realism [26, 72, 94, 136, 161, 190, 209, 213, 219, 227, 228]. However, each of these techniques has its own limitations and

uncertainties, and there is still room for argument and further improvement regarding the perceived accuracy of the auralized spaces that resulted [27, 85, 190, 218].

It is essential to choose the appropriate sound reproduction system based on a consideration of the overall aim of the subjective evaluations. As the current study focuses only on the perception of the influence of variations in monoaural acoustic parameters, as discussed in 6.2, a mono-channel system was used for the reproduction of the auralization results. The anechoic material was convolved with the W-channel of the B-format files obtained from both in-situ measurements and acoustic models.

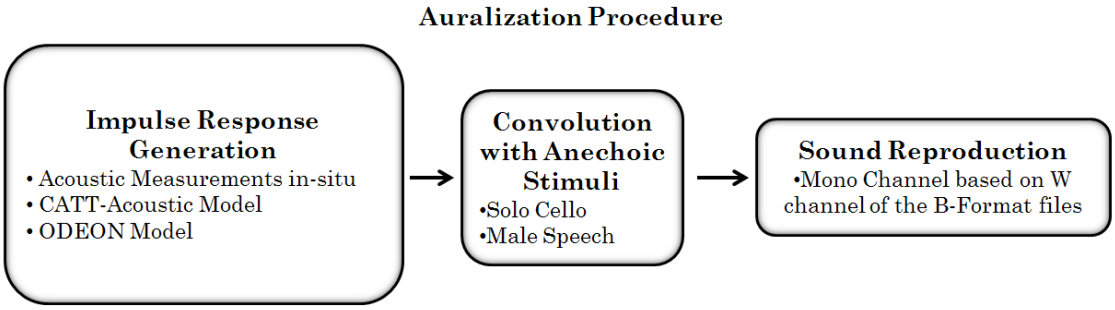

Figure 7.5 For the listening tests a mono-channel system replayed over headphones was used for sound reproduction. The auralization examples were based on the W-channel of the B-format files from both in-situ measurements and acoustic models.

In order to avoid the effect of additional reflections from the architectural characteristics of the listening room on the test samples, it was considered best to use closed-type headphones for the purposes of this study, (SRH440 Professional studio headphones). As two PCs were used simultaneously for the listening tests, it was important to use two identical headphones, calibrated approximately at the same level between 64 and 65 dB (A weighted). Note that the mono-channel auralizations are presented for headphone reproduction by replaying this single-channel convolution over both left and right headphone channels.

Due to the use of headphone reproduction for the listening tests, the influence of the acoustic characteristics of the listening room are actually insignificant [224]. The shape of the room was rectangular, one of the boundaries was an acoustically absorbing curtain and there was carpet on the floor, with an average T_{30} less than 0.4s. The noise level in the room was calculated between 40 and 43 dB (A

weighted). Although the above details should not affect the sound produced through closed-type headphones, it was considered better to "introduce" the participants to a quiet and dry enough room, before the actual listening test.

The comfort of the subjects was considered an important factor that might influence their answers and as a result the reliability of the listening tests [224]. Hence, it was ensured that the heating and the ventilation of the room were confortable. In addition, the window curtains were opened and any irrelevant equipment and furnishings were hidden with curtains, in order to avoid any external distraction.

As the subjects were using a computer interface during the tests, blind listening tests as suggested in [136, 228, 229] were not possible, although a black background desktop monitor screen was set to avoid further possible distractions.

7.6 *Listening Tests Procedure*

The question defined as central to these listening tests pertains to the overall focus of this thesis: **"Can we perceive an acoustic difference when minimal changes have been observed in objective acoustic parameters?".** As described previously, the subjects were asked to compare the selected pairs of samples using the A/B comparison method.

For the investigation of each auralization technique, the selected impulse responses were convolved with the relevant anechoic stimuli (cello, male speech). Hence, for the listening tests for the in-situ measured impulse responses, 40 (20 (pairs) x 2 (stimuli)) question were used in total, and for the listening tests based on the impulse responses from CATT-Acoustic and ODEON models, 36 (18 (pairs) x 2 (stimuli)) questions were used.

In order to ensure the listening tests proceeded smoothly, a graphical user interface (GUI) in Matlab was used[4] (Figure 7.6) in a similar way for all three listening tests. The convolving pairs were loaded and performed in random order

[4] The graphical user interface (GUI) in Matlab was developed by Andrew Chadwick, PhD Candidate in Audio Lab, Department of Electronics, University of York.

for every subject to reduce errors in the responses due to habituation and expectation by playing the samples in a specific order. The interface gave the option to the user to switch in real-time between samples A and B, or to stop each sample and replay it as many times as necessary, as in previous work [136].

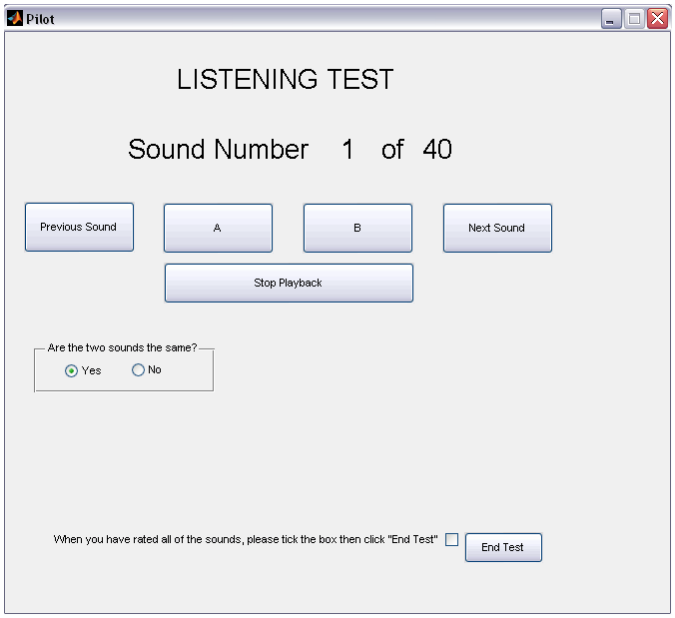

Figure 7.6 The graphical user interface (GUI) in Matlab for the listening test comparing the pairs obtained from the in-situ measurements.

It was considered important to train the subjects before taking the main listening test. This method is commonly used in listening tests, such as in [72, 163, 182, 224] to ensure the subjects are familiar with the interface used. The process of the listening test was explained to the subjects during the training session, where they were given the same tasks but for a reduced number of pairs. For the current tests, however, there was a second purpose for these training sessions for the investigator. The four pairs used were carefully chosen in order to also check the reliability of the participants and their ability to perceive variations using only one of the two chosen stimuli. One of the pairs had exactly the same sample for A and B, and the rest were exposed to evenly increased differentiation across all parameters, within the values used in the main test, compared with the first "reference" sample, as shown in Table 7.11, Table 7.12 and Table 7.13. Similar techniques have been used for investigating the subjects' reliability in previous studies by the current author [133], as well as in [72].

Table 7.11 The groups of pairs used for the training session from the in-situ measured impulse responses. 18 pairs of A/B impulse responses were selected based on their difference in absolute JND values. The colours indicate the acoustic configurations for each impulse response (Blue for Configuration A, Red for configuration B and Green for configuration C).

JND values for Training Session						
Pair	A	B	T30	EDT	C50	C80
1	R19	R19	0	0	0	0
2	R19	R15	1.539028	0.4706821	1.257	0.1075
3	R19	R18	1.0751105	2.0263263	3.469	2.544
4	R19	R18	4.4035346	5.0578381	4.2115	4.189

Table 7.12 The groups of pairs used for the training session from the CATT-Acoustic model impulse responses. 18 pairs of A/B impulse responses were selected based on their difference in absolute JND values. The colours indicate the acoustic configurations for each impulse response (Blue for Configuration A, Red for configuration B and Green for configuration C).

JND values for Training Session						
Pair	A	B	T30	EDT	C50	C80
1	R18	R18	0	0	0	0
2	R18	R26	0.490296	0.675926	1.215	0.738
3	R18	R10	0.776302	3.287037	1.4275	2.2345
4	R18	R21	1.069118	2.62963	3.9915	2.753

Table 7.13 The groups of pairs used for the training session from the ODEON model impulse responses. 18 pairs of A/B impulse responses were selected based on their difference in absolute JND variations. The colours indicate the acoustic configurations for each impulse response (Blue for Configuration A, Red for configuration B and Green for configuration C).

JND values for Training Session						
Pair	A	B	T30	EDT	C50	C80
1	R24	R24	0	0	0	0
2	R24	R9	0.084162	0.104621	0.424	0.382
3	R8	R24	1.208875	0.113339	2.4865	1.4755
4	R24	R16	1.973986	1.14211	3.1715	2.315

Due to the complexity of planning and conducting such rigorous listening tests, the main part of the tests was considered a good opportunity to gather some additional information from the subjects, not directly relevant to the main listening test hypothesis for the current research but certainly a further step towards future work based on this study. Hence, the subjects were asked the "if the sounds are the same" question to define the perceived differentiation in terms of the following:

- Loudness
- Reverberance (Duration)
- Diffusion
- Pitch / Frequency Response
- Clarity
- Attack.

The graphical user interface (GUI) with the additional questions is shown in Figure 7.7. It is well-known [59] that usually these terms are correlated to each other. For instance, in reality clarity is directly related with reverberation time, and frequency response (pitch) is correlated with the reverberance of the space. For this reason, the participants were able to choose more than one of the above terms. However this answer was optional, especially for those cases where the perceived difference could not be explicitly identified.

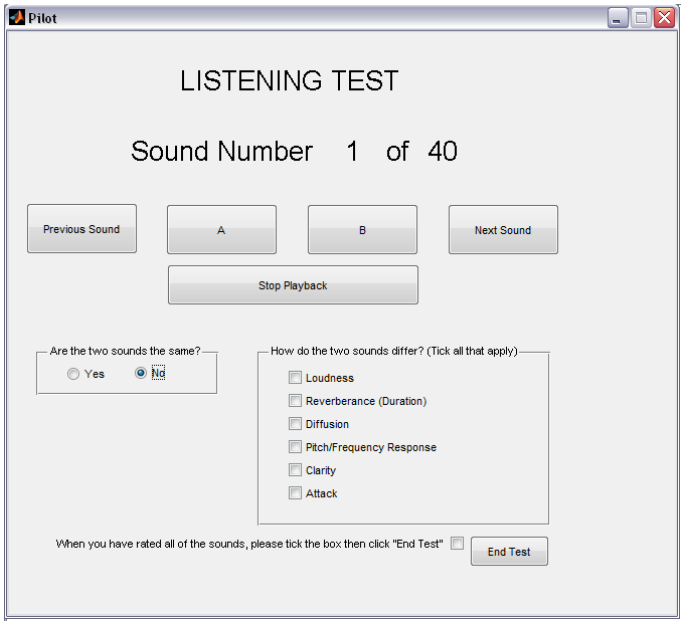

Figure 7.7 The optional graphical user interface (GUI) for the listening test comparing the pairs obtained from in-situ measurements.

These terms could be correlated in future with variations in specific acoustic parameters, as several works have been focused on these subjective terms [43, 59, 80, 82, 101, 163, 207, 215, 217, 230], as shown in . It is interesting to mention, however, the observation, as noted in [82], that there was a different understanding of some of these terms between musicians, acousticians and sound engineers/designers, and further explanation of the use of the terms was necessary in many cases during the training session.

Table 7.14 Correlations between terms used to define the perceived differentiation during the listening tests and objective acoustic parameters, for further work.

Terms	Correlations with Objective Parameters
Loudness	Strength (G), ITDG
Reverberance (Duration)	T_{30}, EDT, C_{50}, C_{80}
Diffusion	C_{50}, C_{80}
Pitch/Frequency Response	T_{30}, EDT, frequency dependence across the octave bands
Clarity	EDT, C_{50}, C_{80}
Attack	EDT, C_{50}, C_{80}, ITDG

7.7 *The Subjects*

The test subjects were musically experienced listeners (either musicians, concert goers or those with audio engineering experience) based on the assumption that if "trained ears" could not perceive any difference between the samples of each pair, naive listeners would require larger differentiations in order to perceive the difference, as has been mentioned in [72]. The subjects were all experienced listeners - either they were musicians, or had many years of musical training, or they were working in audio engineering/acoustics/sound design. Although their hearing was not tested with an audiometric test, 8% of the subjects declared slight hearing problems (such as slightly tinnitus problem in one ear) although the rest declared normal auditory capacity. As explained in the previous section, the reliability of the subjects and their hearing ability were additionally checked through their responses during the training session of the listening tests.

The category of "experienced" listeners has a significant impact on the number of subjects required for listening tests and according to Bech [224] a listening test which requires experienced subjects should involve twenty participants, as was the case in some previous studies [163, 209, 213, 219, 228]. However, in several studies this number was difficult to obtain and the number of subjects varied between 4 and 17 [136, 209, 215, 222, 230]. For the current study, thirteen subjects participated in each test, based on the in-situ measurements, CATT-Acoustic and ODEON impulse responses. Their age varied from 21 to 48 years old. For the in-situ measurements listening test, ten of the subjects were male and three female. For the CATT-Acoustic listening tests, eight of the subjects were male and five female. For the ODEON listening tests, nine of the subjects were male and four of them female.

Before the analysis of the listening tests results, the answers of the subjects were checked for their reliability (post-selection process of the subjects) by comparing with their answers at the training session. It was considered sufficient to exclude those subjects who could not indicate the difference for at least two of the three different pairs from the training session examples. There were no subjects with more than one answer wrong. For the in-situ measurements, three of the thirteen subjects could not hear the difference in one of the pairs, while in the CATT-Acoustic tests, three subjects could not and in for ODEON, two. Note that for each test, the thirteen subjects were not the same participants. However, this was only an indication of their reliability as the procedure could not confirm the reliability of their answers during the main test. Biases such as tiredness, loss of concentration or an unexpected noise event from the outer environment or from the equipment could have affected the perception of the subjects during the listening test.

It was very interesting to observe that one to three subjects in each test indicated as different the pair with exactly the same sample for A and B. This could be explained as a psychological effect due to the wording of the task and their desires/expectations to hear differences that were not there, as explained in [229]. These participants, however, where not excluded from the final analysed results as this attribute at the training session does not necessarily mean they were answering in a similar way during the main test. Their answers were taken into

consideration and it was observed that, overall, their answers in the main test did not deviate from the average answers of the rest of the participants.

Most of the participants characterised the tests as "difficult", meaning that in most cases they could hear a difference between the samples but could not discriminate exactly what the difference they were hearing was. The duration of each test was surprisingly varied, from less than 10 minutes to more than one hour (for three cases). For those cases where the participants needed more time, a short break was usually taken in the middle of the test. A significant difference in the answers of those who had completed the test more quickly than the others and vice versa, was not observed.

7.8 *Listening Test Subjects' Response*

Table 7.15 The answers reported by the thirteen subjects for the in-situ measurement listening test, for each of the two stimuli.

Questions for measurements	**Cello** (Participants out of 13 who perceived a difference)	**Voice** (Participants out of 13 who perceived a difference)
Pair 1	10	10
Pair 2	10	13
Pair 3	12	12
Pair 4	12	9
Pair 5	8	9
Pair 6	9	8
Pair 7	7	11
Pair 8	11	11
Pair 9	3	8
Pair 10	12	3
Pair 11	3	6
Pair 12	10	7
Pair 13	12	7
Pair 14	9	8
Pair 15	9	11
Pair 16	12	6
Pair 17	13	12
Pair 18	12	13
Pair 19	10	9
Pair 20	11	9

Table 7.16 The answers reported by the thirteen subjects for the CATT-Acoustic listening test, for each of the two stimuli.

Questions for CATT-Acoustic	**Cello** (Participants out of 13 who perceived a difference)	**Voice** (Participants out of 13 who perceived a difference)
Pair 1	9	9
Pair 2	11	13
Pair 3	6	11
Pair 4	13	13
Pair 5	4	5
Pair 6	11	10
Pair 7	4	11
Pair 8	12	6
Pair 9	7	9
Pair 10	10	6
Pair 11	12	13
Pair 12	12	12
Pair 13	11	10
Pair 14	9	13
Pair 15	13	13
Pair 16	13	11
Pair 17	11	11
Pair 18	12	13

Table 7.17 The answers reported by the thirteen subjects for the ODEON listening test, for each of the two stimuli.

Questions for ODEON	**Cello** (Participants out of 13 who perceived a difference)	**Voice** (Participants out of 13 who perceived a difference)
Pair 1	11	10
Pair 2	11	9
Pair 3	6	11
Pair 4	10	12
Pair 5	8	7
Pair 6	6	9
Pair 7	5	9
Pair 8	11	12
Pair 9	10	12
Pair 10	7	11
Pair 11	7	11
Pair 12	13	10
Pair 13	9	13
Pair 14	10	12
Pair 15	12	13
Pair 16	5	8
Pair 17	7	12
Pair 18	13	13

7.8.1 **Analysis based on JND values**

As discussed above, based on ISO3382, it was expected that the pairs of samples with less than 1 JND value would be perceived as the same and it was hypothesised that by increasing these JND values, the number of subjects who would perceive the difference would increase as well. Observing the results from all three listening tests (Table 7.15, Table 7.16 and Table 7.17), it is clear this hypothesis was not confirmed as the subjects could indicate a difference between the samples of each pair in most cases even if the objective values claimed the opposite. It is worth mentioning the received responses for the first four pairs, from all three listening tests. These pairs had been chosen as examples in which the differences between all the studied acoustic parameters were observed with less than 1 JND value. However, it is very interesting to observe that the majority of the responses had indicated a perceived difference between these pairs under examination, for all three listening tests.

Statistical analysis could not be applied to these listening tests because the expected result was known a priori. In fact, the test hypothesis was that all thirteen experienced subjects must not perceive the difference between the samples with less than 1 JND value according to ISO3382, therefore giving zero for the expected error of these tests. Additionally, there was not any correlation between the pairs of each group and the number of positive answers due to the non-parametric values of the "Yes" and "No" answer type.

Hence, in order to investigate further the possible reasons for the perceptual difference, an observation of the waveforms was undertaken and the differences between the waveforms of the samples of the hypothesised "identical" pairs analysed. As the impulse responses were all normalised, this fact was not related to the distance of the receivers from the source. However, in all the cases, a difference in the overall energy of the impulse responses was very clear. An example of such pairs is demonstrated in Figure 7.9. This was confirmed with a numerical calculation of the overall energy of the squared impulse responses. It is very important here to note that the clarity parameters (C_{50}/C_{80}) cannot give information about the total amount for energy of an impulse response, as by definition this shows just the ratio of early-to-late energy. This observation raised

the question of why there was no evidence for this energy difference in the objective results for the parameters studied (T_{30}, EDT, C_{50}/C_{80}), as they are often considered as the most important parameters.

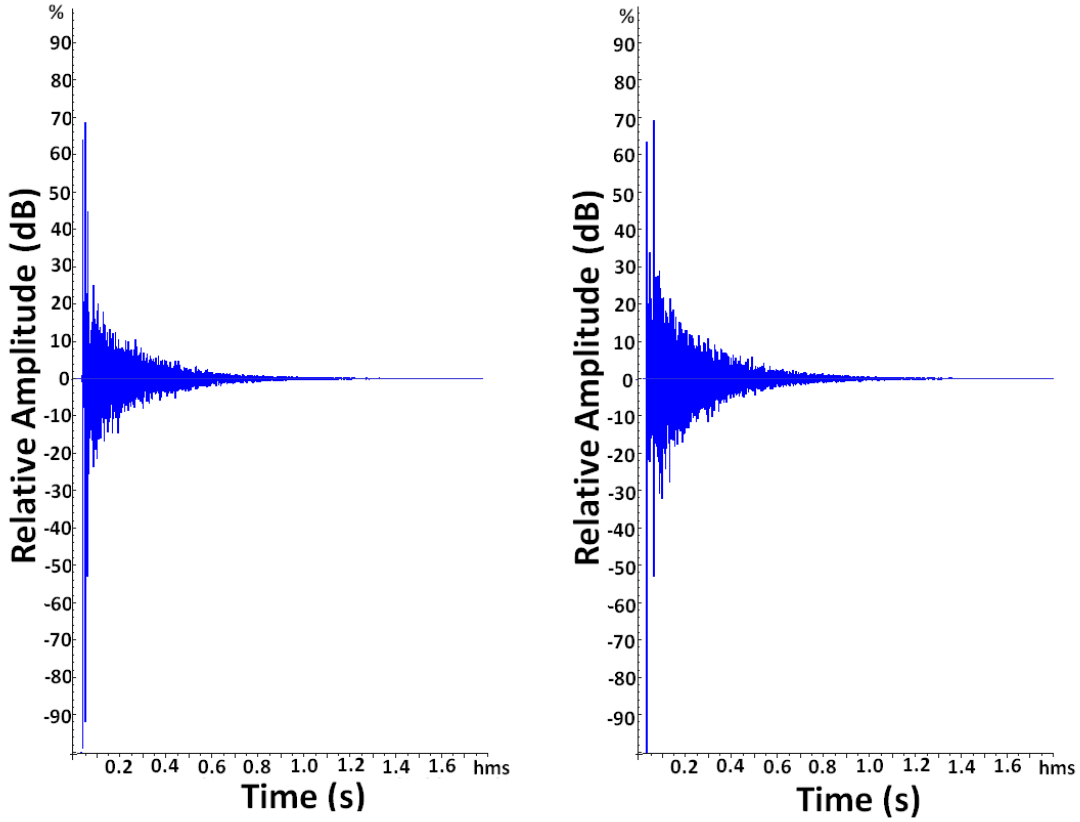

Figure 7.8 Waveforms of the impulse responses for the Pair 3 used for the measurement listening tests are represented, where the samples were assumed to be "identical". On the left the impulse response of the R8, from configuration C is represented and on the right the impulse response of the R18, from the configuration C is represented.

The acoustic parameter values were then examined in each octave band, instead of being averaged across 500Hz and 1000Hz. In order to do this, the same process was followed as explained in section 7.3. The values of each parameter were listed in increasing order and the reference JND value based on the minimum values was used for the comparison between the samples of each pair. It was observed that there were several cases where the average results demonstrated a less than 1 JND values was showing, while the values in either 500Hz and/or 1000Hz bands demonstrated a more than 1 JND value. These new results are represented in Table 7.18, Table 7.19 and Table 7.20, where for each parameter the average values are compared with those from the single octave bands.

Hence, it can be concluded that the JND based on the average of the values in 500Hz and 1000Hz octave bands, as recommended in ISO3382, is not sufficient to show with accuracy the reliability of perceived auralization results. A more detailed analysis is essential in order to observe perceived differences across all the octave bands, and not necessarily only at 500Hz and 1000Hz.

Table 7.18 The JND values at 500Hz and 1000Hz for the in-situ measurements compared with the JND values observed from the average of these two octave bands (Table 7.4). The values with less than 1 JND from the average of the two bands are highlighted in green, while their corresponding values in the single octave bands with more than 1 JND observed are in black font. Note that for clarity of presentation, the values from Table 7.4 have been reduced to three decimal places.

Selected Pairs for in-situ measurements										
			T30		EDT		C50		C80	
			Average of 500Hz,1000Hz		Average of 500Hz,1000Hz		Average of 500Hz,1000Hz		Average of 500Hz,1000Hz	
	A	B	500Hz	1000Hz	500Hz	1000Hz	500Hz	1000Hz	500Hz	1000Hz
1	R26	R5	0.066		0.048		0.176		0.316	
			0.071	0.063	1.349	1.633	1.794	1.443	1.143	0.512
2	R1	R15	0.175		0.074		0.298		0.046	
			0.346	0.739	1.180	1.112	2.706	2.111	1.501	1.592
3	R8	R18	0.287		0.782		0.407		0.285	
			0.395	0.172	1.783	3.793	0.261	1.074	1.624	1.055
4	R23	R12	0.000		0.096		0.847		0.351	
			0.423	0.469	2.635	3.194	0.491	1.202	1.051	1.752
5	R6	R6	1.193		1.907		0.958		0.619	
			0.805	1.643	1.317	2.849	1.503	0.413	0.336	0.901
6	R6	R6	4.801		3.175		1.122		1.290	
			3.783	6.009	4.498	2.142	0.683	1.560	1.027	1.552
7	R6	R6	5.994		5.082		2.080		1.908	
			4.587	7.653	5.815	4.991	2.186	1.973	1.363	2.453
8	R23	R24	1.186		3.845		1.227		2.543	
			1.355	1.017	4.996	3.103	1.197	1.257	3.153	1.933
9	R17	R17	5.074		6.398		0.886		0.387	
			3.571	6.823	8.546	4.900	0.839	0.933	0.511	0.262
10	R9	R8	1.546		0.008		1.568		0.472	
			1.962	1.111	3.213	3.648	0.819	2.316	0.244	0.700
11	R22	R21	0.972		0.343		0.954		0.565	
			0.353	1.674	0.434	1.270	0.499	2.406	0.606	0.523
12	R24	R11	0.118		2.226		0.043		1.077	
			0.085	0.156	0.032	5.027	0.741	0.655	0.346	1.808
13	R3	R20	0.825		3.375		0.180		0.046	
			1.171	0.454	2.056	5.354	0.302	0.057	0.181	0.273
14	R5	R2	0.059		2.002		0.627		0.030	
			0.183	0.329	2.008	2.287	0.104	1.357	1.014	0.954
15	R20	R21	0.339		0.040		2.672		1.743	
			1.214	0.626	2.602	2.849	1.972	3.371	1.887	1.599
16	R20	R20	0.112		0.091		1.786		1.434	

			0.526	0.325	0.670	0.907	1.833	1.738	1.853	1.015
17	**R11**	**R17**	0.042		0.066		4.395		4.093	
			0.235	0.163	2.265	2.293	3.517	5.272	4.365	3.820
18	**R18**	**R15**	0.015		1.875		4.341		2.648	
			0.847	0.970	1.687	2.359	4.258	4.424	2.052	3.244
19	**R3**	**R1**	0.302		0.981		2.381		2.343	
			0.409	0.188	0.386	2.668	4.183	0.578	4.448	0.238
20	**R18**	**R18**	0.280		2.344		2.767		2.802	
			0.498	0.059	4.386	0.154	2.219	3.315	3.797	1.807

Table 7.19 The JND values at 500Hz and 1000Hz for the CATT-Acoustic results, compared with the JND values observed from the average of these two octave bands (Table 7.7). The values with less than 1 JND from the average of the two bands are highlighted in green, while their corresponding values of the single octave bands with more than 1 JND observed are in black font. Note that for clarity of presentation, the values from Table 7.7 have been reduced to three decimal places.

Selected Pairs for CATT												
			Average of 500Hz,1000Hz		Average of 500Hz,1000Hz		Average of 500Hz,1000Hz		Average of 500Hz,1000Hz	
			500Hz	1000Hz	500Hz	1000Hz	500Hz	1000Hz	500Hz	1000Hz
	A	B	T30		EDT		C50		C80	
1	R26	R9	0.409		0.370		0.911		0.940	
			0.858	0.042	0.855	0.111	1.256	3.078	0.473	2.353
2	R1	R10	0.347		0.343		0.056		0.374	
			1.389	0.709	2.974	2.269	0.468	0.579	0.587	0.160
3	R19	R24	0.327		0.676		0.177		0.367	
			0.831	0.181	0.446	1.790	0.516	0.162	0.147	0.881
4	R7	R20	0.184		0.324		0.115		0.251	
			0.722	0.362	0.911	1.550	0.273	0.503	0.771	0.270
5	R6	R6	1.559		1.759		0.173		0.503	
			1.920	1.224	1.599	1.919	0.972	1.317	1.813	0.807
6	R6	R6	6.170		10.287		1.567		1.735	
			6.195	6.273	15.483	5.129	0.535	2.599	0.895	2.575
7	R6	R6	4.610		8.528		1.395		2.238	
			4.275	5.049	13.885	3.210	1.507	1.282	2.708	1.768
8	R12	R12	1.866		0.685		0.787		0.567	
			1.770	2.003	2.621	3.967	1.235	0.338	0.649	0.485
9	R9	R25	1.246		0.537		0.222		0.309	
			1.661	0.848	1.022	0.055	3.177	2.734	1.622	2.240
10	R22	R21	0.218		1.213		0.589		0.138	
			0.477	0.042	0.836	1.587	1.149	0.029	0.578	0.303
11	R8	R1	0.456		2.796		0.429		1.194	
			1.675	0.779	7.807	2.177	1.305	0.448	2.705	0.318
12	R22	R11	0.061		4.889		0.005		0.598	
			0.300	0.431	7.974	1.827	0.248	0.257	1.222	0.027
13	R25	R6	0.123		0.222		1.829		1.585	
			0.000	0.250	0.985	1.421	1.652	2.006	1.830	1.339
14	R8	R4	0.531		0.370		3.513		1.983	
			1.157	0.097	4.591	3.819	3.239	3.786	2.242	1.724
15	R21	R17	0.742		0.944		5.168		4.395	
			0.899	0.598	2.844	4.705	3.765	6.571	3.066	5.723
16	R20	R26	0.014		8.296		3.112		2.766	

			0.340	0.376	6.710	9.871	4.621	1.602	2.323	3.209
17	**R2**	**R17**	0.082		2.796		1.769		1.662	
			1.076	0.932	6.710	1.089	2.540	0.998	3.734	0.410
18	**R21**	**R10**	0.177		3.426		3.480		2.289	
			0.436	0.083	3.104	3.745	2.869	4.091	1.903	2.675

Table 7.20 The JND values at 500Hz and 1000Hz for the ODEON results, compared with the JND values observed from the average of these two octave bands (Table 7.10). The values with less than 1 JND from the average of the two bands are highlighted in green, while their corresponding values of the single octave bands with more than 1 JND observed are in black font. Note that for clarity of presentation, the values from Table 7.10 have been reduced to three decimal places.

Selected Pairs for ODEON												
			Average of 500Hz,1000Hz		Average of 500Hz,1000Hz		Average of 500Hz,1000Hz		Average of 500Hz,1000Hz	
			500Hz	1000Hz	500Hz	1000Hz	500Hz	1000Hz	500Hz	1000Hz
	A	B	T30		EDT		C50		C80	
1	R19	R25	0.520		0.741		0.127		0.401	
			0.742	0.292	0.994	2.546	0.036	0.217	0.095	0.896
2	R19	R25	0.145		0.602		0.180		0.384	
			0.252	0.032	0.110	1.374	0.401	0.761	0.629	1.396
3	R20	R9	0.023		0.636		0.060		0.273	
			0.015	0.065	2.116	0.769	0.664	0.783	1.265	0.720
4	R24	R23	0.008		0.401		0.021		0.163	
			0.045	0.032	1.049	0.201	0.677	0.718	0.446	0.772
5	R6	R6	1.974		0.262		0.740		0.526	
			1.780	2.240	1.049	0.495	1.169	0.311	0.789	0.263
6	R6	R6	6.672		6.181		1.672		1.810	
			6.647	6.883	6.587	6.429	1.827	1.517	1.926	1.693
7	R6	R6	4.698		6.443		0.932		1.284	
			4.866	4.643	7.636	5.934	0.658	1.206	1.137	1.430
8	R7	R23	2.142		0.366		0.505		0.382	
			2.433	1.883	0.846	0.073	0.622	0.387	0.001	0.764
9	R16	R8	1.377		0.349		0.182		0.559	
			1.172	1.640	0.368	0.366	1.262	0.899	0.923	0.195
10	R1	R20	0.130		2.354		0.215		0.958	
			0.163	0.097	5.354	0.385	0.216	0.646	1.089	0.827
11	R10	R25	0.237		1.561		0.792		0.902	
			0.312	2.841	1.546	4.029	0.624	4.649	0.104	4.025
12	R24	R11	0.245		3.435		0.021		0.395	
			0.252	7.166	3.073	4.158	0.016	0.057	0.090	0.700
13	R19	R26	0.099		0.471		2.335		1.525	
			0.312	2.808	1.270	5.403	3.542	3.888	2.430	2.629
14	R2	R3	0.428		0.218		3.594		2.882	
			0.445	0.422	1.141	1.593	2.014	5.173	2.777	2.986
15	R26	R24	0.528		0.070		4.132		2.564	
			0.564	0.503	1.141	0.989	4.952	3.312	2.882	2.246
16	R25	R26	0.054		1.386		2.465		1.648	

			0.386	0.308	1.877	1.044	3.229	1.700	1.771	1.525
17	**R16**	**R17**	0.260		3.418		1.361		1.757	
			0.786	0.308	2.116	5.073	2.148	0.573	2.044	1.469
18	**R10**	**R21**	0.329		2.389		5.496		4.296	
			0.163	0.455	5.317	0.275	5.506	5.486	4.400	4.191

7.8.2 **Analysis based on auralization method**

In order to investigate if the acoustic characteristics of the question groups are perceived in the same way for each of the three auralization methods used for this study, the answers of the common questions were averaged, including the answers for the two different stimuli. In Table 7.21, the questions which were used for this investigation for each question group are reported. Note, however, that for group (6) "difference at T_{30} above 1 JND value and keeping the rest of the parameters with less than 1 JND", only CATT-Acoustic and ODEON have been used. It is interesting to note that for the measurement examples T_{30} was influencing simultaneously C_{50} with similar JND values. Previous studies [29] have shown that the energy parameters C_{50} and C_{80} should have relative changes due to their similar calculation procedure. However, in these results a wide difference between C_{50} and C_{80} values was observed, as well as a correlation between C_{50} and T_{30} values. The author is aware of no relevant work which reports such relationships between these parameters, which may be worth further investigating the possible correlation between the two parameters in the case of actual impulse response measurements.

Table 7.21 The questions from the same group of acoustic characteristics for the three auralization techniques.

	(1) T30/EDT/ C50/C80 <JND	(2) T30/EDT/ C50/C80 ≥ JND	(3) T30/C50/C80 < JND, EDT >JND	(4) T30/EDT < JND, C50/C80 > JND	(5) T30 < JND, C50/C80/ EDT > JND	(6) EDT/C50 /C80 < JND, T30>JND
Measurements	Q1, Q2, Q3, Q4	Q6, Q7, Q8	Q13, Q14	Q15, Q16, Q17	Q18, Q19, Q20	-
CATT-Acoustic	Q1, Q2, Q3, Q4	Q6, Q7	Q10, Q11, Q12	Q13, Q14, Q15	Q16, Q17, Q18	Q8, Q9
ODEON	Q1, Q2, Q3, Q4	Q6, Q7	Q10, Q11, Q12	Q13, Q14,. Q15	Q16, Q17, Q18	Q8, Q9

By presenting the average of the responses as well as their standard deviations in Figure 7.9, it is easier to draw conclusions for each auralization technique.

For the measurements, when only EDT values were changed above 1 JND values (question group (3)), this had less influence on the subjects' perception than when C_{50} and C_{80} values or C_{50}/C_{80} and EDT at the same time were changed above 1 JND values (question groups (4) and (5) respectively).

For CATT-Acoustic, very interestingly, an increased degree of perceptual difference has been observed from changes in T_{30} (question group (6)), EDT (question group (3)), C_{50}/C_{80} (question group (4)) and EDT/C_{50}/C_{80} (question group (5)).

For ODEON, changes in T_{30} (question group (6)) and EDT (question group (3)), as well as when changes above 1 JND values have been observed in all three EDT/C_{50}/C_{80} (question group (5)), were perceived with the same degree of difference from the subjects. On the other hand, changes in C_{50}/C_{80} (question group (4)) are more audible than the other parameters.

Conclusions from the overall average of the three auralization techniques can be drawn as well. Here there is an increased degree of perceptual difference from changes in T_{30} (question group (6)), EDT (question group (3)), C_{50}/C_{80} (question

group (4)). However, the perceived difference in EDT/C_{50}/C_{80} (question group (5)) is less than the latter case of C_{50}/C_{80} (question group (4)).

From all these cases, an overall conclusion is the fact that changes in the energy parameters C_{50}/C_{80} are more audible than changes observed in EDT. Changes in T_{30} were found to have even less influence on the subjects' perception than the other three parameters.

An additional comment on the results shown in Figure 7.9 is that the subjects were more confident about the perceived difference when all the acoustic parameters were hypothesised to be with less than 1 JND value (question group (1)) than those with more than 1 JND value observed across all the studied parameters (question group (2)). One obvious reason for this fact is the variations of the values across the octave bands, as discussed in section 7.8.1.

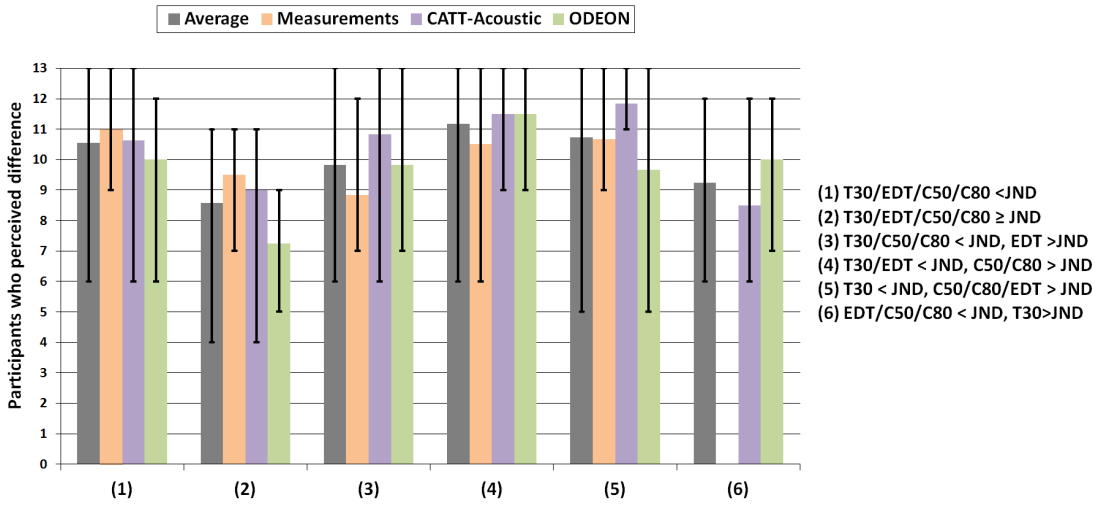

Figure 7.9 The bars represent the average number of subjects who perceived a difference across all three auralization methods, for each group of questions based on the corresponding acoustic characteristics. The first bar is the average of all the listening tests. The standard deviations show the variation in the number of subjects who perceived the difference for each group.

7.8.3 **Analysis based on the stimuli**

As discussed in section 7.4, it has been shown in previous studies that different results can lead to different conclusions in perceptual studies, depending on the original stimulus used for convolution. The current knowledge that we have about the influence of the stimuli on our perception is still limited. For the listening tests in this study, two different stimuli were convolved with the selected impulse responses, and it will be interesting to investigate their effect on results. Hence, in Figure 7.10, Figure 7.11 and Figure 7.12 the percentage of the number of subjects who perceived a difference for each question/pair was calculated for both cases stimuli and the relationship between them compared in each bar.

In the ideal case, where the stimuli do not affect the perception of the acoustic characteristics being tested, the number of subjects for the two stimuli for each question should be equal. This would be represented by the colours for each bar (green for cello and yellow for voice) both reaching the middle of the y-axis.

As observed, however, this was not the case with any of the three auralization techniques. For the in-situ measurements (Figure 7.10), in about 45% of the answers it was observed that the two stimuli had the same effect on the subjects' perception. An interesting point regarding these results was the responses for each stimulus for Q10, where T_{30} and C_{50} parameters differed with more than 1 JND values. The subjects indicated the difference more clearly with the cello as the stimulus rather than with the voice. This was not expected, as from the definition; C_{50} is more relative to speech than music.

For the CATT-Acoustic results (Figure 7.11), for about 50% of the answers the stimuli had the same effect on the responses for each question, while for the rest of the answers - with a few exceptions - pairs with voice as the stimulus were more easily perceived as different.

For the ODEON results (Figure 7.12), for about 30% of the answers the stimuli affected the responses for each question in the same way, while for the rest of the answers voice seemed to have more effect on the perception of the difference between the samples.

Overall, it is concluded that the subjects more often perceived the difference between the samples with the voice excerpt than those with the cello excerpt, as has been also discussed in [72]. In addition to this, one of the main comments made by the participants about the tests was that they found it more difficult to detect differences for the cello excerpts. In the end, though, correlations between the stimuli and the group of questions have not been observed for any of the three listening tests.

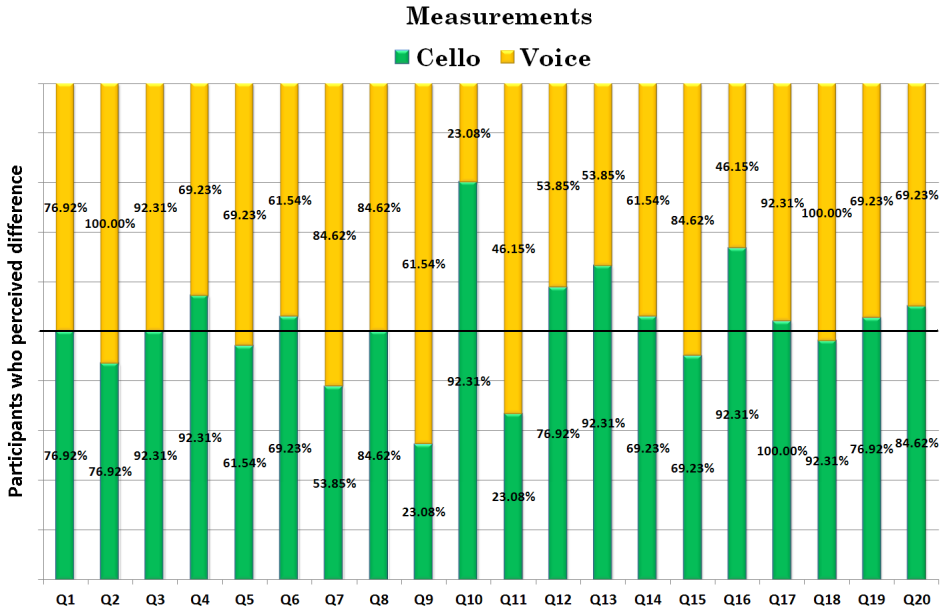

Figure 7.10 Bars showing the effectiveness of each stimulus for each question of the in-situ measurement listening tests. The number of subjects who perceived differences with the cello stimulus are presented in green, while in yellow the corresponding answers for the voice stimulus are presented. The black axis across the x-axis defines the point where the effect of the two stimuli should be balanced.

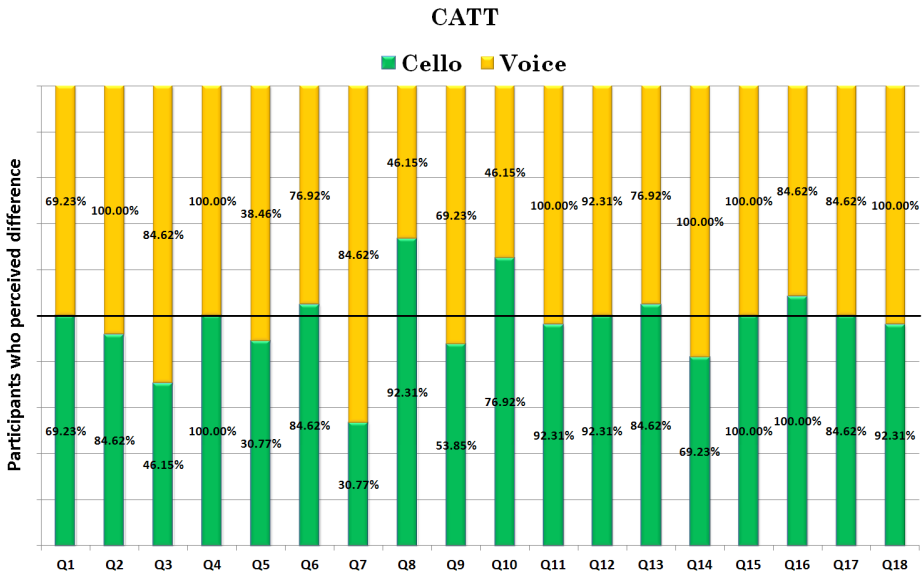

Figure 7.11 Bars showing the effectiveness of each stimulus for each question of the CATT-Acoustic listening tests. In green the number of subjects who perceived differences with the cello stimulus is presented, while in yellow the corresponding answers for the voice stimulus is presented. The black axis across the x-axis defines the point where the effect of the two stimuli should be balanced.

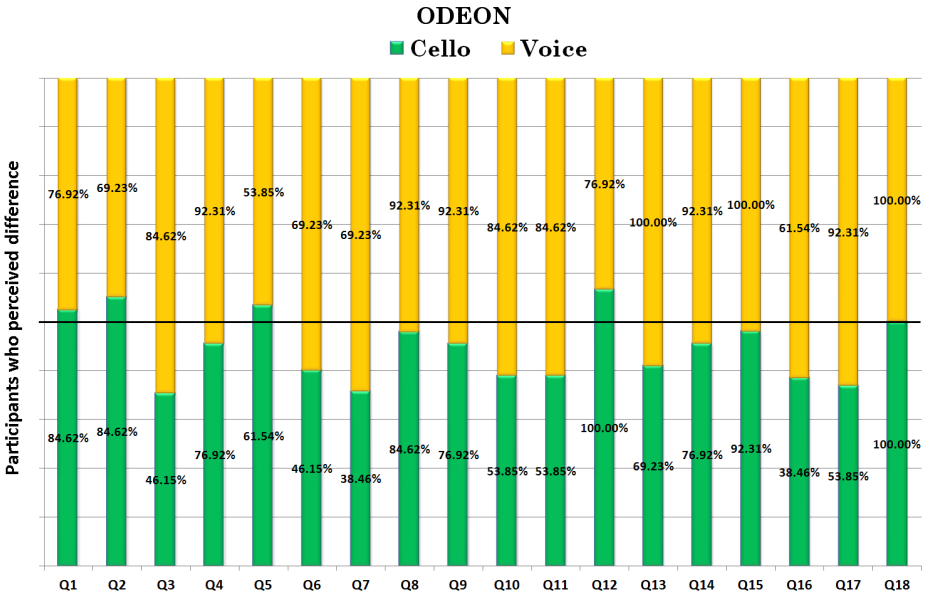

Figure 7.12 The bars show the effectiveness of each stimulus for each question of the ODEON listening tests. In green the number of subjects who perceived differences with the cello stimulus is presented, while in yellow the corresponding answers for the voice stimulus is presented. The black axis across the x-axis defines the point where the effect of the two stimuli should be balanced.

7.9 *Summary*

To evaluate the reliability of auralizations based on the perception of changes in acoustic characteristics, listening tests were conducted and the results have been analysed in this chapter. Each auralization method was investigated independently, hence, three similar listening tests were conducted.

Focusing the investigation on the subjective sensitivity of the listeners to variations in T_{30}, EDT, and $C_{50}/C_{80,}$ the impulse responses had to be carefully selected based on the requirements of the study with respect to JND values. The same process was followed for all three auralization techniques, such that the final test examples were based only on JND values across combination of parameters.

The steps followed were to use appropriate anechoic stimuli and convolve them with the selected impulse responses. The selection of the stimuli was based on the findings of previous studies and the purposes of the current study. Additionally, the sound reproduction system used as well as test planning, the administration and the reporting of the results of the listening tests have been described in detail.

The analysis of the results was based on groups of questions which represented different acoustic conditions, while all different aspects of this study were taken into consideration. It was found that averaging JND values for acoustic parameters across 500Hz and 1000Hz octave bands, as recommended in ISO3382, masks the fact that differences can still be perceived. These differences are revealed by considering non-averaged JND values individually for each octave band.

The results have also been analysed based on the auralization method used, in order to draw conclusions about the effect of each technique on the subjective results. The influence of the two different stimuli was also investigated, showing once more that they can have an effect on the perceptual result observed.

Chapter 8.
Conclusions

Auralization has become a highly useful tool for the acoustic design of spaces, as well as for the acoustic revival of heritage sites. Several auralization techniques have been developed, either based on in-situ acoustic measurements where possible, or on synthesised acoustic virtual environments. Evaluation of the quality of auralization techniques is typically achieved numerically by observing objective acoustic parameters and comparing them with those obtained from in-situ measurements. However, the lack of certainty regarding the accuracy of the perceptual results of these techniques has not been investigated in significant depth. This thesis has been motivated by the need to achieve accurate results in auralization, in term of objective and subjective measures.

The hypothesis on which this research has been based is as follows:

In virtual acoustic reconstructions, perceptual accuracy is dependent on minimising the changes in objective acoustic metrics through optimisation of physical parameters in the auralized space.

In order to support this research hypothesis, the steps below have been followed:

- Theoretical explanations of commonly adopted auralization techniques used have been given, with a presentation of the advantages and limitations of each of these methods.
- A virtual acoustic space has been created by using three of the most common auralization techniques. Impulse responses were captured and produced using each method, by varying the receiver positions, the acoustic configurations of the space and in one of the techniques, the orientation of the sound source.

- Objective studies were carried out in order to observe and analyse the changes in obtained acoustic parameters.
- Finally, the perceptual results of these changes were evaluated through listening tests.

8.1 *Summary*

A theoretical examination of the principles of acoustics has been presented, explaining in detail the characteristic properties of sound propagation in an enclosed space (Chapter 2). The contributions of the acoustic interactions such as sound reflection, sound diffusion, sound absorption or standing waves, have been described. The room impulse response has been introduced as an output of a system, excited by a given input signal, and ideally encapsulating all the acoustic characteristics of the system. The main acoustic parameters, used to objectively represent and evaluate the properties of an impulse response, as recommended in ISO3382, have been defined and discussed. However, these acoustic parameters do not provide sufficient information about the subjective perception of these objective measures. Thus, the relevant just noticeable difference (JND) values had been determined from previous work and used for the subjective evaluations of this thesis.

The concept of auralization and the most well-known auralization techniques have been described (Chapter 3). A considerable amount of theoretical work has resulted in the introduction of a number of different auralization techniques, which can be categorised according to the nature of the impulse responses used, the main difference being those which use impulse responses from an actual space and those relying on synthesised impulse responses from computer-based models. For in-situ measurements, the nature of the excitation signal used, the sound source and microphone properties, as well as the calculation process used for the analysis of the impulse responses affect the accuracy and the reliability of the method.

For computer-based impulse responses, the main difference between existing algorithms is the consideration of the phenomenon of sound as particles or as waves. Geometric acoustic algorithms were examined in detail and their advantages and limitations were presented, in order to identify the most suitable technique for the purposes of this study. The auralization techniques used for this study are based on: 1) in-situ impulse response measurements using the

Exponential-Swept Sine (ESS) Method and 2) two computer simulations using commercial software, CATT-Acoustic and ODEON, both based on geometric acoustic algorithms.

Some pilot studies have been carried out before the main work presented in this thesis (Chapter 4). An experimental shoebox shaped acoustic model was created in ODEON and used in order to study the impact of physical factors and acoustic properties on both objective and subjective results. Physical parameters such as source directivity, source orientation, absorption and scattering coefficients, calculation settings and source/receiver positions are easy to control in such a virtual space. Their impact on T_{30}, EDT and C_{80}/C_{80} was examined and validated in subjective terms through listening tests. The information collected from these pilot studies was then carried over into the main investigation, which was about the influence of the sound source orientation and modelling techniques on the objective values of the space. It was noted that the results of such acoustic simulation models are realistic only when they reflect the geometry, absorption, diffusion and so forth of real spaces.

Thus, for the purpose of this thesis an existing heritage space was used to study the influence of variations in obtained acoustic parameters and their relationship to what a listener perceives. St. Margaret's church was chosen for this study due to the potential to change its physical acoustic characteristics through sets of acoustic panels and drapes (Chapter 5). Hence, variations in the obtained acoustic parameters can be easily controlled by the researcher, for both in-situ measurements, as well as for the computer modelling techniques used. The space was tested in different acoustic configurations, for both measurements and computer models, across a grid of 26 receiver points covering the audience area. Additionally, variations in the orientation of the sound source were applied for the in-situ measurements.

The acoustic characteristics of the captured/synthesised impulse responses were analysed by calculating the acoustic parameters for each auralization technique, acoustic configuration and receiver/source positions (Chapter 6). This research has concentrated on what are assumed to be the most important acoustic parameters. It was considered best to exclude from the study those parameters assumed to be directly affected by the sound source, microphone properties and reproduction

systems. Hence, the investigation was focused on the monoaural parameters T_{30}, EDT and C_{50}/C_{80}.

The importance of studying these objective results in terms of their spatial variation across receiver positions, varying also with frequency has been emphasised in this thesis. For this purpose, a novel way of analysing and representation the data collected - "acoustic floor maps" – has been also introduced. The analysis has included data obtained from the measured impulse responses, as well as the impulses responses produced by CATT-Acoustic and ODEON models. As a comparison between their different auralization techniques was not a goal of this study.

To perceptually evaluate the changes in acoustic characteristics applied to the test space, listening tests were conducted and each auralization technique was studied independently (Chapter 7). For each listening test, impulse responses were selected from the wide data set for each cases based on the observed acoustic parameter values and their changes, due to the measured position and/or the acoustic configuration used. The selection process of the appropriate impulse responses has been explained with respect to the JND value observed for each acoustic parameter, as an average between 500Hz and 1000Hz as recommended in ISO3382.

The selected impulse responses were convolved with two anechoic stimuli, a solo cello and male speech. Pairs of samples with differences in specific acoustic parameter values, with respect to recommended JND, have been examined by using the A/B comparison method. The 39 subjects in total (13 for each listening test/auralization technique) were asked to identify if they could perceive differences between the comparison pairs.

For the analysis of the results of the listening tests, the following aspects were taken into consideration:

- The influence of changes observed amongst specific acoustic parameters, grouped according to JND criteria and varying with both receiver position and acoustic configuration, representing the different acoustic conditions of the measurements and computer auralization results.

- The influence of the auralization method used for each perceptual evaluation (in-situ measurement, CATT-Acoustic, ODEON).
- The effect of the different stimuli used.

A number of conclusions were reached as follows:

- From the listening tests, it is clear that subjects were able to perceive a difference between samples with acoustic parameter values of less than 1 JND value, when averaged across the 500Hz and 1000Hz octave bands. However, further investigation revealed that values above 1 JND were observed in either the 500Hz and 1000Hz octave band, a feature which is then hidden by taking the average measure. A more detailed analysis across octave bands is thus essential for the subjective evaluation of these perceived differences; similarly observations have been made in this thesis regarding the objective representation of the results, via the suggested "acoustic floor maps". **Therefore, it is concluded that in order to achieve accurate results in auralization, optimisation across the octave bands with respect to the JND values is essential, arguing with the ISO3382 recommendations for averaging across 500Ha and 1000Hz.**
- By studying the perceptual results across the three auralization techniques used, it was observed that the subjects had generally given similar responses to the corresponding group of questions for all three listening tests. This reveals that the defined hypothesis for this thesis is not directly affected by the auralization technique used for this study. Summarising these conlcusions:
    - Different auralization techniques did not result different level of the perceived auralization variations,
    - C_{50}/C_{80} changes are more audible than changes observed in EDT.
    - Changes in T_{30} were found to have even less influence on the subjects' perception than the other three parameters.
- It was also confirmed in this study, in line with several previous works, that different perceptual responses can be given to auralizations based on different stimuli. From the results of all three listening tests, changes in the acoustic parameters using the cello excerpt were less audible to the subjects than those obtained by using the voice excerpt. However, no correlation

between stimuli and perceived changes based on specific acoustic parameter groups have been observed.

Therefore, the hypothesis defined for this thesis has been confirmed and it is concluded that: for the perceptual accuracy of virtual acoustic reconstructions it is indeed necessary to minimise changes in the obtained acoustic parameters as perceptual differences are still evident when only a simple acoustic parameter demonstrates a difference of greater than 1 JND in a single frequency band. However, it is essential to add that:

- the perceived differences were not observed to the same degree across all four studied acoustic parameters,
- optimisation of the acoustic parameter values across all the frequency bands is important,
- the overall perception of the changes in the acoustic parameters is independent of the auralization technique used, however, it should be also considered the possibility of non-linear distortions of the resulted auralization results, based on the computer based algorithms.

8.2 *Contributions*

The novel contributions of this thesis are as follow:

- An acoustic study of an existing, unique heritage site and performance venue based on a wide data set obtained from varying the acoustic characteristics of the space, receiver position and sound source orientation, with results obtained from in-situ measurements and two different acoustic modelling techniques.

- The introduction of "acoustic floor maps" as a novel way for representing data for multiple positions in the same space and with respect to their acoustic behaviour across octave bands.

- An investigation of the objective acoustic results observed from three different auralization techniques applied to a single space, all of which were controlled by and dependent on the skills and experience of only one researcher/user.

- An investigation based on both objective and subjective terms for the evaluation of the resulting auralizations.

8.3 *Further Work*

The work presented in this thesis, reporting the results of several research studies, has answered some questions but at the same time has raised some others. The ways in which this research could be developed further are summarised below.

Extension to spatial acoustic parameters

The current study was based only on monoaural acoustic parameters (T_{30}, EDT, C_{50} and C_{80}) and mono sound reproduction of the auralization results. Further work would apply the study of spatial parameters (such as LF and IACC) , following the same approach. It would be very interesting to study how changes in these parameters affect the perception of resulting auralizations, as sound reproduction is now mainly based on multichannel formats. As has been described in Chapter 5, the impulse responses captured in-situ or produced from the acoustic models were B-format files, which are sufficient and high quality data for such an investigation. Additionally, this would require the objective results obtained from these spatial parameters to be studied, as well as a new approach for reproducing the resulting auralizations. Such a study would contribute to the perceptual accuracy of multi-dimensional acoustic representation of a virtual space.

Frequency dependent analysis of JND values

It was observed in this study that the recommended values of JND given by ISO3382 are ultimately not sufficient to describe or minimise differences perceived by a listener. These values are based on an average taken across the two middle octave bands, 500Hz and 1000Hz. It has been proved that variations in a single octave band could determine if a listener can perceive a difference in the resulting auralization. It would be particularly interesting to investigate how changes in the acoustic parameters are perceived across different octave bands. This would require very rigorous listening tests using a broader range of stimuli, in order to study these effects further.

Correlation between C_{50} and T_{30} values

In the case of actual impulse response measurements, carrying out for this research, it was observed that T_{30} and C_{50} values were affected with similar JND values by acoustic variations applied in the space, while the rest of the acoustic parameters were keeping values with less than 1 JND. This is a very interesting observation, as this correlation has not been reported in relevant work, and further more it shows a distinctive differentiation between C_{50} and C_{80} values. It would be worth further investigating the possible correlation between the two parameters, based on real impulse responses, and if so, how this correlation could be described by computer based impulse responses.

Correlation between subjective senses and changes in specific acoustic parameter values

It has been recognised that there is still limited knowledge about the correlation between acoustic factors and their resulting perceptual effect. During the listening tests carried out for this current study, an additional task was given to the subjects, asking them to identify how they had perceived differences between the examined pairs using musical/subjective terms. A further investigation based on these results could show how changes in specific acoustic parameters can be correlated with particular subjective senses.

Appendix A

Architectural Plans for the refurbishment of St. Margaret's Church (1999)

Ground Floor Plan of St. Margaret's Church

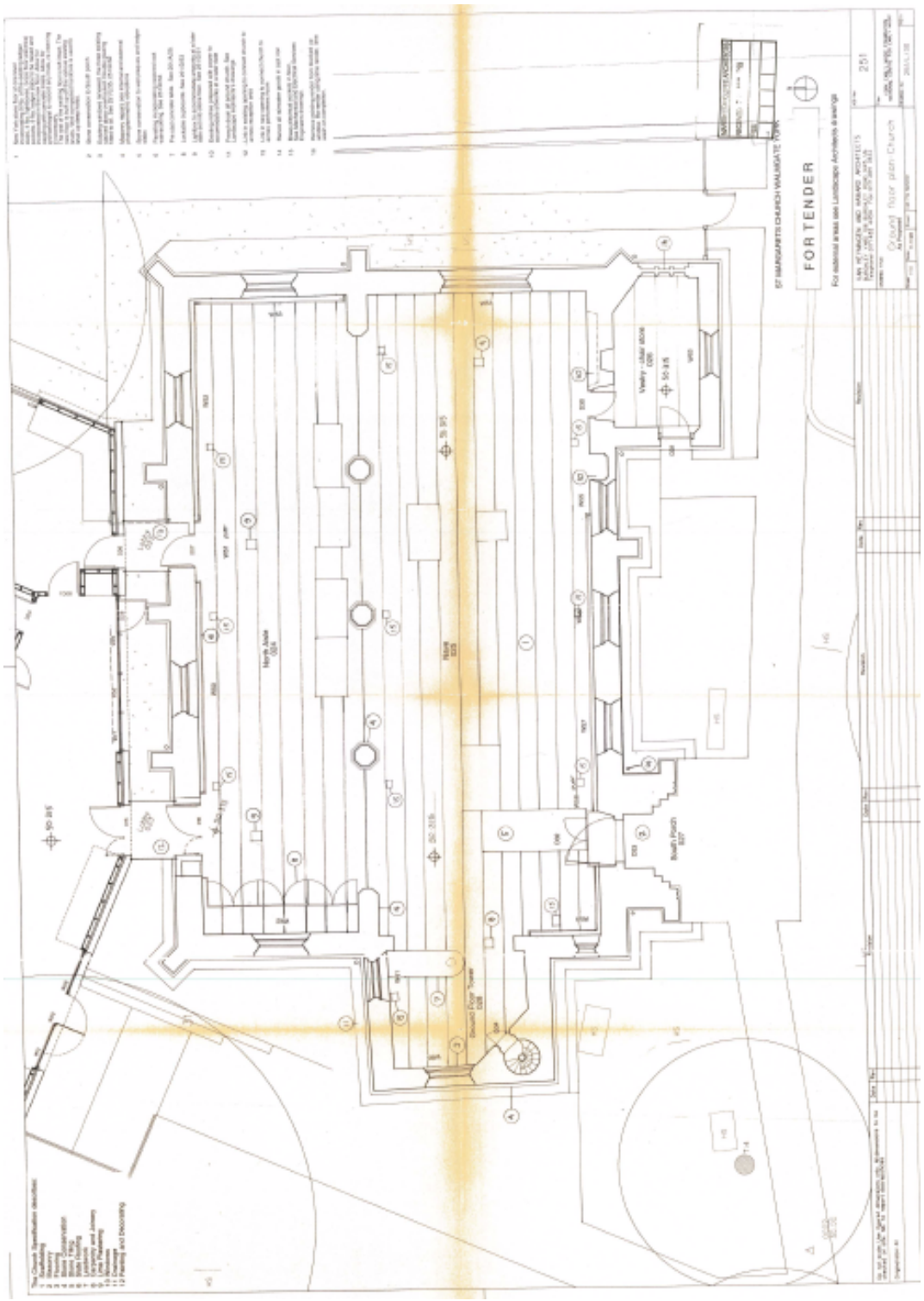

Long Section North of St. Margaret's Church

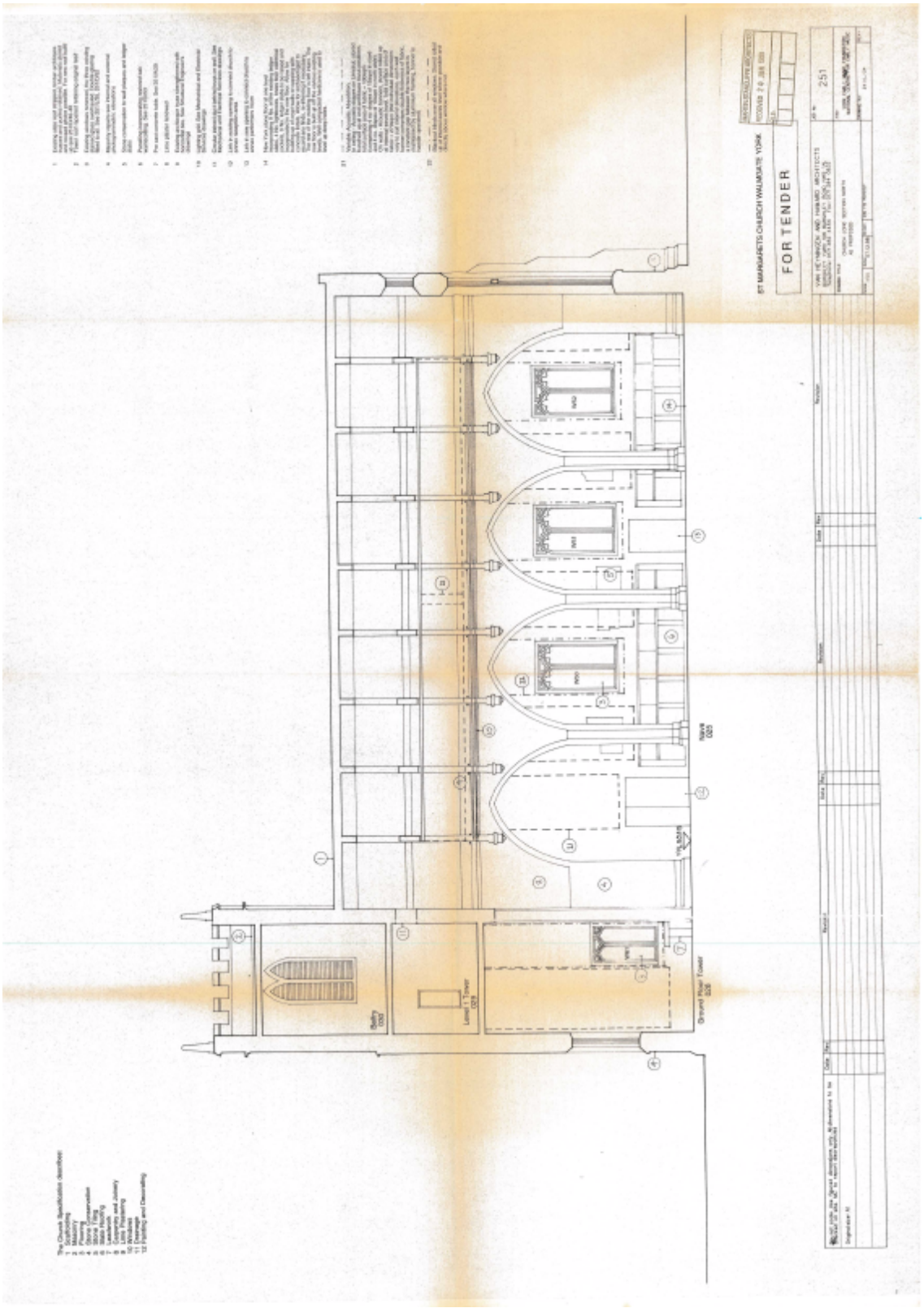

Long Section South of St. Margaret's Church

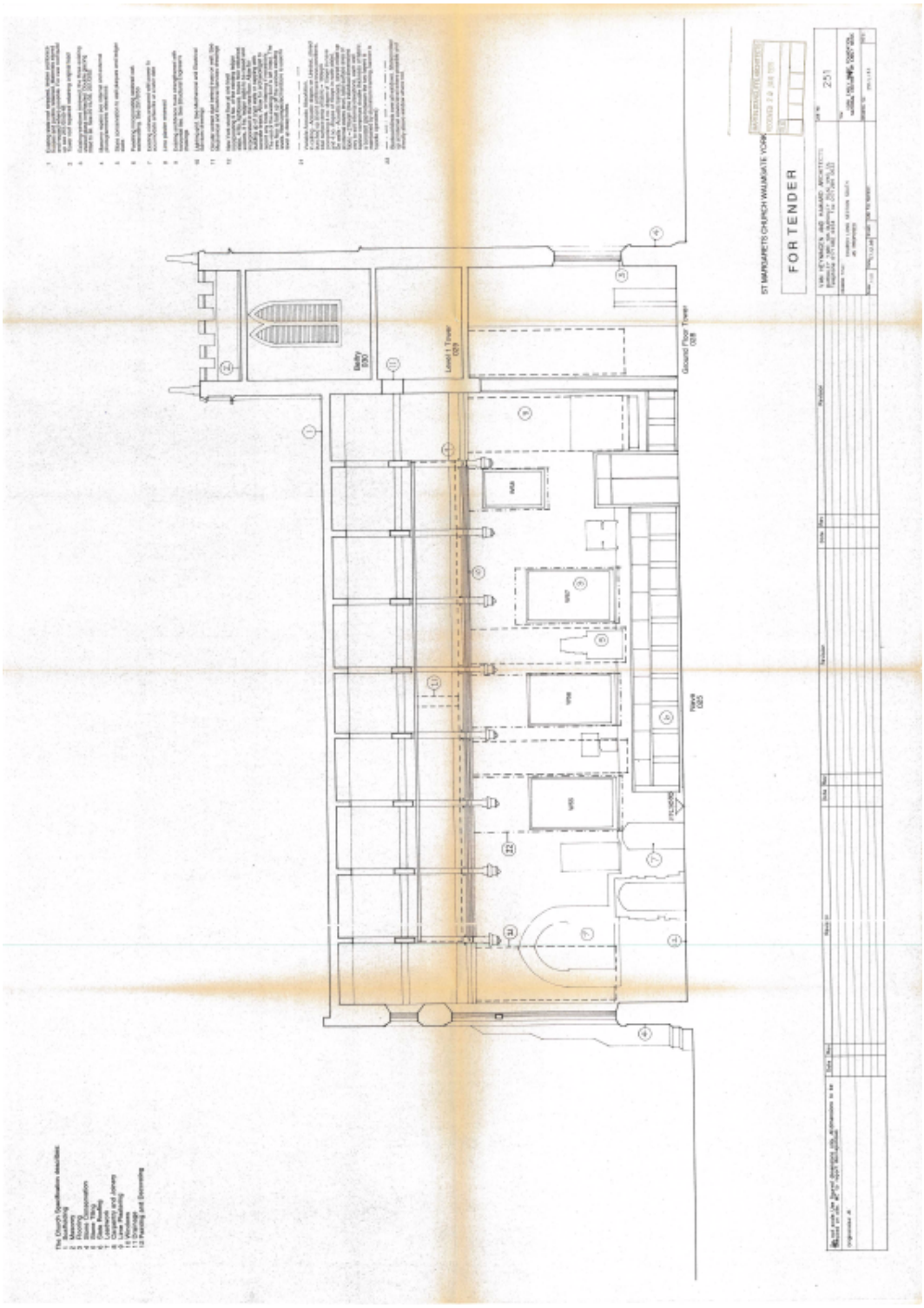

West and East Cross Sections of St. Margaret's Church

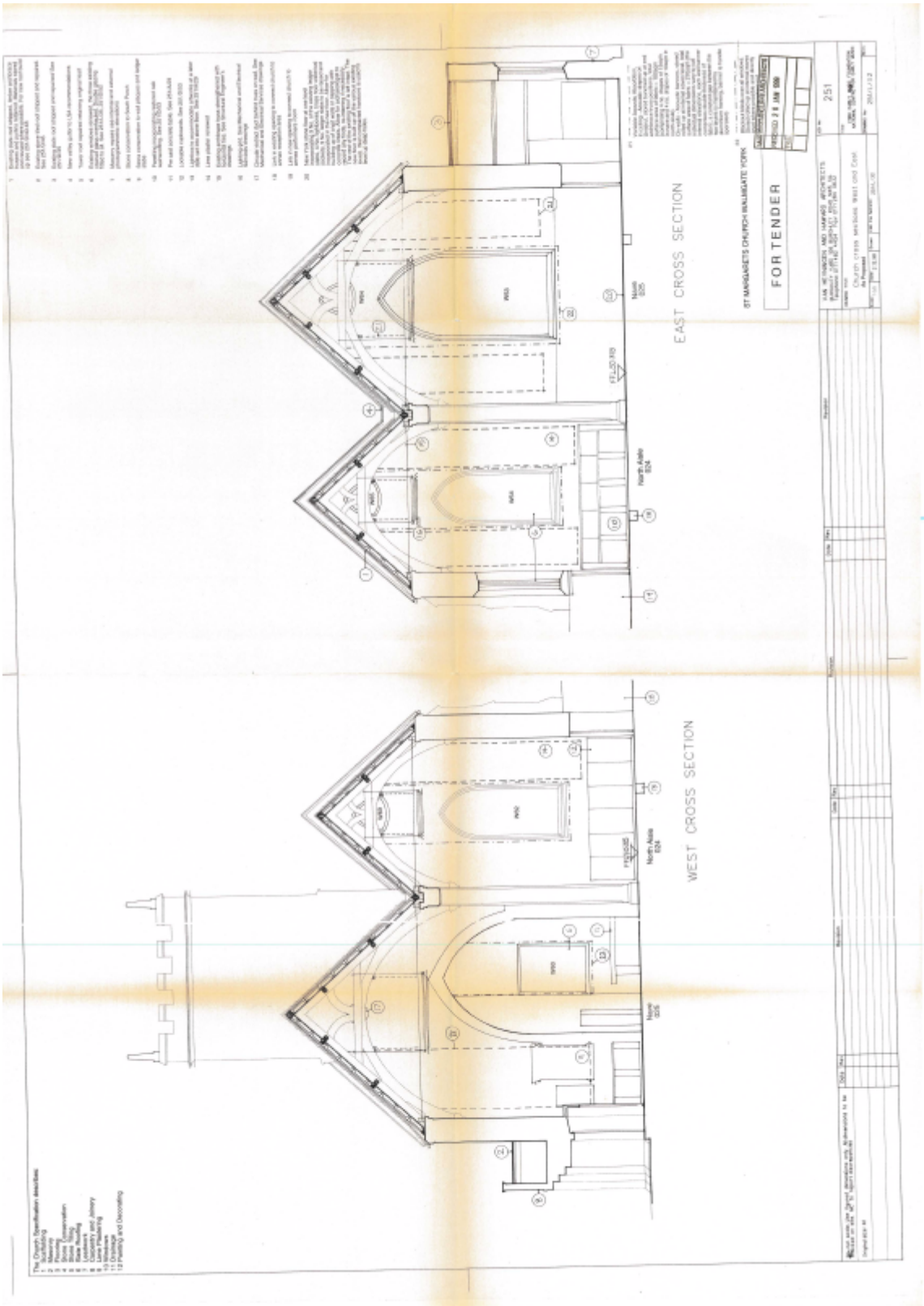

Appendix B

Both sides of the reversible absorbing panels were simulated, giving the user the ability to use them either as opened or closed, depending on the requirements of the configuration in each case. Here an example of the model data in both simulation software is presented, were panel "14)" is used as "opened", by commenting the lines for the "closed" panel.

CATT-Acoustic Model Data for the acoustic panel "14)"

```
;14) opened
[8284 absorption / 8478 8479 8482 8483/ absorption ]
[8285 absorption / 8479-8482 / absorption ]
[8286 diffuser / 8378 8379 8479 8478 / diffuser* ]
[8287 diffuser / 8379 8380 8480 8479 / diffuser* ]
[8288 diffuser / 8380 8381 8481 8480 / diffuser* ]
[8289 diffuser / 8381 8382 8482 8481 / diffuser* ]
[8290 diffuser \ 8382 8482 8483 8383 \ diffuser* ]
[8291 diffuser / 8378 8478 8483 8383 / diffuser* ]
;;14) closed
;[8360 diffuser / 8578 8579 8582 8583 / diffuser* ]
;[8361 diffuser / 8378 8379 8579 8578 / diffuser* ]
;[8362 diffuser / 8382 8383 8583 8582 / diffuser* ]
;[8363 diffuser / 8378 8578 8583 8383 / diffuser* ]
```

ODEON Model Data for the acoustic panel "14)"

```
;14) opened
;Layer "Absorption"     0.769    0.851    0.992
Surf 8284 Apsorption
 8478 8479 8482 8483
Surf 8285 Absorption
 8479>8482
 ;Layer "Diffuser"  0.761    0.996    0.82
Surf 8286 Diffuser
 8378 8379 8479 8478
Surf 8287 Diffuser
 8379 8380 8480 8479
Surf 8288 Diffuser
 8380 8381 8481 8480
Surf 8289 Diffuser
 8381 8382 8482 8481
Surf 8290 Diffuser
 8382 8482 8483 8383
Surf 8291 Diffuser
 8378 8478 8483 8383

;;14) closed
;Surf 8360 Diffuser
; 8578 8579 8582 8583
;Surf 8361 Diffuser
; 8378 8379 8579 8578
;Surf 8362 Diffuser
; 8382 8383 8583 8582
;Surf 8363 Diffuser
; 8378 8578 8583 8383
```

Appendix C

Measurements

Acoustic floor map of EDT values obtained from configuration A across the grid of 26 receiver positions. Note that EDT values for 125Hz and 250Hz increase with an increase in distance.

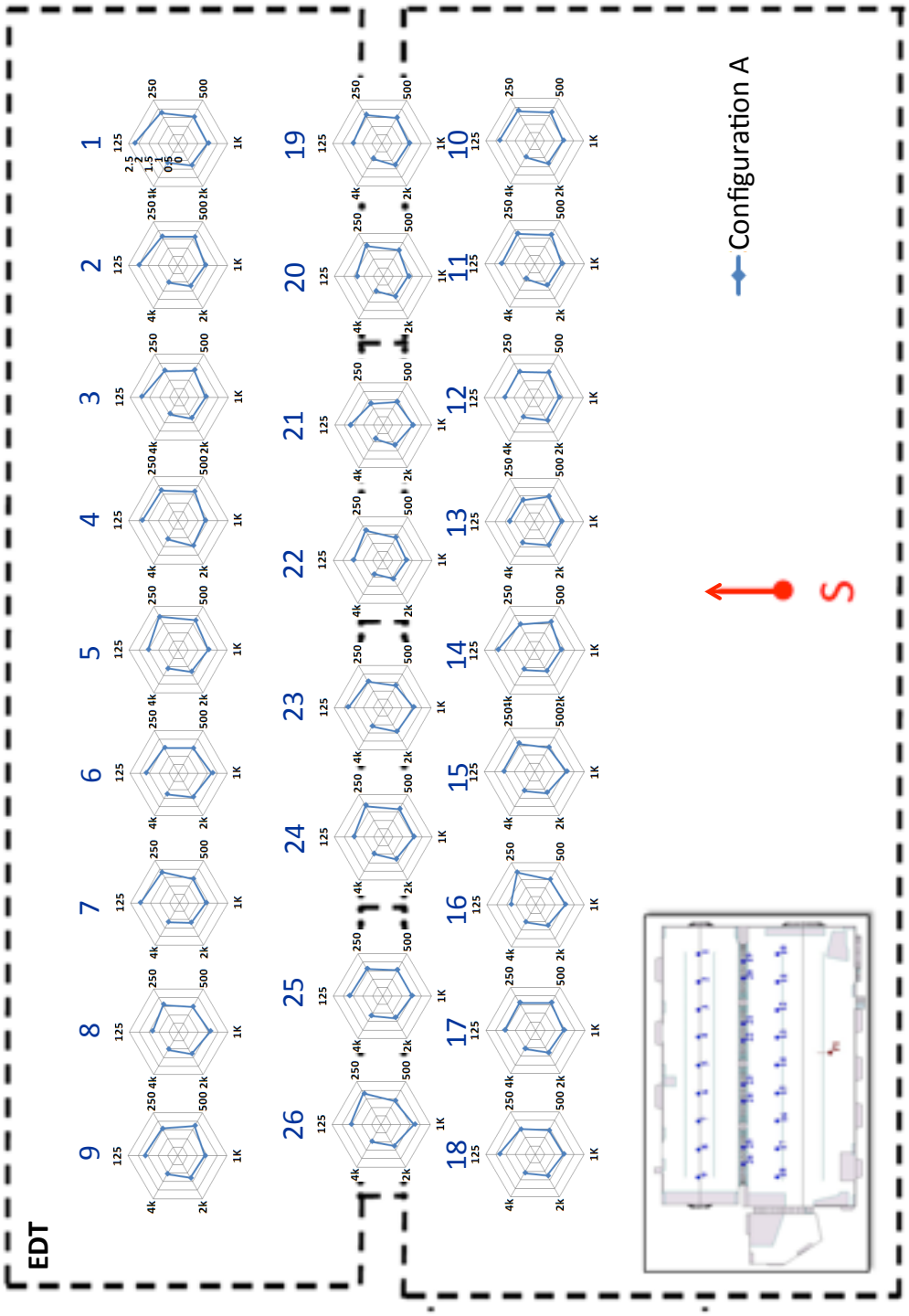

Measurements

Acoustic floor map of EDT values obtained from configuration B across the grid of 26 receiver positions. Note that EDT values for 125Hz and 250Hz increase with an increase in distance.

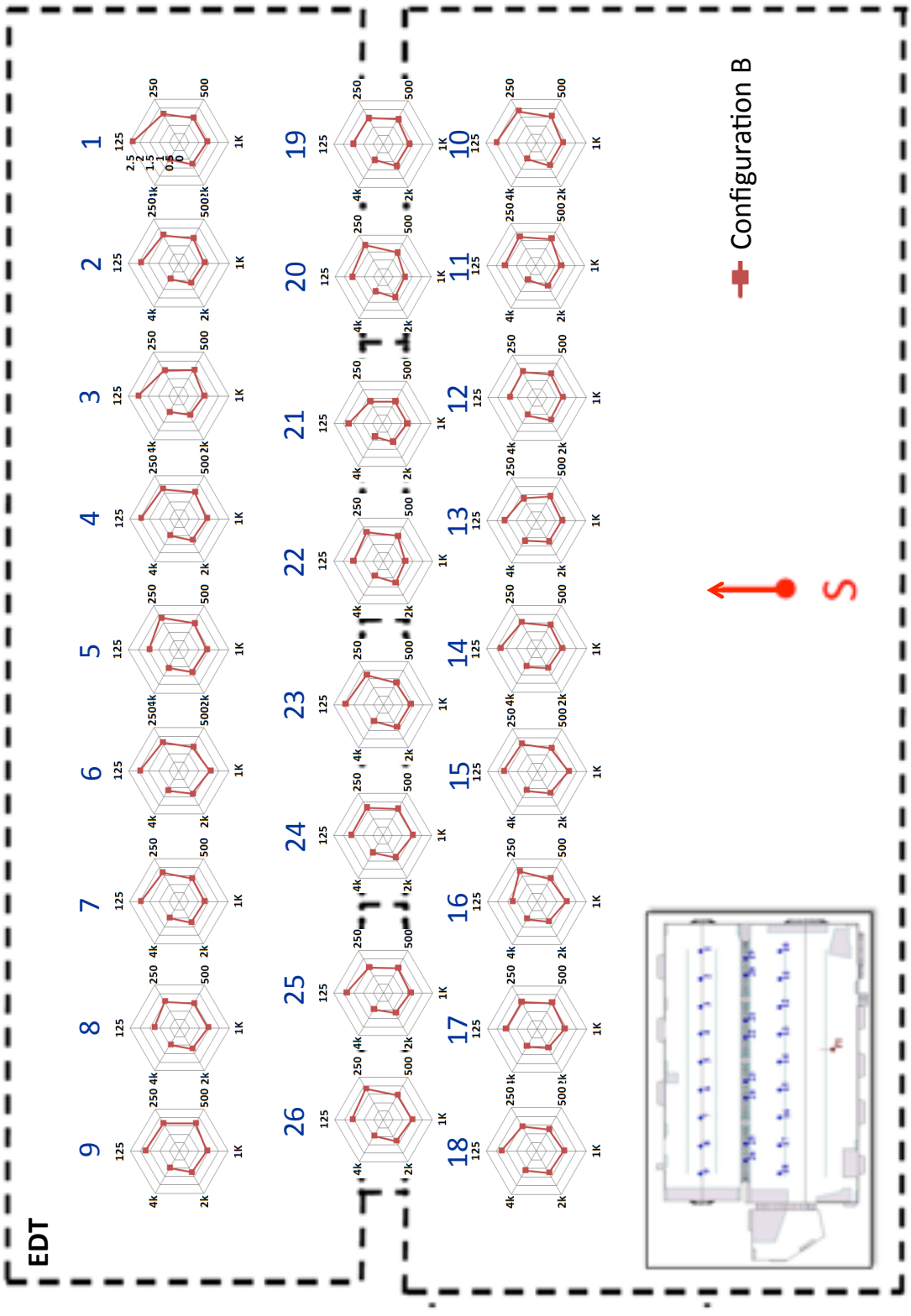

Measurements

Acoustic floor map of EDT values obtained from configuration C across the grid of 26 receiver positions. Note that EDT values for 125Hz and 250Hz increase with an increase in distance.

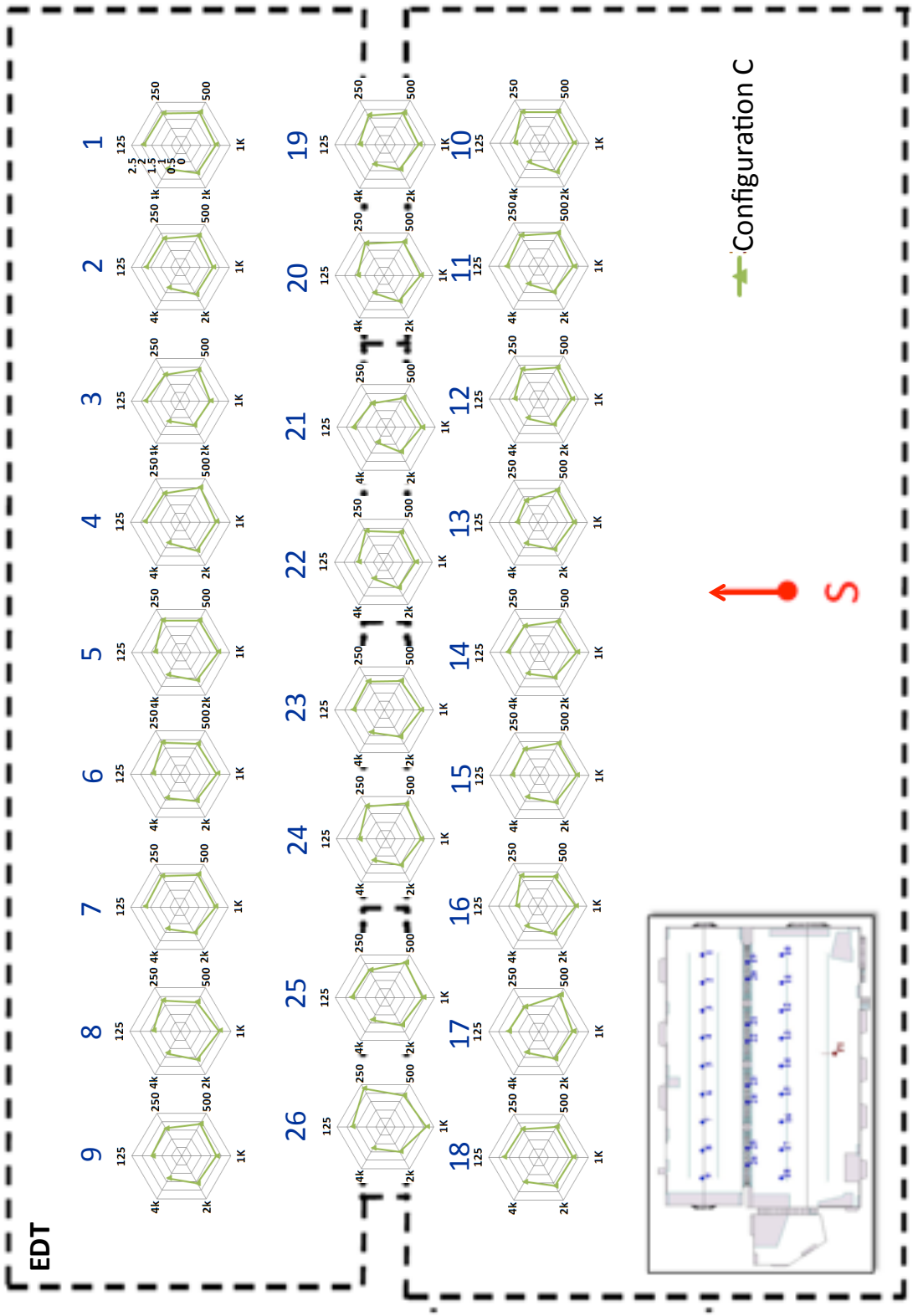

Measurements

Acoustic floor map of C80 values obtained from source orientation at 0° across the grid of 26 receiver positions.

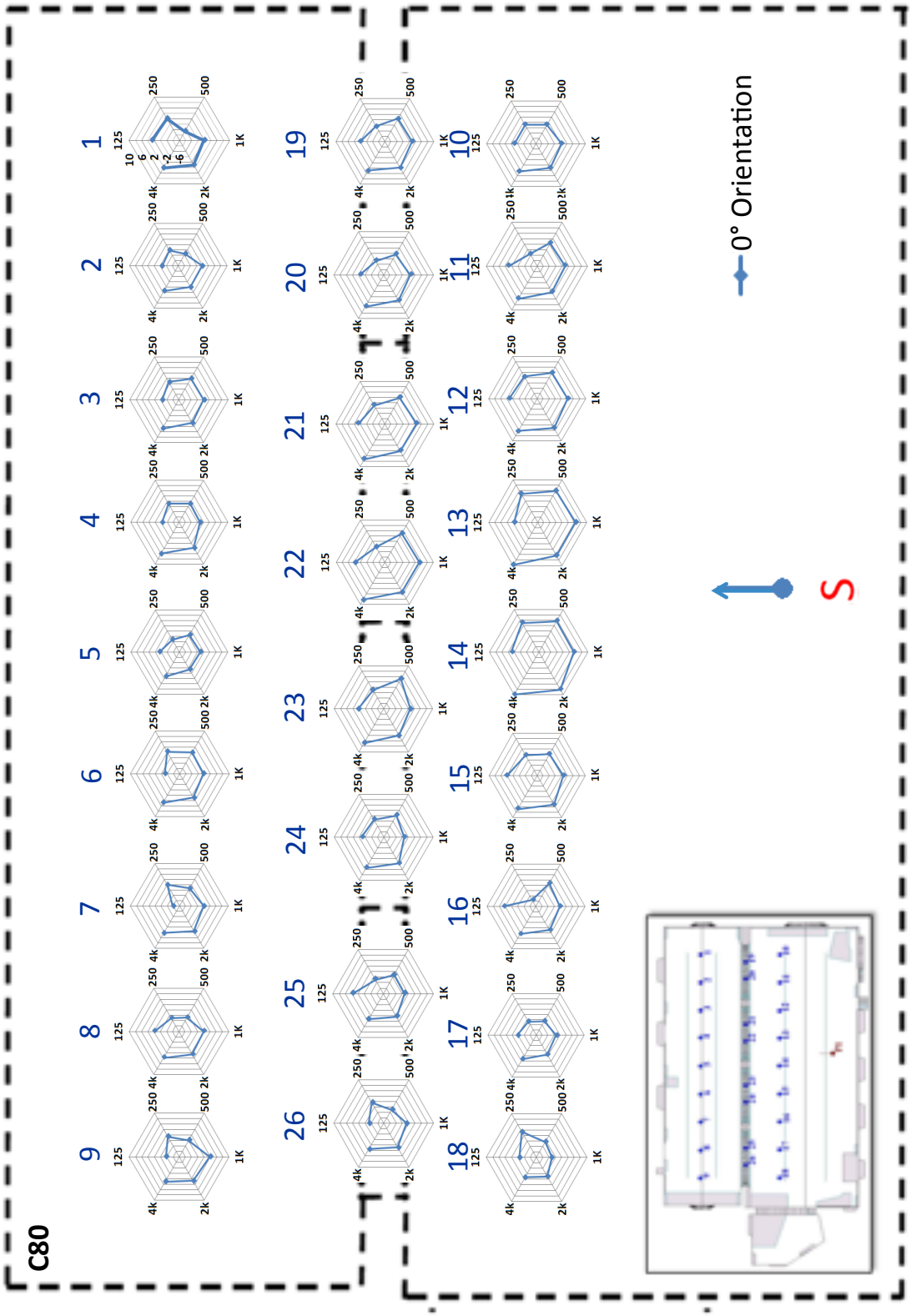

Measurements

Acoustic floor map of C80 values obtained from source orientation at 40° across the grid of 26 receiver positions

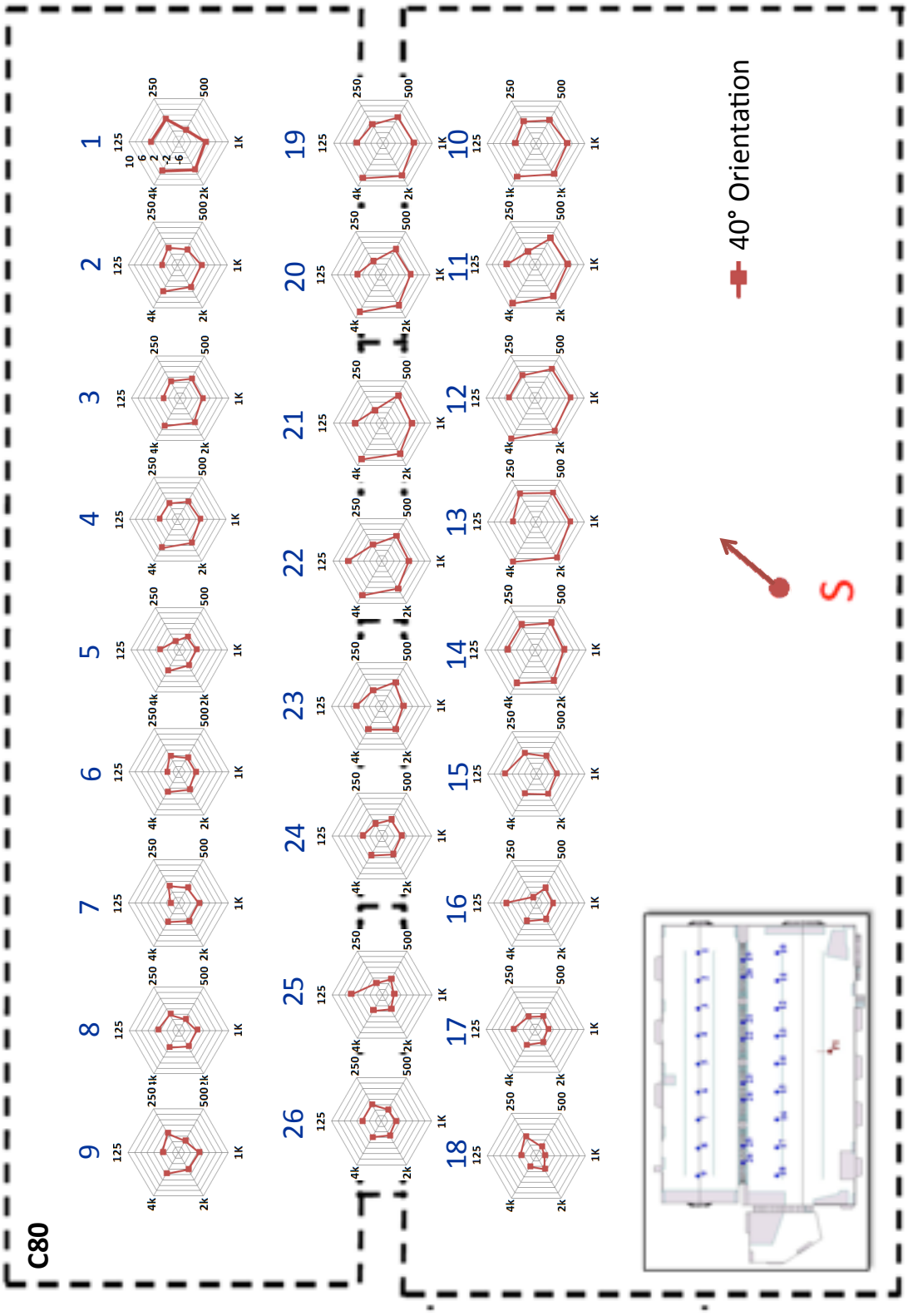

Measurements

Acoustic floor map of C80 values obtained from source orientation at 70° across the grid of 26 receiver positions.

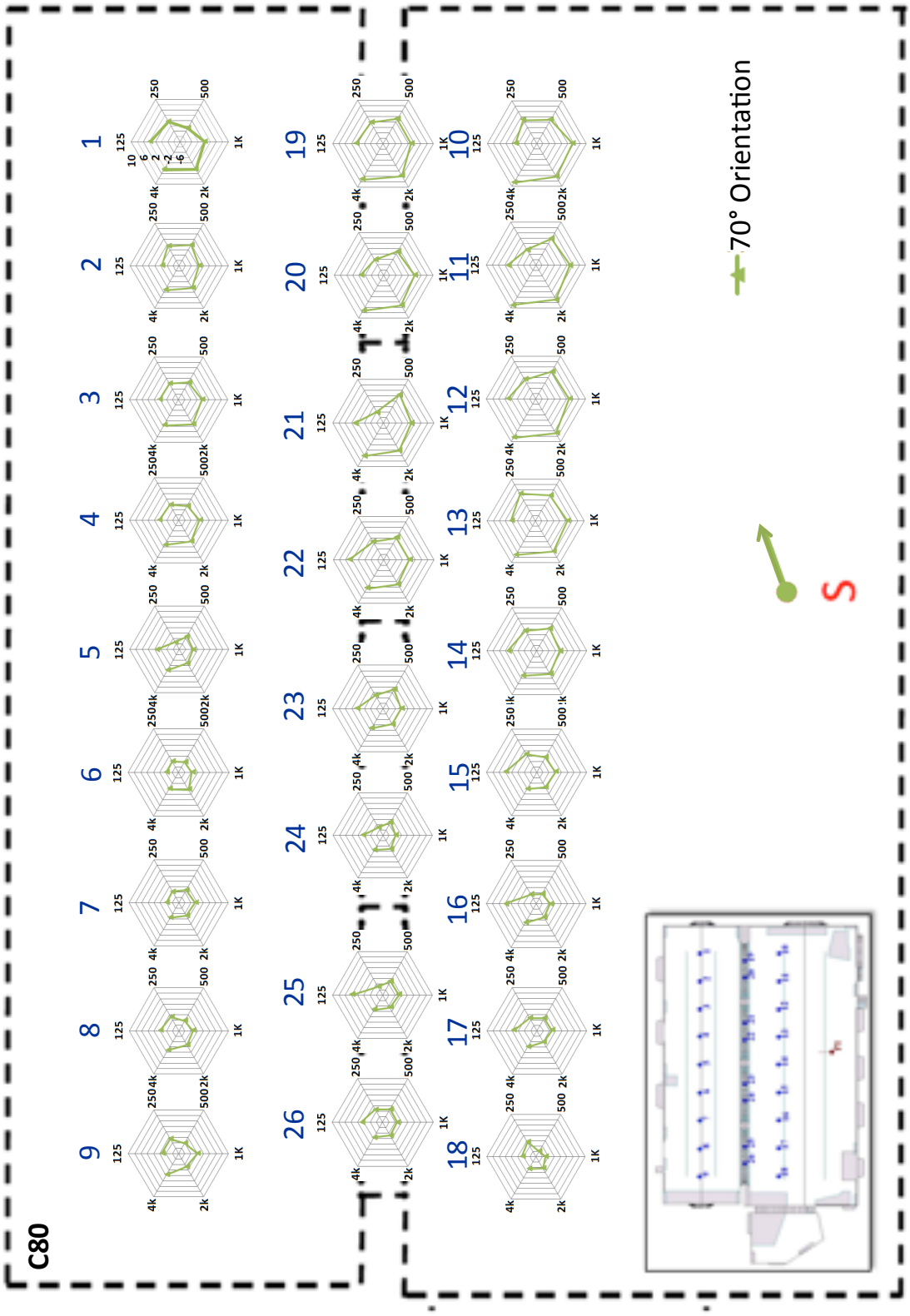

CATT-Acoustic

Acoustic floor map of EDT values obtained from configuration A across the grid of 26 receiver positions.

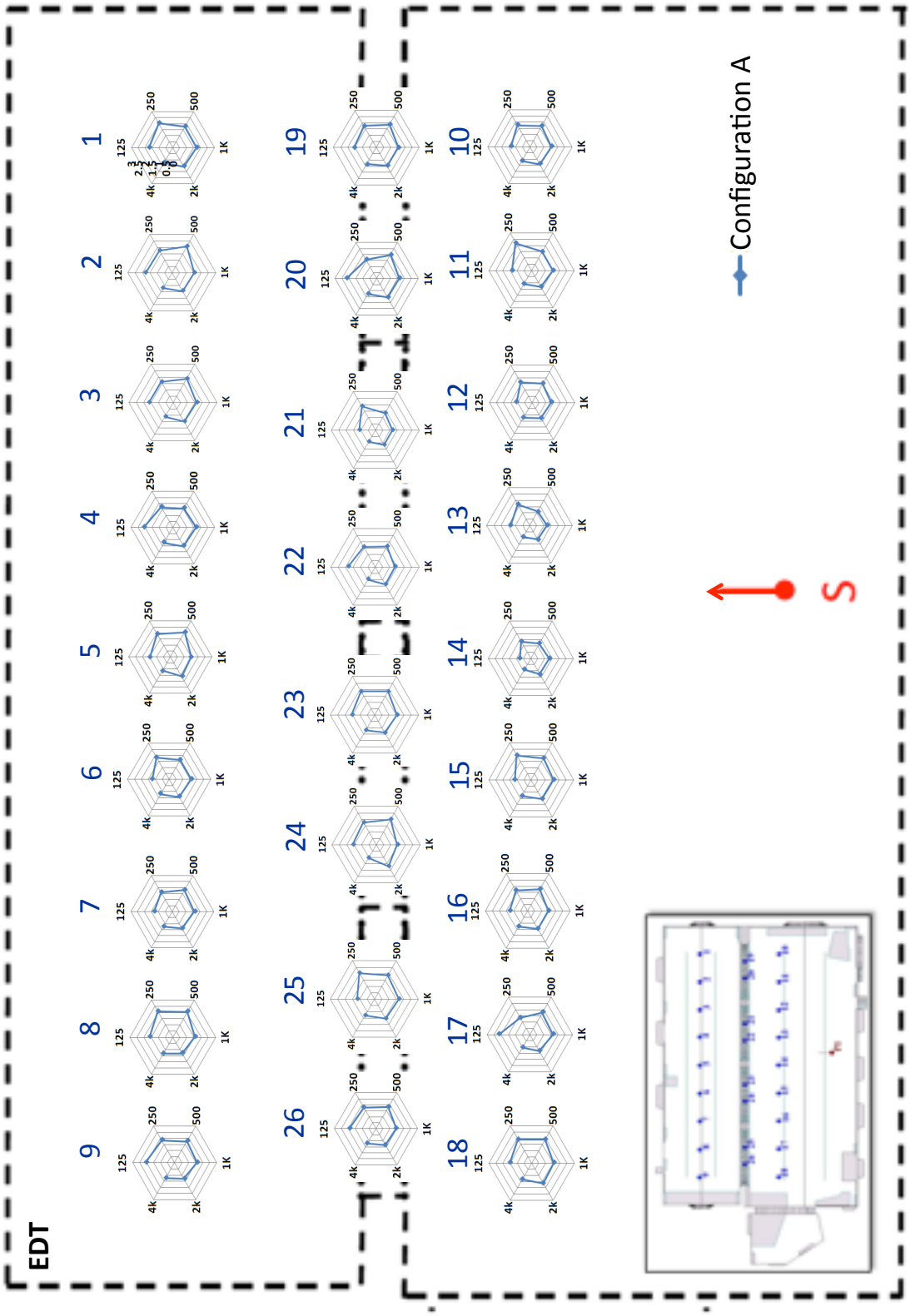

CATT-Acoustic

Acoustic floor map of EDT values observed obtained from configuration B across the grid of 26 receiver positions.

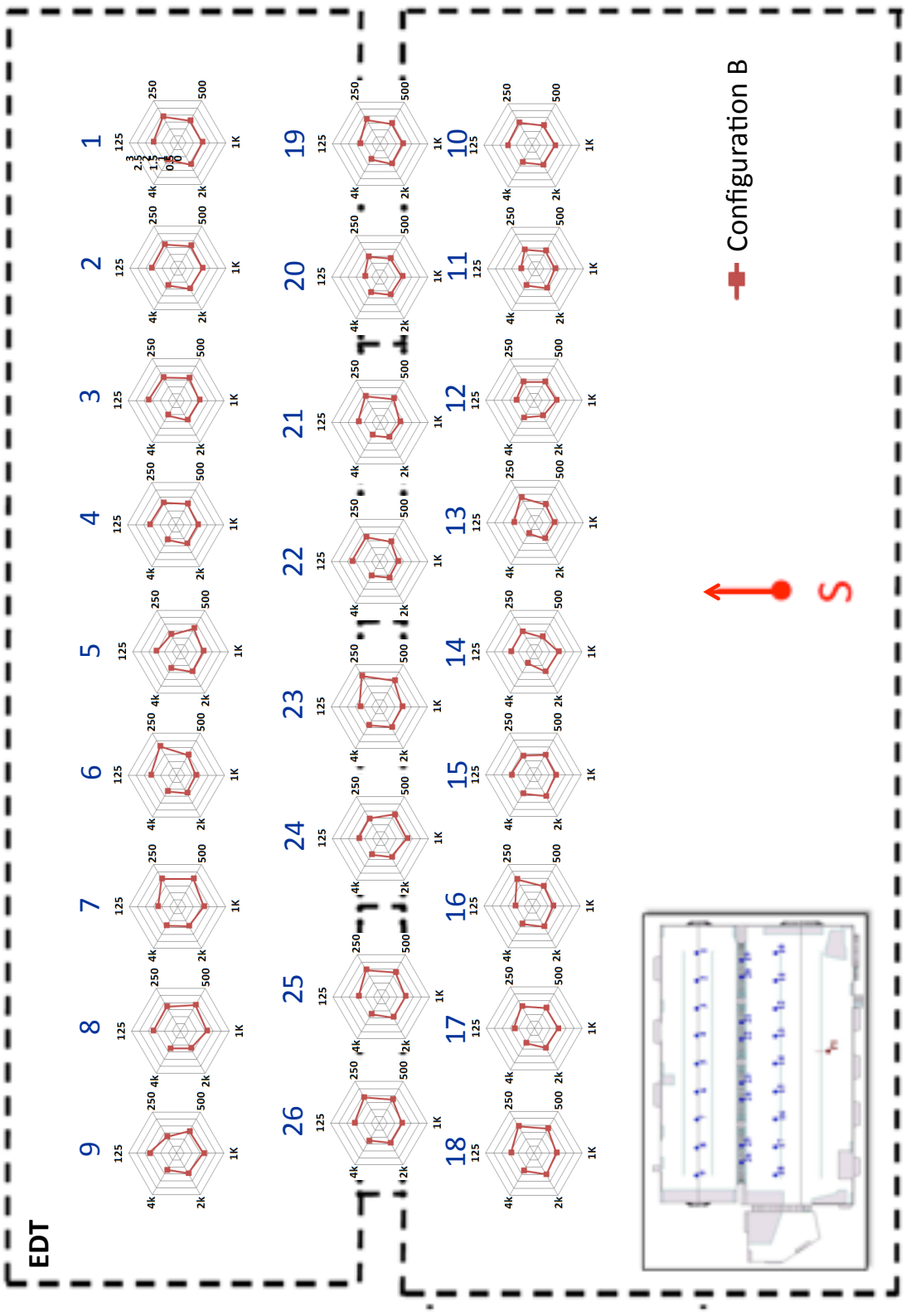

CATT-Acoustic

Acoustic floor map of EDT values obtained from configuration C across the grid of 26 receiver positions .

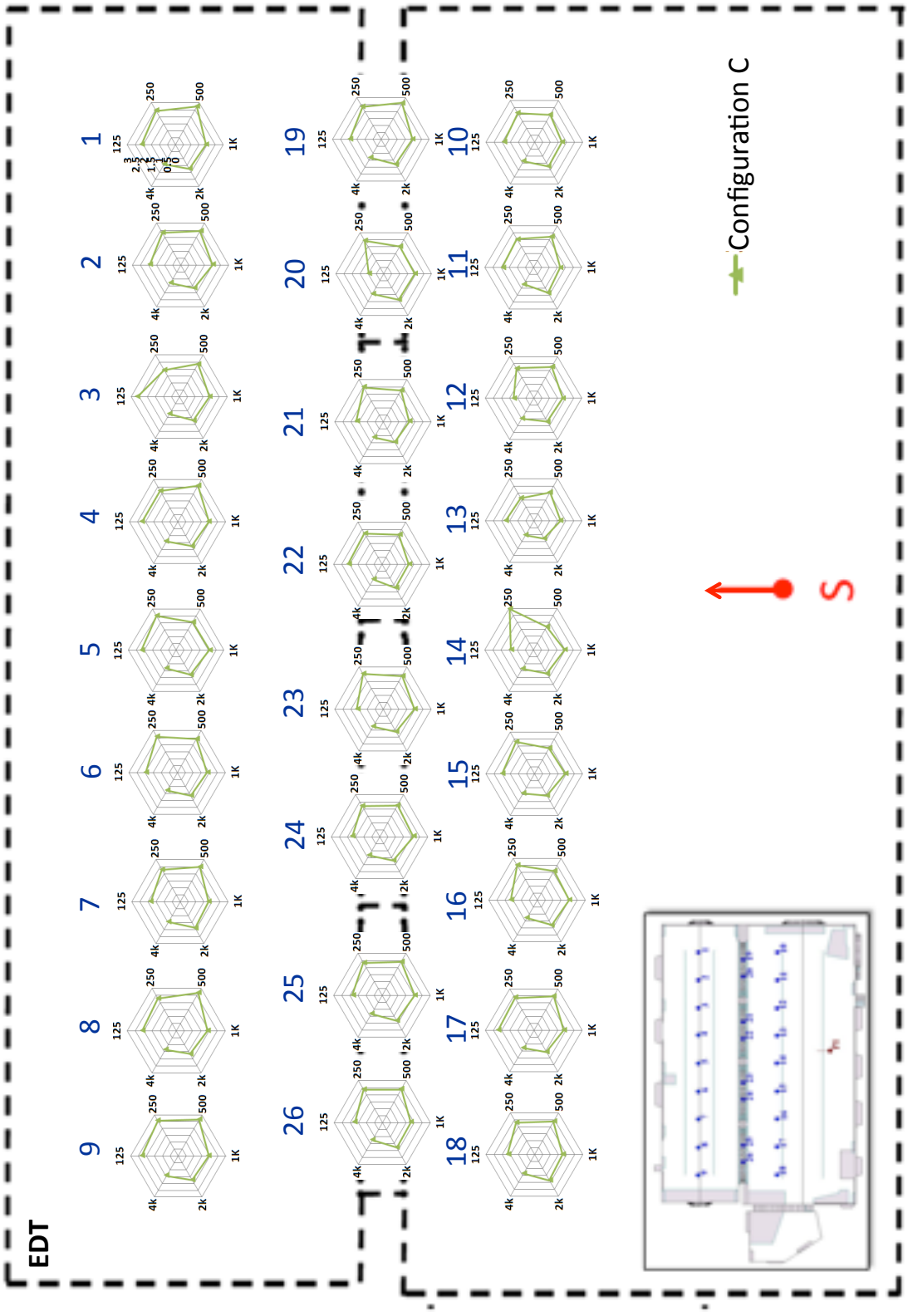

CATT-Acoustic

Acoustic floor map of C80 values obtained from configuration A across the grid of 26 receiver positions.

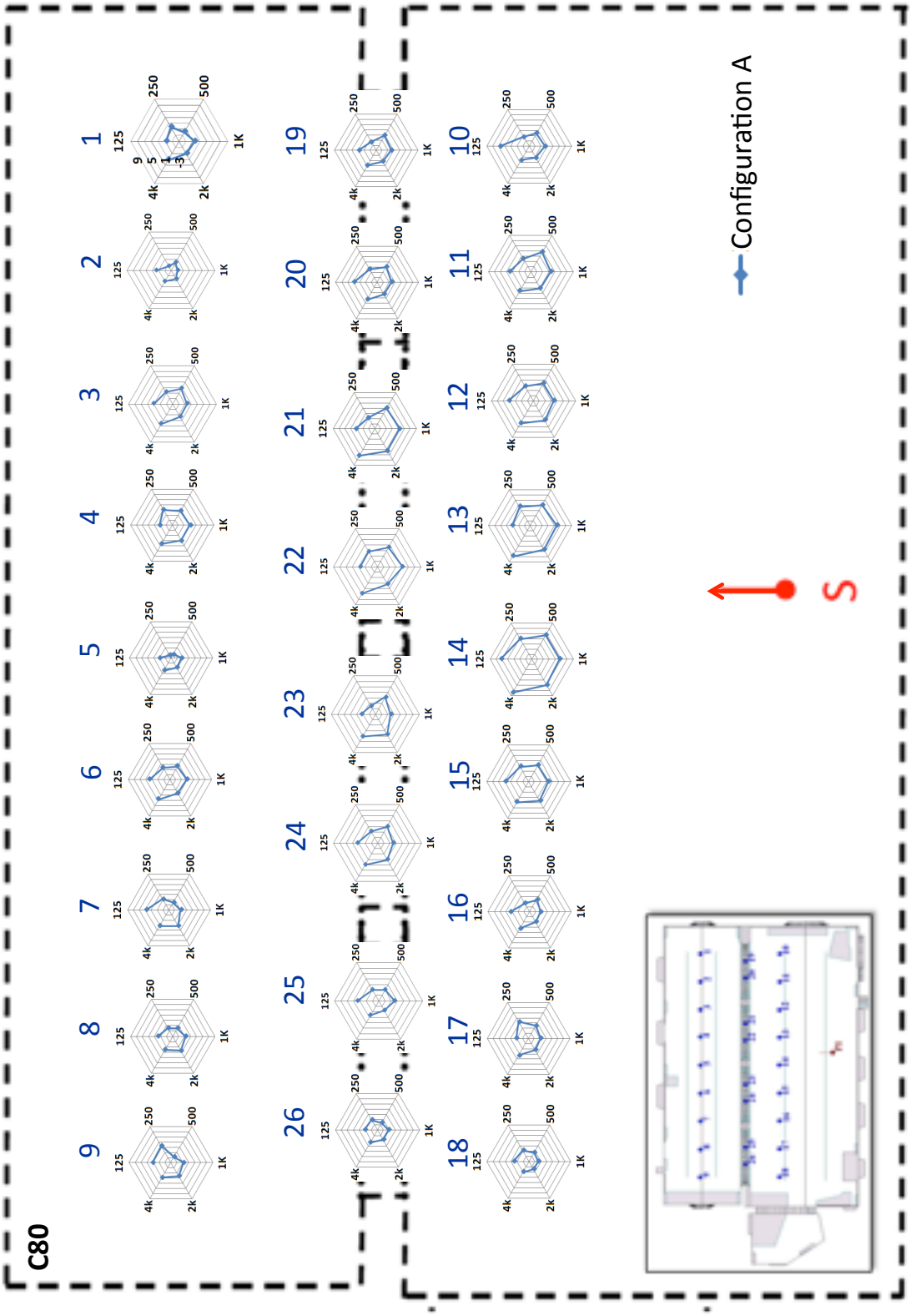

CATT-Acoustic

Acoustic floor map of C80 values obtained from configuration B across the grid of 26 receiver positions.

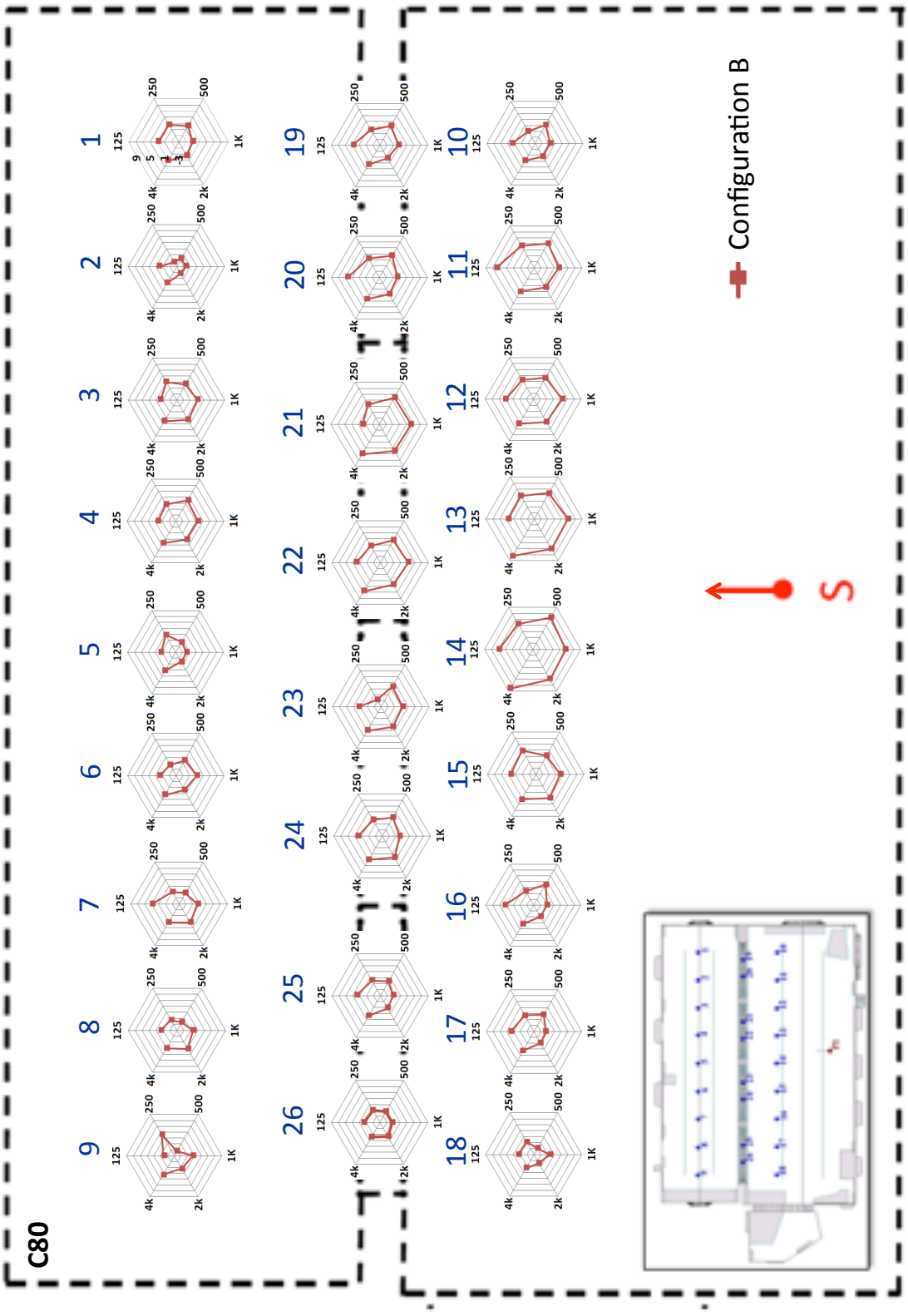

CATT-Acoustic

Acoustic floor map of C_{80} values obtained from configuration C across the grid of 26 receiver positions

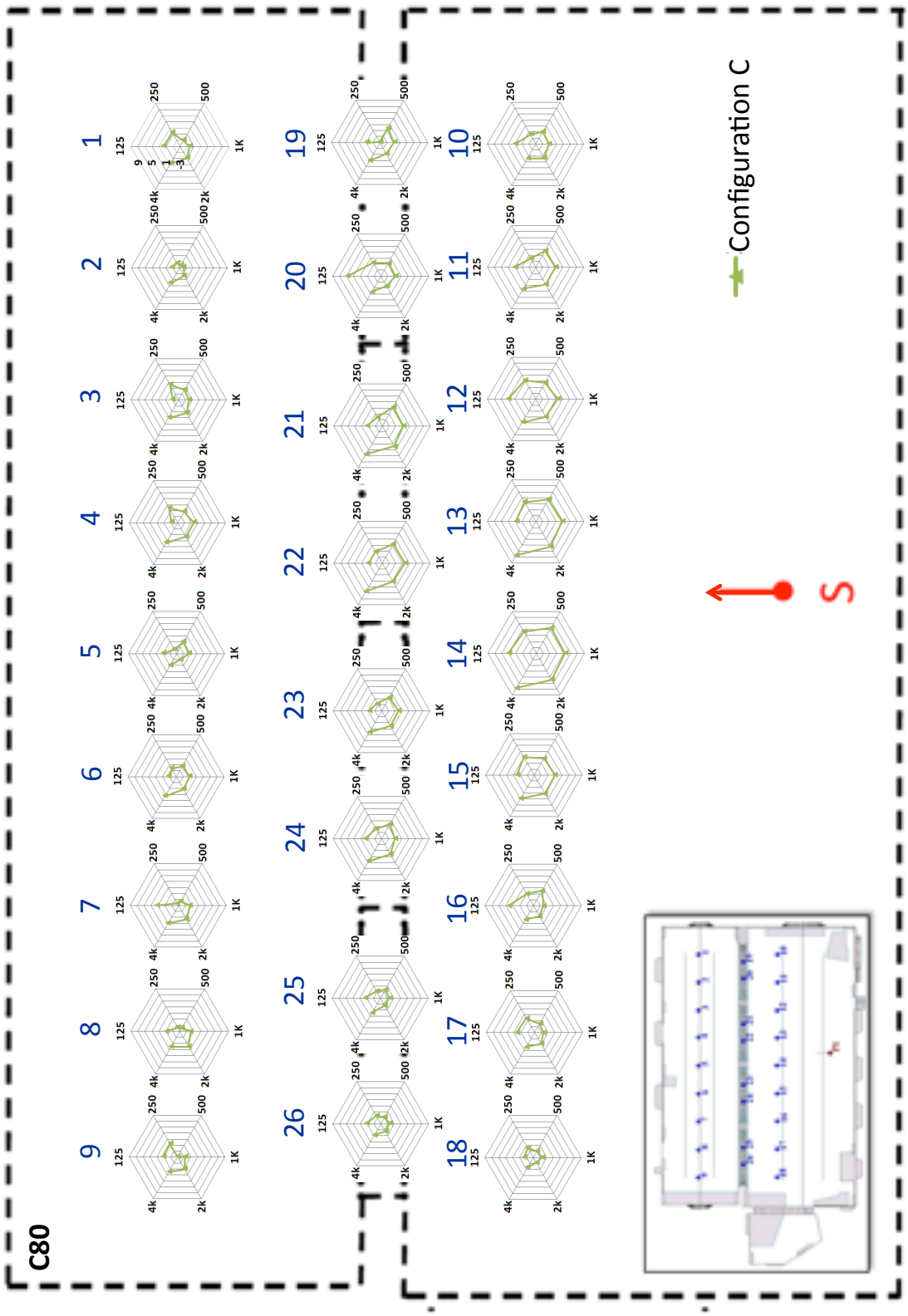

ODEON

Acoustic floor map of EDT values obtained from configuration A across the grid of 26 receiver positions.

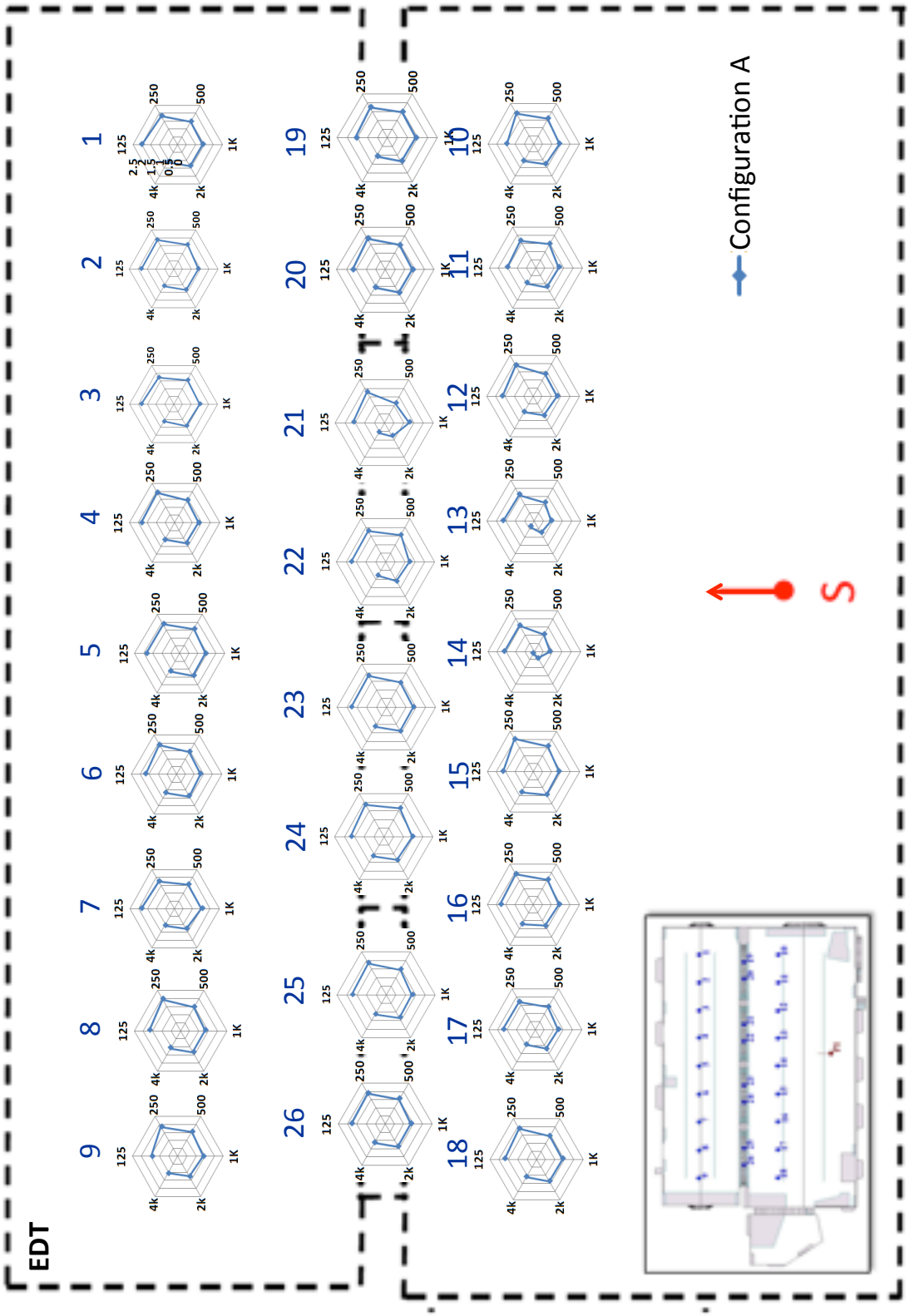

ODEON

Acoustic floor map of EDT values obtained from configuration B across the grid of 26 receiver positions

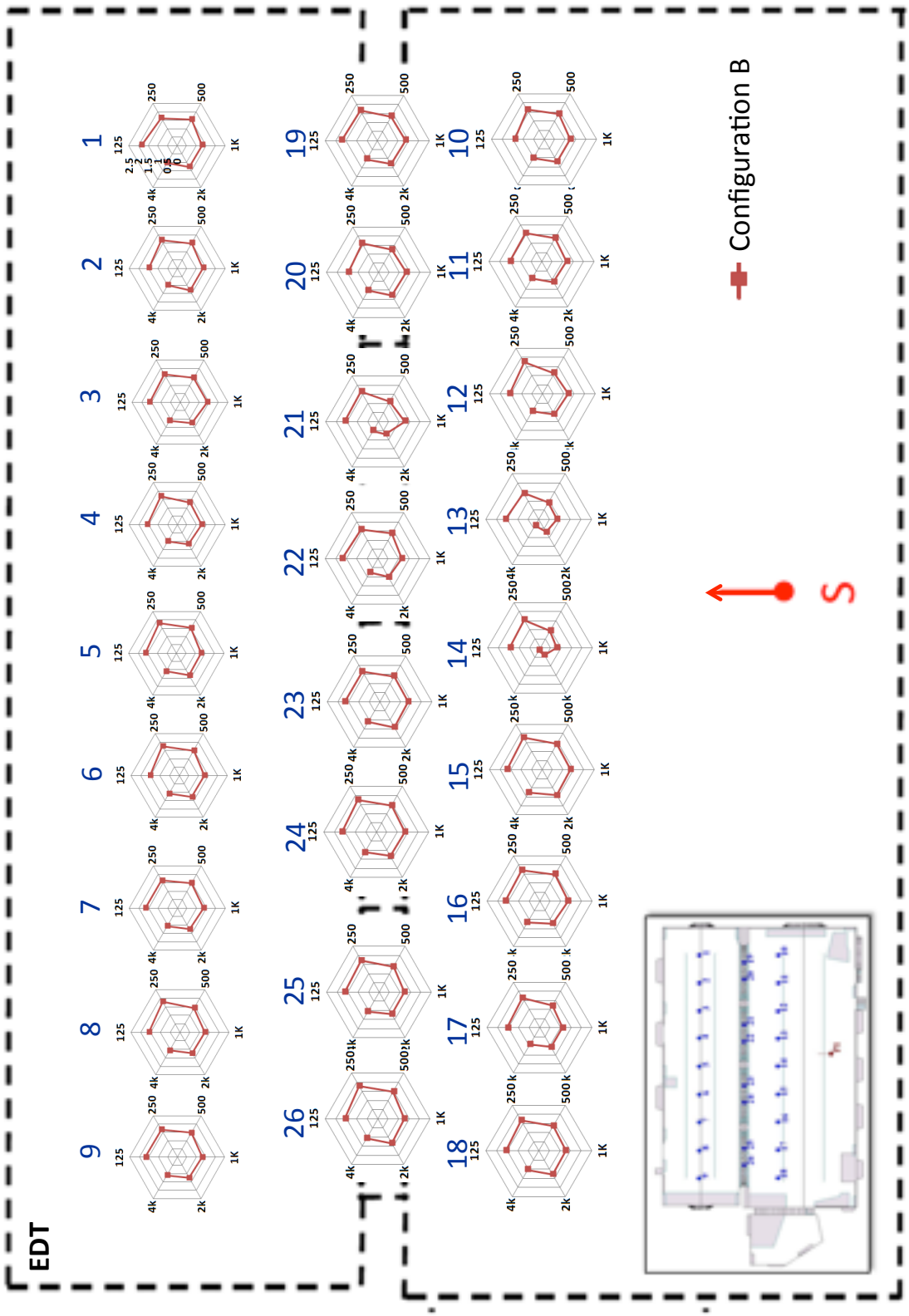

ODEON

Acoustic floor map of EDT values obtained from configuration C across the grid of 26 receiver positions .

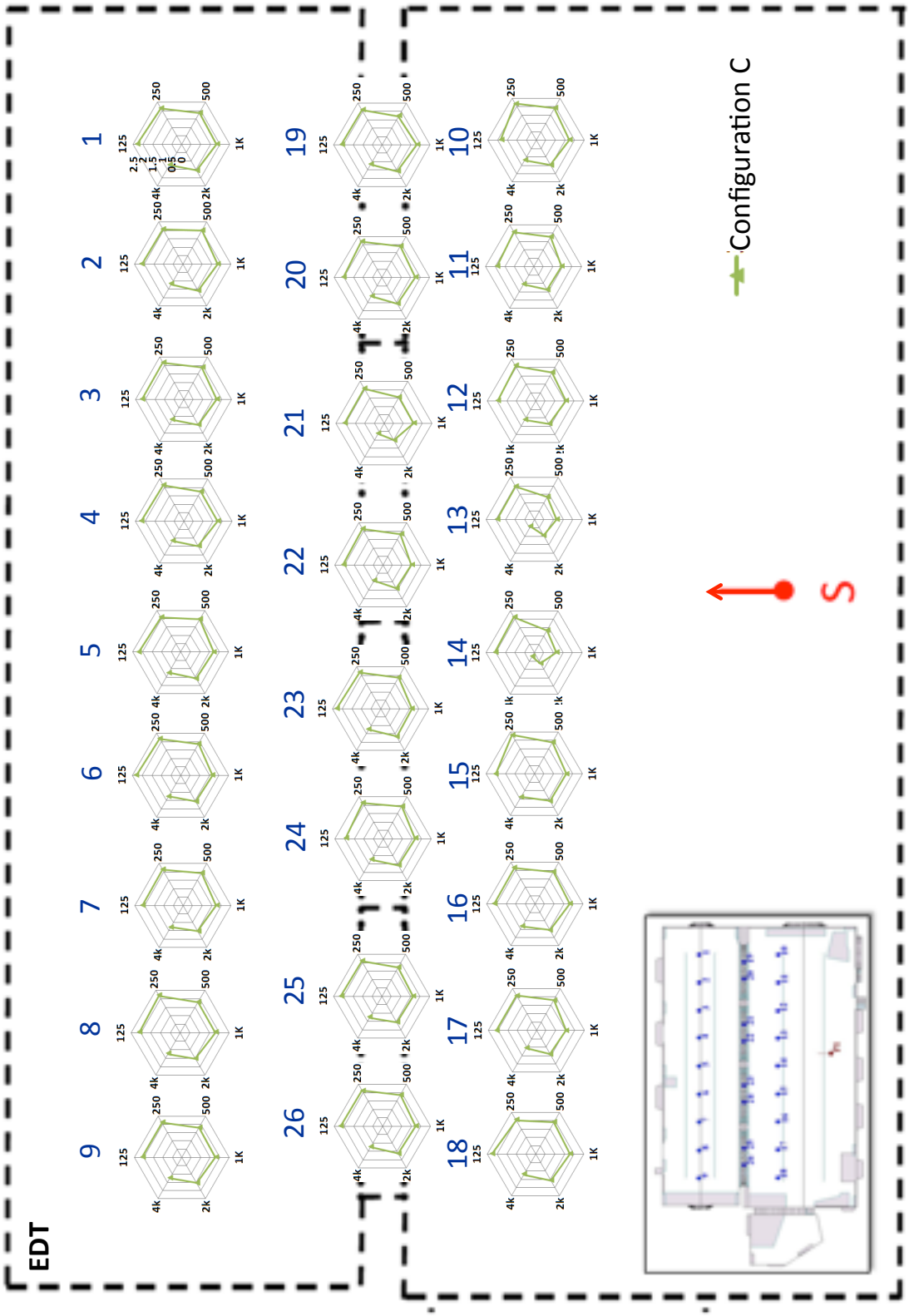

ODEON

Acoustic floor map of C80 values obtained from configuration A across the grid of 26 receiver positions

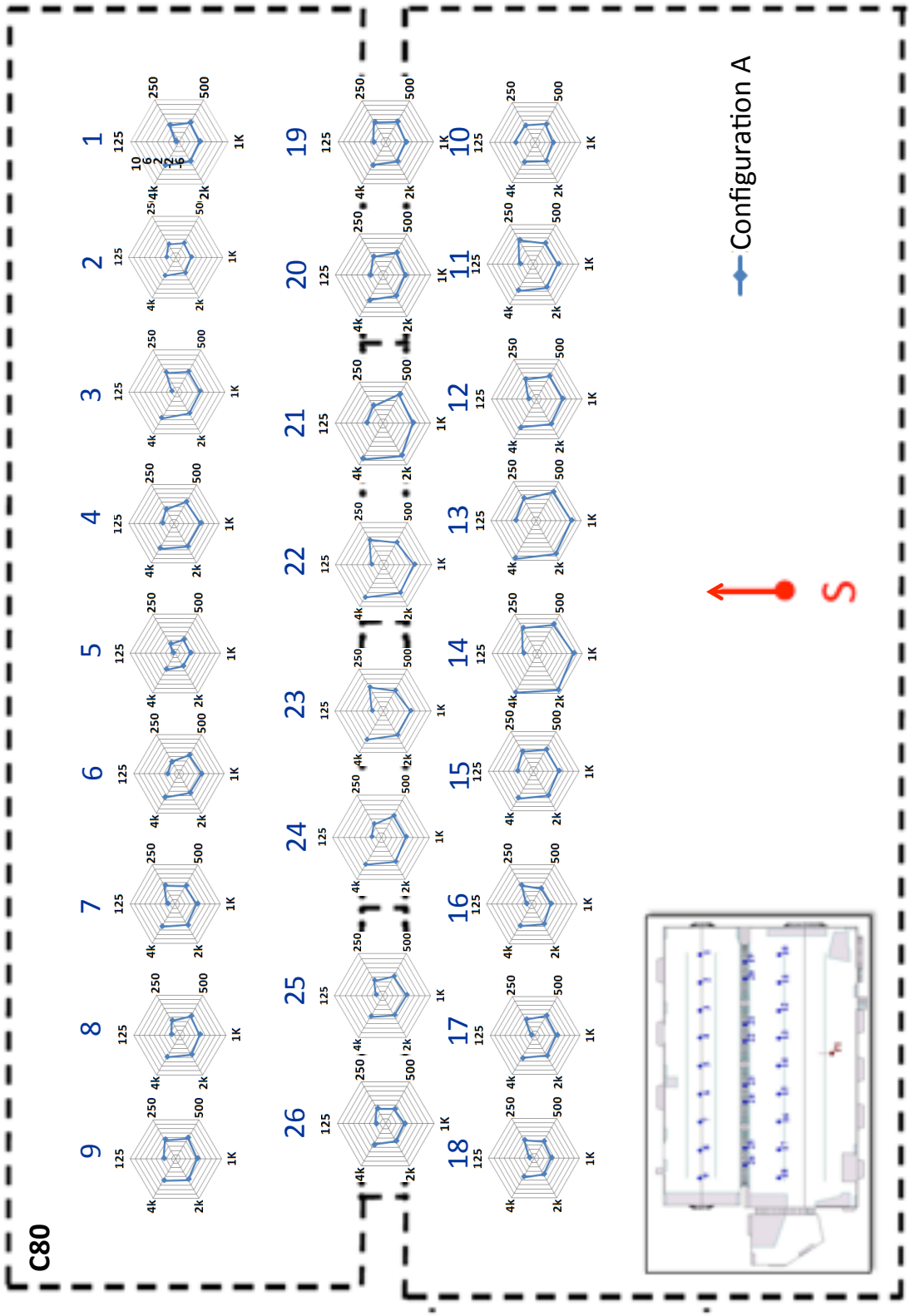

ODEON

Acoustic floor map of C80 values obtained from configuration B across the grid of 26 receiver positions.

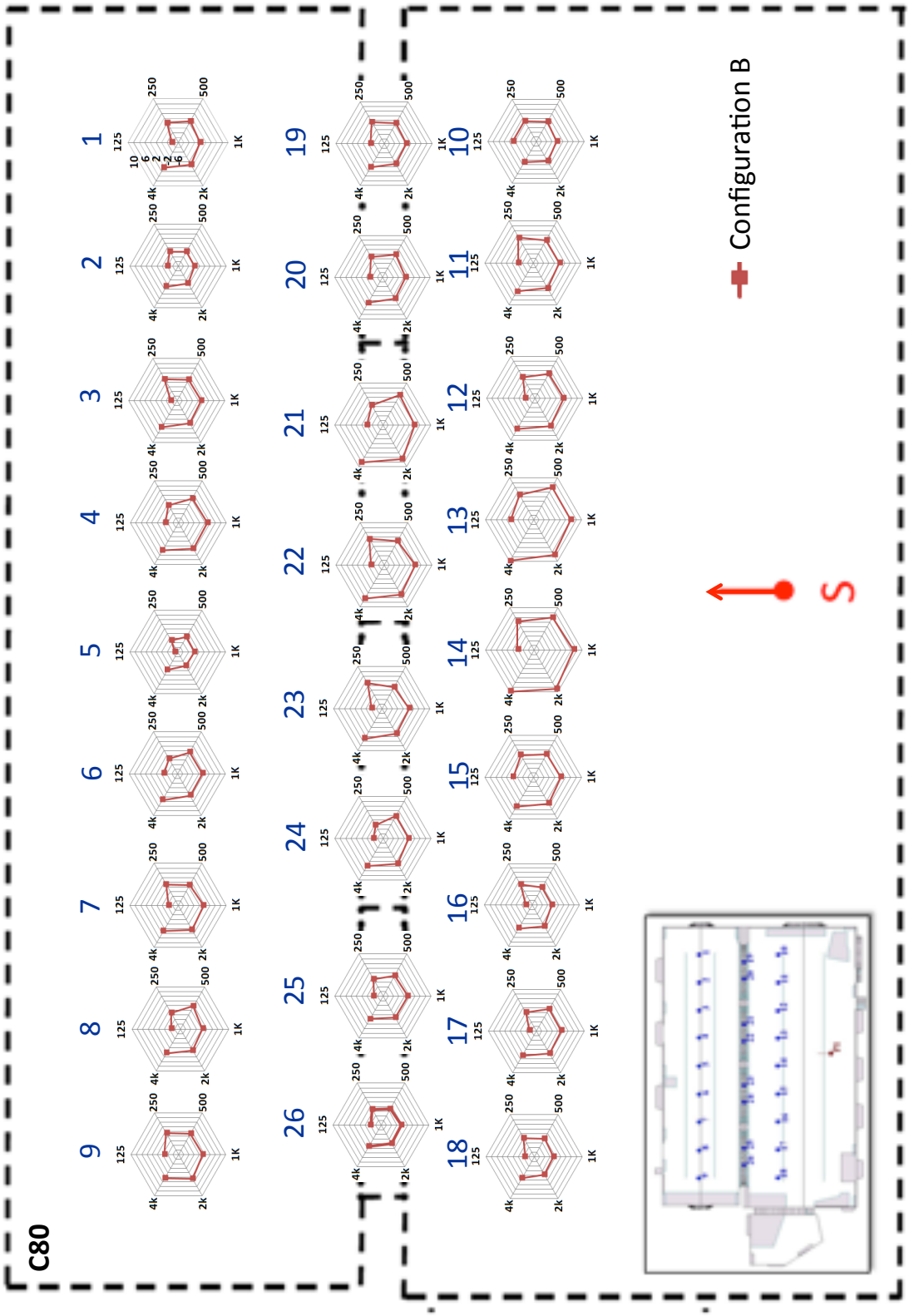

ODEON

Acoustic floor map of C80 values obtained from configuration C across the grid of 26 receiver positions.

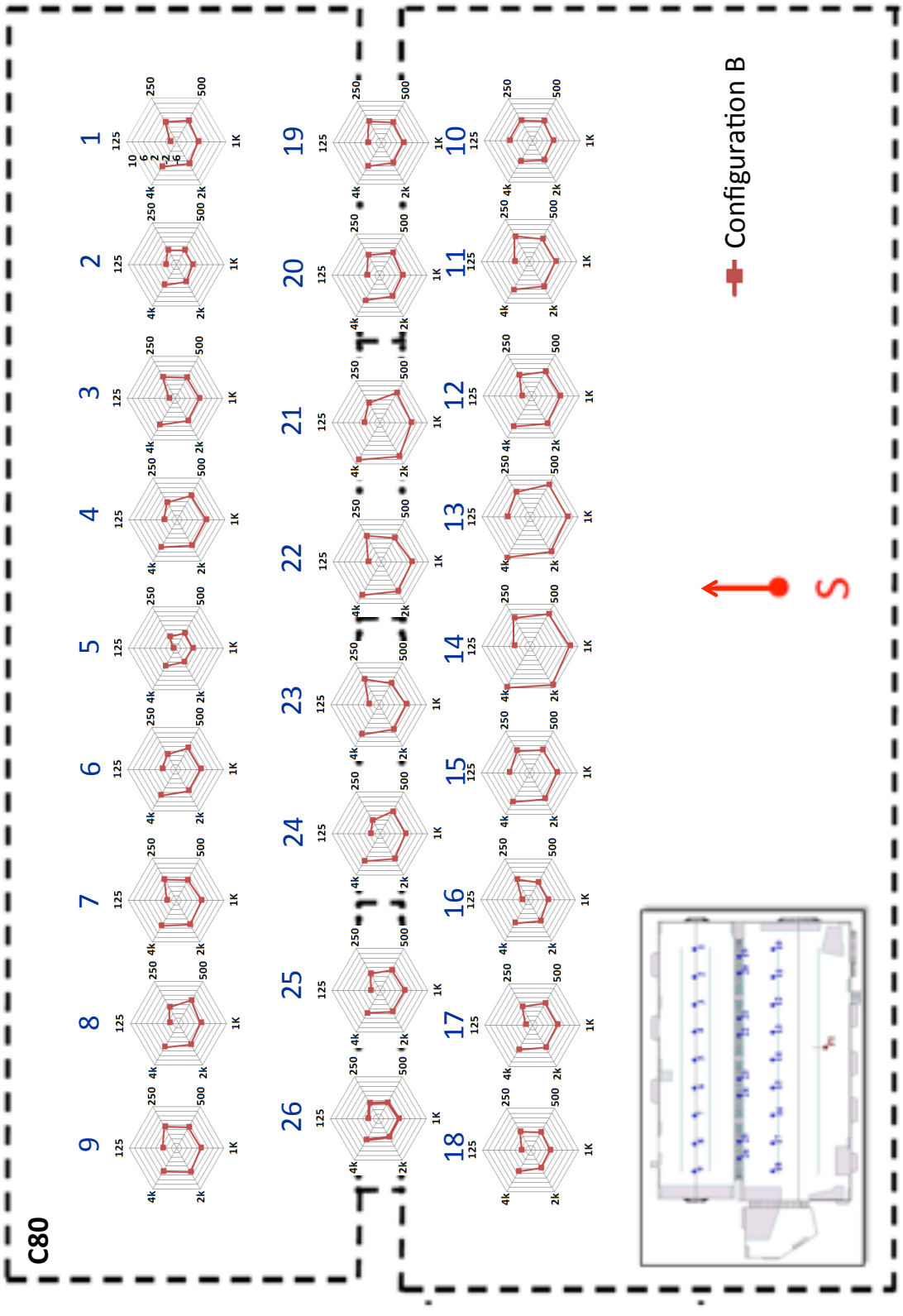

Appendix D

This Appendix contains results observed from the 24 receiver positions for each of the three acoustic configurations and the three sound source orientations, observed from the in-situ measurements, in CATT-Acoustic and ODEON. These results have been used for the subjective evaluations of the resulting auralizations.

For the calculations, the average values of T30, EDT, C50 and C80 over 500Hz and 1000Hz octave bands were used, based on the recommendations of ISO3382. The colours indicate the acoustic configurations for each impulse response (Blue for Configuration A, Red for configuration B and Green for configuration C). Note that two of the positions, R13, and R14, have been excluded from these results for the reasons that have been explained in Chapter 6.

Measurements

Objective results for Configurations A, B and C, sorted in increase order

T30		EDT		C50		C80	
R24	1.358	R22	1.2535	R18	-4.6015	R8	-1.787
R11	1.366	R21	1.275	R18	-4.2625	R18	-1.5025
R15	1.372	R20	1.2775	R8	-4.195	R1	-1.346
R6	1.373	R22	1.2875	R18	-3.859	R25	-0.7815
R8	1.377	R7	1.3075	R1	-3.5455	R18	-0.745
R26	1.378	R12	1.3095	R5	-3.3185	R26	-0.6085
R2	1.3785	R18	1.3115	R26	-3.262	R2	-0.579
R5	1.3825	R2	1.314	R25	-3.1525	R5	-0.4895
R9	1.3855	R23	1.3145	R17	-3.0455	R4	-0.395
R20	1.387	R3	1.3635	R1	-2.796	R1	-0.38
R22	1.387	R19	1.367	R2	-2.6835	R17	-0.3015
R12	1.3915	R12	1.3765	R8	-2.6455	R9	-0.068
R4	1.393	R7	1.391	R6	-2.437	R10	-0.002
R18	1.4035	R20	1.394	R26	-2.3915	R17	0.085
R17	1.4065	R25	1.4035	R26	-2.357	R26	0.127
R21	1.41	R1	1.404	R25	-2.321	R18	0.1425
R7	1.417	R16	1.4105	R5	-2.306	R2	0.1575
R19	1.4185	R8	1.412	R4	-2.3015	R24	0.228
R10	1.4195	R10	1.415	R5	-2.1815	R17	0.3205
R25	1.4195	R11	1.416	R17	-2.1595	R1	0.3455
R3	1.425	R18	1.4275	R2	-2.077	R26	0.472

R1	1.4375	R19	1.4385	R9	-2.0695	R6	0.4985
R23	1.4385	R5	1.4395	R8	-2.0615	R8	0.5185
R16	1.44	R23	1.4415	R10	-2.0395	R5	0.713
R17	1.4495	R26	1.4425	R19	-1.9745	R2	0.7575
R18	1.4505	R17	1.446	R17	-1.9665	R5	0.7875
R6	1.454	R4	1.4515	R1	-1.942	R25	0.8
R24	1.4645	R3	1.4555	R7	-1.8735	R7	0.804
R9	1.4645	R21	1.458	R25	-1.872	R20	0.84
R11	1.4655	R6	1.468	R3	-1.7435	R3	0.886
R15	1.4665	R15	1.468	R20	-1.564	R4	0.9455
R20	1.468	R2	1.4955	R2	-1.555	R9	0.9905
R2	1.4685	R4	1.4985	R7	-1.347	R19	1.0835
R12	1.4725	R15	1.502	R16	-1.3435	R15	1.1455
R21	1.473	R17	1.5065	R6	-1.3155	R8	1.166
R26	1.4735	R25	1.507	R24	-1.2965	R11	1.235
R22	1.476	R16	1.513	R4	-1.197	R16	1.2485
R19	1.4765	R1	1.517	R9	-1.078	R7	1.2835
R10	1.4845	R11	1.5215	R20	-1.01	R24	1.3105
R4	1.4865	R26	1.5245	R4	-0.889	R10	1.61
R7	1.487	R9	1.5325	R10	-0.795	R25	1.692
R8	1.4905	R8	1.533	R11	-0.708	R7	1.698
R1	1.4935	R9	1.5445	R9	-0.6325	R6	1.788
R5	1.4955	R10	1.5545	R7	-0.608	R24	1.8025
R25	1.4975	R24	1.5555	R20	-0.426	R9	1.8895
R3	1.514	R6	1.5875	R3	-0.4155	R3	1.963
R23	1.517	R24	1.608	R16	-0.4015	R20	2.01
R16	1.52	R5	1.6145	R19	-0.39	R10	2.065
R26	1.7535	R22	1.6775	R6	-0.3575	R4	2.1725
R24	1.7585	R3	1.705	R11	-0.356	R16	2.179
R21	1.7735	R19	1.734	R10	-0.276	R15	2.397
R18	1.7755	R2	1.752	R15	-0.2605	R6	2.4065
R15	1.7765	R18	1.7555	R19	-0.1765	R11	2.629
R6	1.78	R12	1.761	R16	-0.1485	R3	2.63
R7	1.781	R23	1.767	R24	-0.138	R19	2.6865
R25	1.7865	R21	1.768	R11	0.09	R23	2.785
R20	1.7935	R10	1.77	R3	0.1255	R20	2.7935
R17	1.794	R6	1.7865	R24	0.133	R15	2.794
R8	1.795	R8	1.8045	R23	0.3285	R16	2.8435
R11	1.795	R9	1.8195	R15	0.345	R11	2.8795
R22	1.796	R16	1.825	R22	0.621	R21	3.0115
R10	1.7965	R1	1.828	R15	0.867	R12	3.1355
R16	1.8005	R11	1.835	R23	1.1015	R19	3.3325
R19	1.8005	R7	1.871	R21	1.123	R22	3.8475
R9	1.802	R5	1.873	R12	1.175	R12	3.886
R12	1.8165	R15	1.873	R22	1.292	R23	3.9435
R23	1.8165	R4	1.89	R23	1.36	R21	4.0585

R2	1.8265	R17	1.9075	R22	1.9005	R12	4.2015
R4	1.8295	R20	1.9165	R12	2.009	R23	4.3455
R5	1.8305	R24	1.939	R21	2.035	R21	4.5365
R1	1.837	R25	1.959	R21	2.2455	R22	5.101
R3	1.8495	R26	1.9935	R12	2.272	R22	5.3155

The relevant JNDs have been calculated based on the following minimum observed values.

	T30		EDT		C50		C80	
Minimum Values	R24	1.358	R22	1.2535	R18	-4.6015	R8	-1.787
JND		0.0679		0.062675		1		1

Objective results for Configurations A, B and C, sorted based on the JND values in increase order

JND values							
T30		EDT		C50		C80	
R24	0	R22	0	R18	0	R8	0
R11	0.11782	R21	0.343039	R18	0.339	R18	0.2845
R15	0.206186	R20	0.382928	R8	0.4065	R1	0.441
R6	0.220913	R22	0.542481	R18	0.7425	R25	1.0055
R8	0.279823	R7	0.861588	R1	1.056	R18	1.042
R26	0.294551	R12	0.893498	R5	1.283	R26	1.1785
R2	0.301915	R18	0.925409	R26	1.3395	R2	1.208
R5	0.360825	R2	0.965297	R25	1.449	R5	1.2975
R9	0.405007	R23	0.973275	R17	1.556	R4	1.392
R20	0.427099	R3	1.755086	R1	1.8055	R1	1.407
R22	0.427099	R19	1.810929	R2	1.918	R17	1.4855
R12	0.493373	R12	1.962505	R8	1.956	R9	1.719
R4	0.515464	R7	2.193857	R6	2.1645	R10	1.785
R18	0.670103	R20	2.241723	R26	2.21	R17	1.872
R17	0.714286	R25	2.393299	R26	2.2445	R26	1.914
R21	0.765832	R1	2.401276	R25	2.2805	R18	1.9295
R7	0.868925	R16	2.504986	R5	2.2955	R2	1.9445
R19	0.891016	R8	2.528919	R4	2.3	R24	2.015
R10	0.905744	R10	2.576785	R5	2.42	R17	2.1075
R25	0.905744	R11	2.59274	R17	2.442	R1	2.1325
R3	0.986745	R18	2.776227	R2	2.5245	R26	2.259
R1	1.170839	R19	2.951735	R9	2.532	R6	2.2855
R23	1.185567	R5	2.96769	R8	2.54	R8	2.3055
R16	1.207658	R23	2.999601	R10	2.562	R5	2.5

R17	1.34757	R26	3.015556	R19	2.627	R2	2.5445
R18	1.362297	R17	3.0714	R17	2.635	R5	2.5745
R6	1.413844	R4	3.159154	R1	2.6595	R25	2.587
R24	1.568483	R3	3.222976	R7	2.728	R7	2.591
R9	1.568483	R21	3.262864	R25	2.7295	R20	2.627
R11	1.583211	R6	3.422417	R3	2.858	R3	2.673
R15	1.597938	R15	3.422417	R20	3.0375	R4	2.7325
R20	1.620029	R2	3.861189	R2	3.0465	R9	2.7775
R2	1.627393	R4	3.909055	R7	3.2545	R19	2.8705
R12	1.686303	R15	3.964898	R16	3.258	R15	2.9325
R21	1.693667	R17	4.036697	R6	3.286	R8	2.953
R26	1.701031	R25	4.044675	R24	3.305	R11	3.022
R22	1.73785	R16	4.140407	R4	3.4045	R16	3.0355
R19	1.745214	R1	4.204228	R9	3.5235	R7	3.0705
R10	1.863034	R11	4.276027	R20	3.5915	R24	3.0975
R4	1.892489	R26	4.323893	R4	3.7125	R10	3.397
R7	1.899853	R9	4.451536	R10	3.8065	R25	3.479
R8	1.951399	R8	4.459513	R11	3.8935	R7	3.485
R1	1.995582	R9	4.643	R9	3.969	R6	3.575
R5	2.025037	R10	4.802553	R7	3.9935	R24	3.5895
R25	2.054492	R24	4.818508	R20	4.1755	R9	3.6765
R3	2.297496	R6	5.329079	R3	4.186	R3	3.75
R23	2.341679	R24	5.656163	R16	4.2	R20	3.797
R16	2.385862	R5	5.759872	R19	4.2115	R10	3.852
R26	5.824742	R22	6.765058	R6	4.244	R4	3.9595
R24	5.89838	R3	7.203829	R11	4.2455	R16	3.966
R21	6.119293	R19	7.666534	R10	4.3255	R15	4.184
R18	6.148748	R2	7.95373	R15	4.341	R6	4.1935
R15	6.163476	R18	8.009573	R19	4.425	R11	4.416
R6	6.215022	R12	8.097327	R16	4.453	R3	4.417
R7	6.22975	R23	8.193059	R24	4.4635	R19	4.4735
R25	6.310751	R21	8.209015	R11	4.6915	R23	4.572
R20	6.413844	R10	8.240925	R3	4.727	R20	4.5805
R17	6.421208	R6	8.504188	R24	4.7345	R15	4.581
R8	6.435935	R8	8.791384	R23	4.93	R16	4.6305
R11	6.435935	R9	9.030714	R15	4.9465	R11	4.6665
R22	6.450663	R16	9.118468	R22	5.2225	R21	4.7985
R10	6.458027	R1	9.166334	R15	5.4685	R12	4.9225
R16	6.516937	R11	9.278022	R23	5.703	R19	5.1195
R19	6.516937	R7	9.852413	R21	5.7245	R22	5.6345
R9	6.539028	R5	9.884324	R12	5.7765	R12	5.673
R12	6.752577	R15	9.884324	R22	5.8935	R23	5.7305
R23	6.752577	R4	10.15556	R23	5.9615	R21	5.8455
R2	6.899853	R17	10.43478	R22	6.502	R12	5.9885
R4	6.944035	R20	10.57838	R12	6.6105	R23	6.1325
R5	6.958763	R24	10.93738	R21	6.6365	R21	6.3235

R1	7.054492	**R25**	11.25648	**R21**	6.847	**R22**	6.888
R3	7.238586	**R26**	11.80694	**R12**	6.8735	**R22**	7.1025

Objective results for Source Orientations 0°, 40°and 70° sorted in increase order

The colours here indicate the source orientation configurations for each impulse response (Blue for the 0° orientation of the source, Red for the 40° and Green for the 70°).

T30		EDT		C50		C80	
R18	1.4305	R10	1.2115	R18	-7.0295	R18	-3.547
R22	1.4315	R22	1.2535	R18	-6.4505	R18	-2.974
R6	1.438	R20	1.324	R26	-5.653	R6	-1.982
R19	1.442	R10	1.3355	R8	-5.3785	R16	-1.943
R22	1.446	R12	1.353	R26	-5.375	R8	-1.8775
R11	1.4465	R12	1.3765	R25	-5.3395	R26	-1.5955
R6	1.4485	R21	1.3805	R8	-5.191	R17	-1.5685
R17	1.4495	R7	1.391	R17	-5.0915	R24	-1.426
R4	1.4495	R20	1.394	R9	-4.922	R5	-1.3935
R18	1.4505	R20	1.3995	R7	-4.8345	R25	-1.3585
R23	1.4505	R22	1.401	R16	-4.6505	R26	-1.34
R11	1.451	R21	1.414	R25	-4.643	R17	-1.331
R17	1.452	R22	1.4185	R6	-4.376	R8	-1.1575
R18	1.4535	R18	1.4275	R5	-4.3195	R9	-1.1405
R6	1.454	R19	1.4385	R18	-4.2625	R7	-0.9965
R23	1.4555	R23	1.4415	R24	-4.1295	R25	-0.9675
R26	1.459	R19	1.4525	R17	-4.1145	R5	-0.798
R24	1.4595	R3	1.4555	R9	-3.794	R6	-0.7805
R5	1.461	R21	1.458	R5	-3.4285	R18	-0.745
R19	1.462	R12	1.4615	R16	-3.2685	R9	-0.5865
R15	1.4625	R11	1.469	R6	-3.011	R16	-0.549
R26	1.4635	R4	1.4715	R15	-2.868	R1	-0.38
R12	1.4635	R3	1.472	R1	-2.796	R15	-0.289
R24	1.464	R19	1.475	R8	-2.6455	R17	0.085
R24	1.4645	R16	1.4775	R7	-2.6385	R7	0.0935
R9	1.4645	R16	1.491	R4	-2.4705	R4	0.097
R11	1.4655	R24	1.492	R26	-2.3915	R24	0.1195
R15	1.4665	R1	1.493	R25	-2.321	R26	0.127
R20	1.468	R2	1.4955	R24	-2.308	R2	0.1575
R2	1.4685	R4	1.4985	R5	-2.306	R23	0.389
R17	1.4685	R15	1.502	R17	-2.1595	R1	0.509
R21	1.469	R17	1.5065	R23	-2.0945	R8	0.5185
R8	1.4705	R25	1.507	R2	-2.077	R15	0.601
R10	1.4705	R11	1.5105	R3	-1.918	R1	0.6465
R12	1.4725	R16	1.513	R1	-1.7505	R2	0.6675
R21	1.473	R1	1.517	R2	-1.5845	R5	0.713

R26	1.4735	R11	1.5215	R4	-1.563	R25	0.8
R1	1.475	R26	1.5245	R1	-1.471	R4	0.9455
R10	1.4755	R18	1.527	R7	-1.347	R3	0.985
R12	1.4755	R2	1.53	R6	-1.3155	R4	1.0305
R22	1.476	R8	1.533	R2	-1.239	R2	1.176
R20	1.476	R3	1.5395	R4	-1.197	R7	1.2835
R25	1.4765	R8	1.541	R15	-1.1735	R24	1.3105
R19	1.4765	R9	1.5445	R20	-1.01	R3	1.386
R2	1.478	R15	1.546	R10	-0.795	R10	1.61
R16	1.478	R1	1.5505	R3	-0.786	R6	1.788
R9	1.479	R7	1.5535	R23	-0.7115	R23	1.836
R2	1.48	R10	1.5545	R9	-0.6325	R9	1.8895
R15	1.4815	R26	1.5545	R22	-0.4495	R3	1.963
R16	1.4835	R15	1.5575	R3	-0.4155	R20	2.01
R10	1.4845	R25	1.5615	R16	-0.4015	R22	2.1095
R4	1.4865	R18	1.5695	R19	-0.39	R16	2.179
R21	1.4865	R23	1.5735	R11	-0.356	R15	2.397
R7	1.487	R24	1.5825	R24	-0.138	R11	2.629
R25	1.4895	R25	1.5865	R22	0.043	R19	2.6865
R5	1.49	R6	1.5875	R20	0.3065	R19	2.9365
R8	1.4905	R7	1.606	R15	0.345	R22	3.1225
R3	1.4915	R2	1.607	R19	0.7555	R20	3.388
R20	1.492	R24	1.608	R20	0.7755	R10	3.434
R1	1.4935	R9	1.61	R21	0.8195	R20	3.444
R9	1.494	R8	1.613	R19	0.9735	R21	3.6135
R8	1.494	R5	1.6145	R23	1.1015	R19	3.744
R7	1.4945	R23	1.6165	R22	1.292	R12	3.886
R5	1.4955	R4	1.6385	R21	1.593	R23	3.9435
R7	1.4955	R17	1.6455	R10	1.666	R21	4.0325
R25	1.4975	R26	1.688	R12	2.009	R21	4.0585
R3	1.4975	R9	1.6965	R21	2.035	R10	4.166
R4	1.5	R6	1.7025	R11	2.235	R11	4.1775
R3	1.514	R17	1.7205	R12	2.2705	R11	4.372
R23	1.517	R5	1.7235	R10	2.4855	R12	4.4875
R16	1.52	R5	1.752	R11	2.642	R22	5.101
R1	1.523	R6	1.788	R12	3.163	R12	5.1545

The relevant JNDs have been calculated based on the following minimum observed values.

	T30		EDT		C50		C80	
Minimum Values	R18	1.4305	R10	1.2115	R18	-7.0295	R18	-3.547
JND		0.071525		0.060575		1		1

Objective results for Source Orientations 0°, 40° and 70° sorted based on the JND values in increase order

JND values							
T30		EDT		C50		C80	
R18	0	R10	0	R18	0	R18	0
R22	0.013981	R22	0.693355	R18	0.579	R18	0.573
R6	0.104858	R20	1.857202	R26	1.3765	R6	1.565
R19	0.160783	R10	2.047049	R8	1.651	R16	1.604
R22	0.216707	R12	2.335947	R26	1.6545	R8	1.6695
R11	0.223698	R12	2.723896	R25	1.69	R26	1.9515
R6	0.25166	R21	2.78993	R8	1.8385	R17	1.9785
R17	0.265641	R7	2.963269	R17	1.938	R24	2.121
R4	0.265641	R20	3.012794	R9	2.1075	R5	2.1535
R18	0.279623	R20	3.103591	R7	2.195	R25	2.1885
R23	0.279623	R22	3.128353	R16	2.379	R26	2.207
R11	0.286613	R21	3.342963	R25	2.3865	R17	2.216
R17	0.300594	R22	3.417251	R6	2.6535	R8	2.3895
R18	0.321566	R18	3.565827	R5	2.71	R9	2.4065
R6	0.328556	R19	3.747421	R18	2.767	R7	2.5505
R23	0.349528	R23	3.796946	R24	2.9	R25	2.5795
R26	0.398462	R19	3.978539	R17	2.915	R5	2.749
R24	0.405453	R3	4.028064	R9	3.2355	R6	2.7665
R5	0.426424	R21	4.069336	R5	3.601	R18	2.802
R19	0.440405	R12	4.127115	R16	3.761	R9	2.9605
R15	0.447396	R11	4.250929	R6	4.0185	R16	2.998
R26	0.461377	R4	4.2922	R15	4.1615	R1	3.167
R12	0.461377	R3	4.300454	R1	4.2335	R15	3.258
R24	0.468368	R19	4.349979	R8	4.384	R17	3.632
R24	0.475358	R16	4.391251	R7	4.391	R7	3.6405
R9	0.475358	R16	4.614115	R4	4.559	R4	3.644
R11	0.489339	R24	4.630623	R26	4.638	R24	3.6665
R15	0.503321	R1	4.647132	R25	4.7085	R26	3.674
R20	0.524292	R2	4.688403	R24	4.7215	R2	3.7045
R2	0.531283	R4	4.737928	R5	4.7235	R23	3.936
R17	0.531283	R15	4.795708	R17	4.87	R1	4.056
R21	0.538273	R17	4.869996	R23	4.935	R8	4.0655
R8	0.559245	R25	4.87825	R2	4.9525	R15	4.148
R10	0.559245	R11	4.93603	R3	5.1115	R1	4.1935
R12	0.587207	R16	4.977301	R1	5.279	R2	4.2145
R21	0.594198	R1	5.043335	R2	5.445	R5	4.26
R26	0.601188	R11	5.117623	R4	5.4665	R25	4.347
R1	0.62216	R26	5.167148	R1	5.5585	R4	4.4925
R10	0.629151	R18	5.208419	R7	5.6825	R3	4.532
R12	0.629151	R2	5.257945	R6	5.714	R4	4.5775

R22	0.636141	R8	5.30747	R2	5.7905	R2	4.723
R20	0.636141	R3	5.414775	R4	5.8325	R7	4.8305
R25	0.643132	R8	5.439538	R15	5.856	R24	4.8575
R19	0.643132	R9	5.497317	R20	6.0195	R3	4.933
R2	0.664103	R15	5.52208	R10	6.2345	R10	5.157
R16	0.664103	R1	5.596368	R3	6.2435	R6	5.335
R9	0.678085	R7	5.645894	R23	6.318	R23	5.383
R2	0.692066	R10	5.662402	R9	6.397	R9	5.4365
R15	0.713037	R26	5.662402	R22	6.58	R3	5.51
R16	0.741	R15	5.711927	R3	6.614	R20	5.557
R10	0.754981	R25	5.777961	R16	6.628	R22	5.6565
R4	0.782943	R18	5.910029	R19	6.6395	R16	5.726
R21	0.782943	R23	5.976063	R11	6.6735	R15	5.944
R7	0.789934	R24	6.124639	R24	6.8915	R11	6.176
R25	0.824886	R25	6.190673	R22	7.0725	R19	6.2335
R5	0.831877	R6	6.207181	R20	7.336	R19	6.4835
R8	0.838868	R7	6.512588	R15	7.3745	R22	6.6695
R3	0.852849	R2	6.529096	R19	7.785	R20	6.935
R20	0.859839	R24	6.545605	R20	7.805	R10	6.981
R1	0.880811	R9	6.578622	R21	7.849	R20	6.991
R9	0.887801	R8	6.628147	R19	8.003	R21	7.1605
R8	0.887801	R5	6.65291	R23	8.131	R19	7.291
R7	0.894792	R23	6.685927	R22	8.3215	R12	7.433
R5	0.908773	R4	7.049113	R21	8.6225	R23	7.4905
R7	0.908773	R17	7.164672	R10	8.6955	R21	7.5795
R25	0.936735	R26	7.866281	R12	9.0385	R21	7.6055
R3	0.936735	R9	8.006603	R21	9.0645	R10	7.713
R4	0.971688	R6	8.105654	R11	9.2645	R11	7.7245
R3	1.167424	R17	8.402806	R12	9.3	R11	7.919
R23	1.209367	R5	8.452332	R10	9.515	R12	8.0345
R16	1.251311	R5	8.922823	R11	9.6715	R22	8.648
R1	1.293254	R6	9.517128	R12	10.1925	R12	8.7015

CATT-Acoustic

Objective results for Configurations A, B and C, sorted in increase order

T30		EDT		C50		C80	
R26	1.4685	R21	1.08	R2	-3.882	R18	-1.428
R7	1.48	R22	1.1455	R2	-3.844	R9	-1.3695
R6	1.4845	R11	1.212	R5	-3.618	R2	-1.313
R9	1.4985	R11	1.291	R9	-3.418	R17	-1.103
R12	1.5035	R20	1.3175	R8	-3.209	R8	-0.923
R18	1.5045	R10	1.365	R25	-3.126	R25	-0.819
R8	1.5055	R4	1.368	R5	-3.0905	R26	-0.7025
R5	1.5115	R24	1.3805	R26	-3.079	R5	-0.678
R17	1.5135	R15	1.3895	R5	-3.0615	R2	-0.2415
R11	1.516	R21	1.4005	R17	-3.0545	R5	-0.2405
R2	1.5195	R3	1.403	R18	-2.9045	R9	0.0465
R4	1.5215	R19	1.408	R1	-2.7805	R2	0.137
R25	1.522	R20	1.435	R26	-2.74	R5	0.2245
R22	1.5225	R3	1.4455	R2	-2.734	R1	0.2705
R15	1.5235	R16	1.453	R9	-2.408	R3	0.4325
R3	1.5275	R17	1.4685	R8	-2.3475	R7	0.4495
R19	1.537	R22	1.476	R26	-2.343	R18	0.46
R21	1.5385	R8	1.5065	R18	-2.055	R6	0.606
R7	1.5465	R18	1.5425	R16	-2.032	R26	0.6285
R9	1.549	R6	1.545	R8	-1.613	R8	0.768
R1	1.5515	R5	1.5695	R9	-1.432	R26	0.8205
R24	1.5515	R1	1.5725	R3	-1.3795	R19	0.828
R23	1.552	R23	1.575	R10	-1.3665	R16	0.8835
R16	1.5585	R26	1.579	R25	-1.2105	R17	0.9805
R1	1.5585	R9	1.599	R16	-1.1535	R23	0.983
R10	1.5615	R25	1.6155	R7	-1.14	R10	1.0025
R16	1.565	R19	1.6165	R18	-1.128	R7	1.083
R20	1.565	R2	1.6195	R17	-0.965	R24	1.195
R26	1.566	R25	1.628	R16	-0.94	R4	1.2065
R10	1.577	R6	1.64	R20	-0.9315	R25	1.2595
R21	1.583	R18	1.6405	R17	-0.905	R20	1.3335
R8	1.5845	R4	1.6435	R25	-0.8935	R18	1.3665
R19	1.586	R8	1.6635	R7	-0.8165	R1	1.3875
R25	1.59	R12	1.6745	R19	-0.8005	R25	1.39
R2	1.5915	R17	1.6875	R6	-0.776	R7	1.42
R6	1.599	R2	1.701	R23	-0.703	R9	1.5685
R15	1.6015	R16	1.704	R24	-0.6235	R10	1.761
R3	1.6035	R12	1.7115	R3	-0.5805	R17	1.799
R24	1.6055	R5	1.7335	R4	-0.5375	R16	1.8135

R18	1.607	R7	1.738	R7	-0.2645	R8	1.8885
R17	1.6155	R26	1.7655	R10	-0.219	R16	2.1005
R20	1.617	R24	1.7985	R1	-0.1635	R12	2.311
R23	1.6215	R9	1.809	R3	-0.1595	R6	2.341
R4	1.6235	R23	1.8345	R10	0.2995	R19	2.427
R22	1.6285	R15	1.8415	R20	0.3715	R1	2.431
R11	1.633	R10	1.845	R12	0.492	R22	2.508
R5	1.6395	R7	1.8535	R11	0.5965	R20	2.6935
R12	1.6405	R1	1.8635	R6	0.6185	R11	2.7085
R25	1.8745	R21	1.9515	R1	0.7405	R4	2.751
R8	1.8845	R17	2.0025	R22	0.774	R15	2.7785
R10	1.9075	R22	2.061	R6	0.791	R3	2.8315
R26	1.916	R15	2.0735	R24	0.9105	R6	2.844
R1	1.918	R6	2.1005	R20	0.9265	R3	3.0185
R23	1.9185	R11	2.128	R19	0.936	R4	3.0915
R18	1.92	R10	2.1365	R15	1.031	R24	3.092
R21	1.9205	R24	2.1375	R4	1.165	R21	3.2915
R19	1.9235	R2	2.138	R19	1.19	R24	3.294
R9	1.9265	R23	2.1395	R4	1.2135	R19	3.3105
R16	1.934	R4	2.153	R23	1.504	R23	3.4475
R4	1.935	R25	2.163	R23	1.544	R15	3.5325
R6	1.9375	R19	2.174	R12	1.548	R20	3.5865
R12	1.9405	R5	2.193	R24	1.587	R10	3.601
R3	1.9415	R18	2.2095	R22	1.9635	R23	3.6445
R7	1.947	R16	2.219	R11	1.968	R22	4.042
R22	1.9475	R12	2.234	R15	2.057	R21	4.1195
R24	1.9475	R26	2.24	R22	2.0935	R12	4.1215
R5	1.9525	R3	2.2425	R21	2.1135	R11	4.5565
R2	1.956	R1	2.252	R12	2.3345	R11	4.6395
R11	1.9585	R9	2.279	R11	2.4775	R15	4.67
R20	1.9605	R7	2.3165	R15	2.633	R12	4.6885
R17	1.975	R20	2.334	R21	2.6825	R21	4.81
R15	2.002	R8	2.403	R21	2.8635	R22	4.9475

The relevant JNDs have been calculated based on the following minimum observed values.

	T30	EDT	C50	C80
Minimum Values	R26 1.4685	R21 1.08	R2 -3.882	R18 -1.428
JND	0.073425	0.054	1	1

Objective results for Configurations A, B and C, sorted based on the JND values in increase order

JND values							
T30		EDT		C50		C80	
R26	0	R21	0	R2	0	R18	0
R7	0.156622	R22	1.212963	R2	0.038	R9	0.0585
R6	0.217909	R11	2.444444	R5	0.264	R2	0.115
R9	0.40858	R11	3.907407	R9	0.464	R17	0.325
R12	0.476677	R20	4.398148	R8	0.673	R8	0.505
R18	0.490296	R10	5.277778	R25	0.756	R25	0.609
R8	0.503916	R4	5.333333	R5	0.7915	R26	0.7255
R5	0.585632	R24	5.564815	R26	0.803	R5	0.75
R17	0.61287	R15	5.731481	R5	0.8205	R2	1.1865
R11	0.646919	R21	5.935185	R17	0.8275	R5	1.1875
R2	0.694586	R3	5.981481	R18	0.9775	R9	1.4745
R4	0.721825	R19	6.074074	R1	1.1015	R2	1.565
R25	0.728635	R20	6.574074	R26	1.142	R5	1.6525
R22	0.735444	R3	6.768519	R2	1.148	R1	1.6985
R15	0.749064	R16	6.907407	R9	1.474	R3	1.8605
R3	0.803541	R17	7.194444	R8	1.5345	R7	1.8775
R19	0.932925	R22	7.333333	R26	1.539	R18	1.888
R21	0.953354	R8	7.898148	R18	1.827	R6	2.034
R7	1.062308	R18	8.564815	R16	1.85	R26	2.0565
R9	1.096357	R6	8.611111	R8	2.269	R8	2.196
R1	1.130405	R5	9.064815	R9	2.45	R26	2.2485
R24	1.130405	R1	9.12037	R3	2.5025	R19	2.256
R23	1.137215	R23	9.166667	R10	2.5155	R16	2.3115
R16	1.225741	R26	9.240741	R25	2.6715	R17	2.4085
R1	1.225741	R9	9.611111	R16	2.7285	R23	2.411
R10	1.266599	R25	9.916667	R7	2.742	R10	2.4305
R16	1.314266	R19	9.935185	R18	2.754	R7	2.511
R20	1.314266	R2	9.990741	R17	2.917	R24	2.623
R26	1.327886	R25	10.14815	R16	2.942	R4	2.6345
R10	1.477698	R6	10.37037	R20	2.9505	R25	2.6875
R21	1.559414	R18	10.37963	R17	2.977	R20	2.7615
R8	1.579843	R4	10.43519	R25	2.9885	R18	2.7945
R19	1.600272	R8	10.80556	R7	3.0655	R1	2.8155
R25	1.65475	R12	11.00926	R19	3.0815	R25	2.818
R2	1.675179	R17	11.25	R6	3.106	R7	2.848
R6	1.777324	R2	11.5	R23	3.179	R9	2.9965
R15	1.811372	R16	11.55556	R24	3.2585	R10	3.189
R3	1.838611	R12	11.69444	R3	3.3015	R17	3.227
R24	1.86585	R5	12.10185	R4	3.3445	R16	3.2415
R18	1.886279	R7	12.18519	R7	3.6175	R8	3.3165

R17	2.002043	R26	12.69444	R10	3.663	R16	3.5285
R20	2.022472	R24	13.30556	R1	3.7185	R12	3.739
R23	2.083759	R9	13.5	R3	3.7225	R6	3.769
R4	2.110998	R23	13.97222	R10	4.1815	R19	3.855
R22	2.179094	R15	14.10185	R20	4.2535	R1	3.859
R11	2.240381	R10	14.16667	R12	4.374	R22	3.936
R5	2.328907	R7	14.32407	R11	4.4785	R20	4.1215
R12	2.342526	R1	14.50926	R6	4.5005	R11	4.1365
R25	5.529452	R21	16.13889	R1	4.6225	R4	4.179
R8	5.665645	R17	17.08333	R22	4.656	R15	4.2065
R10	5.97889	R22	18.16667	R6	4.673	R3	4.2595
R26	6.094654	R15	18.39815	R24	4.7925	R6	4.272
R1	6.121893	R6	18.89815	R20	4.8085	R3	4.4465
R23	6.128703	R11	19.40741	R19	4.818	R4	4.5195
R18	6.149132	R10	19.56481	R15	4.913	R24	4.52
R21	6.155941	R24	19.58333	R4	5.047	R21	4.7195
R19	6.196799	R2	19.59259	R19	5.072	R24	4.722
R9	6.237657	R23	19.62037	R4	5.0955	R19	4.7385
R16	6.339803	R4	19.87037	R23	5.386	R23	4.8755
R4	6.353422	R25	20.05556	R23	5.426	R15	4.9605
R6	6.38747	R19	20.25926	R12	5.43	R20	5.0145
R12	6.428328	R5	20.61111	R24	5.469	R10	5.029
R3	6.441948	R18	20.91667	R22	5.8455	R23	5.0725
R7	6.516854	R16	21.09259	R11	5.85	R22	5.47
R22	6.523664	R12	21.37037	R15	5.939	R21	5.5475
R24	6.523664	R26	21.48148	R22	5.9755	R12	5.5495
R5	6.59176	R3	21.52778	R21	5.9955	R11	5.9845
R2	6.639428	R1	21.7037	R12	6.2165	R11	6.0675
R11	6.673476	R9	22.2037	R11	6.3595	R15	6.098
R20	6.700715	R7	22.89815	R15	6.515	R12	6.1165
R17	6.898195	R20	23.22222	R21	6.5645	R21	6.238
R15	7.265918	R8	24.5	R21	6.7455	R22	6.3755

ODEON

Objective results for Configurations A, B and C, sorted in increase order

T30		EDT		C50		C80	
R2	1.307	R17	1.147	R5	-4.8025	R5	-1.237
R20	1.318	R21	1.176	R2	-4.5655	R2	-1.0275
R1	1.3265	R12	1.1775	R26	-4.112	R26	-0.461
R18	1.3295	R21	1.191	R5	-4.055	R18	-0.212
R19	1.3305	R11	1.2315	R2	-3.71	R16	-0.016
R10	1.3315	R22	1.254	R2	-3.29	R2	-0.016
R3	1.335	R20	1.29	R5	-3.2145	R5	0.0255
R7	1.335	R25	1.29	R18	-3.1055	R2	0.184
R11	1.335	R4	1.2985	R26	-2.978	R5	0.432
R15	1.3355	R17	1.305	R26	-2.511	R10	0.532
R16	1.341	R18	1.312	R16	-2.406	R1	0.547
R6	1.3435	R10	1.313	R18	-2.3365	R26	0.6435
R12	1.344	R12	1.318	R10	-1.9715	R8	0.9785
R9	1.3465	R19	1.3325	R8	-1.8705	R18	1.022
R4	1.351	R8	1.3475	R25	-1.789	R9	1.1065
R21	1.351	R11	1.3545	R16	-1.702	R25	1.108
R22	1.3515	R26	1.3695	R18	-1.648	R19	1.1105
R24	1.352	R4	1.375	R19	-1.5975	R16	1.212
R23	1.3525	R23	1.377	R10	-1.255	R26	1.35
R5	1.3585	R22	1.3795	R1	-1.213	R20	1.379
R26	1.361	R6	1.3805	R16	-1.1985	R3	1.3805
R8	1.363	R25	1.386	R3	-1.134	R6	1.4455
R25	1.3645	R8	1.3935	R6	-1.1095	R7	1.4455
R17	1.3725	R5	1.394	R17	-1.0455	R16	1.4925
R8	1.431	R9	1.394	R10	-1.0195	R18	1.528
R1	1.432	R15	1.3945	R8	-1.017	R10	1.65
R17	1.432	R6	1.3955	R7	-0.966	R17	1.7405
R15	1.438	R23	1.3975	R20	-0.746	R1	1.8335
R7	1.4445	R24	1.4	R9	-0.6865	R8	2.0515
R11	1.446	R18	1.409	R19	-0.6435	R10	2.1015
R12	1.448	R20	1.412	R25	-0.4635	R24	2.103
R5	1.449	R16	1.4135	R1	-0.3345	R19	2.168
R2	1.4535	R2	1.415	R17	-0.286	R1	2.2795
R4	1.454	R7	1.4185	R8	-0.2105	R23	2.2985
R18	1.456	R19	1.4205	R6	-0.1775	R7	2.469
R10	1.4575	R1	1.425	R19	-0.173	R11	2.498
R22	1.459	R3	1.4275	R25	-0.0465	R25	2.5515
R19	1.4635	R1	1.431	R24	0.02	R19	2.5975
R21	1.4655	R26	1.4475	R3	0.0345	R3	2.6855

R3	1.468	R2	1.465	R11	0.0405	R6	2.729
R26	1.47	R9	1.465	R17	0.092	R15	2.817
R6	1.4725	R16	1.4655	R7	0.117	R17	2.836
R9	1.473	R10	1.4755	R3	0.3035	R4	2.9435
R25	1.473	R5	1.4765	R20	0.338	R20	2.9485
R24	1.4735	R15	1.4775	R1	0.375	R9	2.958
R23	1.475	R7	1.5225	R23	0.418	R8	2.9975
R16	1.481	R3	1.525	R6	0.5625	R25	2.998
R20	1.489	R24	1.5515	R20	0.59	R7	3.057
R22	1.75	R21	1.5525	R9	0.593	R3	3.0655
R17	1.7615	R11	1.6035	R7	0.812	R24	3.1415
R12	1.7655	R12	1.626	R11	0.895	R9	3.145
R21	1.773	R22	1.6625	R4	0.9365	R12	3.1775
R16	1.7785	R17	1.6675	R24	0.983	R20	3.2375
R6	1.7795	R25	1.6685	R11	1.0055	R6	3.255
R15	1.7815	R23	1.7435	R15	1.0065	R17	3.313
R4	1.782	R6	1.75	R9	1.0455	R23	3.4385
R10	1.7835	R4	1.755	R12	1.056	R22	3.5085
R3	1.7865	R19	1.7565	R23	1.3165	R24	3.527
R2	1.787	R15	1.7725	R24	1.4695	R11	3.619
R24	1.789	R9	1.779	R23	1.49	R23	3.69
R18	1.79	R8	1.7935	R15	1.77	R11	3.8015
R7	1.792	R26	1.7965	R12	1.844	R15	3.803
R20	1.792	R24	1.8005	R4	1.9125	R15	4.0745
R9	1.7935	R3	1.809	R22	1.939	R4	4.299
R23	1.7965	R10	1.813	R15	1.96	R12	4.301
R5	1.7975	R20	1.8155	R12	2.0445	R22	4.435
R11	1.805	R7	1.833	R4	2.4705	R12	4.672
R19	1.8105	R1	1.837	R22	2.6655	R4	4.723
R25	1.815	R18	1.8385	R22	3.201	R21	4.7615
R1	1.819	R5	1.8425	R21	3.2525	R22	4.884
R26	1.8235	R16	1.8635	R21	4.02	R21	5.9505
R8	1.826	R2	1.906	R21	4.4765	R21	6.397

The relevant JNDs have been calculated based on the following minimum observed values.

	T30	EDT	C50	C80
Minimum Values	R2 1.307	R17 1.147	R5 -4.8025	R5 -1.237
JND	0.06535	0.05735	1	1

Objective results for Configurations A, B and C, sorted based on the JND values in increase order

JND values							
T30		EDT		C50		C80	
R2	0	R17	0	R5	0	R5	0
R20	0.168324	R21	0.505667	R2	0.237	R2	0.2095
R1	0.298393	R12	0.531822	R26	0.6905	R26	0.776
R18	0.3443	R21	0.767219	R5	0.7475	R18	1.025
R19	0.359602	R11	1.473409	R2	1.0925	R16	1.221
R10	0.374904	R22	1.865737	R2	1.5125	R2	1.221
R3	0.428462	R20	2.493461	R5	1.588	R5	1.2625
R7	0.428462	R25	2.493461	R18	1.697	R2	1.421
R11	0.428462	R4	2.641674	R26	1.8245	R5	1.669
R15	0.436113	R17	2.755013	R26	2.2915	R10	1.769
R16	0.520275	R18	2.877071	R16	2.3965	R1	1.784
R6	0.558531	R10	2.894507	R18	2.466	R26	1.8805
R12	0.566182	R12	2.981691	R10	2.831	R8	2.2155
R9	0.604438	R19	3.234525	R8	2.932	R18	2.259
R4	0.673298	R8	3.496077	R25	3.0135	R9	2.3435
R21	0.673298	R11	3.618134	R16	3.1005	R25	2.345
R22	0.680949	R26	3.879686	R18	3.1545	R19	2.3475
R24	0.6886	R4	3.975588	R19	3.205	R16	2.449
R23	0.696251	R23	4.010462	R10	3.5475	R26	2.587
R5	0.788064	R22	4.054054	R1	3.5895	R20	2.616
R26	0.82632	R6	4.071491	R16	3.604	R3	2.6175
R8	0.856924	R25	4.167393	R3	3.6685	R6	2.6825
R25	0.879878	R8	4.298169	R6	3.693	R7	2.6825
R17	1.002295	R5	4.306888	R17	3.757	R16	2.7295
R8	1.897475	R9	4.306888	R10	3.783	R18	2.765
R1	1.912777	R15	4.315606	R8	3.7855	R10	2.887
R17	1.912777	R6	4.333043	R7	3.8365	R17	2.9775
R15	2.004591	R23	4.367916	R20	4.0565	R1	3.0705
R7	2.104055	R24	4.411508	R9	4.116	R8	3.2885
R11	2.127008	R18	4.568439	R19	4.159	R10	3.3385
R12	2.157613	R20	4.62075	R25	4.339	R24	3.34
R5	2.172915	R16	4.646905	R1	4.468	R19	3.405
R2	2.241775	R2	4.67306	R17	4.5165	R1	3.5165
R4	2.249426	R7	4.734089	R8	4.592	R23	3.5355
R18	2.280031	R19	4.768963	R6	4.625	R7	3.706
R10	2.302984	R1	4.847428	R19	4.6295	R11	3.735
R22	2.325937	R3	4.89102	R25	4.756	R25	3.7885
R19	2.394797	R1	4.952049	R24	4.8225	R19	3.8345
R21	2.425402	R26	5.239756	R3	4.837	R3	3.9225
R3	2.463657	R2	5.5449	R11	4.843	R6	3.966

R26	2.494262	R9	5.5449	R17	4.8945	R15	4.054
R6	2.532517	R16	5.553618	R7	4.9195	R17	4.073
R9	2.540168	R10	5.727986	R3	5.106	R4	4.1805
R25	2.540168	R5	5.745423	R20	5.1405	R20	4.1855
R24	2.547819	R15	5.76286	R1	5.1775	R9	4.195
R23	2.570773	R7	6.547515	R23	5.2205	R8	4.2345
R16	2.662586	R3	6.591107	R6	5.365	R25	4.235
R20	2.785004	R24	7.053182	R20	5.3925	R7	4.294
R22	6.778883	R21	7.070619	R9	5.3955	R3	4.3025
R17	6.954858	R11	7.959895	R7	5.6145	R24	4.3785
R12	7.016067	R12	8.352223	R11	5.6975	R9	4.382
R21	7.130834	R22	8.988666	R4	5.739	R12	4.4145
R16	7.214996	R17	9.07585	R24	5.7855	R20	4.4745
R6	7.230298	R25	9.093287	R11	5.808	R6	4.492
R15	7.260903	R23	10.40105	R15	5.809	R17	4.55
R4	7.268554	R6	10.51439	R9	5.848	R23	4.6755
R10	7.291507	R4	10.60157	R12	5.8585	R22	4.7455
R3	7.337414	R19	10.62772	R23	6.119	R24	4.764
R2	7.345065	R15	10.90671	R24	6.272	R11	4.856
R24	7.375669	R9	11.02005	R23	6.2925	R23	4.927
R18	7.390972	R8	11.27289	R15	6.5725	R11	5.0385
R7	7.421576	R26	11.3252	R12	6.6465	R15	5.04
R20	7.421576	R24	11.39494	R4	6.715	R15	5.3115
R9	7.444529	R3	11.54316	R22	6.7415	R4	5.536
R23	7.490436	R10	11.6129	R15	6.7625	R12	5.538
R5	7.505738	R20	11.6565	R12	6.847	R22	5.672
R11	7.620505	R7	11.96164	R4	7.273	R12	5.909
R19	7.704667	R1	12.03139	R22	7.468	R4	5.96
R25	7.773527	R18	12.05754	R22	8.0035	R21	5.9985
R1	7.834736	R5	12.12729	R21	8.055	R22	6.121
R26	7.903596	R16	12.49346	R21	8.8225	R21	7.1875
R8	7.941852	R2	13.23452	R21	9.279	R21	7.634

Appendix E

Supporting materials on DVD

Supporting material of this research can be found on the accompanying DVD, providing results, audio examples and digital copies of the thesis and the author's publications. The DVD is designed to be used as a website, thus the *index.html* file should be used for the navigation to the contents. The contents of the DVD are:

A. Impulse Responses from:
    a. acoustic measurements in St. Margaret's Church
    b. CATT-Acoustic model of St. Margaret's Church
    c. ODEON model of St. Margaret's Church

B. CAD model
    a. in CATT-Acoustic
    b. in ODEON

C. Listening tests data:
    a. Documentation
    b. Anechoic Stimuli
    c. Sound Examples
    d. Subjective Responses

D. Publications:
    a. PhD Thesis (pdf file)
    b. Conference Papers

References

1. Commins, D., Pompoli, R., Farina, A., Fausti, P., Prodi, N., *Acoustics of Teatro Degli Archimboli in Milano Design, Computer and Scale Models, Details, Results*. Proceedings of the Institute of Acoustics, 2002. **24**(Pt 4).
2. Farina, A., Cocchi, A., Garai, M., Semprini, G. *Old Churches as Concert Halls: a Non-Sabinian Approach to Optimum Design of Acoustic Correction*. in *Proc. of 14th I.C.A.* . 1992. Beijing, China.
3. Exton, P., Marshall, H. *The Room Acoustic design of the Guangzhou Opera House. Proceedings of the Institute of Acoustics*. in *Proc. of the Institute of Acoustics*. 2011. Dublin, Ireland.
4. Dilworth, C., Smyth, S. *The Acoustic Requirements of the Irish Chamber Orchestra*. in *Proc. of the Institute of Acoustics*. 2011. Dublin, Ireland.
5. Facondini, M., Ponteggia, D. *Acoustics of the Restored Petruzzelli Theater*. in *Proc. of the 128th AES Convention* 2010. London, UK.
6. Buen, A., Strand, L., *Room Acoustics in the Scene II in the New Oslo Opera and the Ridehuset - Two Variable Acoustics Coupled Space Venues*. Proc. of the Institute of Acoustics, 2008. **30**(2): p. 240-260.
7. *A virtual acoustic walkthrough animation in St. Margaret's Church, York*. the Open AIR Library [cited 2011]; Available from: http://www.openairlib.net/auralizationdb/content/st-margarets-church-national-centre-early-music.
8. Fazenda, B., Drumm, I. *Recreating the Sound of Stonehenge*. in *The Acoustics of Ancient Theatres Conference*. 2011. Patras.
9. Murphy, D., *Archaeological Acoustic Space Measurement for Convolution Reverberation and Auralization Applications*. Proc. Of the 9th Int.Conference on Digital Effects (DAFx-06), 2006: p. 221-226.
10. Niaounakis, T.I. *The Acoustics of Ancient Theatre of Hephastia - Limnos Island, Greece*. in *The Acoustics of Ancient Theatres Conference*. 2011. Patras.
11. Vassilantonopoulos, S.L., Hatziantoniou, P., Tatlas, N-A., Zakynthizons, T., Mourjopoulos, J.N. . *Measurements and Analysis of the Acoustics of the Ancient Theatre of Epidaurus*. in *The Acoustics of Ancient Theatres Conference*. 2011. Patras.
12. Iannace, G., Maffei, L., Trematerra, P. *The Acoustic Evolution of the Large Theatre of Pompeii*. in *The Acoustics of Ancient Theatres*. 2011. Patras.
13. Rindel, J.H., Lisa, M. *The ERATO project and its contribution to our understanding of the acoustics of ancient Greek and Roman theatres*. in *ERATO Project Symposium*. 2006. Istanbul, Turkey.
14. Rindel, J.H. *The Erato Project and its Contribution to our Understanding of the Acoustics of Ancient Theatres*. in *The Acoustics od Ancient Theatres*. 2011. Patras.
15. Prodi, N., Farnetani, A., Pompoli, R., Fausti, P. *Acoustics and Architecture in Ancient Open Air Theatres*. in *The acoustics of Ancient Theatres Conference*. 2011. Patras.
16. Lisa, M., Rindel, J.H. and Christensen, C.L. *Predicting the Acoustics of Ancient Open-Air Theaters: The importance of Calculation Methods and Geometrical Details*. in *Joint Baltic-Nordic Acoustics Meeting*. 2004.
17. Rindel, J.H., Gade, A.C., Lisa, M., *The Virtual Reconstruction of the Ancient Roman Concept Hall in Aphrodisias, Turkey*. Proc. of the Institute of Acoustics, 2006. **28**(2): p. 316-323.

18. Dragonetti, R., Ianniello, C., Mercoglaino, F., Romano, R. *The Acoustics of two Ancient Roman Theatres in Pompeii*. in *9th International Congress on Acoustics*. 2007. Madrid.
19. Fausti, P., Pompoli, R., Prodi, N. *Comparing the Acoustics of Mosques and Byzantine Churches*. in *19th International Symposium CIPA*. 2003. Antalya, Turkey.
20. Boren, B., Longair, M. *A Method for Acoustic Modelling of Past Soundscapes*. in *The acoustics of Ancient Theatres Conference*. 2011. Patras.
21. Foteinou, A., Murphy, D., Masinton, A. *Verification of Geometric Acoustics Based Auralization*. in *Proc. of the128th AES Convention*. 2010. London.
22. Foteinou, A., Murphy D. and Masinton, A. *Investigation of Factors Influencing Acoustic Characteristics in Geometric Acoustics Based Auralization*. in *Proc. of the 13th Int. Conference on Digital Audio Effects (DAFx-10)*. 2010. Graz, Austria.
23. Masinton, A., *A Sacred Space: priorities, perception and the presence of God in late medieval Yorkshire parish churches*, in *Medieval Studies*. 2006, University of York: York.
24. Álvarez, L., Alonso, A., Zamarreño, T., Girón, S., Galindo, M. . *Virtual Acoustics of the Cathedral of Malaga (Spain)*. in *Proc. of Forum Acusticum 2011*. 2011. Aalborg, Denmark.
25. *Temple of Decision (video installation)*. Re-sounding Falkland [cited 2010]; Available from: http://resoundingfalkland.com/video.html.
26. Farina, A., Ayalon, R. *Recording Concert Hall Acoustics for Posterity*. in *AES 24th International Conference on Multichannel Audio*. 2003. Banff, Canada.
27. Farina, A., Armelloni, E., Martignon, P. *An experimental comparative study of 20 Italian opera houses: measurement techniques*. in *147th Meeting of the Acoustical Society of America*. 2004. New York (USA).
28. *The Open AIR Library*. [cited 2010]; Available from: http://www.openairlib.net/.
29. Bork, I., *A comparison of Room Simulation Software - The 2nd Round Robin on Room Acoustical Computer Simulation*. Acta Acustica, 2000. **86**: p. 943-956.
30. Christensen, C.L., Nielsen, G., Rindel, J.H., *Danish Acoustical Society Round Robin on Room Acoustic Computer Modeling*. 2008, Odeon A/S: Lyngby, Denmark.
31. Bork, I., *Simulation and Measurement of Auditorium Acoustics – The Round Robins on Room Acoustical Simulation*. Proceedings of the Institute of Acoustics, 2002. **24**(Pt. 4).
32. Bork, I. *Evaluation of Room Acoustical Simulation Software*. in *CFA/DAGA'04*. 2004. Strasbourg.
33. Bork, I., *Report on the 3rd Round Robin on Room Acoustical Computer Simulation – Part I: Measurements*. Acta Acustica United with Acustica, 2005. **91**: p. 740-752.
34. Bork, I., *Report on the 3rd Round Robin on Room Acoustical Computer Simulation - Part II: Calculations*. Acta Acustica United with Acustica, 2005. **91**: p. 753-763.
35. Everest, F.A., *Master Handbook of Acoustics*. 4th ed. 2001, USA: McGraw-Hill.
36. *Inverse-square law*. Wikipedia: The Free Encyclopedia [cited 15 August 2009]; Available from: http://en.wikipedia.org/wiki/File:Inverse_square_law.svg].

37. Evans, L.B., Bass, H.E., Sutherland, L.C., *Atmospheric Absorption of Sound: Theoretical Predictions.* Journal of Acoustical Society of America, 1972. **51**(5 (Part 2)): p. 1565-1575.
38. Bass, H.E., Bauer, H.-J., Evans, L.B., *Atmospheric Absorption of Sound: Analytical Expressions.* Journal of Acoustical Society of America, 1972. **52**(3 (Part2)): p. 821-825.
39. Lisa, M., Rindel, J.H., Gade, A.C. and Christensen, C.L. , *Acoustical Computer Simulations of the Ancient Roman Theatres.* ERATO Project Symposium, 2006: p. 20-26.
40. Howard, D., Murphy, D., *Voice Science Acoustics and Recording*. 2008: Plural Publishing.
41. Howard, D., Angus, J., *Acoustics and Psychoacoustics*. 2nd ed. 2001, UK: Focal Press.
42. Allen, J.B., Berkley, D.A., *Image Method for Efficiently Simulating Small-room Acoustics.* Journal of Acoustical Society of America, 1979. **65**(4): p. 943-950.
43. Vorländer, M., *Auralization*. 1st ed, ed. Springer. 2008, Berlin.
44. Kuttruff, H., *Room Acoustics*. 5th ed. Elsevier Applied Science. 2009, Netherlands.
45. ISO354, *Acoustics - Measurement of sound absorption in a reverberation room*. ISO. 1985.
46. Beranek, L.L., *Acoustics*. 1952, New York: McGraw-Hill.
47. Bolt, R., H., *Note on Normal Frequency Statistics for Rectangular Rooms.* Acoustical Society of America, 1946. **18**(1).
48. Gilford, C.L.S., *The acoustic design of talk studios and listening rooms.* Journal of Audio Engineering Society, 1979. **27**: p. 17-31.
49. Louden, M.M., *Dimension ratios of rectangular rooms with good distribution of eigentones.* Acustica, 1971. **24**: p. 101-104.
50. Skålevik, M. *Schroeder Frequency Revisited*. in *Forum Acusticum*. 2011. Aalborg, Denmark.
51. Schroeder, M., R., *The "Schroeder frequency" revisited.* Acoustical Society of America, 1996. **99**((5)).
52. Farina, A. *Simultaneous Measurement of Impulse Response and Distortion with a Swept-Sine technique*. in *108th AES Convention*. 2000
53. Murphy, D., *Digital waveguide mesh topologies in room acoustics modelling*, in *Electronics D.Phil. thesis*. 2000, University of York: York.
54. Lynn, P.A., *Digital Signals, Processors and Noise.* First ed. 1992, London: Macmillan New Electronics Series.
55. ISO3382, I.S.-. *Acoustics - Measurement of room acoustic parameters, Part 1: Performance spaces*, ed. B. Standards. 2009.
56. Schroeder, M., R., *New Method of Measuring Reverberation Time.* Journal of Acoustical Society of America, 1965. **37**: p. 409-412.
57. Barron, M., *Non-linear Decays in Simple Spaces and their Possible Exploitation.* Proceedings of the Institute of Acoustics, 2011. **34**(2).
58. Beranek, L., *Subjective Rank-Orderings and Acoustical Measurements for Fifty-Eight Concert Halls.* Acta Acustica United with Acustica, 2003. **89**: p. 494-508.
59. Beranek, L., *Acoustics and Musical Qualities.* Journal of Acoustical Society of America, 1996. **99**(5): p. 2647-2652.
60. ISO3382, I.S.-. *Acoustics – Measurement of reverberation time of rooms with reference to other acoustical parameters*. 2nd ed. ISO. 1997

61. Popa, V., Culda, T., Negrescu, C. *Software Library for Managing a Complete Audio Chain Intended for Determining Acoustic Room Parameters and Spatial Impression*. in *SISOM 2012 and Session of the Commission of Acoustics*. 2012. Bucharest.
62. Reichardt, W., Schmidt, W., *The detectability of changes in sound field parameters for music.* Acustica, 1967. **18**: p. 275-282.
63. Cremer, L., Muller, H.A., *Principles and Applications of Room Acoustics*. Applied Science. Vol. 1. 1982, London.
64. Niaounakis, T.I., Davies, W.J., *Perception of reverberation time in small listening rooms.* Journal of Audio Engineering Society, 2002. **50**: p. 343-350.
65. Cox, T.J., Davies, W.J., Lam, Y.W., *The Sensitivity of Listeners to Early Sound Field Changes in Auditoria.* Acustica, 1993. **79**: p. 27-41.
66. Bradley, J.S., Reich, R., Norcross, S.G., *A just noticeable difference in C50 for speech.* Applied Acoustics, 1999. **58**: p. 99-108.
67. Bradley, J.S., Halliwell, R.E., *Making Auditorium Acoustics More Quantitative.* Journal of Sound and Vibration, 1989. **23**: p. 16-23.
68. Bradley, J.S. *Hall average characteristics of 10 halls.* in *Proc. 13th International Congress on Acoustics (ICA).* 1989. Belgrade.
69. Ahearn, M.J., Schaeffler, M.J., Celmer, R.D., Vigeant, M.C., *The just noticeable difference of the clarity index of music, C80.* Journal of Acoustical Society of America, 2009. **126**(2288).
70. Witew, I., Dietrich, P., de Vries, D.,Vorländer, M. *Uncertainty of room acoustic measurements – How many measurement positions are necessary to describe the conditions in auditoria?* in *Proceedings of the International Symposium on Room Acoustics, ISRA* 2010. Melbourne, Australia.
71. Witew, I. *Is the perception of listener envelopment in concert halls affected by clarity?* in *Proc. DAGA*. 2006. Munich.
72. Martellotta, F., *The Just Noticeable Difference of Center Time and Clarity Index in Large Reverberant Spaces.* Acoustical Society of America, 2010. **128**(2): p. 654-663.
73. Vorländer, M. *International Round Robin on Room Acoustical Computer Simulations*. in *15th International Congress on Acoustics*. 1995. Trondheim, Norway.
74. Foteinou, A., Murphy, D.T. *Evaluation of the psychoacoustic perception of geometric acoustic modeling based auralization*. in *Proc. of the130th AES Convention*. 2011. London.
75. Kleiner, M., Dalenbäck, B.-I., Svensson, P., *Auralization - An Overview.* Journal of Acoustical Society of America, 1993. **41**(11): p. 861-875.
76. Svensson, P., *The Early History of Ray Tracing in Room Acoustics*, in *Reflections on Sound. In honour of Professor Emeritus Asbjørn Krokstad, .* 2008: Trondheim.
77. Cocchi, A., Tronchin, L., Farina, A., Cesare, M., *A Comparison Between Some Measurement Techniques in the Foligno Auditorium*. Proceedings of the Institute of Acoustics, 2002. **24**(2002).
78. Fausti, P., Farina, A., *Acoustic Measurements in Opera Houses: Comparison Between Different Techniques and Equipment.* Journal of Sound and Vibration, 2000. **232**(1): p. 213-229.
79. Müller, S., Massarani, P., *Transfer-Function Measurement with Sweeps.* Journal of Autio Engineering Society, 2001. **49**(6): p. 443-471.
80. Lewers, T.H., Anderson, J.S., *Some Acoustical Properties of St Paul's Cathedral, London.* Journal of Sound and Vibration, 1984. **92**(2): p. 285-297.

81. Tronchin, L., Farina, A., *Acoustics of the Former Teatro "La Fenice" in Venice*. Journal of Audio Engineering Society, 1997. **45**(12): p. 1051-1062.
82. Farina, A., *Acoustic Quality of Theatres: Correlations between Experimental Measures and Subjective Evaluations*. Applied Acoustics, 2001. **62**: p. 889-916.
83. Farina, A. *Impulse Response Measurements*. in *23rd Norbic Sound Symposium*. 2007.
84. James, A., *Results of the NPL Study into Comparative Room Acoustic Measurement Techniques Part 1, Reverberation Time in Large Rooms*. Proceedings of the Institute of Acoustics, 2003. **25**(4).
85. Farina, A., Tronchin, L. *New Measurement Technique for 3D Sound Characterization in Theatres*. in *The Acoustics of Ancient Theatres Conference*. 2011. Patras.
86. Merimaa, J., Peltonen, T., Lokki, T., *Concert Hall Impulse Responses - Pori, Finland: Reference*, in *a free documented room response database available at http://www.acoustics.hut.fi/projects/poririrs/*. 2005.
87. Meng, Q., Sen, D., Wang, S., Hayes, L. *Impulse response measurement with sine sweeps and amplitude modulation schemes*. in *2nd International Conference on Signal Processing and Communication Systems*. 2008. Gold Coast
88. Farina, A., Commins, D. E., Prodi, N. *Experimental Analysis of the acoustical behaviour of Musikverein in Concert and Ballet Configurations*. in *Acoustics'08*. 2008. Paris.
89. Farina, A., Tronchin, L., Tarabusi, V. *Comparison between Opera houses: Italian and Japanese cases*. in *Awaji Yumebutai International Conference Center*. 2004. Hyogo, Japan.
90. Witew, I.B., Behler, G.K. *Uncertainties in measurement of single number parameters in room acoustics*. in *Forum Acusticum*. 2005. Budapest.
91. Behler, G. *Uncertainties of measured parameters in room acoustics caused by the directivity of source and/or receiver*. in *3rd European Congress on Acoustics*. 2002. Sevilla Forum Acusticum
92. Bassuet, A.A.A. *Acoustics of a Selection of Famous 18th Century Opera Houses: Versailles, Markgräfliches, Drottningholm, Schweitzingen*. in *Proc. of Acoustics '08*. 2008. Paris.
93. Lundeby, A., Vigran, T.E., Bietz, H., Vorländer, M., *Uncertainties of Measurements in Room Acoustics*. Acustica, 1995. **81**: p. 344-355.
94. Gerzon, M., *Recording concert hall acoustics for posterity*. JAES, 1975. **23**(Number 7): p. 569.
95. Ueda, L.K., Figueiredo, F.L., Iazzetta, F., Kon, F. *A User-Friendly Graphical System for Room Acoustics Measurement and Analysis*. In Anais do 10.o Simpósio Brasileiro de Computação Musical. . Belo Horizonte: Sociedade Brasileira de Computação.
96. Peltonen, T., Lokki, T., Gouatarbès, B., Merimaa, J., Karjalainen, M. *A System for Multi-Channel and Binaural Room Response Measurements*. in *Proc. of 110th AES Convention*. 2001. Amsterdam, The Netherlands.
97. Queiroz, M., Iazzetta, F., Kon, F., Gomes, M. H. A., Fiqueiredo, F. L., Masiero, B., Ueda, L. K., Dias, L., Torres, M. H. C., Thomaz, L. F., *AcMus: an Open, Integrated Platform for Room Acoustics Research*. Journal of the Brazilian Computer Society, 2008. **14 (3)**: p. 87-103.
98. Katz, B.F.G., *International Round Robin on Room Acoustical Impulse Response Analysis Software 2004*. Acoustics Research Letters Online, 2004. **5**: p. 158-164.

99. Karjalainen, M., Antsalo, P., Mäkivirta, A., Peltonen, T., Välimäki, V., *Estimation of Modal Decay Parameters from Noisy Response Measurements.* Journal of Audio Engineering Society, 2002. **50**(11): p. 867-878.
100. Bradley, J.S., *An International Comparison of Room Acoustics Measurement Systems*, in *IRC Internal Report*. 1996.
101. Bradley, J.S. *Review of Objective Room Acoustics Measures and Future Needs*. in *Proceedings of the International Symposium on Room Acoustics, ISRA*. 2010. Melbourne, Australia.
102. Chu, W.T., *Comparison of Reverberation Measurements Using Schroeder's Impulse Method and Decay-curve Averaging Method.* Journal of Acoustical Society of America, 1978. **63**(5): p. 1444-1450.
103. Hirata, Y., *A method of eliminating noise in power responses (Letter to the editor).* Journal of Sound and Vibration, 1982. **82**(4): p. 593-595.
104. Witew, I., Vorländer, M. *Uncertainties of room acoustical measurements - influence of the exact source and receiver positions*. in *Proceedings of the Institute of Acoustics (IoA)*. 2011.
105. Allred, J.C., Newhouse, A., *Applications of the Monte Carlo Method to Architectural Acoustics.* Journal of Acoustical Society of America, 1958. **30**(1): p. 1-3.
106. Krokstad, A., Strøm, S., Sørsdal, S., *Calculating the Acoustical Room Response by the Use of a Ray Tracing Technique.* Journal of Sound and Vibration, 1968. **8**(1): p. 118-125.
107. Rindel, J.H., *The Use of Computer Modeling in Room Acoustics.* Journal of Vibroengineering, 2000. **Vol.3**(5): p. 219-224.
108. Southern, A., Murphy, D., Campos, G., Dias, P. *Finite Difference Room Acoustic Modelling on a General Purpose Graphics Processing Unit*. in *Proc. of the 128th AES Convention*. 2010. London, UK.
109. Webb, C.J., Bilbao, S. *Virtual Room Acoustics : A Comparison of Techniques for computing 3D-FDTD schemes using CUDA*. in *Proc. of the 130th AES Convention*. 2011. London, UK.
110. Southern, A., Siltanen, S., Savioja, L. *Spatial Room Impulse Responses with a Hybrid Modelling Method*. in *Proc. of the 130th AES Convention*. 2011. London, UK.
111. Southern, A., *The Synthesis and Auralization of Physically Modelled Soundfields*, in *Department of Electronics*. 2010, University of York.
112. Murphy, D.T., Kelloniemi, A., Mullen, J., Shelley, S., *Acoustic Modelling using the Digital Waveguide Mesh.* IEEE Signal Processing Magazine, 2007. **24**(2): p. 55-66.
113. Kelloniemi, A., Huang, P., Välimäki, V., Savioja, L. *Hyper-dimensional Digital Waveguide Mesh for Reverberation Modeling*. in *Proc. of the 10th Int. Conference on Digiral Audio Effects (DAFx-07)*. 2007. Bordeaux, France.
114. Siltanen, S., Lokki, T., Kiminki, S., Savioja, L., *The Room Acoustic Rendering Equation.* Journal of Acoustical Society of America, 2007. **122**(3): p. 1624-1635.
115. Siltanen, S., Lokki, T., Savioja, L. *Room Acoustics Modeling with Acoustic Radiance Transfer*. in *Proc. of the ISRA*. 2010. Melbourne, Australia.
116. Kang, J. *Application of Radiosity Method in Acoustic Simulation*. in *18th International Conference on Acoustics (ICA)*. 2004. Kyoto, Japan.
117. Borish, J., *Extension of the image model to arbitrary polyhedra.* Journal of Acoustical Society of America, 1984. **75**(6): p. 1827-1836.
118. Stephenson, U., *Comparison of the Mirror Image Source Method and the Sound Particle Simulation Method.* Applied Acoustics, 1990. **29**: p. 35-72.

119. Rindel, J.H. *Computer Simulation Techniques for Acoustical Design of Rooms - How to Treat Reflections in Sound Field Simulation.* in *Proc. of ASVA 97*. 1997. Tokyo.
120. Christensen, C.L., *ODEON Room Acoustics Program Version 7.0 Industrial, Auditorium and Combined Editions*. 2003.
121. Alpkocak, A., Sis, M.K., *Computing Impulse Response of Room Acoustics Using the Ray-Tracing Method in Time Domain.* Archives of Acoustics, 2010. **35**(4): p. 505-519.
122. van Maercke, D., *Simulation of Sound Fields in Time and Frequency Domain using a Geometrical Model.* Acta Acustica United with Acustica, 1996. **82**(3): p. 517-525.
123. Vian, J.P., van Maercke, D. *Calculation of the Room Impulse Response using a Ray-tracing Method*. in *Proc. of 12th ICA Symposium*. 1986. Vancouver.
124. Farina, A. *RAMSETE - A New Pyramid Tracer for Medium and Large Scale Acoustic Problems*. in *Proc. of EURO-NOISE 95 Conference*. 1995. Lyon.
125. Lewers, T., *A Combined Beam Tracing and Radiant Exchange Computer Model of Room Acoustics.* Applied Acoustics, 1993. **38**: p. 161-178.
126. Noisternig, M., Katz, B.F.G., Siltanen, S., Savioka, L., *Framework for Real-time Auralization in Architectural Acoustics.* Acta Acustica United with Acustica, 2008. **94**: p. 1000-1015.
127. Arnošt, V. *Discrete Simulation of Sound Wave Propagation*. in *Proceedings of 34th Spring International Conference on Modelling and Simulation of Systems (MOSIS 2000)*. 2000. Rožnov pod Radhošt□m, CZ.
128. Farina, A., *Pyramid Tracing vs. Ray Tracing for the simulation of sound propagation in large rooms*, in *Computational Acoustics and its Environmental Applications*, C.A. Brebbia, Editor. 1995: Southampton (GB) p. 109-116.
129. Funkhouser, T., Tsingos, N., Carlbom, I., Elko, G., Sondi, M., West, J.E., Pingali, G., Min, P., Ngan, A., *A beam tracing method for interactive architectural acoustics.* Journal of Acoustical Society of America, 2004. **115**(2): p. 739-756.
130. Farina, A. *Verification of the accuracy of the Pyramid Tracing algorithm by comparison with experimental measurements by objective parameters.* in *ICA95 (International Conference on Acoustics)*. 1995. Trondheim (Norway).
131. Walsh, J.P., Rivard, M.T. *Signal Processing Aspects of Godot: A System for Computer-aided Room Acoustics Modeling and Simulation*. in *Proc. of th 72nd AES Convention*. 1982. Anaheim, California.
132. Laine, S., Siltanen, S., Lokki, Savioja, L., *Accelerated Beam Tracing Algorithm*. Applied Acoustics, 2008. **70**(1): p. 172-181.
133. Foteinou, A., Murphy, D.T. *Perceptual validation in the acoustic modelling and auralization of heritage sites: The Acoustics Measurement and Modelling of St Margaret's Church, York, UK.* in *Proc. of Conference of Ancient Theatres*. 2012. Patras, Greece.
134. Christensen, C.L. *Modelling Large sound sources in a room acoustical calculation program*. in *Joint Meeting of the Acoustical Society of America and the European Acoustics Association*. 1999. Berlin.
135. Savioja, L., Huopaniemi, J., Lokki, T., Väänänen, R., *Creating Interactive Virtual Acoustic Environments.* Journal of Audio Engineering Society, 1999. **47**(9).
136. Farina, A., Fontana, S., Campanini, S. *New Method for Auralizing the Results of Room Acoustics Simulations*. in *19th International Congress on Acoustics Simulations (ICA)*. 2007. Madrid.

137. Cox, T.J., D'Antonio, P. *Room Optimizer: A Computer Program to Optimize the Placement of Listener, Loudspeakers, Acoustical Surface Treatment and Room Dimensions in Critical Listening Rooms*. in *103rd Convention of the Audio Engineering Society*. 1997. New York.
138. Vorländer, M., *Simulation of the Transient and Steady-State Sound Propagation in Rooms using a New Combined Ray-Tracing/Image-Source Algorithm*. Journal of Acoustical Society of America, 1989. **86**(1): p. 172-178.
139. Southern, A., Siltanen, S., Murphy, D.T., Savioja, L. , *Room Impulse Response Synthesis and Validation Using a Hybrid Acoustic Model*. IEEE Transactions on Audio, Speech, and Language Processing, 2013. **21**(9).
140. van Maercke, D., Jacques, M., *The Prediction of Echograms and Impulse Responses within the Epidaure Software*. Applied Acoustics, 1993. **38**.
141. Tenenbaum, R.A., Camilo, T.S., Torres, J.C.B., Gerges, S.N.Y., *Hybrid Method for Numerical Simulation of Room Acoustics: Part 1 - Theoretical and Numerical Aspects*. J. of Braz. Soc. of Mech Sci. & Eng., 2007. **29**(2): p. 222-231.
142. Tenenbaum, R.A., Camilo, T.S., Torres, J.C.B., Stutz, L.T., *Hybrid Method for Numerical Simulation of Room Acoustics: Part 2 - Validation of the Computational Code RAIOS 3*. J. of Braz. Soc. of Mech Sci. & Eng., 2007. **29**(2): p. 222-231.
143. Otani, M., Iwaya, Y., Saito, F., Suzuki, Y., Yamada, Y., Hidaka, T. *Hybrid Auralization of Concert-hall Acoustics based on Scale Model Measurement and Geometric Acoustics Simulation*. in *Proc. of the EAA Symposium on Auralization*. 2009. Espoo, Finland.
144. Wang, H., Huang, K., *Simulation of Room Impulse Response by using Hybrid Method of Wave and Geometric Acoustics*. J. Temporal Des. Arch. Environ., 2009. **9**(1): p. 9-13.
145. Aretz, M., Nöthen, R., Vorländer, M., Schröder, D. *Combined Broadband Impulse Responses using FEM and Hybrid Ray-based Methods*. in *Proc. of the EAA Symposium on Auralization*. 2009. Espoo, Finland.
146. Lokki, T., Southern, A., Siltanen, S., Savioja, L. *Studies of Epidaurus with a Hybrid Room Acoustics Modelling Method*. in *The Acoustics of Ancient Theatres Conference*. 2011. Patras.
147. Gomes, M.H.A. *Implementation and Comparison of Room Acoustical Simulation Methods and an Auralisation Tool*. in *19th International Congress on Acoustics*. 2007. Madrid.
148. Dalenbäck, B.-I., *Room Acoustic Prediction based on a Unified Treatment of Diffuse and Specular Reflection*. Journal of Acoustical Society of America, 1996. **100**(2): p. 899-909.
149. *CATT-Acoustic v8.0g, User's Manual*. 2002.
150. James, A., Dalenbäck, B.-I., Naqvi, A., *Computer Modelling with CATT-Acoustic - Theory and Practice of Diffuse Reflection and Array Modelling*, in *Technical Paper by Adrian James Acoustics*: UK.
151. Laird, I., Murphy, D., Chapman, P, Jouan, S. *Development of a Virtual Performance Studio with Application of Virtual Acoustic Recording Methods*. in *Proc. of the 130th Convention*. 2011. London, UK.
152. Vallejo-Ortega, G., Sánchez-Rivera, J.I., de la Iglesia, M.Á. *Acoustic Study of a Roman Theatre in Hispania: Colonia Clunia Sulpicia*. in *The Acoustics of Ancient Theatres Conference*. 2011. Patras.
153. Galindo, M., Zamarreño, T., Girón, S., *Acoustic Simulations of Mudejar-Gothic Churches*. Journal of Acoustical Society of America, 2009. **126**(3): p. 1207-1218.

154. Vassilantonopoulos, S.L., Mourjopoulos, J.N., Hatziantoniou, P., Zarouhas, T. *The Acoustics of Roman Odeion of Patras*. in *Acoustics 2006 (In Greek)*. 2006. Herakleion, Creta.
155. Vassilantonopoulos, S.L., Mourjopoulos, J.N., *The Acoustics of Roofed Ancient Odeia: The Case of Herodes Atticus Odeion*. Acta Acustica United with Acustica, 2009. **95**: p. 291-299.
156. Segura, J., Giménez, A., Romero, J., Cerdá, S., *A Comparison of Different Techniques for Simulating and Measuring Acoustic Parameters in a Place of Worship: Sant Jaume Basílica in Valencia, Spain*. Acta Acustica United with Acustica, 2011. **97**: p. 155-170.
157. Berardi, U., *Simulation of acoustical parameters in rectangular churches*. Journal of Building Performance Simulation, 2013. **6**(7).
158. Naylor, G.M., *ODEON - Another Hybrid Room Acoustical Model*. Applied Acoustics, 1993. **38**: p. 131-143.
159. Naylor, G.M., Rindel, J.H. *Predicting Room Acoustical Behaviour with the ODEON Computer Model*. in *124th ASA Meeting*. 1992. New Orleans.
160. Naylor, G. *Treatment of Early and Late Reflections in a Hybrid Computer Model for Room Acoustics*. in *124th ASA meeting*. 1992. New Orleans.
161. Bradley, J.S., Sato, H., Picard, M., *On the Importance of Early Reflections for Speech in Rooms*. Journal of Acoustical Society of America, 2003. **113**(6): p. 3233-3243.
162. Vigeant, M.C., Wang, L.M., Rindel, J.H., *Objective and Subjective evaluations of the multi-channel auralization technique as applied to solo instruments*. Applied Acoustics, 2011. **72**: p. 311-323.
163. Vigeant, M.C., Celmer, R.D., Dick, D.A. *Investigation of the Correlation between Late Lateral Sound Level and Total Acoustic Absorption, and an Overview of a Related SUbjective Study*. in *Proc. of the International Symposium on Room Acoustics, ISRA 2010*. 2010. Melbourne, Australia.
164. Rathsam, J., Wang, L.M., Rindel, J.H., Christensen, C.L. *Reflector Responses: A Comparison between ODEON's Modified Ray Tracing Algorithm and a Filtered Boundary Element Method Model*. in *DAGA*. 2007. Stuttgart, Germany.
165. Reich, R., Bradley, J., *Optimizing Classroom Acoustics using Computer Model Studies*. Canadian Acoustics, 1998. **26**(4): p. 15-21.
166. Rindel, J.H. *Room Acoustic Prediction Modelling*. in *23rd Encontro da Sociedade Brasileira de Acústica*. 2010. Salvador - BA.
167. Rindel, J.H. *Echo Problems in Ancient Theatres and a Comment to the 'Sound Vessels' Described by Vitruvius*. in *The Acoustics of Ancient Theatres Conference*. 2011. Patras.
168. Iannace, G., Maffei, L., Aletta, F. *Computer Simulation of the Effect of the Audience on the Acoustics of the Roman Theatre of Beneventum (Italy)*. in *The Acoustics of Ancient Theatres*. 2011. Patras.
169. Skålevik, M., *Room Acoustic Parameters and their Distribution over Concert Hall Seats*. www.akutek.info, 2008. **30** (2).
170. Klosak, A.K., Gade, A.C. *Relationship between Room Shape and Acoustics of Rectangular Concert Halls*. in *Acoustic' 08*. 2008. Paris.
171. Shiokawa, H., Rindel, J.H., *Comparisons between Computer Simulations of Room Acoustical Parameters and Those Measured in Concert Halls*, in *Report of the Research Institute of Industrial Technology*. 2007, Nibon University.

172. Støfringsdal, B., *Integrated Room Acoustic and Electro-acoustic Design -The Concept Venue at Rockheim, Norway*. Proc. of the Institute of Acoustics, 2011. **33**(2): p. 273-277.
173. Vigeant, M.C., Wang, L.M., Rindel, J.H., *Effects of Changing the Amount of Absorption in a Computer Model of Queen's Hall, Copenhagen, Denmark*. Proc. of the Institute of Acoustics, 2006. **28**(2): p. 247-254.
174. Wang, L.M., Rathsam, J., Ryherd, S. *Interactions of Model Detail Level and Scattering Coefficients in Room Acoustic Computer Simulation*. in *International Symposium on Room Acoustics: Design and Science*. 2004. Kyoto, Japan.
175. Weitze, C.A., Rindel, J.H., Christensen, C.L., Gade, A.C. *The Acoustical History of Hagia Sophia revived through Computer Simulation*. in *Forum Acusticum*. 2002. Sevilla.
176. Bradley, D. *The Effect of Source Directivity and Side-Wall Scattering on Binaural Hearing Objective Measures*. in *Forum Acusticum*. 2011. Aalborg.
177. Vorländer, M. *Prediction tools in acoustics - Can we trust the PC?* in *BNAM*. 2010. Bergen, Norway.
178. Vorländer, M. *Performance of Computer simulations for Architectural Acoustics*. in *Proc. of 20th International Congress on Acoustics, ICA*. 2010. Sydney, Australia.
179. Vorländer, M., *Computer Simulations in Room Acoustics: Concepts and Uncertainties*. Journal of Acoustical Society of America, 2013. **133**(3): p. 1203-1213.
180. Lokki, T., Savioja, L. *State-of-the-art in Auralization of Concert Hall Models - What is still missing?* in *Joint Baltic-Norbic Acoustics Meeting*. 2008. Reykjavik, Iceland.
181. Tsingos, N., Carlbom, I., Elko, G., Funkhouser, T., Kubli, B., *Validation of Acoustical Simulations in the "Bell Labs Box*. IEEE CG&A, 2002(Special Issue on Virtual World, Real Sound).
182. Foteinou, A., Murphy, D.T. *The Control of Early Decay Time on Auralization Results based on Geometric Acoustic Modelling*. in *Joint Baltic-Nordic Acoustics Meeting (BNAM)*. 2012. Odense, Denmark.
183. ISO3382-2, I.S.-. *Acoustics - Measurement of room acoustic parameters, Part 2: Reverberation time in ordinary rooms*. ISO. 2008.
184. *The Church of St Margaret*. The National Centre for Early Music [cited 12 December 2010]; Available from: http://www.ncem.co.uk/?idno=245.
185. *NCEM Site Development History*. The National Centre for Early Music [cited 12 December 2010]; Available from: http://www.ncem.co.uk/code/download.aspx?name=NCEM%20Site%20Development%20History&file=/uploads/ncem/mainsite/downloads/website_content/attachments/NCEM%20Site%20Development%20History.pdf.
186. *NCEM History*. The National Centre for Early Music [cited 12 December 2010]; Available from: http://www.ncem.co.uk/?idno=175.
187. *Architectural Plans as proposed for York Early Music Foundation - National Centre for Early Music*. 1998, Van Heyningen and Haward Architects.
188. Farina, A. *AURORA Plug-ins, .* [cited 7th August 2009]; Available from: http://www.aurora-plugins.com/.
189. Farina, A. *Presentation at 24th AES International Conference (slide 16)*. 2003 [cited 7th August 2009]; Available from: http://pcfarina.eng.unipr.it/Public/Presentations/AES24-Presentation_files/frame.htm.

190. Lokki, T., *Subjective comparison of four concert halls based on binaural impulse responses*. Acoust. Sci. & Tech. , 2005. **26**(2).
191. Ma□ecki, P., Wiciak, J. *Acoustic Parameters of Chosen Orthodox Churches Overview and Preliminary Psychoacoustic Tests Using Choral Music*. in *130th AES Convention*. 2011. London, UK.
192. the SoundField SPS422B studio microphone system [cited 15 April 2013]; Available from: http://www.soundfield.com/downloads/sps422b.pdf.
193. CATT-Acoustic, *User's Manual v8g*. 2007, Gothenburg, Sweden: CATT
194. ODEON, *User Manual, version 10.0*. 2009, Lyngby, Denmark: ODEON A/S.
195. Farina, A. *Measurement of Surface Scattering Coefficient: Comparison of the Mommertz/Vorlander approach with the new Wave Field Synthesis method*. in *International SYmposium on Surface Diffusion in Room Acoustics*. 2000. Liverpool, (GB.
196. Garai, *Measurement of sound-absorption coefficient in-situ: The reflection method using periodic pseudo-random sequences of maximum length*. Applied Acoustics, 1993. **39**: p. 119-139.
197. Mommertz, E., *Angle-dependent in-situ measurements of reflection coefficients using a subtraction technique*. Applied Acoustics, 1995. **46**(3): p. 251-263.
198. Gade, A., Lynge, C., Lisa, M., Rindel, J. *Matching simulations with measured acoustic data from Roman Theatres using the ODEON programme*. in *Forum Acusticum*. 2005. Budapest.
199. Kamisi□ski, T., Rubacha, J., Pilch, A., *The Study of Sound Scattering Structures for the Purposes of Room Acoustic Enhancement*. Acta Physica Polonica A, 2010. **118**(1): p. 83-86.
200. Pulkki, V., Lokki, T., *Visualization of Edge Diffraction*. Acoustics Research Letters Online (ARLO), 2003. **4**(4): p. 118-123.
201. Cox, T.J., Dalenback, B.-I. L., D'Antonio, P., Embrechts, J. J., Jeon, J. Y., Mommertz, E., Vorländer, M., *A Tutorial on Scattering and Diffusion Coefficients for Room Acoustic Surfaces*. Acta Acustica United with Acustica, 2006. **92**: p. 1-15.
202. Cox, T.J., D'Antonio, P. *Surface characterization for room acoustic modelling and design*. in *International Symposium on Room Acoustics: Design and Science* 2004. Kyoto, Japan.
203. Gomes, M.H.A., Vorländer, M., Gerges, S.N.Y. *Measurement and use of scattering coefficients in room acoustic computer simulations*. in *Acústica*. 2004. Guimarães - Portugal.
204. Christensen, C.L., Rindel, J.H. *A new scattering method that combines roughness and diffraction effects*. in *Forum Acusticum*. 2005. Budapest.
205. Skålevik, M. *On the Struggle to Find a Set of Room Acoustical Parameters that explains and Predicts Subjective Ranking of Concert Halls*. in *Auditorium Acoustics, IOA*. 2011. Dublin.
206. Jordan, V., L., *A Group of Objective Acoustical Criteria For Concert Halls*. Applied Acoustics, 1981. **14**: p. 253-266.
207. Merimaa, J., Peltonen, T., Lokki, T., *Concert Hall Impulse Responses - Pori, Finland: Analysis results*, in *a free documented room response database available at http://www.acoustics.hut.fi/projects/poririrs/*. 2005.
208. Angelakis, K., Rindel, J.H., Gade, A.C. *Theatre of the Sanctuary of Asklepios at Epidaurus and the Theatre of Ancient Epidaurus: Objective measurements and computer simulations*. in *Proc. of The Acoustics of Ancient Theatres Conference*. 2011. Patras, Greece.

209. Lokki, T., Pätynen, J., Kuusinen, A., Tervo, S., *Disentangling preference ratings of concert hall acousics using subjective sensory profiles*. Journal of Acoustical Society of America, 2012. **132**(5): p. 3148-3161.
210. □opa, M.D., Toma, N., Kirei, B. S., S□r□cu□, I., Farina, A., *Experimental Acoustic Evaluation of an Auditorium*. Advances in Acoustics and Vibration, 2012. **Volume 2012**.
211. Hak, C., Vertegaal, H. *What Exactly is Time Infinity for Acoustical Parameters*. in *The Sixteen International Congress on Sound and Vibration (ICSV16)*. 2009. Kraków, Poland.
212. Stettner, A., Greenberg, D. P. *Computer Graphics Visualization For Acoustic Simulation*. in *Computer Graphics*. 1989. New York: Proc. Siggraph 89.
213. Farina, A., Martignon, P., Azzali, A., Capra, A. *Listening Tests Performed Inside a Virtual Room Acoustic Simulator*. in *I seminario Música Ciênca e Tecnologia "Acústica Musical"*. 2004. São Paolo do Brasil.
214. Merimaa, J., Pulkki, V. , *Spatial Impulse Response Rendering I: Analysis and Synthesis*. Journal of Audio Engineering Society, 2005. **53**(12): p. 1115-1127.
215. Okano, T., Beranek, L.L., Hidaka, T., *Relations among interaural cross-correlation coefficient (IACCE), lateral fraction (LFE), and apparent source width (ASW) in concert halls*. Journal of Acoustical Society of America, 1998. **104**(1): p. 255-265.
216. Barron, M., Lee, L-J., *Energy relations in concert auditoriums. I*. Journal of Acoustical Society of America, 1988. **84**(2): p. 618.
217. Beranek, L., *The sound strength parameter G and its importance in evaluating and planning the acoustics of halls for music*. Journal of Acoustical Society of America, 2011. **129**(5): p. 3020-3026.
218. Kessler, R. *An Optimized Method for Capturing Multidimensional "Acoustic Fingerprints"*. in *118th AES Convention*. 2005. Barcelona, Spain.
219. Capra, A., Binelli, M., Marmiroli, D., Martignon, P., Farina, A. *Correlation Between Subjective Descriptors and Objective Parameters of Theatres and Auditoria Acoustics Simulated with Binaural Sound Systems*. in *13th International Congress on Sound and Vibration (ICSV13)*. 2006. Vienna, Austria.
220. Barron, M., *Sybjective Study of British Symphony Concert Halls*. Acta Acustica - Acustica, 1988. **66**(1): p. 1-14.
221. Farina, A., Farina, A. *Realtime Auralization Employing a Not-linear, Not-time-invariant Convolver*. in *123rd AES Convention*. 2007. New York, USA.
222. Ando, Y., Gottlob, D., *Effects of Early multiple reflections on subjective preference judgments of music sound fields*. Journal of Acoustical Society of America, 1979. **65(2)**(0001-4966/79-020524-04$00.80): p. 524-529.
223. Merimaa, J., Pulkki, V. *Spatial Impulse Response Rendering*. in *Proc. of the 7th Int. Conference on Digital Audio Effects (DAFx'04)*. 2004. Naples, Italy.
224. Bech, S., Zacharov, N., *Perceptual Audio Evaluation - Theory, Method and Application*, ed. Wiley. 2006, Chichester, England.
225. Bang&Olufsen, *Music for Archimedes Project, CD reproduced for CATT-Acoustic auralization*. 1992.
226. Farina, A. *Auralization Software for the Evaluation of a Pyramid Tracing Code: Results of Subjective Listening Tests*. in *ICA95 (International Conference on Acoustics)*. 1995. Trondheim (Norway).

227. Kearney, G., *Auditory Scene Synthesis using Virtual Acoustic Recording and Reproduction*, in *Department of Electronic and Electrical Engineering*. 2009, Trinity College: Dublin.
228. Lokki, T., Vertanen, H., Kuusinen, A., Pätynen, J., Tervo, S. *Auditorium Acoustics Assessment with Sensory Evaluation Methods*. in *Proceedings of the International Symposium on Room Acoustics, ISRA*. 2010. Melbourne, Australia.
229. Zielinski, S. *On some biases encountered in modern listening tests*. in *Spatial Audio & Sensory Evaluation Techniques*. 2006. Guildford, UK.
230. Bradley, J.S., Soulobre, G.A., *The Influence of Late Arriving Energy on Spatial Impression*. Journal of Acoustical Society of America, 1995. **97**(4): p. 2263-2271.